Photoinduced Electron Transfer in Dyads and Triads with d^6 Metal Complexes and Anthraquinone

Dissertation

zur Erlangung des mathematisch-naturwissenschaftlichen Doktorgrades

"Doctor rerum naturalium"

der Georg-August-Universität Göttingen

vorgelegt von

Jihane Hankache

aus Libanon

Göttingen, 2012

Referent: Prof. Dr. Oliver Wenger
Koreferent: Prof. Dr. Franc Meyer
Tag der mündlichen Prüfung: 21.06. 2012

To my Boss

Behind every 'successful' student.....a 'horrible' boss

Table of Contents

General Introduction

Nowadays, given the rapid technology progress and the growth of the population, the world energy consumption rate is expected to grow from 13.5 TW to 40.8 TW by 2050 [1]. Until now, the required energy is mostly produced by fossil fuels (oil, coal, natural gas). These fuels contribute to the increase of air pollution and lead to high amounts of carbon dioxide (CO_2) causing global warming. Moreover, this energy supply is closed to reach the limit. Searching for alternative energy sources is mandatory and has become recently one of the most important scientific and technical challenges facing humanity in the 21st century.

It has been reported that the amount of solar energy that reaches the earth in one hour (4.3×10^{20} J) is more than the amount of fossil fuels that is consumed by humans in an entire year (4.1×10^{20} J) [2]. The possibility of exploiting this enormous amount of energy to produce a clean and renewable energy source received significant attention from scientists worldwide. However, the main scientific challenge is that this solar energy must be captured, converted, and stored [3]. Solar capture and conversion may be accomplished by photovoltaics (PVs), but the high cost of the materials should be taken into account. The most attractive and cheapest method for solar energy conversion and storage is in the form of chemical bonds. This method is inspired from a natural process called photosynthesis.

Natural photosynthesis is a series of reactions that take place in green plants, algae and bacteria which capture sunlight and convert it into chemical energy. This energy is used to

reduce the carbon dioxide to carbohydrates and to oxidize water to molecular oxygen. In general, photosynthesis could be described by the reaction shown in equation 1 [4]:

$$6CO_2 + 6H_2O + \text{sunlight} \rightarrow C_6H_{12}O_6 + 6O_2 \qquad \text{(eq. 1)}$$

This reaction occurs in the thylakoid membranes of the chloroplasts in which two large protein complexes are localized: Photosystem I (PS I) which absorbs photons with a wavelength of 700 nm, and Photosystem II (PS II) which absorbs photons at a wavelength of 680 nm. PS II provides the oxidizing potentials necessary to split water into protons, electrons, and oxygen (eq. 2).

$$2H_2O + 4\,h\nu \rightarrow O_2 + 4e^- + 4H^+ \qquad \text{(eq. 2)}$$

The electrons liberated in this reaction reduce benzoquinone to hydroquinone and transfer reductive equivalents to PS I in which CO_2 is converted into carbohydrate [5,6].

Water splitting is one of the most important chemical reactions on the planet. Figure 1 provides a general overview about the series of electron transfer reactions that happen in PS II which leads to water oxidation. Absorption of a photon in PS II leads to the formation of an excited state of the chlorophyll species called P^*_{680}. The excited P^*_{680} is then oxidized through an electron transfer reaction to a primary acceptor, the pheophytine (Ph), creating a charge-separated state, $P_{680}^+Ph^-$. The lifetime of this state is crucial for the storage of solar energy. In order to prevent charge-recombination, Ph^- donates an electron in a few hundred picoseconds to a tightly bound quinone (Q_A). Therefore the distance between the charges ($P_{680}^+Q_A^-$) is increased. The oxidized P_{680}^+ is reduced through a rapid electron transfers from a nearby tyrosine residue (Tyr). This electron transfer appears to be coupled to proton transfer to histidine (His_{190}), resulting in the original P_{680} and a neutral tyrosine radical. The $Tyr^{\cdot}Q_A^-$ radical pair is further stabilized by electron transfer to a second quinone (Q_B). The tyrosine radical oxidizes the manganese cluster. This cluster consists of four manganese ions and plays a crucial role in the charge accumulating process and very probably as the active site for water oxidation. The tyrosine is an intermediate reactant in the electron transfer from the manganese cluster to the oxidized P_{680}^+ (Figure 1).

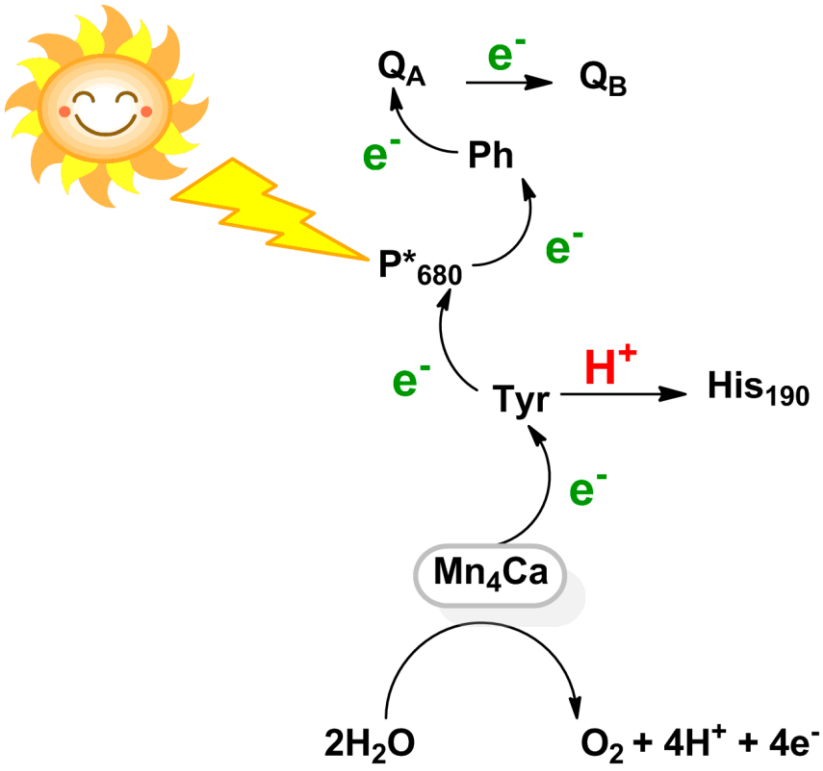

Figure 1. Illustration of light induced electron transfer reactions in PS II resulting in the oxidation of water.

The concept of photosynthesis attracted researchers who have made significant efforts in order to understand this natural process by designing artificial systems that mimic the photosynthesis mechanism. One of the challenges is to have donor-acceptor system (D-A) as far away as possible in order to prevent charge-recombination. A long-lived charge-separated state (D^+-A^-) will be then formed. This state can react with water and produce a clean fuel such as hydrogen which can replace the fossil fuels [3].

Electron transfer reactions leading to charge-separated states are not only present in photosynthesis but play a pivotal role in many biological processes [7-9] for example in respiration. Being interested in this field, my effort in this thesis has been devoted to studying photoinduced electron transfer in artificial dyad and triad systems containing an electron donor (D), a photosensitizer, and a quinone as electron acceptor (A).

One of my challenges is to increase the lifetime of the charge-separated state (τ_{CS}) in these systems either by increasing the number of bridge units between the donor and the acceptor, or via hydrogen-bonding in presence of a proton source. The latter method is found to have a significant effect on the increase of τ_{CS} and could be a way for storing light energy.

Before tackling my Ph.D. work in detail, a brief theoretical discussion about the electron transfer mechanism is useful. Then, the photophysical and redox properties of the ruthenium(II) polypyridyl complex will be presented since the ruthenium complex is used as a chromophore in most of the dyad and triad systems investigated in this work. The last part of this introduction will be devoted to shed light on some important previous research in the field of photoinduced electron transfer.

1. Photoinduced electron transfer

Absorption of light by a molecule results in an electronic transition of the molecule from its ground state (S_0) to its first excited state. When the electron is promoted to an excited state, its spin usually does not change due to spin restrictions. Consequently, the excited state formed is called singlet excited state (S_1). From S_1, the molecule first relaxes to the lowest vibrational level through thermal relaxation. This relaxation is generally faster than other photophysical and photochemical processes ($k_{vib} = 10^{11} - 10^{12}$ s^{-1}).

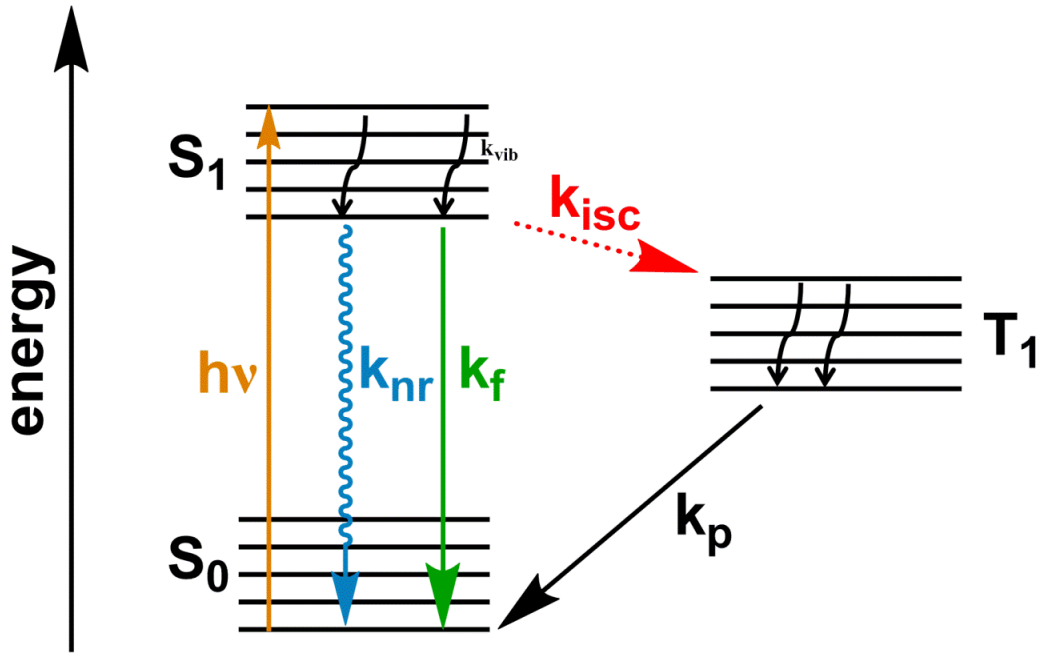

Scheme 1. Jablonski diagram illustrating the different energy levels involved and the different transitions that can occur upon absorption of a photon by a molecule.

The singlet excited state S_1 can undergo two types of deactivation back to the ground state S_0: either through a non-radiative decay (k_{nr}) as heat, or via a radiative deactivation manifested by emission of light and it corresponds to fluorescence ($k_f = 10^9\ s^{-1}$).

If the spin of the excited electron flips, the spin multiplicity for the excited state becomes three and this process is called intersystem crossing (k_{isc}). The resulting state is a triplet excited state (T_1). Intersystem crossing is a forbidden process due to spin restrictions, but it can happen in systems with strong spin-orbit coupling. Hence, this triplet excited state (T_1) undergoes radiative decay which is called phosphorescence. This process is relatively slow ($k_p = 10^3 - 10^6\ s^{-1}$).

Each decay step is characterized by its own rate constant k_i and each excited state is characterized by its lifetime τ given by the formula:

$$\tau = 1/\sum_i ki$$

$\sum_i ki$ is the sum of the rate constants of the deactivation pathways that causes the relaxation of the corresponding excited state.

When the lifetime of the excited state is sufficiently long, there is a possibility that this state interacts with other molecules, therefore additional deactivation pathways could take place such electron or energy transfer processes.

Photoinduced electron transfer occurs between at least two redox units: an electron donor (D) and an electron acceptor (A). Photoexcitation of a D-A system at a given wavelength results in a population of an excited state of either *D-A or D-*A (* denotes an excited state). The excitation is followed by an intramolecular electron transfer from the donor to the acceptor allowing the formation of a charge-separated state D^+-A^-.

$$\mathbf{D\text{-}A} \xrightarrow{h\nu} \mathbf{{}^*D\text{-}A} \xrightarrow{k_{ET}} \mathbf{D^+\text{-}A^-}$$

According to Marcus theory [10-19] developed in the late of 1950s, the parameters that control such an electron transfer reaction are the driving force (-ΔG), arising from the difference in

the oxidation potentials of D and A, and the reorganization energy (λ), needed for the nuclear rearrangements that accompany the electron transfer. Therefore, the electron transfer rate k_{ET} can be estimated from the driving force and the reorganization energy according to equation 3.

$$k_{ET} = A \cdot \exp\left(-\frac{(\Delta G + \lambda)^2}{4 \cdot \lambda}\right) \qquad \text{(eq.3)}$$

Rate expression in equation 3 has the form of a Gaussian function. Consequently there are three different regimes for electron transfer rate:

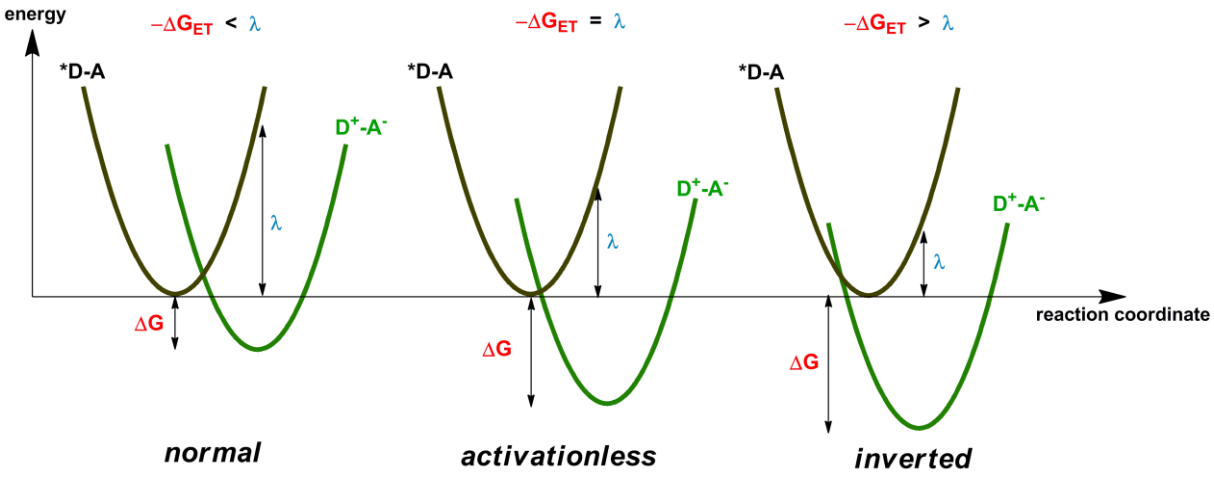

Figure 2. Potential energy surfaces for electron transfer from a photoexcited donor (*D) to an acceptor (A) in three different regimes.

Activationless electron transfer leads to a maximum rate. This rate decreases with decreasing driving force in the Marcus normal regime. On the other hand, Marcus theory also predicts an inverted region, where the rate decreases with increasing driving force.

In photoinduced electron transfer processes charge separation is often in the Marcus normal region ($-\Delta G_{ET} < \lambda$) and charge recombination is frequently in the inverted region ($-\Delta G_{ET} > \lambda$).

2. $Ru(bpy)_3^{2+}$ complex as photosensitizer

In nature, chlorophylls play the role of photosensitizers. They absorb sunlight that creates the excited state, which undergoes electron transfer reactions leading to the formation of the charge-separated state that is important for the conversion of solar energy into chemical energy. Chlorophylls are natural porphyrins. Hence designing artificial molecular systems comprised of porphyrins as chromophores[20-22] have taken a vital part in research. However, the $Ru(bpy)_3^{2+}$ complex is widely used as photosensitizer due to its remarkable chemical stability and photophysical properties [23-29].

2.1 Photochemical and photophysical properties of $Ru(bpy)_3^{2+}$

$Ru(bpy)_3^{2+}$ is a d^6 transition metal with nearly octahedral geometry. The local symmetry at the Ru site is D_3. The absorption spectrum in the visible region is dominated by an intense metal-to-ligand charge transfer (^{1}MLCT) band at 450 nm (Figure 3) caused by the transition from a dπ metal orbital (t_{2g}) to a ligand based orbital (π_L^*). The other intense band around 290 nm is due to a promotion of an electron from π_L to π_L^*.This transition is called ligand-centered bands (LC). The weak shoulder around 320 nm corresponds to the metal-centered transition (MC) from t_{2g} to e_g [24,25,30,31].

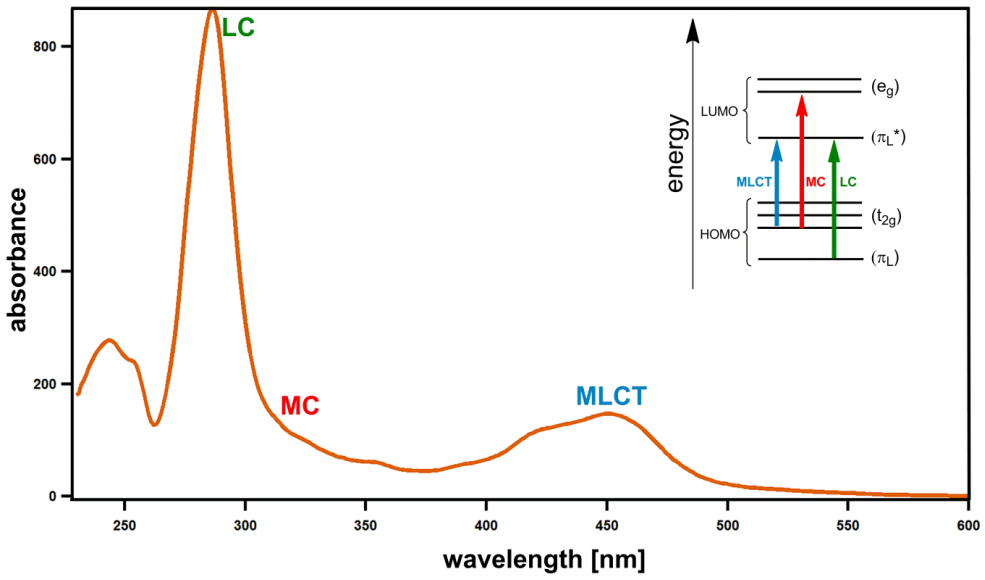

Figure 3. Absorption spectrum of $Ru(bpy)_3^{2+}$ in acetonitrile solution showing the different types of electronic transitions.

The ^{1}MLCT state decays rapidly within 300 fs via intersystem crossing (φ_{isc} = 1) [24,32-35] to a ^{3}MLCT excited state which has a lifetime (τ) of around 0.8 μs in acetonitrile at room temperature [36]. This long-lived excited state of $Ru(bpy)_3^{2+}$ can transfer its energy to another molecule (a quencher), either by energy transfer or electron transfer. In the absence of a quencher, the excited state undergoes deactivation through both nonradiative and radiative decay pathways with an emission quantum yield (φ) of 0.06 in deaerated acetonitrile solution at room temperature (Figure 4).

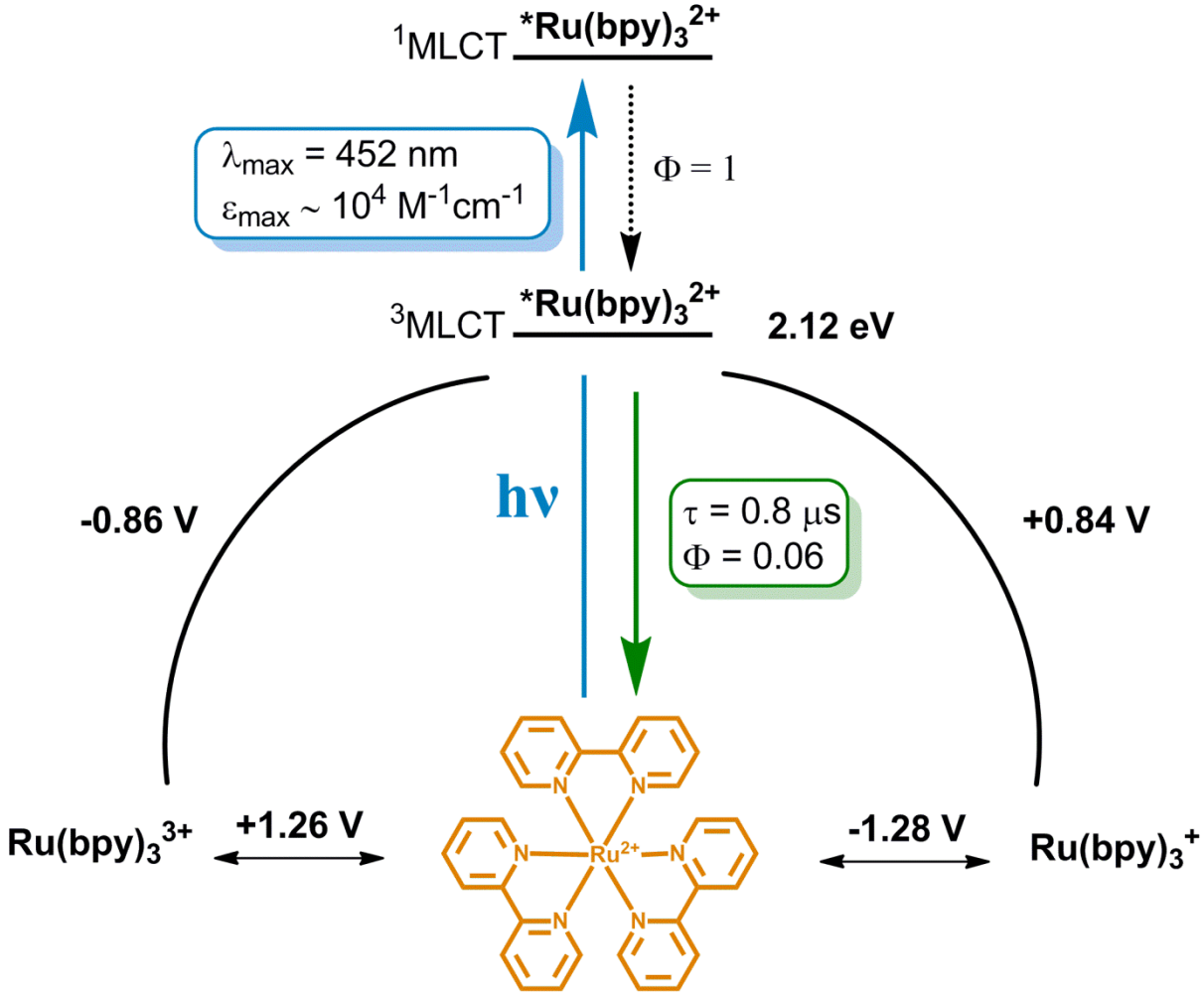

Figure 4. Photophysical and electrochemical properties of $Ru(bpy)_3^{2+}$ in acetonitrile solution. The redox potentials are reported versus SCE.

2.2 Redox properties of $Ru(bpy)_3^{2+}$

The oxidation of $Ru(bpy)_3^{2+}$ occurs at positive potentials (E_{ox} = +1.26 V vs. SCE) which involves the removal of one electron from a metal-centered orbital (Ru^{3+}/Ru^{2+}). On the other hand, three reduction waves of the ruthenium complex occur at negative potential (between -1.28 V and – 1.70 V vs. SCE) and are all ligand centered [37] (Figure 4).

The redox potentials for reduction and oxidation of $*Ru(bpy)_3^{2+}$ are +0.84 V and -0.86 V respectively. In other words, $*Ru(bpy)_3^{2+}$ can act as a good electron donor or electron acceptor at the same time. The redox potentials of the excited state can be estimated according to the following equations [24]:

$$E(Ru^{3+}/*Ru^{2+}) = E(Ru^{3+}/Ru^{2+}) - E_{00}$$
$$E(*Ru^{2+}/Ru^{+}) = E(Ru^{2+}/Ru^{+}) + E_{00}$$

$E(Ru^{3+}/Ru^{2+})$ and $E(Ru^{2+}/Ru^{+})$ are the potentials for the ground state oxidation and reduction respectively. E_{00} is the excitation energy (2.12 eV).
Adding electron-withdrawing or electron-donating substituents on two of the bipyridine ligands lead to a change of the ground state redox potentials and therefore a change in the excited state potentials [38,39].

3. Photoinduced electron transfer in artificial systems

Since photoinduced electron transfer (PET) plays important roles in natural photosynthesis and in biological systems, this field has become an active area of research. Large number of books, reviews and articles have been published in this field [40-53]. In this section, I have selected some papers where the PET in different systems leads to a charge-separation state with different lifetimes and quantum yields. These systems usually consist of a photosensitizer, an electron donor and/or an electron acceptor.

3.1 Dyad and triad systems with d^6 metal complexes

Sauvage and co-workers have reported the results obtained upon photoexcitation of a rigid linear triad system based on an iridium(III) terpyridine complex with an amine donor and a

bisimide electron acceptor (Scheme 2) [54]. The key finding behind this study was the photogeneration of a long-lived charge-separated state with a lifetime on the order of 120 μs. This state was stable in the presence of air. This system has an important disadvantage regarding the low yield (10 %) of the formation of the fully charge-separated state.

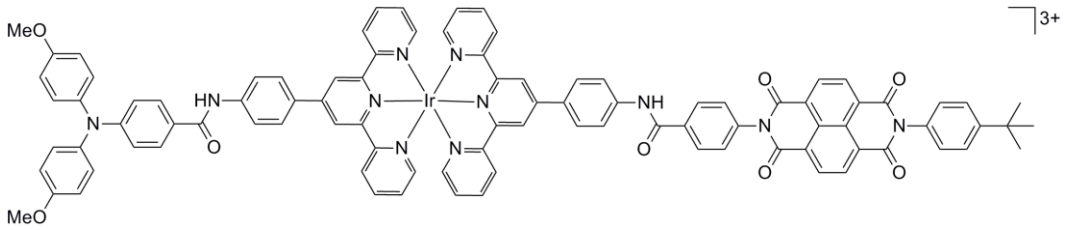

Scheme 2

Meyer and co-workers studied the photoinduced intramolecular electron transfer in ruthenium(II) bipyridine-quinone complexe [55] (Scheme 3). This system incorporates a phenothiazine unit as an electron donor, anthraquinone moieties as electron acceptors, and the $Ru(bpy)_3^{2+}$ complex as a photosensitizer.

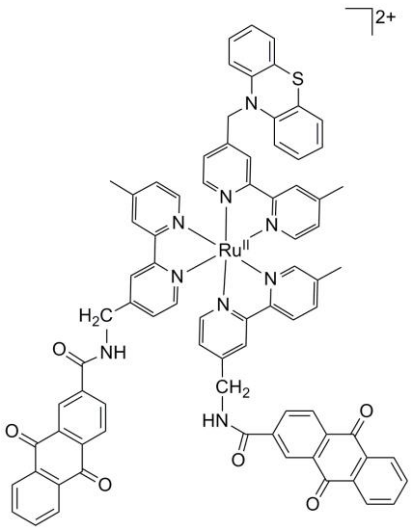

Scheme 3

Excitation of this molecule leads to the formation of a charge-separated state (PTZ^+/AQ^-) in approximately 40 % yield. This state undergoes back electron transfer with τ = 150 ns corresponding to a rate constant of $6.7 \cdot 10^6$ s^{-1}. Since the tris-substituted triad in Scheme 3 is heteroleptic, there is the possibility of formation of multiple isomers. This may complicate the analysis of the photophysical properties of the triad.

To overcome the problem of isomeric mixtures and non-optimized spatial organization, Meyer and co-workers have designed a helical oligoproline assembly bearing three different redox sites : A phenothiazine electron donor, a tris(bipyridine)ruthenium(II) chromophore, and an anthraquinone electron acceptor. These redox sites are in a linear array on one side of the helical rod [56] (Scheme 4). A charge-separated state was formed in 53 % yield and this state decayed exponentially with a lifetime of 175 ns ($k = 5.6 \cdot 10^6\ s^{-1}$), and stored 1.65 eV of energy.

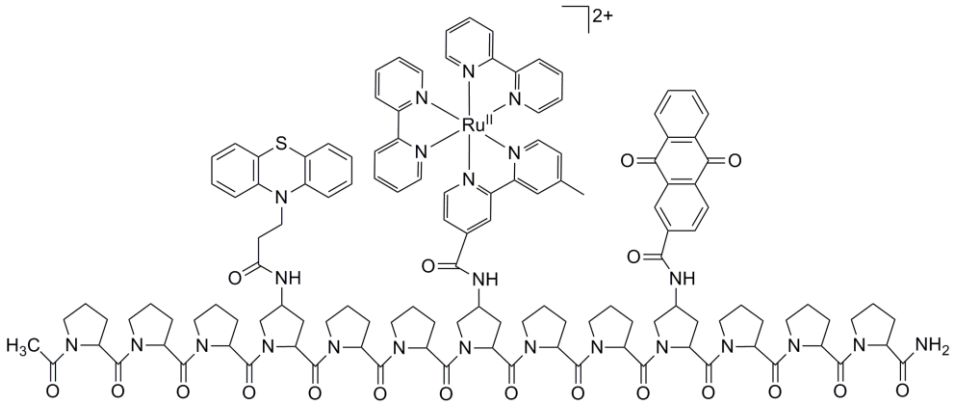

Scheme 4

The triad shown in Scheme 5 has been investigated by Hammarström and co-workers [57]. This triad is based on benzoquinone (BQ) as electron acceptor, a phenothiazine (PTZ) as electron donor and $Ru(bpy)_3^{2+}$ acting as chromophore. The PTZ^+-Ru^{2+}-BQ^- charge-separated state is formed via a sequence of Ru^{2+} to BQ and PTZ to Ru^{3+} electron transfer steps. This state is formed with a high yield (> 90 %), it exhibits a lifetime of 80 ns and stores 1.32 eV of the excitation energy. However this molecule turned out to be photolabile.

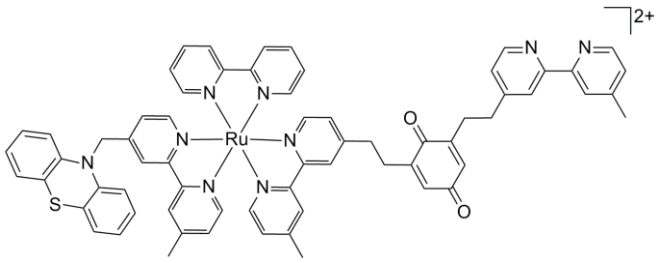

Scheme 5

The same group synthesized a linear triad based on $Ru(dqp)_2^{2+}$ for vectorial electron transfer [58] (Scheme 6). The choice of this photosensitizer with bis(diquinolinyl)pyridine

ligands is due to the large bite angle creating a strong ligand field leading to photophysical properties similar to those of $Ru(bpy)_3^{2+}$. The fully charge-separated state is formed with more than 50 % yield.

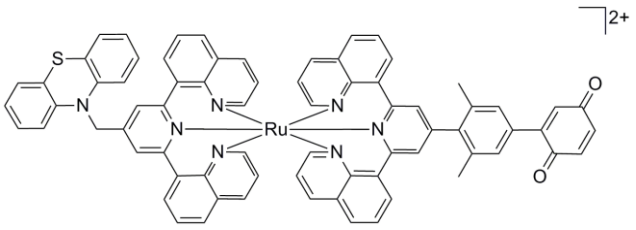

Scheme 6

Wenger and co-workers [59-61] have synthesized rigid molecular dyads comprised of a phenothiazine as electron donor and $Ru(bpy)_3^{2+}$ as the chromophore. These two redox center are separated either with oligo-*p*-xylene units or with oligo-*p*-dimethoxybenzene (Scheme 7). Despite the fact that these two wires are structurally very similar, electron transfer across the tetra-*p*-dimethoxybenzene wire is 1000 times faster than across the tetra-*p*-xylene spacer.

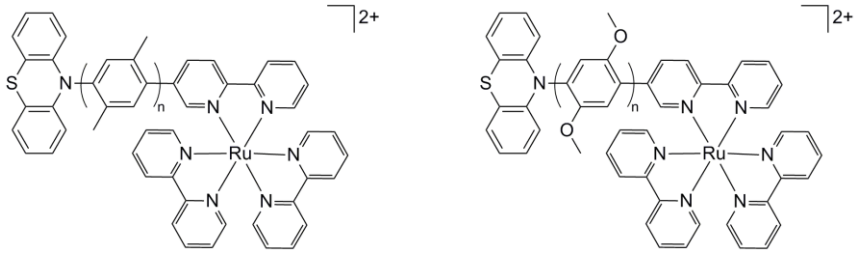

Scheme 7

3.2 Electron transfer with quinone acceptors

Quinones are extensively used as electron acceptors since they play a key role in natural photosynthesis [62,63]. In addition to their capacity of accepting electrons, quinones are easy to be protonated and able to form hydrogen-bonds. These two factors facilitate the reduction of quinones.

Linschitz and co-workers focused on hydrogen-bonding and protonation effects in electrochemical reduction of quinones in aprotic solvents in presence of small amounts of hydrogen-bond donors or Brønsted acids [64]. It has been demonstrated that upon addition of

hydroxylic additives to a solution of quinone in CH_2Cl_2, the reduction waves of the quinone shift positively and electrochemical reduction becomes easier with increasing of hydrogen-bond donor strength. Moreover, the redox waves maintain their reversibility. This finding has been attributed to hydrogen-bonding between the alcoholic solvent and the reduced quinone.

The same group has demonstrated that upon photoexcitation of fullerene (C_{60}), oxidative quenching of the lowest triplet excited state of C_{60} to C_{60}^{+} by a quinone molecules (chloranil) becomes more efficient when the chloranil is hydrogen-bonded to an hexafluoroisopropanol (HFIP) molecule [65,66].

Quinones have been well explored electrochemically in protic solvents. By contrast, a lack of studies has been noted concerning their investigation in light induced redox chemistry. For this reason, it was decided to give through this thesis a close insight regarding the effect of hydrogen-bonding with these quinones on the photoinduced electron transfer reactions.

References

[1] Lewis, N. S.; Nocera, D. G., *Proc. Natl. Acad. Sci. U. S. A.* **2006,** *103*, 15729.

[2] United Nations Development Program (2003) *World Energy Assessment Report*: *Energy and the Challenge of Sustainability* (United Nations, New York).

[3] McDaniel, N. D.; Bernhard, S., *Dalton Transactions* **2010,** *39*, 10021.

[4] Barber, J.; Andersson, B.; *Nature* **1994**, *370*, 31

[5] Meyer, T. J.; Huynh, M. H. V.; Thorp, H. H., *Angew. Chem.-Int. Edit.* **2007,** *46*, 5284.

[6] Renger, G.; Renger, T., *Photosynth. Res.* **2008,** *98*, 53.

[7] Hoganson, C. W. and Babcock, G. T. *Science*, **1997**, *277*, 1953

[8] Babcock, G. T., *Proc. Natl. Acad. Sci. U. S. A.* **1999**, *96*, 12971

[9] Howard, J. B. and Rees, D. C., *Proc. Natl. Acad. Sci. U. S. A.* **2006**, *103*, 17088.

[10] R. A. Marcus, *Pure Appl. Chem.* **1997**, *69*, 13.

[11] R. A. Marcus, *Faraday Discuss. Chem. Soc.* **1960**, *29*, 21.

[12] R. A. Marcus; H. Eyring, *Ann. Rev. Phys. Chem.* **1964**, *15*, 155.

[13] R. A. Marcus, *J. Chem. Phys.* **1965**, *43*, 679.

[14] N. Sutin, *J. Phys. Chem.* **1986**, *90*, 3465.

[15] R. A. Marcus, *J. Chem. Phys.* **1956**, *24*, 966.

[16] R. A. Marcus, *J. Chem. Phys.* **1956**, *24*, 979.

[17] R. A. Marcus, *J. Chem. Phys.* **1957**, *26*, 867.

[18] R. A. Marcus, *J. Chem. Phys.* **1957**, *26*, 872.

[19] R. A. Marcus, *Can. J. Chem.* **1959**, *37*, 155.

[20] Bonnett, R., *Chem. Soc. Rev.***1995,** *24* (1), 19.

[21] Guldi, D. M., *Chem. Soc. Rev.***2002,** *31*, 22.

[22] Gust, D.; Moore, T. A.; Moore, A. L., *Acc. Chem. Res.* **2001,** *34*, 40.

[23] Gaffney, H.; Adamson, A. W.; *J. Am. Chem. Soc.* **1972**, *94*, 8238.

[24] Juris, A.; Balzani, V.; Barigelletti, F.; Campagna, S.; Belser, P.; von Zelewsky, A. *Coord. Chem. Rev*. **1988**, *84*, 85.

[25] Kalyanasundaram, K. *Photochemistry of Polypyridine and Porphyrin Complexes*; Academic Press Limited: London, 1992; pp 87-212.

[26] Sabbatini, N.; Balzani, V., *J. Am. Chem. Soc.* **1972**, *94*, 7587.

[27] Wenger, O. S., *Coord. Chem. Rev.* **2009,** *253*, 1439.

[28] Navon, G.; Sutin, N., *Inorg. Chem.* **1974**, *13*, 2159.

[29] Dearmond, M. K.; Myrick, M. L. *Acc. Chem. Res.* **1989,** *22*, 364-370.

[30] Crosby, G. A., *Acc. Chem. Res.* **1975,** *8*, 231-238.

[31] Kalyanasundaram, K., *Coord. Chem. Rev.* **1982,** *46*, 159.

[32] Damrauer, N. H.; Cerullo, G.; Yeh, A.; Boussie, T. R.; Shank, C. V.; McCusker, J. K., *Science* **1997**, *275*, 54.

[33] Yeh, A. T.; Shank, C. V.; McCusker, J. K., *Science* **2000,** *289*, 935-938.

[34] Demas, J. N.; Taylor, D. G., *Inorg. Chem.* **1979,** *18*, 3177.

[35] Demas, J. N.; Crosby, G. A., *J. Am. Chem. Soc.* **1971,** *93*, 2841.

[36] Young, R. C.; Meyer, T. J.; Whitten, D. G., *J. Am. Chem. Soc.* **1976,** *98*, 286.

[37] Tokel-Takvoryan, N. E.; Hemingway, R. E.; Bard, A. J., *J. Am. Chem. Soc.* **1973,** *95*, 6582.

[38] Balzani, V.; Scandola, F., *J. Chem. Educ.* **1983**, *60*, 834.

[39] Sutin, N.; Creutz, C., *J. Chem. Educ.* **1983**, *60*, 809.

[40] Kavarnos. G. J. *Fundamentals of Photoinduced Electron Transfer*, VCH, New York, **1993**.

[41] Fox, M. A.; Chanon, M. (Eds.). *Photoinduced Electron Transfer. Parts. A - D*, Elsevier, Amsterdam, **1988**.

[42] Mattay, J. (Ed.), *Photoinduced Electron Transfer. Parts. I - IV***,** Springer-Verlag, Berlin, **1990**.

[43] Balzani, V., *Electron transfer in chemistry*. VCH Wiley: Weinheim, 2001; Vol. 3.

[44] Sutin, N.; Creutz, C., *Pure Appl. Chem.* **1980,** *52*, 2717.

[45] Sutin, N., *Journal of Photochemistry* **1979,** *10*, 19.

[46] Delaive, P. J.; Sullivan, B. P.; Meyer, T. J.; Whitten, D. G., *J. Am. Chem. Soc.* **1979,** *101*, 4007.

[47] Sariciftci, N. S.; Smilowitz, L.; Heeger, A. J.; Wudl, F., *Science* **1992,** *258*, 1474.

[48] Sauvage, J. P.; Collin, J. P.; Chambron, J. C.; Guillerez, S.; Coudret, C.; Balzani, V.; Barigelletti, F.; Decola, L.; Flamigni, L., *Chemical Reviews* **1994,** *94*, 993.

[49] Murphy, C. J.; Arkin, M. R.; Jenkins, Y.; Ghatlia, N. D.; Bossmann, S. H.; Turro, N. J.; Barton, J. K., *Science* **1993,** *262*, 1025.

[50] Wenger, O. S., *Chem. Soc. Rev.* **2011,** *40*, 3538-3550.

[51] Oevering, H.; Paddonrow, M. N.; Heppener, M.; Oliver, A. M.; Cotsaris, E.; Verhoeven, J. W.; Hush, N. S., *J. Am. Chem. Soc.* **1987,** *109*, 3258.

[52] Wasielewski, M. R., *Chem. Rev.* **1992,** *92*, 435.

[53] Wrobel, D.; Graja, A., *Coordination Chemistry Reviews* **2011,** *255*, 2555.

[54] Flamigni, L.; Baranoff, E.; Collin, J. P.; Sauvage, J. P., *Chem. -Eur. J.* **2006,** *12*, 6592.

[55] Opperman, K. A.; Mecklenburg, S. L.; Meyer, T. J., *Inorg. Chem.* **1994,** *33*, 5295.

[56] McCafferty, D. G.; Friesen, D. A.; Danielson, E.; Wall, C. G.; Saderholm, M. J.; Erickson, B. W.; Meyer, T. J., *Proc. Natl. Acad. Sci. U. S. A.* **1996,** *93*, 8200.

[57] Kumar, R. J.; Karlsson, S.; Streich, D.; Jensen, A. R.; Jager, M.; Becker, H. C.; Bergquist, J.; Johansson, O.; Hammarström, L., *Chem.-Eur. J.* **2010,** *16*, 2830.

[58] Borgström, M.; Johansson, O.; Lomoth, R.; Baudin, H. B.; Wallin, S.; Sun, L. C.; Åkermark, B.; Hammarström, L., *Inorg. Chem.* **2003,** *42*, 5173.

[59] Hanss, D.; Wenger, O. S., *Inorg. Chem.* **2008,** *47*, 9081.

[60] Hanss, D.; Wenger, O. S., *Eur. J. Inorg. Chem.* **2009**, 3778.

[61] Walther, M. E.; Wenger, O. S., *ChemPhysChem* **2009,** *10*, 1203.

[62] Gunner, M. R.; Dutton, P. L., *J. Am. Chem. Soc.* **1989,** *111*, 3400.

[63] Renger, G., *Angew. Chem.-Int. Ed. Engl.* **1987,** *26*, 643.

[64] Gupta, N.; Linschitz, H., *J. Am. Chem. Soc.* **1997,** *119*, 6384.

[65] Biczok, L.; Gupta, N.; Linschitz, H., *J. Am. Chem. Soc.* **1997,** *119*, 12601.

[66] Biczok, L.; Linschitz, H., *J. Phys. Chem. A* **2001,** *105*, 11056.

Abstract

Over the past years, designing molecular systems that mimic natural processes has become the center of much research in the field of chemistry. Many of these artificial systems are synthesized in order to study photoinduced intramolecular electron transfer. These models are usually consisting of a photosensitizer, an electron acceptor, and/or an electron donor, and are considered attractive candidates for the conversion and storage of solar energy. The molecular dyads investigated in this thesis are comprised of a d^6 metal diimine complex acting as photosensitizer and an anthraquinone as electron acceptor. In addition to the d^6 metal photosensitizer and the anthraquinone acceptor, a tertiary amine has been used as an electron donor in the triads. Photoexcitation of these systems in presence of a strong hydrogen-bond donor strongly influences the thermodynamics and kinetics of the photoinduced electron transfer reaction. In fact, hydrogen-bonding between protic solvent and reduced anthraquinone has a great impact on the excited state deactivation of the dyads by electron transfer from ruthenium to anthraquinone. In the triads, this hydrogen-bonding leads to a significant increase of the lifetime of the charge-separated state containing an oxidized tertiary amine and reduced anthraquinone. This long-lived charge-separated state is interesting in terms of storing light energy in chemical bonds. In both the dyads and triads, the overall photoinduced reaction in presence of protic solvent may be regarded as a variant of stepwise proton-coupled electron transfer (PCET) in which proton density is transferred from the hydrogen-bond donor solvent to photoreduced anthraquinone.

Chapter I
Photoinduced Long-range Electron Transfer in Ruthenium-Anthraquinone Dyads

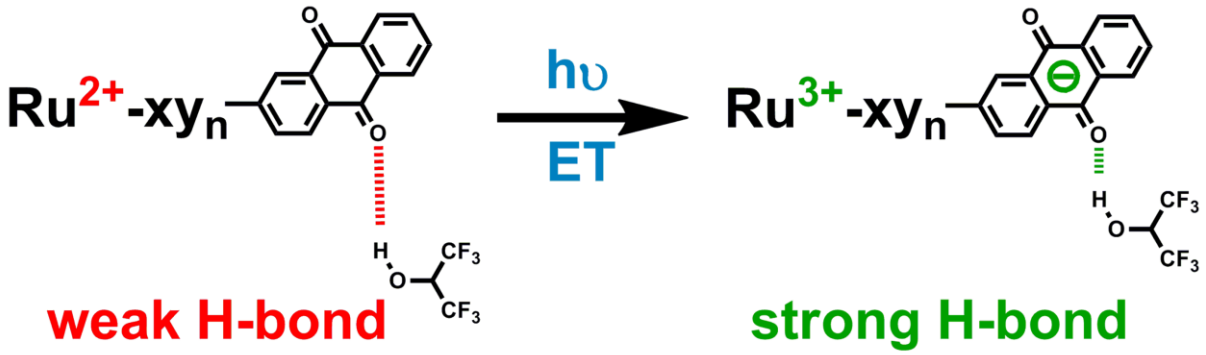

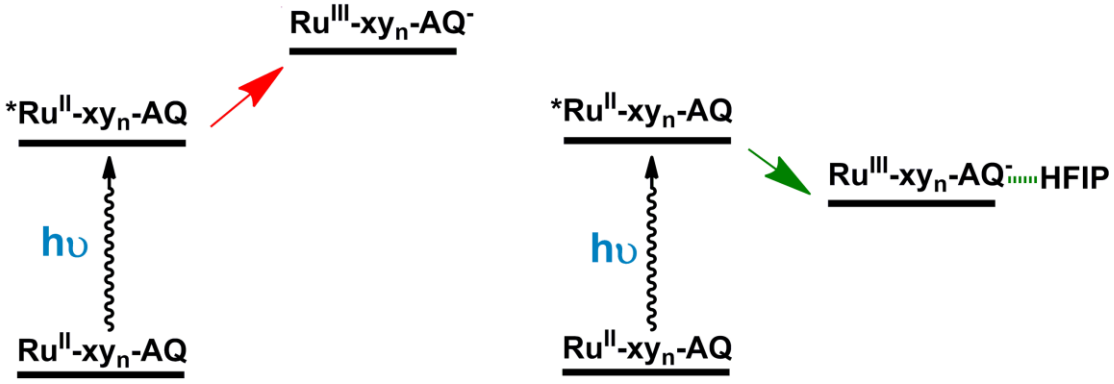

Introduction

Our group had previously synthesized several systems wherein the electron is transferred through variable-length bridges comprised of *p*-xylene, *p*-dimethoxybenzene, and *p*-phenylene units. These bridges connected an electron donor, the phenothiazine group and an electron acceptor, the $Ru(bpy)_3^{2+}$ (bpy= 2,2' –bipyridine) complex.

One of my initial research goals was to study by flash quenching the distance dependent electron transfer, but this time between anthraquinone as an electron acceptor and the ruthenium complex from above as electron donor.

In the first section of this chapter I will evoke our first target, what difficulties had faced us, and how our attention turned towards other perspectives: (i) the effect of solvent polarity on the photoinduced electron transfer, (ii) changing the donor-bridge energy gap by replacing the *p*-xylene with *p*-dimethoxybenzene bridge, as well as (iii) changing the driving force by substituting two of the three bipyridine ligands on $Ru(bpy)_3^{2+}$ by *tert*-butyl groups.

In the second part, other parameters will be studied: how hydrogen-bonding between the carbonyl group of anthraquinone unit and the hydroxyl group of hexafluoroisopropanol will affect the intramolecular electron transfer in the dyad systems. In both parts, synthetic strategies and all the spectroscopic measurements will be described in detail.

I-1. Synthesis

A series of rigid rod-like donor-bridge-acceptor molecules composed of $Ru(bpy)_3^{2+}$ (bpy = 2,2' –bipyridine) as an electron donor, a variable-length (n = 0 - 4) *p*-xylene bridge, and 9,10-anthraquinone as electron acceptor has been synthesized (Scheme 1.1).

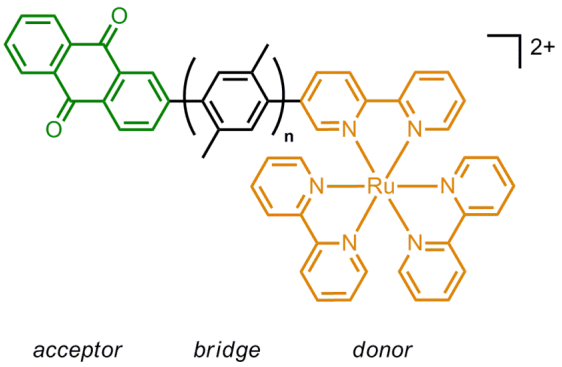

Scheme 1.1: Representative scheme for the dyads investigated in this work, with n = 0 – 4.

The $Ru(bpy)_3^{2+}$ complex was used due to its favorable photophysical and electrochemical properties [1,2]. While anthraquinone is well known as electron acceptor [3], a rigid bridge was necessary in order to have a fixed distance between the two moieties. For this purpose, *p*-xylene is used as a molecular bridging unit, with which we can easily build bridges comprised of up to four units without having solubility problems.

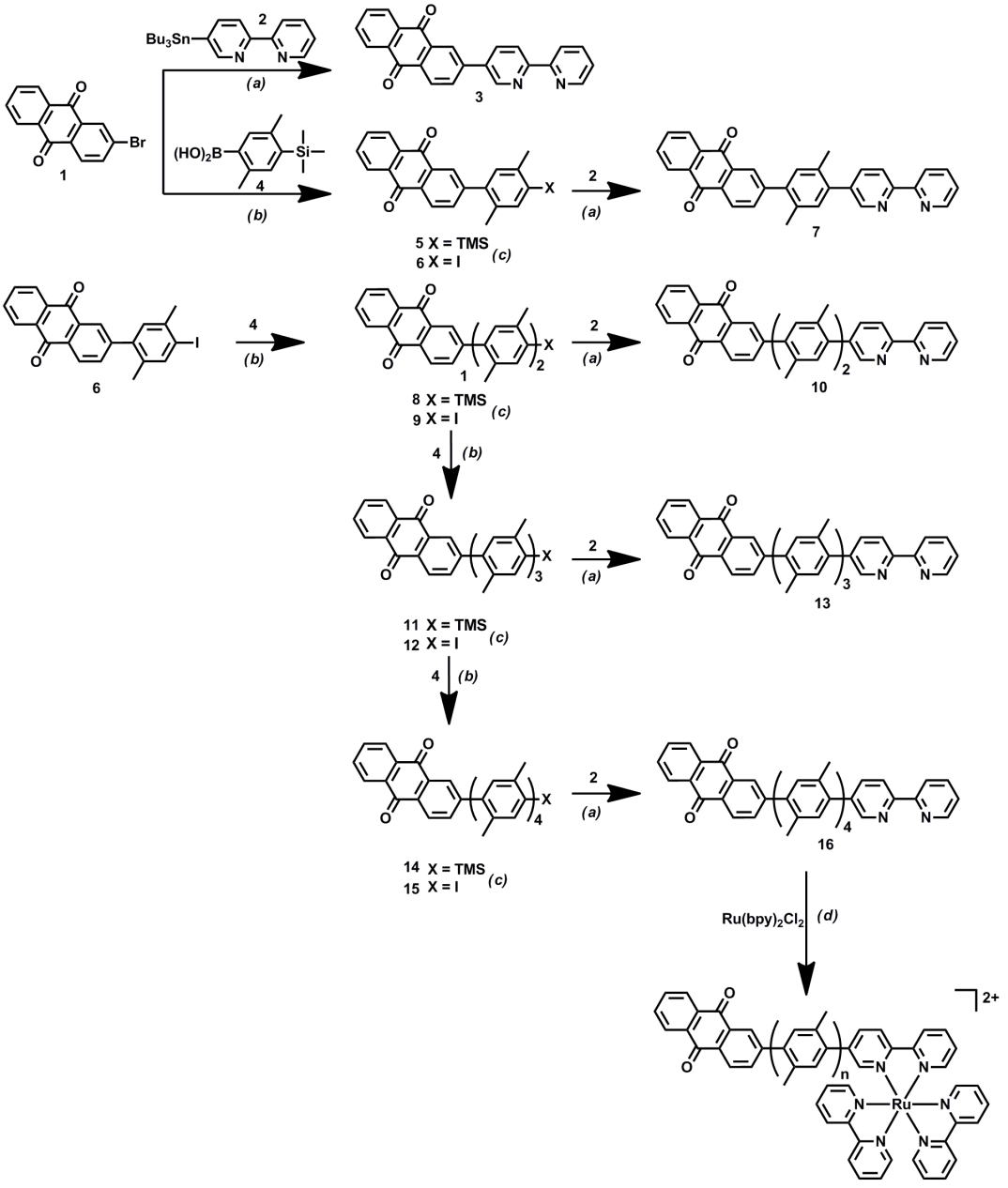

(a) $Pd(PPh_3)_4$, m-xylene (reflux), (b) $Pd(PPh_3)_4$, Na_2CO_3, toluene/ethanol/water 85:1:5 (reflux), (c) ICl, CH_3CN/CH_2Cl_2 3:1 (RT), (d) ethanol/chloroform 10:3 (reflux).

Scheme 1.2: Synthetic steps for the preparation of the dyads.

Scheme 1.2 summarizes the different synthetic steps to prepare all the five dyads. Two main types of reactions are used to synthesize these particular molecules: Suzuki and Stille coupling reactions.

In order to synthesize the first ligand (**3**) wherein the donor and the acceptor are directly connected to each other, Stille coupling reaction occured between the commercial compound 2-bromoanthraquinone (**1**) and 5-(tri-*n*-butyltin)-2,2'-bipyridine (**2**).

To start building the bridge between the donor and the acceptor, a building block TMS-xy-Br (**4**) is used. Consequently, the strategy used to synthesize the four ligands is as follows: molecule **1** is coupled to molecule **4** via Suzuki coupling. The resulting TMS product **5** is deprotected with ICl in essentially quantitative yield to give molecule **6**. Then, one crop of the compound **6** is coupled to molecule **2** in 38 % yield and the first ligand (**7**) with one *p*-xylene unit is ready to be complexed with $Ru(bpy)_2Cl_2$. The second crop of **6** is cross-coupled to molecule **4** yielding compound **8** with two *p*-xylene units. The latter should be deprotected by TMS/halogen exchange reaction with iodine monochloride, and product **9** is obtained. Once again, **9** is either coupled to molecule **2** to give the ligand **10** in 35 % yield, or coupled to molecule **4** leading to compound **11** with three *p*-xylene units which reacts with ICl to give compound **12**. The synthesis proceeds either by a Stille coupling with **2** to get the ligand **13** in 26 % yield, or by Suzuki coupling with **4** to give compound **14**. Therefore, to synthesize the last ligand **16** with four *p*-xylene units, **14** should be first deprotected **15** and then coupled to molecule **2**.

In order to get the Ru-xy_{0-4}-AQ complexes, the ligands **3**, **7**, **10**, **13**, and **16** are then reacted with $Ru(bpy)_2Cl_2$. The overall yield from molecule **1** until molecule **16** is 12 %. The most difficult part was the purification of the ligands which were subjected to at least two column chromatographies.

I-2. Optical spectroscopy

I-2.1 Optical absorption

The absorption spectra of the Ru-xy_{0-4}-AQ molecules are represented in Figure 1.1. These spectra are measured in pure acetonitrile solution, and $Ru(bpy)_3^{2+}$ complex was used as a reference. The term Ru-xy_0-AQ is used for the dyad in which the redox partners Ru and AQ are linked directly, while Ru-xy_{1-4}-AQ corresponds to the dyads in which Ru and AQ are linked together by one up to four *p*-xylene units.

The most prominent absorption bands are located at 450 and 290 nm. These bands are respectively assigned to a metal-to-ligand charge transfer band (MLCT) of $Ru(bpy)_3^{2+}$ and to a bpy-localized π-π* transition. At first glance, the UV-Vis spectra of the dyads with n = 1 – 4 look very similar to each other. But at wavelengths shorter than 265 nm, the extinction coefficient increases with increasing number of *p*-xylene units.

Based on our previous investigations [4-8], the similarity in the absorption spectra can be explained by the fact that π-conjugation is weak between the oligo-*p*-xylene units when increasing the bridge length.

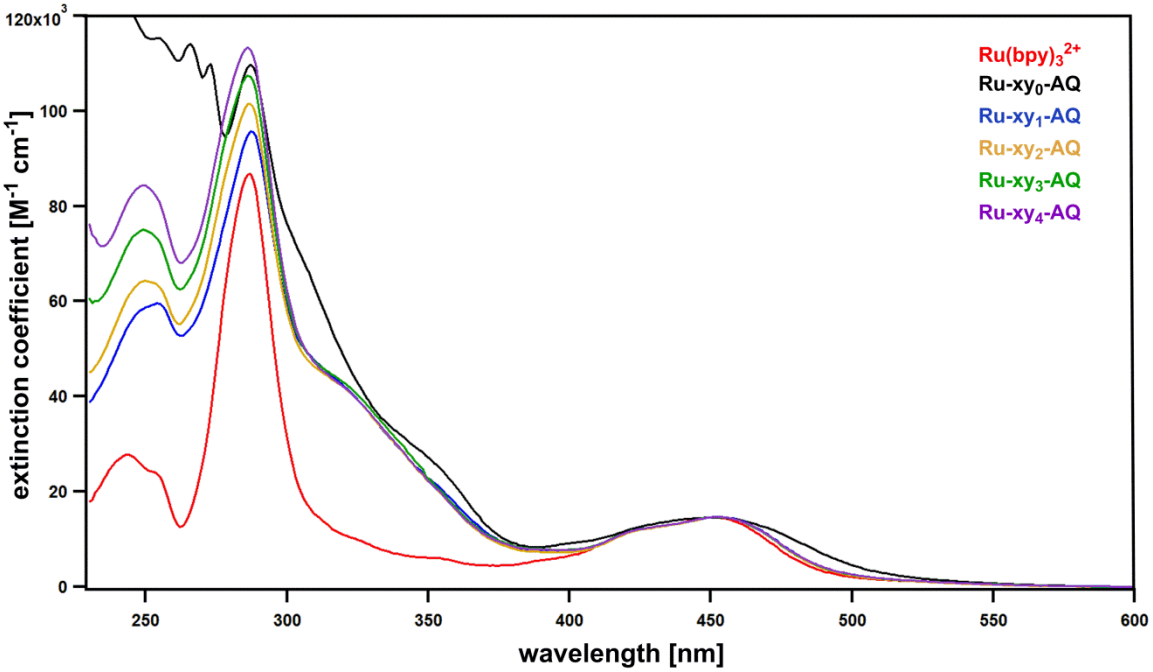

Figure 1.1: Optical absorption spectra of Ru-$xy_{0\text{-}4}$-AQ and $Ru(bpy)_3^{2+}$ in acetonitrile solution.

What is unusual is the behavior of Ru-xy_0-AQ. We have noticed several differences in the absorption spectra of Ru-xy_0-AQ compared to those of Ru-$xy_{1\text{-}4}$-AQ. At 450 nm the MLCT band presents a tail which extends to longer wavelengths. Between 380 nm and 295 nm, the extinction is larger than in the case of Ru-$xy_{1\text{-}4}$-AQ, while around 250 nm Ru-xy_0-AQ absorbs much more strongly than the other dyads. The peculiar behavior of Ru-xy_0-AQ is presumably due to strong electronic coupling between the two redox species, since $Ru(bpy)_3^{2+}$ and anthraquinone are directly connected to each other.

I-2.2 Steady-state luminescence spectroscopy

The luminescence spectra of the investigated complexes which are presented in Figure 1.2 correspond to the forbidden electronic transition from the ^{3}MLCT excited state to the ground state. For Ru-xy$_{1\text{-}4}$-AQ molecules and the reference complex these bands have a maximum at 600 nm, while for Ru-xy$_0$-AQ, the maximum of the emission band is red-shifted by 30 nm and the intensity is weaker by a factor of 7. This is consistent with the interpretation of strong electronic coupling between ruthenium and anthraquinone, as discussed above.

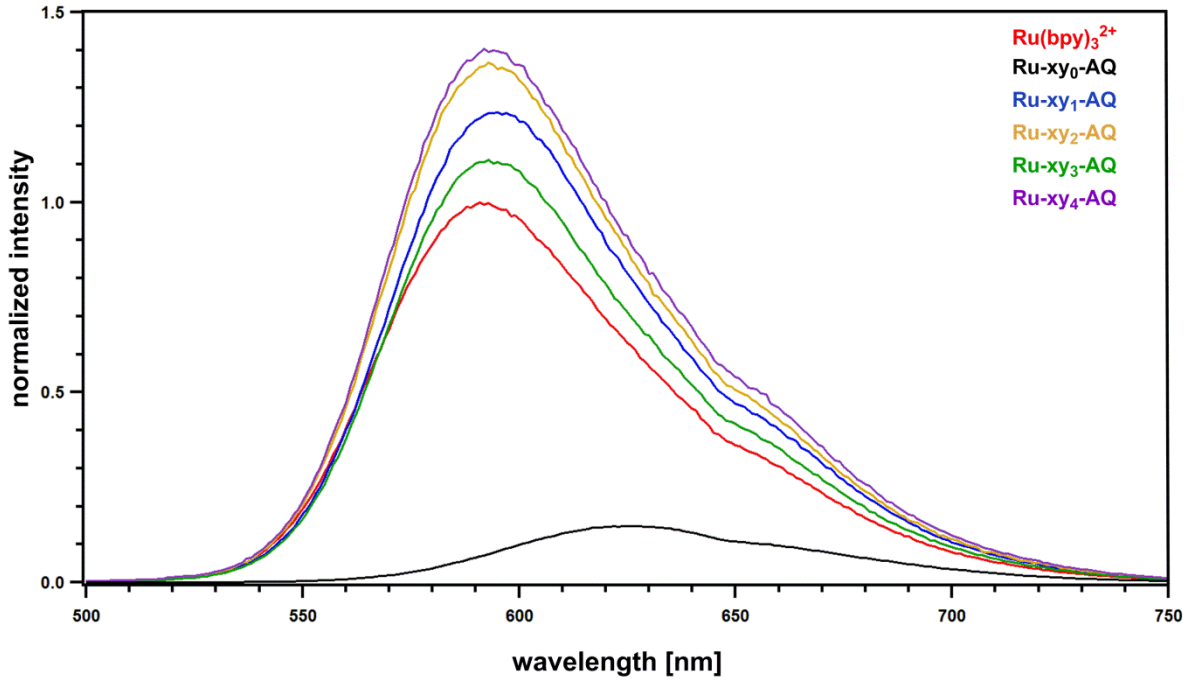

Figure 1.2: Steady-state luminescence spectra of Ru-xy$_{0\text{-}4}$-AQ and Ru(bpy)$_3^{2+}$ in deoxygenated dichloromethane solution after excitation at 450 nm.

I-3. Electrochemistry

Cyclic voltammogrammetry with the Ru-xy$_n$-AQ compounds and the Ru(bpy)$_3^{2+}$ complex was carried out in deoxygenated acetonitrile solution at room temperature (Figure 1.3). A platinum disk is used for the working electrode. The counter wire is made of platinum, while the reference electrode is made of silver. Ferrocene was added as an internal reference substance, and therefore the redox potentials in Figure 1.3 are reported versus this reference.

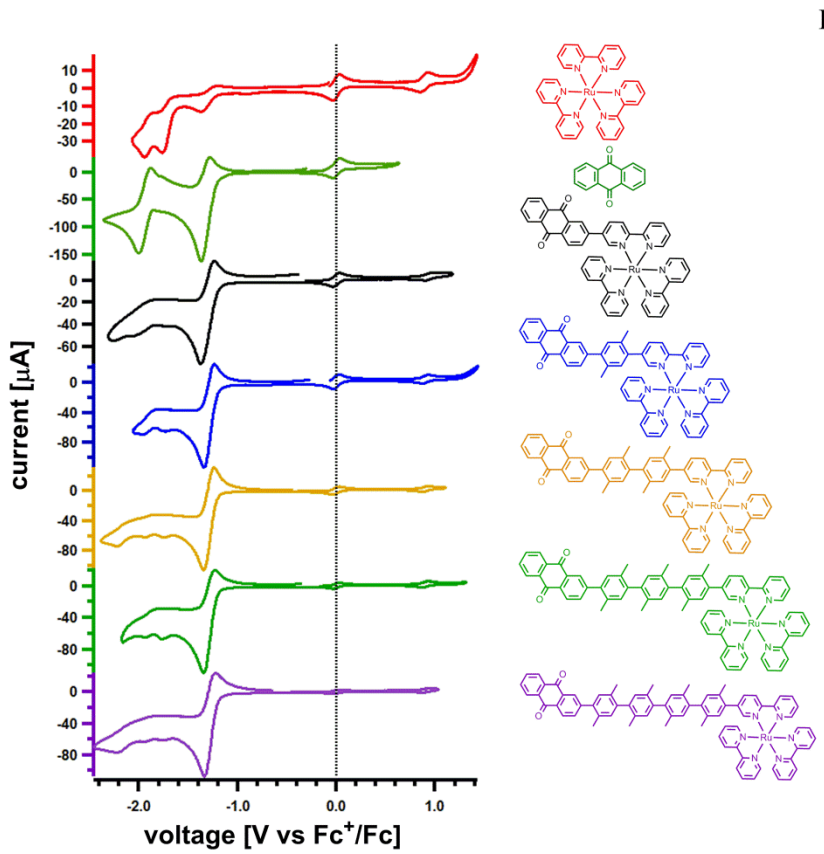

	R_{DA} [Å]	E_{ox} [V]	E_{red} [V]
		0.88	
			-1.32
	9.0	0.94	-1.30
	13.3	0.90	-1.28
	17.6	0.90	-1.28
	21.9	0.90	-1.29
	26.2	0.90	-1.29

Figure 1.3: Cyclic voltammograms for Ru-xy$_{0\text{-}4}$-AQ, Ru(bpy)$_3^{2+}$ and AQ measured in dry and deoxygenated acetonitrile solution in presence of 0.1 M $TBAPF_6$ electrolyte.

The ruthenium oxidation wave (Ru^{3+}/Ru^{2+}) occurs at a potential of 0.9 V in the dyads with n = 1 – 4, which is similar to the redox potential of the free Ru(bpy)$_3^{2+}$ complex (0.88 V). In the dyad with in n = 0 the respective oxidation potential is more positive by 0.04 V. The wave for anthraquinone reduction in Ru-xy$_{0\text{-}4}$-AQ (AQ/AQ^-) appears around -1.3 V, and that of the free 9,10- anthraquinone is at -1.32 V. Except for the Ru-xy$_0$-AQ complex, the similarity of the redox potentials with those of the reference compounds indicates weak electronic interaction between ruthenium and antraquinone units over the *p*-xylene bridge.

I-4. Electron transfer in dichloromethane solution

Time-resolved luminescence spectroscopy and transient absorption spectroscopy are useful experimental techniques to obtain kinetic information about photoinduced electron transfer and the formation of any radical species.

I-4.1 Transient absorption spectroscopy

Based on the electrochemical data, photoexcitation of the dyads at 450 nm should lead to the formation of Ru^{3+} and AQ^{-}. Hence, we are expecting a negative signal at 450 nm due to the bleach of the ^{1}MLCT absorption band indicating the formation of Ru^{3+} which has a weak extinction coefficient at this wavelength [9,10]. Moreover, a band around 570 nm and 380 nm should also be expected due to the formation of anthraquinone monoanion [11-13].

Our expectations were not fulfilled while exciting Ru-xy_{0-4}-AQ in dichloromethane solution. There was neither the bleach at 450 nm of the MLCT absorption band revealing the presence of the oxidized form of ruthenium (Ru^{3+}), nor the two absorption bands at 570 nm and 380 nm characteristic of the reduced form of anthraquinone (AQ^{-}). This result does not imply that there is no electron transfer at all. Therefore, time-resolved luminescence experiments were carried out.

I-4.2 Time-resolved luminescence spectroscopy

Figure 1.4 shows the luminescence decays of the Ru-xy_{0-4}-AQ dyads and of the isolated ruthenium reference complex. These decays are the dynamic counterpart to the steady state luminescence data from Figure 1.2. The measurements were carried out in deoxygenated CH_2Cl_2 solution after excitation at 407 nm or 450 nm. The detection was at 610 nm.

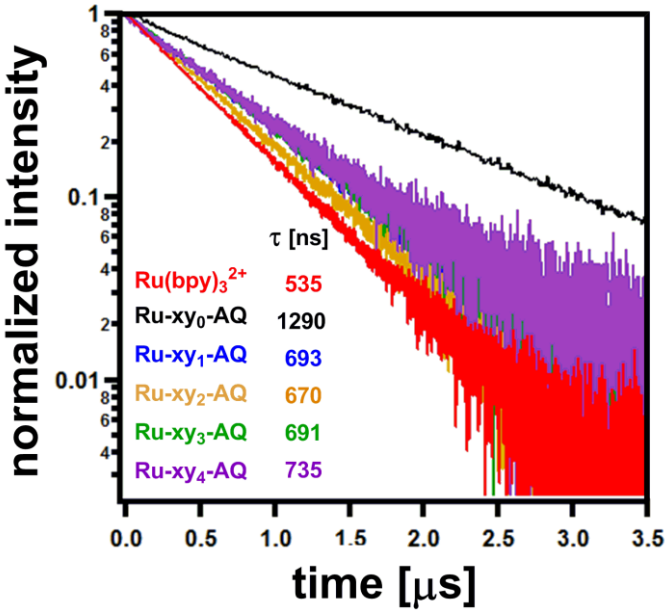

Figure 1.4: Luminescence decays and lifetimes of the $Ru(bpy)_3^{2+}$ reference complex and the five Ru-xy_{0-4}-AQ dyads in dichloromethane solution.

Fits to these single exponential decays give the luminescence lifetimes in the inset of Figure 1.4. Ru-$xy_{1\text{-}4}$-AQ exhibit similar lifetimes with an average value of 698 ns. This is a factor of 1.3 larger than the luminescence lifetime of $Ru(bpy)_3^{2+}$ (535 ns).
Despite the slight increase in the lifetimes of the Ru-$xy_{1\text{-}4}$-AQ dyads, their lifetimes are considered close to the lifetime of $Ru(bpy)_3^{2+}$. Therefore, one may conclude that there is no additional deactivation process of the ^{3}MLCT state in the Ru-$xy_{1\text{-}4}$-AQ dyads. In other words, the excited state of these dyads decays in the same way as in the isolated $Ru(bpy)_3^{2+}$ complex, namely through radiative and nonradiative processes, and not an electron transfer mechanism.

By contrast, Ru-xy_0-AQ continues to behave differently, because its luminescence lifetime in CH_2Cl_2 (1290 ns) is a factor of 2.4 longer than that of $Ru(bpy)_3^{2+}$ (535 ns), despite the fact that its steady-state luminescence intensity is a factor of 7 weaker. We suppose that this peculiar observation is, as mentioned previously, due to the strong electronic coupling between the donor and the acceptor. Based on the transient absorption data and the absence of luminescence quenching in Ru-$xy_{0\text{-}4}$-AQ, it seems clear that the photoinduced electron transfer from the ^{3}MLCT excited state of the ruthenium Ru^{2+} to anthraquinone is absent in dichloromethane solution.

For this reason, our attention turned to a flash-quench technique where we can photogenerate Ru^+ species and therefore the intramolecular electron transfer will occur from the ground state instead of the excited state. The photogenerated Ru^+ species is a far better electron donor than photoexcited $Ru(bpy)_3^{2+}$, hence there should be more driving force for electron transfer from Ru^+ to AQ.

I-5. Electron transfer by flash-quench experiments

The excited form of ruthenium ($*Ru^{2+}$) acts as strong oxidant as well as a strong reducing agent. The strategy of the flash quench procedure is as follows (Scheme 1.3): Photoexcitation of Ru(II)-xy-AQ complex in solution leads to an MLCT excited state *Ru(II)-xy-AQ (upper left). In presence of an appropriate quencher Q, the MLCT state will be quenched reductively in intermolecular fashion to form Ru(I)-xy-AQ and Q^+ (upper right). Then, intramolecular electron transfer occurs from Ru^+ to AQ across the *p*-xylene bridge, whereby the initial Ru (II) complex is recovered and an anthraquinone radical anion is formed (Ru(II)-xy-AQ^-).

Bimolecular recombination between AQ^- and Q^+ leads back to the initial state Ru(II)-xy-AQ. This is so-called electron transfer by flash quenching.

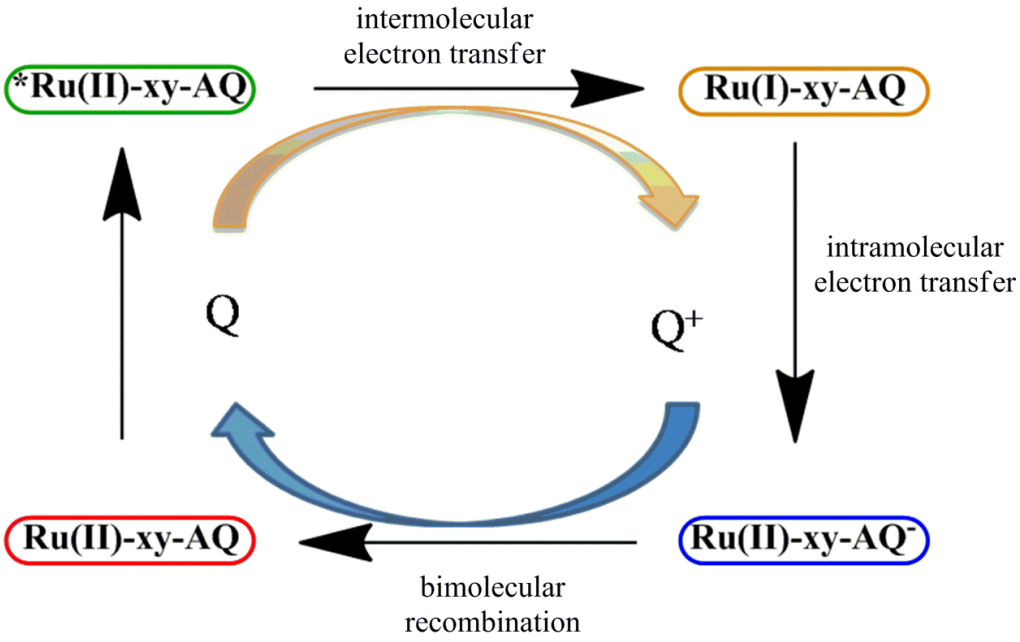

Scheme 1.3: Reaction steps occurring after excitation of Ru(II) in presence of a reversible quencher.

In order to reduce the excited form of Ru(II) to Ru(I), the quencher Q should have a redox potential lower than that of ruthenium. Moreover, the oxidized form of the quencher (Q^+) should exhibit absorption bands different from that of Ru^+ and AQ^- in order to distinguish the different radical species. Several quenchers have been used in our experiments:

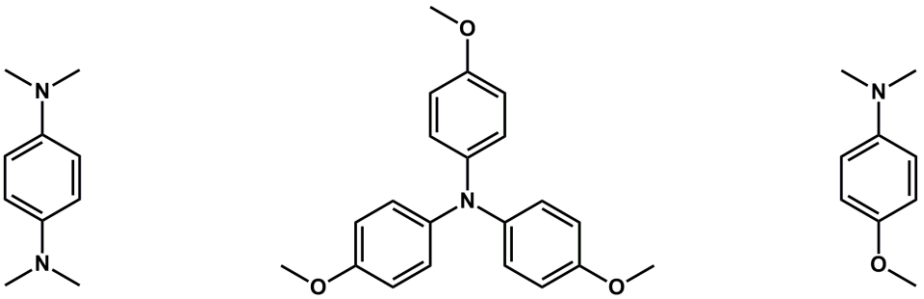

Unfortunately, none of these quenchers were suitable, and we were unable to detect any formation of radical species as evidence for a possible electron transfer in our ruthenium-anthraquinone systems.

The absence of the photoinduced and phototriggered electron transfer in dichloromethane solution forced us to change different parameters which may have an important influence on the electron transfer mechanism.

I-6. Solvent polarity effect on the photoinduced electron transfer: Investigation in CH_3CN solvent

According to equation 1.1 [14,15], an increase in solvent dielectric constant will lead to an increase of the driving force for photoinduced electron transfer.
Based on this fact, our hope was to change the driving force in our system just by increasing the polarity of the solvent. Hence, the energy level structure will change and therefore ET could become possible.

$$\Delta G_{ET} = e\cdot(E_{ox} - E_{red}) - E_{00} - e^2/(4\pi\varepsilon_0\varepsilon_s R_{DA}) \qquad \text{(eq. 1.1)}$$

E_{ox} oxidation potential for ruthenium
E_{red} reduction potential for AQ
E_{00} energy of the photoactive ^{3}MLCT state = 2.12 eV for $Ru(bpy)_3^{2+}$
E elemental charge
R_{DA} center-to-center donor–acceptor distance
ε_0 vacuum permittivity
ε_s dielectric constant of the solvent

When changing from dichloromethane to acetonitrile solvent, the dielectric constant increases from 8.93 to 35.94 [16]. This increase had a significant effect on the luminescence lifetimes. The decays and their corresponding lifetimes are reported in Figure 1.5.
The ^{3}MLCT state of the reference complex decays with τ = 866 ns, while the Ru-xy_n-AQ systems yield τ = 14 ns for n = 0, τ = 300 ns for n = 1, and τ > 1000 ns for the systems with n = 2 – 4. Thus it is obvious that at least in the Ru-xy_0-AQ and Ru-xy_1-AQ dyads an additional (nonradiative) excited-state deactivation process has become competitive.

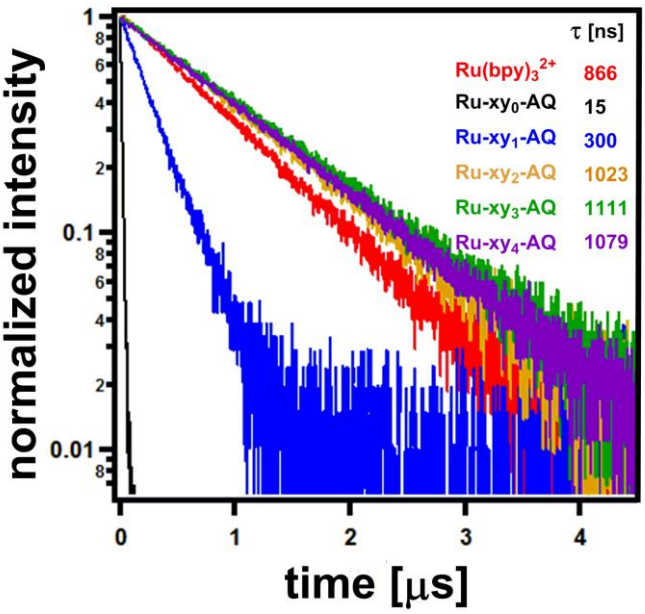

Figure 1.5: ^{3}MLCT luminescence decays and corresponding lifetimes of the investigated dyads and the reference complex in deoxygenated acetonitrile solution.

By transient absorption spectroscopy we would expect, as mentioned previously, a ^{1}MLCT bleach around 450 nm indicating the formation of Ru^{3+}, and two absorption bands at 570 nm and 380 nm as evidence for the formation of anthraquinone radical anion (AQ^{-}). Unfortunately, all our efforts to detect any bands at these specific wavelengths failed. The reason could be the rapid disappearance of these radical species, even in the longest bridge of the Ru-xy$_4$-AQ molecule. Hence, we do not have direct evidence for the electron transfer between Ru and AQ in CH_3CN, and only luminescence lifetimes remain as indirect evidence for the intramolecular electron transfer.

However, the quenching of the ^{3}MLCT excited-state in Ru-xy$_{0\text{-}1}$-AQ can be interpreted in this case either by an electron transfer process or by a triplet-triplet energy transfer from Ru to AQ. In fact, the lowest triplet excited state of the free anthraquinone is at 2.69 eV [17], while the ^{3}MLCT excited-state of $Ru(bpy)_3^{2+}$ is at 2.12 eV. Thus, the triplet-triplet energy transfer from Ru to AQ is endergonic by 0.57 eV, and therefore this process is ruled out. Consequently, the luminescence quenching in Ru-xy$_{0\text{-}1}$-AQ compared to $Ru(bpy)_3^{2+}$ could be only attributed to an electron transfer mechanism.

Based on the calculation of ΔG_{ET} in equation 1.1 using the redox potentials shown in Figure 1.3 and ε_{CH3CN} = 35.94, the driving force is estimated to be only very weakly endergonic (ΔG_{ET} = + 0.07 eV). By changing the dielectric constant to that of dichloromethane (ε_s =

8.93), photoinduced electron transfer between ruthenium and anthraquinone can thermodynamically not occur, because the driving force is significantly endergonic ($\Delta G_{ET} \approx$ +0.3 eV).

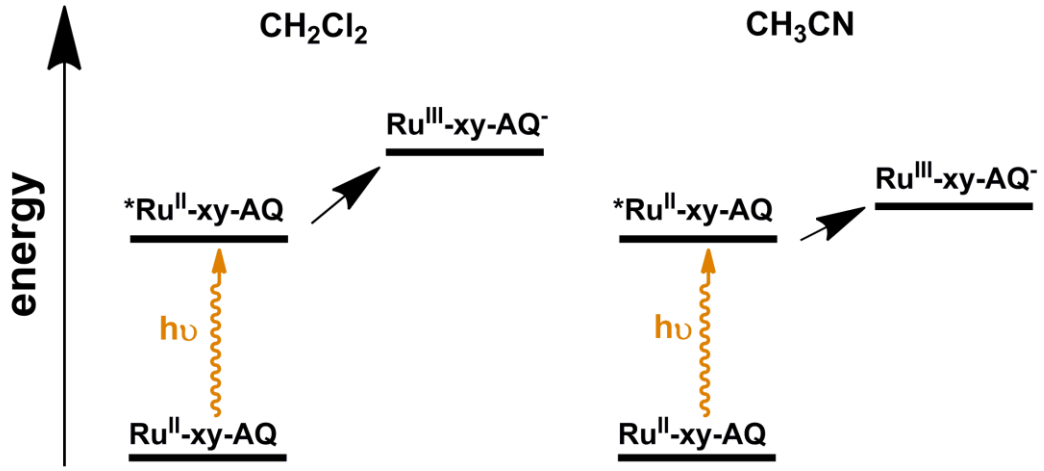

Scheme 1.4: Energetic levels for photoinduced electron transfer in CH_2Cl_2 (left) and CH_3CN (right).

This result explains why in our previous experiments in CH_2Cl_2 we were unable to detect any radical species by transient absorption spectroscopy, and it explains the absence of luminescence quenching in this apolar solvent. On the other hand, it demonstrates that by increasing the polarity of the solvent from CH_2Cl_2 to CH_3CN the photoinduced electron transfer becomes more efficient (less endergonic) (Scheme 1.4), and thereby it explains the luminescence quenching in the dyads.

I-7. Effect of bridge variation and change of the driving force by chemical substitution

I-7.1 Changing the donor-bridge energy gap

It has been previously demonstrated in our group that the replacement of *p*-xylene bridge by a *p*-dimethoxybenzene unit affects the hole transfer rates [18,19]. This has been attributed to the change in the energy gap between the donor and the bridge.

To study how important this effect will be on the photoinduced electron transfer, a molecule comprised of $Ru(bpy)_3^{2+}$ as an electron donor, *p*-dimethoxybenzene unit as a bridge, and 9,10-anthraquinone as an electron acceptor has been synthesized (Scheme 1.5).

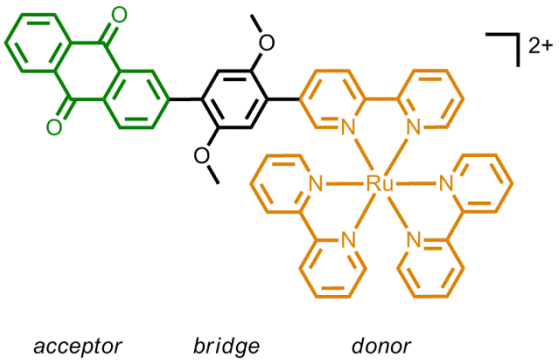

Scheme 1.5: Molecular structure of a Ru-dmb-AQ complex.

To synthesize this molecule, the same strategy is followed as for the Ru-xy_1-AQ dyad (Scheme 1.6). In this case the building block which has been used is 2,5-dimethoxy-4-trimethylsilylphenylboronic acid **17**. It is cross-coupled to 2-bromoanthraquinone **1**. The resulting product **18** reacts with iodine monocloride ICl to give compound **19**. The latter undergoes a Stille coupling reaction with molecule **2**. The ligand (**20**) obtained is complexed with $Ru(bpy)_2Cl_2$ yielding the desired complex (**21**) in overall yield of 32 %.

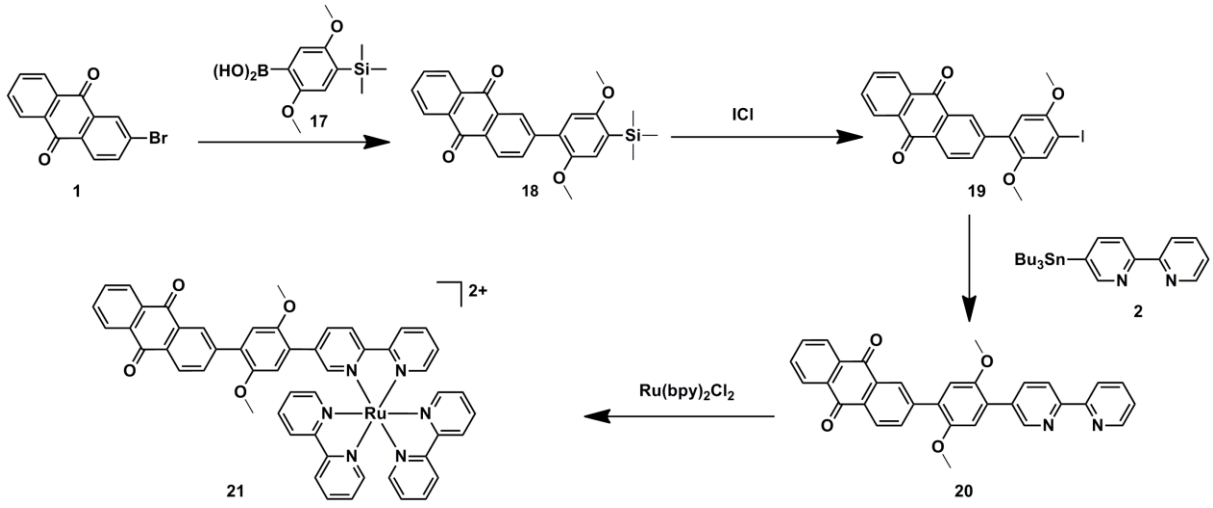

Scheme 1.6: Synthetic steps for preparing the Ru-dmb-AQ dyad.

I-7.1.1 Optical absorption and steady-state luminescence spectroscopy

The optical absorption and luminescence spectra of Ru, Ru-xy-AQ and Ru-dmb-AQ in aerated acetonitrile solution are shown in Figure 1.6.

Compared to the absorption spectra of Ru and Ru-xy-AQ, Ru-dmb-AQ exhibits an additional absorption band between 370 nm and 450 nm which is assigned to an electronic transition from the *p*-dimethoxybenzene unit to the ruthenium complex.

The luminescence appears to be more quenched in Ru-dmb-AQ than in Ru-xy-AQ with respect to the reference complex. We may conclude that nonradiative deactivation in Ru-dmb-AQ is slightly more efficient than in Ru-xy-AQ.

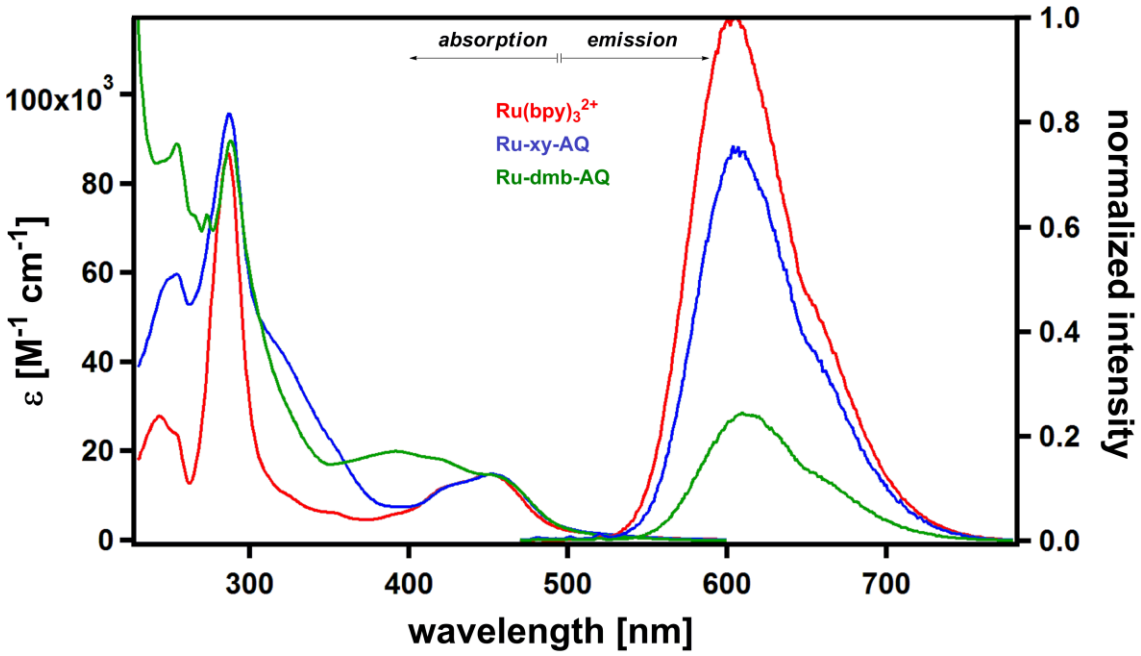

Figure 1.6: Optical absorption and luminescence spectra of the investigated dyads in aerated acetonitrile solution. Excitation occurred at 450 nm.

I-7.1.2 Electrochemistry

Figure 1.7 shows the cyclic voltammograms of the three relevant dyads measured in deoxygenated acetonitrile solution. In all voltammograms there is a wave at 0.0 V caused by the ferrocenium/ferrocene (Fc^+/Fc) couple, which was used as an internal reference.

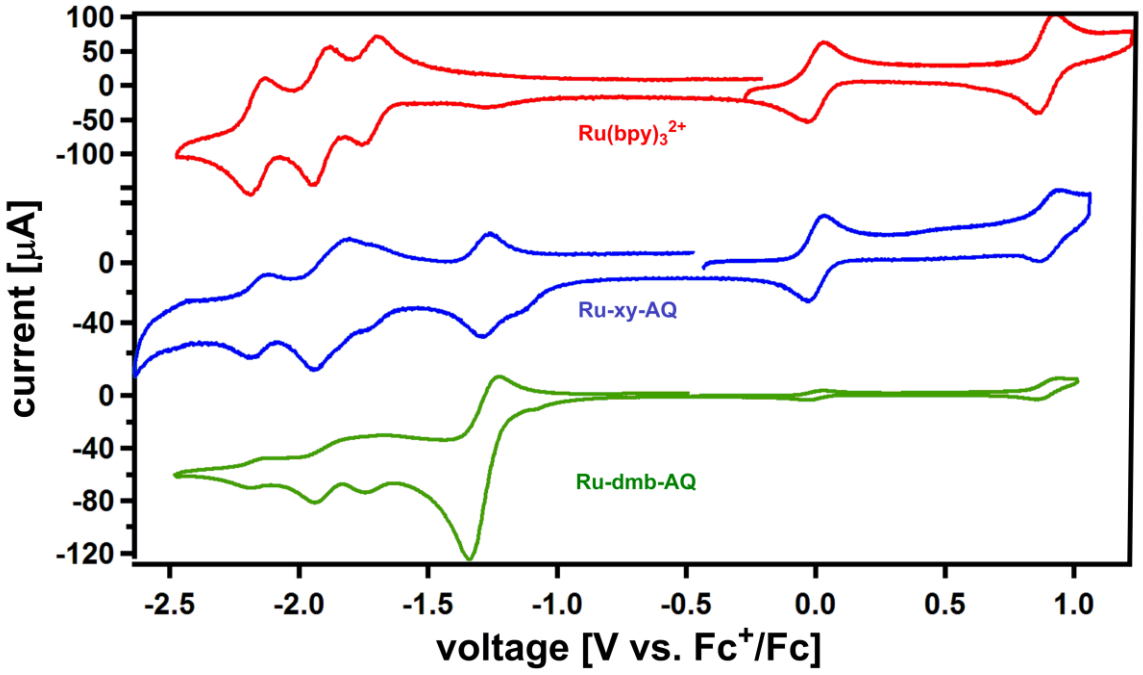

Figure 1.7: Cyclic voltammograms measured in dry and deoxygenated acetonitrile solution in presence of 0.1 M of $TBAPF_6$.

The oxidation of ruthenium (Ru^{3+}/Ru^{2+}) occurs at 0.9 V in all three dyads, while the reduction of anthraquinone ($AQ^{0/-}$) takes place at -1.27 V in Ru-xy-AQ and at -1.29 V in Ru-dmb-AQ.
In the present case, we intended to investigate excited-state electron transfer from Ru(II) to AQ, or equivalently, hole transfer from anthraquinone to photoexcited ruthenium(II).
Based on electrochemical potentials, *p*-dimethoxybenzene is oxidized much more easily than *p*-xylene [19]. Therefore the hole injection from AQ to *p*-dimethoxybenzene (E_{ox} = 1.1 V vs Fc^+/Fc) is energetically uphill by ~2.4 eV, whereas in case of *p*-xylene (E_{ox} > 1.7 V vs Fc^+/Fc), the respective injection is more than 3.0 eV uphill.

The question that might be asked is: Does the difference of 0.6 eV in the donor-bridge energy gap between Ru-xy-AQ and Ru-dmb-AQ has an influence on the photoinduced electron transfer? To answer this question, luminescence lifetime data are useful.

I-7.1.3 Time-resolved luminescence spectroscopy

The luminescence lifetime of Ru-dmb-AQ measured in deoxygenated acetonitrile solution is 124 ns (Figure 1.8). Compared to those of Ru (866 ns) and Ru-xy-AQ (300 ns) (Figure 1.5); Ru-dmb-AQ clearly has the shortest ^{3}MLCT lifetime.

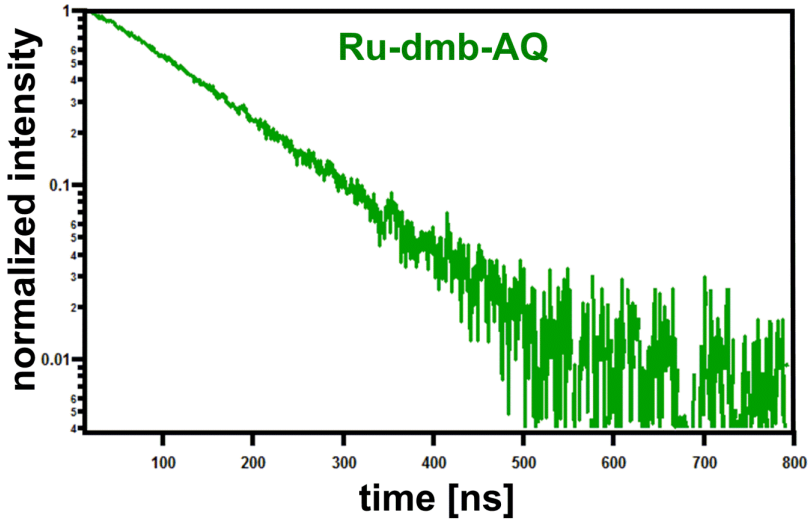

Figure 1.8: Luminescence decay of the Ru-dmb-AQ complex in deoxygenated acetonitrile solution. Excitation occurred at 450 nm, detection was at 610 nm.

By applying equation 1.2 to the acetonitrile data, this procedure results in k_Q-values of $2.2 \cdot 10^6$ s^{-1} for Ru-xy-AQ and $6.9 \cdot 10^6$ s^{-1} for Ru-dmb-AQ.

$$k_Q = \tau_{dyad}^{-1} - \tau_{ref}^{-1} \qquad \text{(eq. 1.2)}$$

In equation 1.2, τ_{dyad} is the luminescence lifetimes of the ruthenium-bridge-anthraquinone, and τ_{ref} is the luminescence lifetime of the isolated $Ru(bpy)_3^{2+}$ complex.
Therefore, the decrease in the donor-bridge energy gap by replacing a *p*-xylene spacer with a *p*-dimethoxybenzene unit leads to an increase in the electron transfer rates by a factor of 3.5 (Scheme 1.7).

I-7.2 Changing the driving force by chemical substitution of bpy ligands

Introduction of *tert*-butyl substituents at the ancillary bipyridine ligands of the Ru-xy-AQ complex increases the electronic density around the metal. Thus, the oxidation of ruthenium becomes easier: E_{ox} (Ru^{3+}/Ru^{2+}) shifts from 0.9 V in Ru-xy-AQ to 0.79 V in Ru(^{t}Bu)-xy-AQ (Figure 1.9) leading to a possible change in the driving force for photoinduced electron transfer.

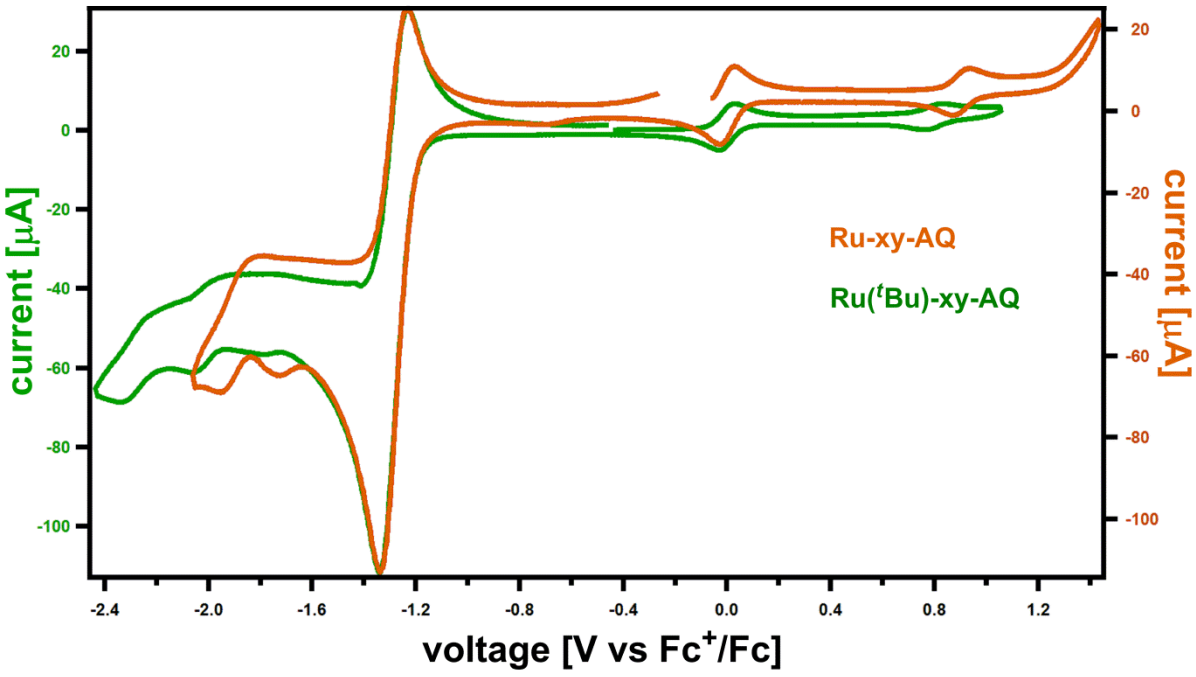

Figure 1.9: Oxidation waves of Ru-xy-AQ and Ru(^{t}Bu)-xy-AQ complexes in deoxygenated acetonitrile solution. The wave at 0.0 V corresponds to the oxidation of ferrocene (Fc^+/Fc) which was added as an internal reference.

In order to estimate the driving force for photoinduced electron transfer from ruthenium to anthraquinone, equation 1.1 was used. Using the redox potentials extracted from the data in Figure 1.9, the driving force seems to change from slightly endergonic in Ru-xy-AQ (ΔG_{ET} = +0.07 eV) to slightly exergonic in Ru(^{t}Bu)-xy-AQ (ΔG_{ET} = -0.11 eV). This change in the driving force leads to a fast decay of the ^{3}MLCT excited-state. The lifetime goes from 300 ns in Ru-xy-AQ to 47 ns in Ru(^{t}Bu)-xy-AQ (Figure 1.10). In fact, the Ru(^{t}Bu)-xy-AQ dyad exhibits biexponential decay with a fast decay yielding lifetime of 47 ns. The slow decay is attributed to emission of Ru(^{t}Bu) impurity present in the Ru(^{t}Bu)-xy-AQ sample.

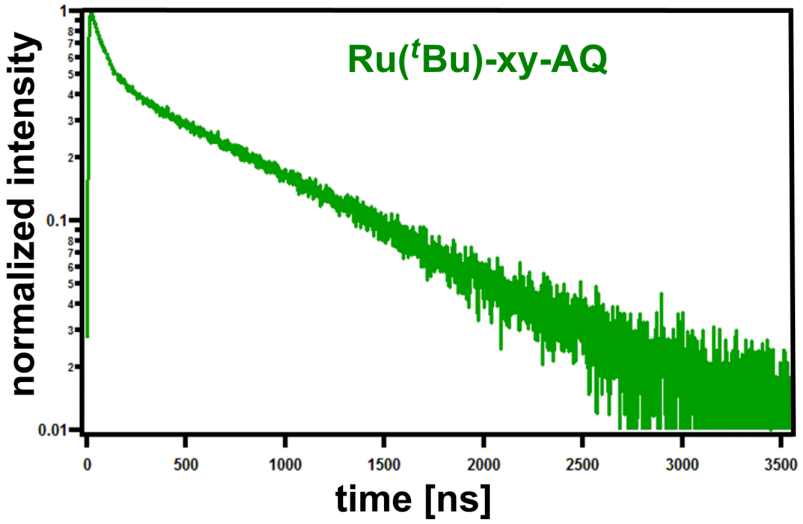

Figure 1.10: Luminescence decay of the Ru(^{t}Bu)-xy-AQ complex in deoxygenated acetonitirle solution. Excitation occurred at 450 nm, detection was at 610 nm.

Hence, the introduction of electron-donating *tert*-butyl substituents in the bpy ancillary ligands and the associated increase in the driving force by ~0.2 eV entails an acceleration by an order of magnitude (k_Q = $2.2 \cdot 10^6$ s^{-1} for Ru-xy-AQ to $2.0 \cdot 10^7$ s^{-1} for Ru(^{t}Bu)-xy-AQ (Scheme 1.7).

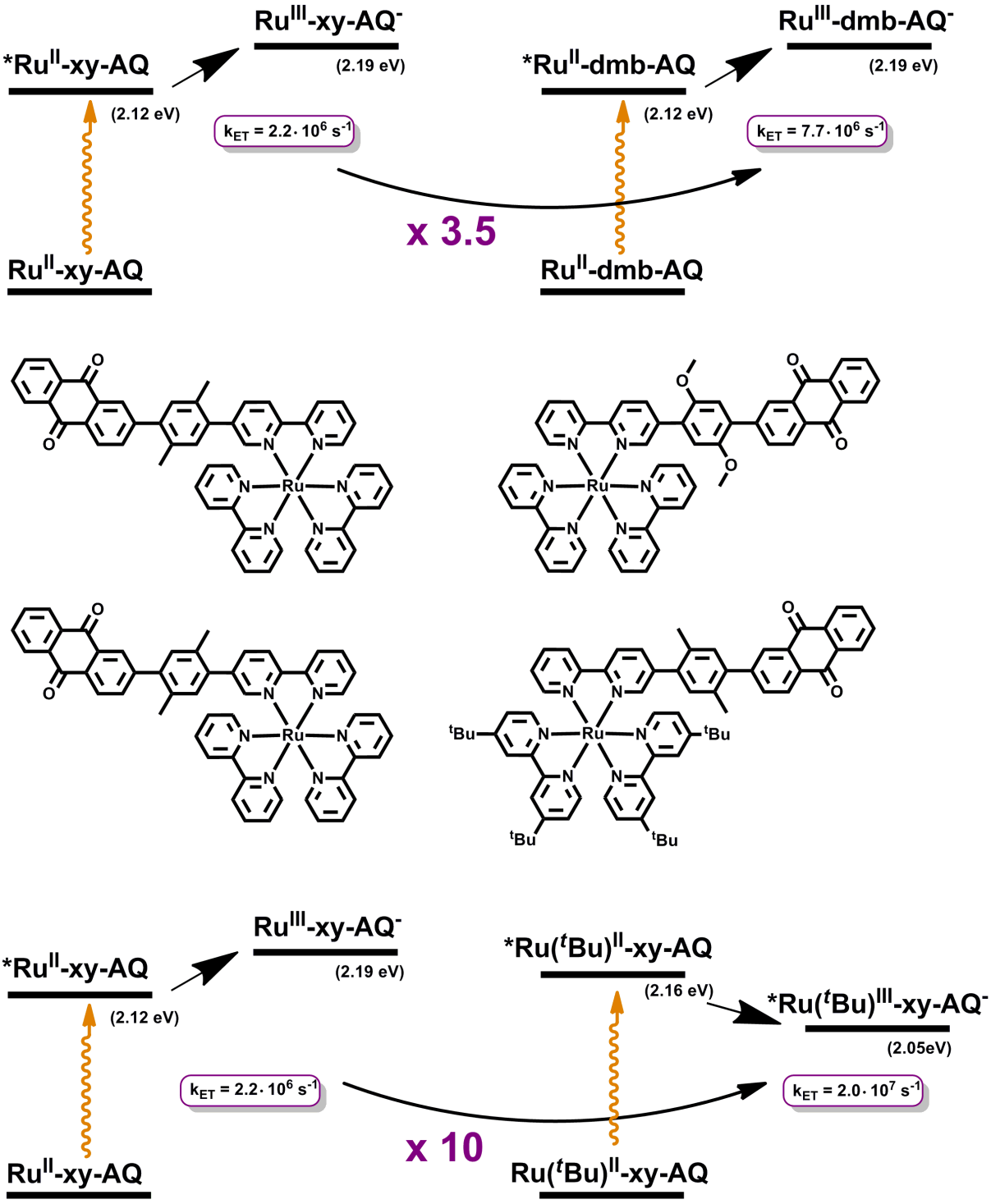

Scheme 1.7: Energetics and kinetics of photoinduced electron transfer as a function of bridge modulation and changes in bpy-substitution.

I-8. Influence of hydrogen-bonding solvent on photoinduced electron transfer

I-8.1 Investigations in CH_3CN/H_2O solvent mixtures at pH 7

Dry acetonitrile contains no source of acidic protons; hence we expect excited-state deactivation in Ru-xy_0-AQ and Ru-xy_1-AQ to occur via a pure electron transfer mechanism. At some point we decided to involve a protic solvent in order to enlarge our investigation to a proton coupled electron transfer mechanism (PCET). Water was used, with a dielectric constant of 78.3, and its ability to form hydrogen bonds with anthraquinone, in order to facilitate the PCET process.

Due to solubility problems in pure water, the Ru-xy_n-AQ dyads were dissolved in a 1:1 acetonitrile/water mixture. This mixture has a dielectric constant of 55.7 [20]. The decays and the lifetimes obtained under these conditions are shown in Figure 1.11.

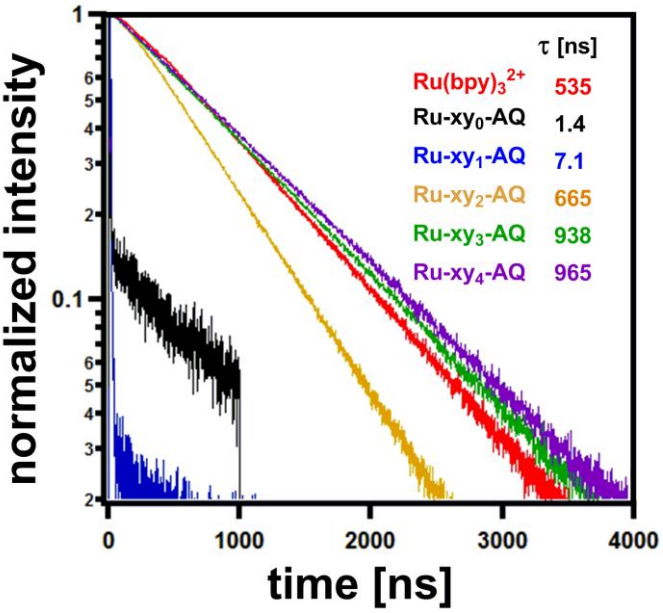

Figure 1.11: Luminescence decays and their lifetimes in a deoxygenated mixture of 1:1 CH_3CN/H_2O. Excitation occurred at 407/450 nm, detection was at 610 nm.

Comparison to the lifetimes determined in pure acetonitrile shows that in the CH_3CN/H_2O mixture more significant shortening of the luminescence lifetimes occurs. For example, in Ru-xy_0-AQ τ = 1.4 ns in CH_3CN/H_2O while in pure acetonitrile τ = 14 ns. For Ru-xy_1-AQ, the

lifetimes in the two solvents are 7.1 ns and 300 ns respectively, whereas for Ru-xy_2-AQ τ = 665 ns in CH_3CN/H_2O and 1023 ns in pure CH_3CN.

In order to understand the reason of the shortening of the lifetimes in Ru-$xy_{0\text{-}1}$-AQ in CH_3CN/H_2O, a thermodynamic "square scheme" is useful to illustrate the different possible reaction pathways (Scheme 1.8).

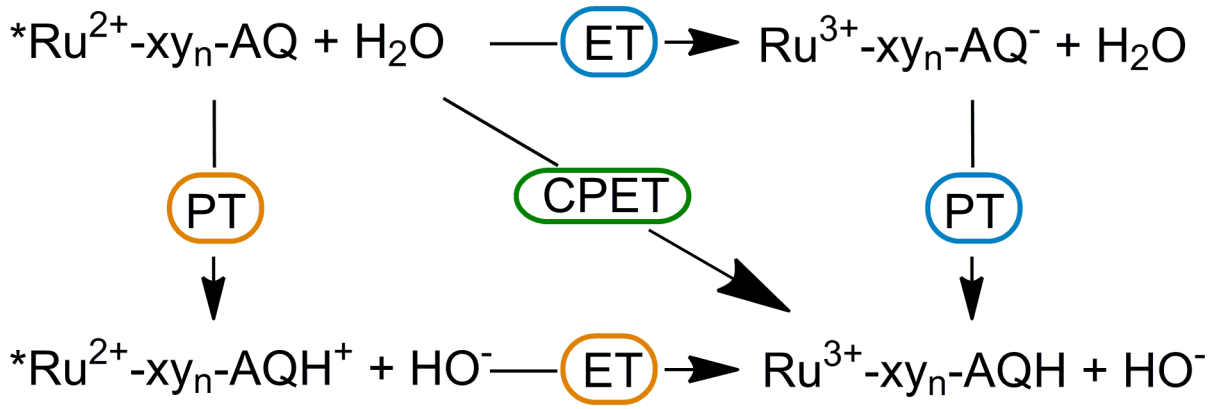

Scheme 1.8: PTET, ETPT and CPET reaction pathways in Ru-xy_n-AQ / H_2O system.

According to the above square scheme, ^{3}MLCT deactivation in CH_3CN/H_2O mixtures could occur via three pathways: electron transfer followed by proton transfer (**ETPT**) or the opposite sequence comprised of proton transfer followed by electron transfer (**PTET**). Alternatively, the deactivation could occur through concerted proton-electron transfer (**CPET**) whereby the electron and the proton are transferred at the same time. In all three cases, the overall mechanism is known as proton-coupled electron transfer (**PCET**).

A proton transfer from H_2O to AQ seems possible, particularly in view of the fact that water can form hydrogen-bonds with the carbonyl group of anthraquinone. However, the pK_a values must be considered: The pK_a value of the conjugate acid of AQ in H_2O is -8.2 [21]. Water has a pK_a of 15.7. Therefore it is thermodynamically highly unlikely that H_2O protonates AQ. Hence, the PTET mechanism from Scheme 1.8 is ruled out.

The pK_a value of the conjugate acid of anthraquinone monoanion is 5.3 [22]. Therefore H_2O with a pK_a of 15.7 still cannot protonate the AQ^- despite the fact that the latter is a far better acceptor of protons than the neutral AQ. Thus, if electron transfer happens, it cannot be followed by a proton transfer. Hence ETPT is also ruled out.

In order to explore the possibility of a CPET mechanism, kinetic isotope effects (KIEs) were investigated.

For this experiment, H_2O has been replaced by D_2O. The decays and the lifetimes are shown in Figure 1.12. The excited-state decay rate constants (k_Q) are given in Table 1.1.

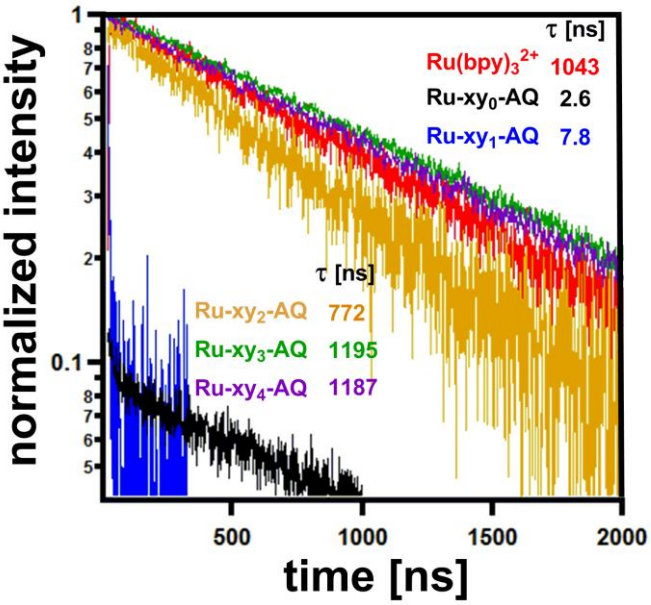

Figure 1.12: Luminescence decays and their lifetimes in a deoxygenated mixture of 1:1 CH_3CN/D_2O. Excitation occurred at 407/450 nm, detection was at 610 nm.

species	τ [ns] CH_3CN-H_2O	τ [ns] CH_3CN-D_2O	k_Q [s^{-1}] CH_3CN-H_2O	k_Q [s^{-1}] CH_3CN-D_2O
$Ru(bpy)_3^{2+}$	930	1043	-	-
Ru-xy_0AQ	1.4	2.6	$7.1\cdot10^8$	$3.8\cdot10^8$
Ru-xy_1AQ	7.1	7.8	$1.4\cdot10^8$	$1.3\cdot10^8$
Ru-xy_2AQ	665	772	$4.5\cdot10^8$	$4.6\cdot10^8$
Ru-xy_3AQ	938	1195	-	-
Ru-xy_4AQ	965	1187	-	-

Table 1.1: Luminescence lifetimes (τ) and excited-state decay rate constants (k_Q) acetonitrile-water mixtures at pH 7 determined after exciting deoxygenated solutions at 407/405 nm. Detection occurred at 610 nm.

For calculation of k_Q, equation 1.2 has been used for this purpose:

$$k_Q = \tau_{dyad}^{-1} - \tau_{ref}^{-1} \quad \text{(eq. 1.2)}$$

τ_{dyad} is the luminescence lifetimes of the dyads. It would appear logical to use the lifetime of the isolated $Ru(bpy)_3^{2+}$ complex as τ_{ref}, but we note that in all cases considered so far, the Ru-xy_3-AQ and Ru-xy_4-AQ dyads exhibit lifetimes which are somewhat longer than that of $Ru(bpy)_3^{2+}$. Thus it seems appropriate to use the average of the Ru-xy_3-AQ and Ru-xy_4-AQ lifetimes as τ_{ref} values.

For determination of the kinetic isotope effect (KIE), we used equation 1.3

$$KIE = k_{Q,H}/k_{Q,D} \quad \text{(eq. 1.3)}$$

As seen from the k_Q values given in Table 1.1 (third and fourth column), the lifetimes increase by a factor of 1.2 when going from CH_3CN/H_2O to CH_3CN/D_2O. Hence, the excited-state decay rate constants k_Q remains very similar between CH_3CN/H_2O and CH_3CN/D_2O. Usually, CPET processes exhibit KIEs ≥ 2 [23-26], and therefore we can assume that the CPET mechanism is inactive.

Given the finding that a PCET process is not responsible for the ^{3}MLCT deactivation in Ru-xy_0-AQ and Ru-xy_1-AQ, the difference in the shortening of the excited-state lifetime between CH_3CN and CH_3CN/H_2O has to be interpreted as a polarity effect on simple electron transfer. On the other hand there may be an influence of hydrogen-bonding from water which facilitates the simple electron transfer process without involving the actual transfer of an entire proton.

I-8.2 Investigations in CH_3CN/H_2O solvent mixtures at pH 2

Based on calculated estimates of the driving forces for electron transfer and proton transfer in our investigated dyads at pH = 2 (Scheme 1.9), CPET appears to be the most exergonic reaction step for the luminescence quenching in acidic solution (ΔG_{CPET} = -0.33 eV). By contrast, PTET is highly improbable due the strongly endergonic nature of the initial proton transfer step (ΔG_{PT} = +0.39 eV).

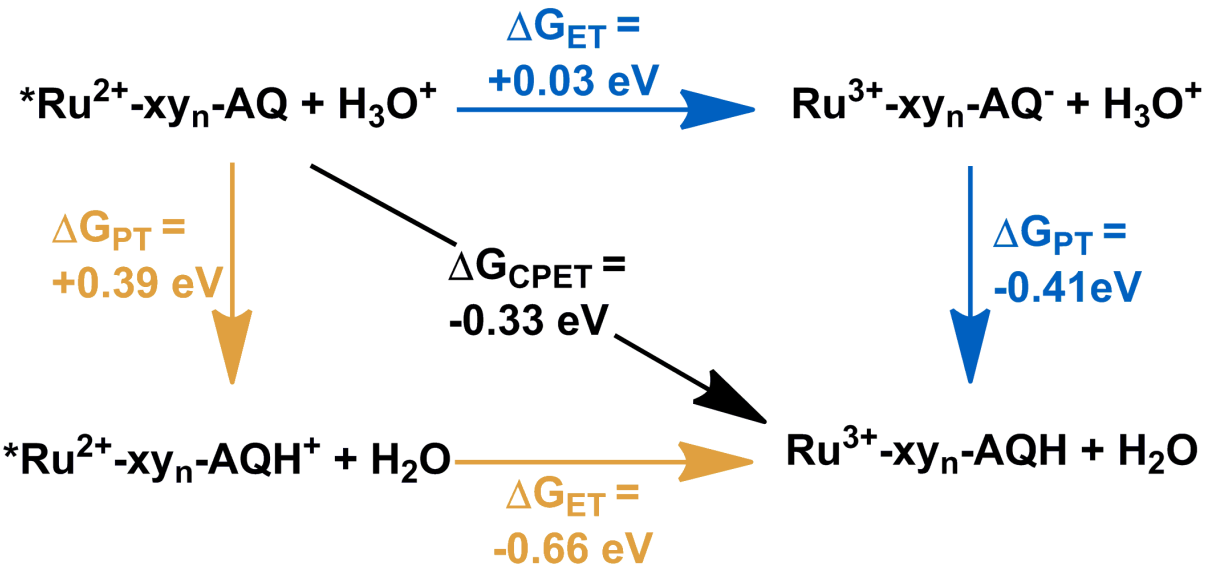

Scheme 1.9: PTET, ETPT and CPET reaction pathways in Ru-xy_n-AQ / H_3O^+ system at low pH and their thermodynamics of the individual processes.

In Scheme 1.9, the driving forces are estimated by using the following data:

E_{red} (AQ) -1.32 V vs Fc^+/Fc (Figure 1.3)

E_{red} ($AQH^·$) -0.56 V vs Fc^+/Fc [22]

E_{ox} ($*Ru^{2+}$) -1.24 V vs Fc^+/Fc

pK_a $AQH^·$ 5.3 [21]

pK_a AQH^+ -8.2 [21]

pK_a H_2O 15.7

pK_a H_3O^+ -1.7

By representing the data from Scheme 1.9 in a Jablonski-type energy level scheme, we can notice that the initial proton transfer step and electron transfer step are uphill processes, whereas the CPET mechanism is a downhill process (Scheme 1.10).

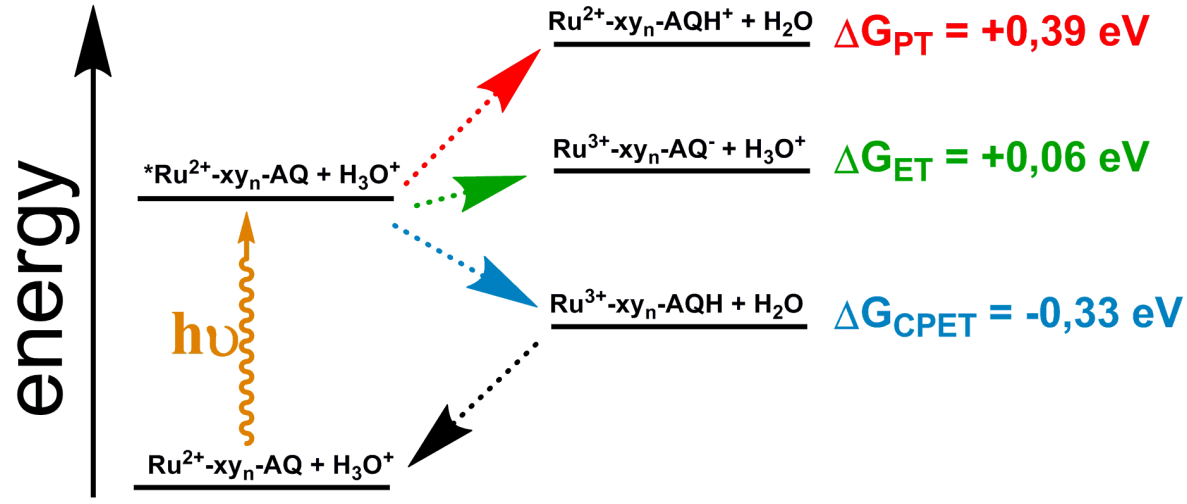

Scheme 1.10

Through addition of HCl the apparent pH of the CH_3CN/H_2O mixture was changed from 7 to 2. Surprisingly, this was found to have essentially no effect on the excited-state deactivation (second column in Table 1.2). Likewise, while adding DCl to the CH_3CN/D_2O mixture, the lifetimes did not present any significant changes compared to HCl (third column in Table 1.2).

species	τ [ns] CH_3CN-H_2O HCl	τ [ns] CH_3CN-D_2O DCl	k_Q [s^{-1}] CH_3CN-H_2O HCl	k_Q [s^{-1}] CH_3CN-D_2O DCl
$Ru(bpy)_3^{2+}$	856	970	-	-
Ru-xy_0AQ	2.0	3.2	$5.0\cdot10^8$	$3.1\cdot10^8$
Ru-xy_1AQ	6.2	3.1	$1.6\cdot10^8$	$3.2\cdot10^8$
Ru-xy_2AQ	544	618	$8.3\cdot10^8$	$6.5\cdot10^8$
Ru-xy_3AQ	1005	1080	-	-
Ru-xy_4AQ	982	981	-	-

Table 1.2: Luminescence lifetimes (τ) and excited-state decay rate constants (k_Q) in acetonitrile-water mixtures at pH 2 determined after exciting deoxygenated solutions at 407/405 nm. Detection occurred at 610 nm.

The absence of a significant kinetic isotope effect at pH 2 suggests that the ^{3}MLCT excited-state could not be deactivated through a CPET mechanism, whereas it could be deactivated

through a sequence of electron transfer and proton transfer (ETPT). According to the pK_a values of the conjugate acid of anthraquinone monoanion (5.3) and that of the hydronium ion (-1.7), it is thermodynamically possible to protonate AQ^- by H_3O^+. Therefore, the photoinduced electron transfer occurs first from ruthenium to anthraquinone, and then once AQ^- is formed it is likely to be protonated by H_3O^+.

I-8.3 Hydrogen-bonding between hexafluoroisopropanol and anthraquinone in apolar CH_2Cl_2 solution

Since water has a high dielectric constant and at the same time the possibility to form hydrogen bonds, it becomes more difficult to understand and interpret the results from the prior section. It is hard to differentiate whether the polarity effect or the hydrogen-bonding control the rates for photoinduced electron transfer. For this reason, it was necessary to use a solvent with a relatively low dielectric constant, but able to form hydrogen-bonds. HFIP (1,1,1,3,3,3-hexafluoro-2-propanol) is a good choice with ε_s = 16.6, because it is one of the strongest hydrogen-bond donors.

In the following parts, my studies were restricted to the Ru-xy_1-AQ molecule.

In order to study the effect of HFIP on our molecule, it is meaningful to start first by searching for evidence for hydrogen-bonding between HFIP and free anthraquinone. We assume that the results from such experiments will be applicable to the AQ unit when it is attached to the Ru complex.
In first step, our experiments were carried out on charge-neutral AQ, and then on the AQ radical anion (AQ^-).

I-8.3.1 Hydrogen-bonding between hexafluoroisopropanol and charge-neutral AQ in dichloromethane

I-8.3.1.1 Optical absorption spectroscopy

Figure 1.13 shows the absorption spectra of a 10^{-4} M solution of free 9,10-anthraquinone in CH_2Cl_2 without and after the addition of increasing amounts of HFIP. Prior to HFIP addition, the absorption spectrum presents two prominent bands at 327 nm and 273 nm. While adding

small amounts of HFIP, a red-shift occurs: on the one hand the band at 327 nm shifts to 332 nm at a concentration of 0.5 M in HFIP, and on the other hand the band at 273 nm shifts to 275 nm.

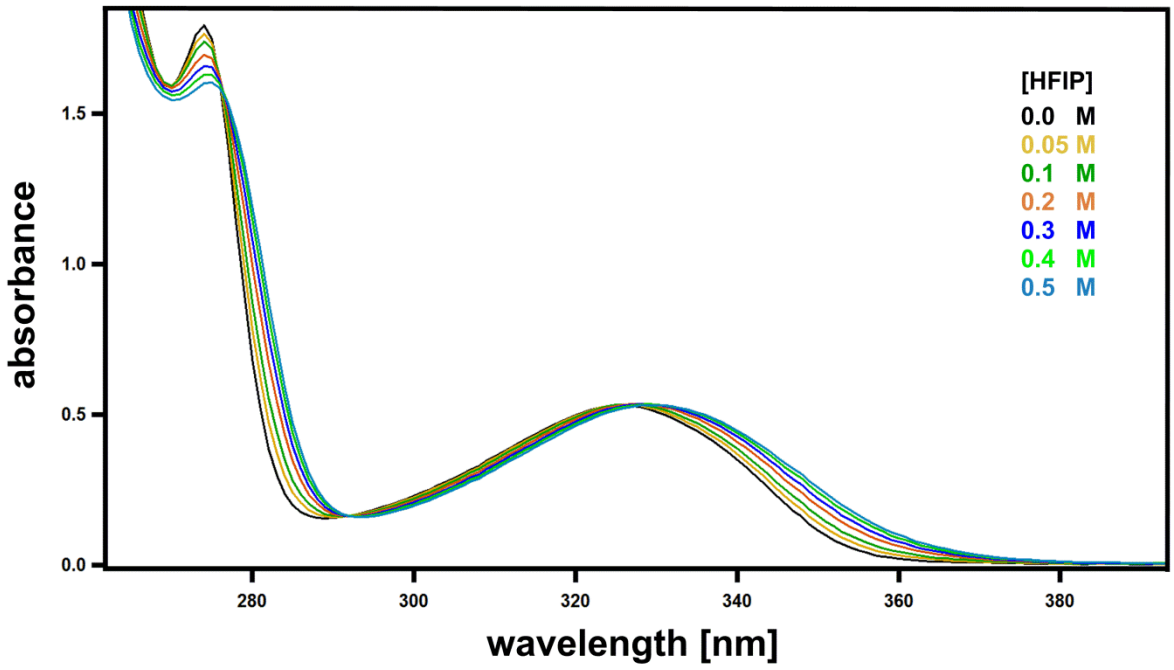

Figure 1.13: Optical absorption of a ~10^{-4} M solution of 9,10-anthraquinone (AQ) in CH_2Cl_2 in presence of increasing concentrations of hexafluoroisopropanol (HFIP).

Two isosbestic points at 277 nm and 292 nm reveal the presence of only two distinct species, presumably free AQ and AQ which is accepting a hydrogen bond from HFIP (AQ-HFIP). Thus we assume that these two species are in chemical equilibrium:

$$AQ + HFIP \leftrightarrow AQ\text{-}HFIP \qquad \text{(eq. 1.4)}$$

From this measurement, and based on the Mataga and Tsuno equation [27-29] (eq. 1.5), important information could be obtained: the equilibrium constant $K_{eq}^{(AQ)}$ for the chemical equilibrium of equation 1.4.

$$(1-A_0/A)_\lambda / [HFIP] = - K_{eq}^{(AQ)} + K_{eq}^{(AQ)} \cdot (\varepsilon_{AQ\text{-}HFIP}/\varepsilon_{AQ})_\lambda \cdot (A_0/A)_\lambda \qquad \text{(eq. 1.5)}$$

[HFIP] concentration of HFIP in mol/l

A_0 absorbance of AQ in absence of HFIP

A absorbance of AQ in presence of HFIP

$\varepsilon_{AQ\text{-}HFIP}$ extinction coefficient of hydrogen-bonded AQ at wavelength λ in $M^{-1}cm^{-1}$

ε_{AQ} extinction coefficient of free AQ at wavelength λ in $M^{-1}cm^{-1}$

The observation wavelength λ was chosen to be 283 nm because there are particularly significant special changes at this wavelength (Figure 1.13). Figure 1.14 shows a plot of $(1-A_0/A)_\lambda$ / [HFIP] versus $(A_0/A)_\lambda$ for this wavelength. Linear regression fit to the data yields a slope of 7.28 and an intercept of -1.76 with a correlation factor $R^2 = 0.9987$. Hence, from the intercept we obtain $K_{eq}^{(AQ)}$ equal to 1.76 M^{-1}. This order of magnitude is reasonable in view of other comparable hydrogen-bonded (charge-neutral) systems in aprotic solvents [30].

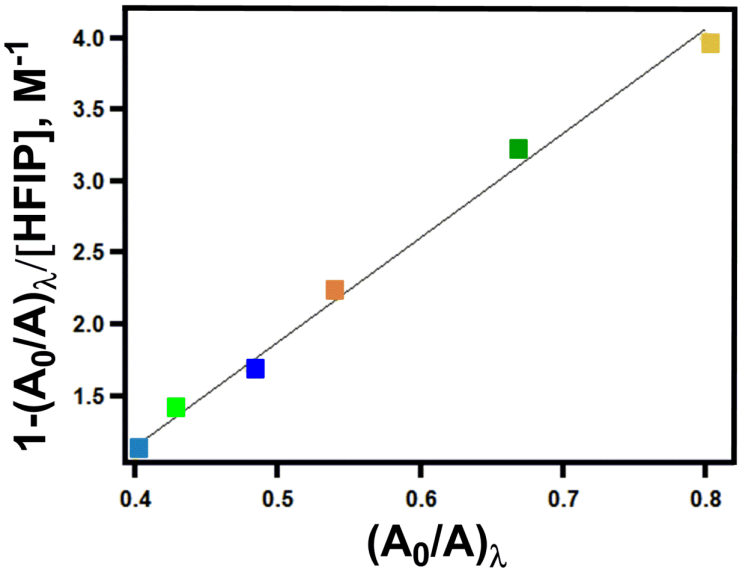

Figure 1.14: Plot of the experimental absorbance data at a wavelength of 283 nm according to equation 1.5; the color code is the same as in Figure 1.13.

I-8.3.1.2 Infrared spectroscopy

Infrared spectroscopy has the potential to provide more direct evidence for the presence of hydrogen-bond between AQ and HFIP. Our hope was to find a change in the C=O stretch IR absorption of AQ upon addition of HFIP. An approximately 1 M solution of AQ in CH_2Cl_2 was used for this experiment. In agreement with other studies the CO stretch appears at 1678

cm^{-1} [31,32] (blue trace). While adding 0.1 M of HFIP to this solution, this peak shifts by -4 cm^{-1} (Figure 1.15).

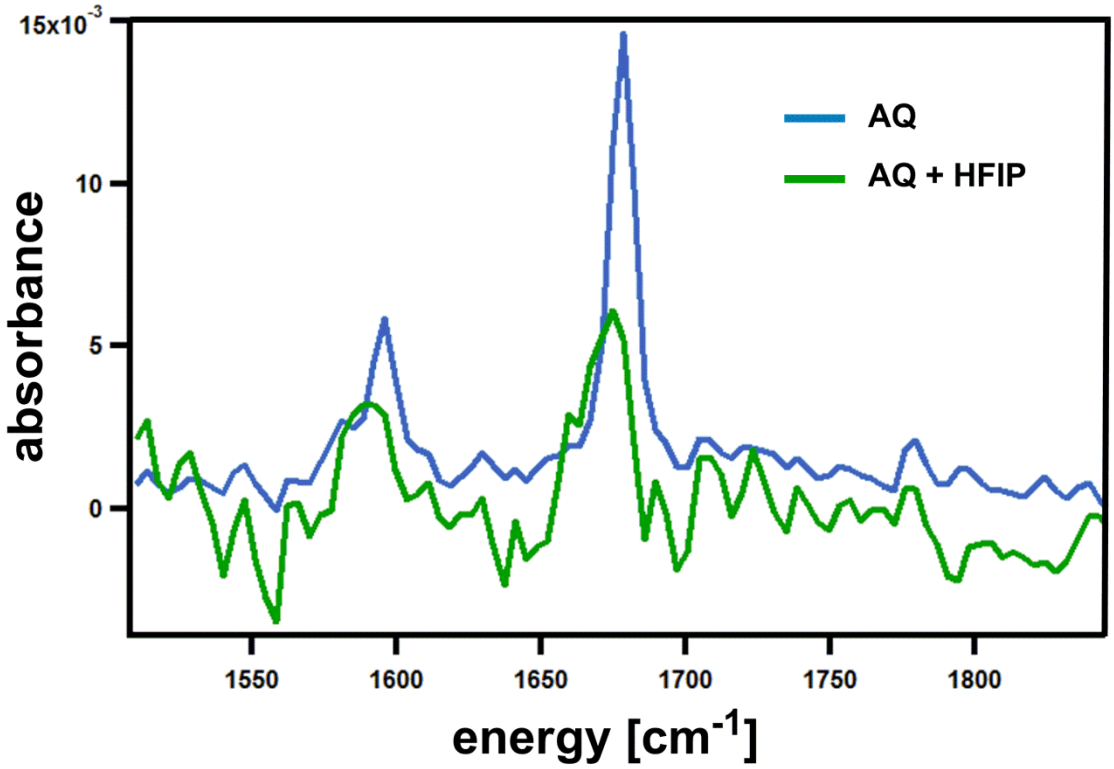

Figure 1.15: Blue trace: Infrared spectrum of a 1 M solution of 9,10-anthraquinone (AQ) in CH_2Cl_2. The green trace was measured on the same solution after adding ~ 0.1 M of HFIP.

Despite the fact that this shift is relatively small, we are positive that it is not an instrumental artifact. Changes in dielectric constant may cause shifts in IR frequencies, but in our case relatively small amounts of HFIP (0.1 M; ε_s = 16.6) were added. Consequently it appears possible that the small shift in the CO stretch upon HFIP addition is indeed due to the hydrogen bonding.

I-8.3.2 Hydrogen-bonding between hexafluoroisopropanol and AQ^- monoanion in dichloromethane

I-8.3.2.1 Cyclic voltammetry

By reducing AQ to AQ^- electrochemically, the formation of hydrogen-bonds with HFIP can be expected to become even more important than in the case of neutral AQ.

Figure 1.16 shows a series of voltammograms of Ru-xy$_1$-AQ in CH_2Cl_2 in presence of different concentrations of HFIP. The waves at 0.0 V belong to the oxidation of the ferrocene substance which was added as an internal reference.

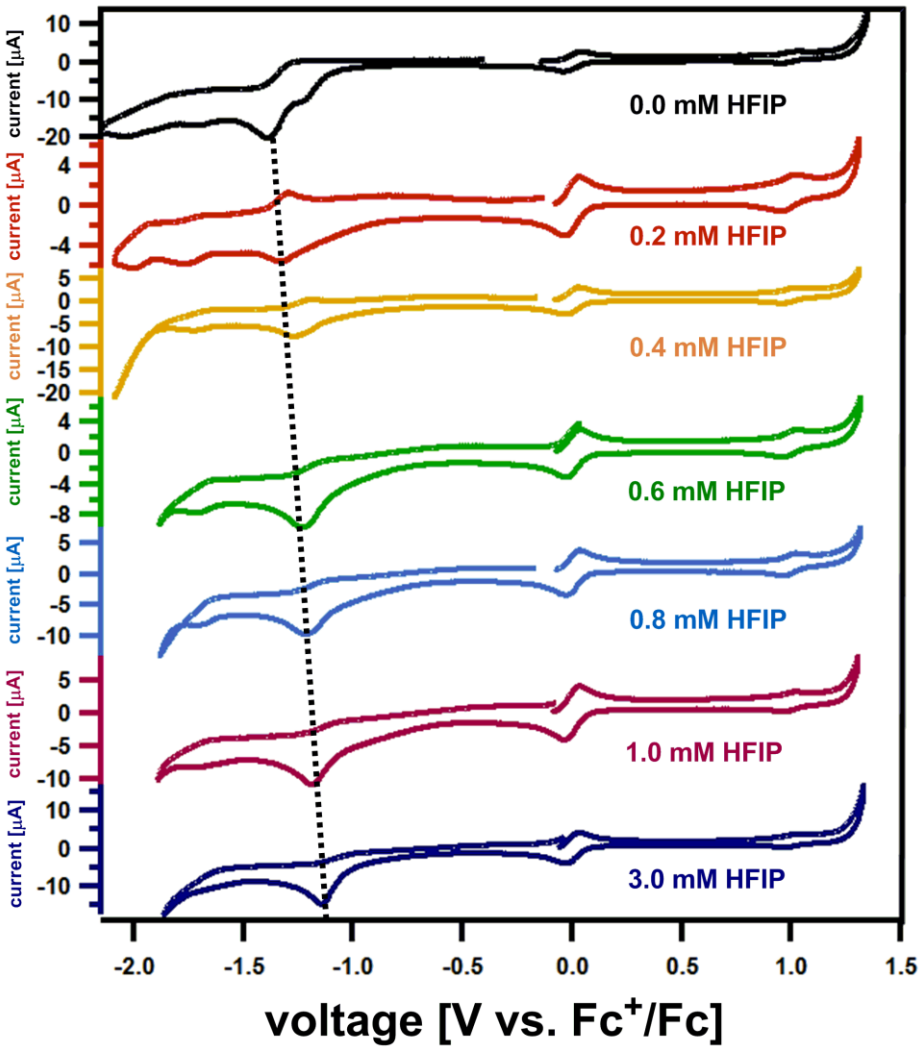

Figure 1.16: Cyclic voltammograms measured on the Ru-xy$_1$-AQ dyad in dry and deoxygenated CH_2Cl_2 in presence of increasing concentrations of hexafluoroisopropanol.

By increasing the amount of HFIP from 0.2 mM to 3.0 mM, the reduction wave of AQ at -1.39 V shifts to the more positive potentials until we reach -1.14 V with 3.0 mM of HFIP. The oxidation waves of Ru^{3+}/Ru^{2+} near 1.0 V remain unaffected in the presence of HFIP.

The following question might be asked: Is this shift due to protonation or simply due to strong hydrogen bonds between the AQ and HFIP? In fact, as mentioned before, the pK_a value of the conjugate acid of AQ^- is 5.3 in DMF, while that of HFIP is 17.9 in DMSO. Thus, the

protonation of AQ^- by HFIP is thermodynamically unlikely. The shift is therefore likely due to hydrogen-bonding effects.

As for the neutral AQ, a chemical equilibrium is established between AQ^- and HFIP:

$$AQ^- + n\text{HFIP} \leftrightarrow AQ^-\text{-HFIP}_n \qquad \text{(eq. 1.6)}$$

n represents the number of HFIP molecules connected by hydrogen-bonds to AQ^-. This number can be determined using the following expression [33,34]:

$$\Delta E_{red} = n\cdot\cdot(R\cdot T/F)\cdot \ln([\text{HFIP}]) + (R\cdot T/F)\cdot \ln(K_{eq}^{(AQ-)}) \qquad \text{(eq. 1.7)}$$

ΔE_{red} the difference between the electrochemical reduction at a given HFIP concentration above 0.0 mM and the potential at [HFIP] = 0.

R the gas constant = 8.31 J mol^{-1} l^{-1}

T the temperature in Kelvin (K)

F the Faraday constant = 96485 C mol^{-1}

Plotting ΔE_{red} versus ln([HFIP]) yields a straight line (Figure 1.17) as expected from eq. 1.7. A linear regression fit gives a slope of 0.15 V and an intercept of 0.62 with $R^2 = 0.9815$.

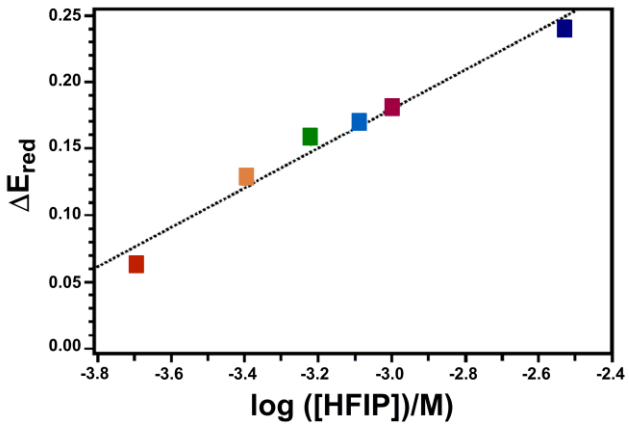

Figure 1.17: Plot of the shift in AQ/AQ^- reduction potential (ΔE_{red}) within increasing HFIP concentration as observed experimentally in the data from Figure 1.16 (with the same color code). This semilogarithmic plot serves to determine $K_{eq}^{(AQ-)}$ according to equation 1.7.

According to equation 1.7, the slope corresponds to $2.3 \cdot n \cdot (R \cdot T/F)$, and from this we obtain $n \approx 2.5$. This value suggests that by reducing AQ to AQ^-, the number of HFIP molecules bonded to AQ through hydrogen-bond increases from 1 to 2.5.

From the intercept, one may estimate the equilibrium constant $K_{eq}^{(AQ-)}$ for the binding of 2.5 HFIP molecules per anthraquinone monoanion which is around $3.6 \cdot 10^{11}$ $M^{-2.5}$. When calculating a mean association constant per individual HFIP molecule, one obtains $(3.6 \cdot 10^{11}\ M^{-2.5})^{1/2.5} = 1.6 \cdot 10^4\ M^{-1}$.

To conclude, the number of HFIP molecules bound to the anthraquinone unit via hydrogen-bonding increases from 1 to 2.5 when AQ is reduced. Moreover, the binding to AQ^- becomes stronger than to charge-neutral AQ (Scheme 1.11). In fact, the binding constant increases from ~1 M^{-1} to $1.6 \cdot 10^4$ M^{-1} per hydrogen bond.

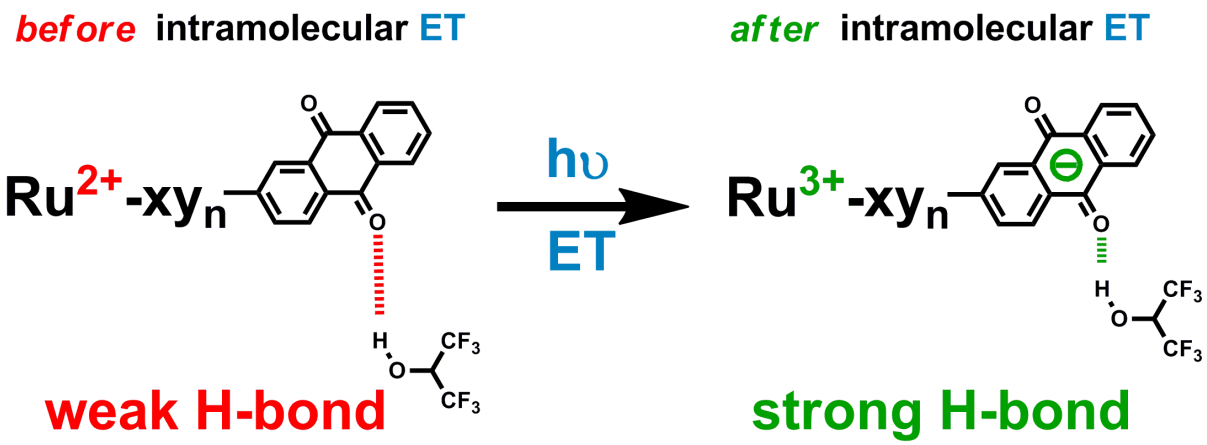

Scheme 1.11: Hydrogen-bonding between anthraquinone and hexafluoroisopropanol before and after intramolecular Ru-to-AQ electron transfer.

After collecting relevant experimental evidence for the presence of hydrogen-bonds between HFIP and AQ, it is time to study its influence on photoinduced electron transfer in Ru-xy_1-AQ.

I-8.4 Influence of HFIP on photoinduced electron transfer in the Ru-xy_1-AQ dyad

Upon addition of HFIP to a deoxygenated dichloromethane solution of Ru-xy_1-AQ, the reduction of anthraquinone becomes easier (Figure 1.16). Therefore, one would expect more

driving force for intramolecular electron transfer between photoexcited $Ru(bpy)_3^{2+}$ and AQ. Indeed, by calculating the driving force in presence of HFIP, we found ΔG_{ET} = -0.12 eV. This value has been estimated by using the reduction potential of -1.14 V for anthraquinone in presence of 3.0 mM of HFIP (Figure 1.16).

Consequently, the thermodynamics for photoinduced electron transfer change from being endergonic in absence of HFIP to slightly exergonic in presence of HFIP (Scheme 1.12).

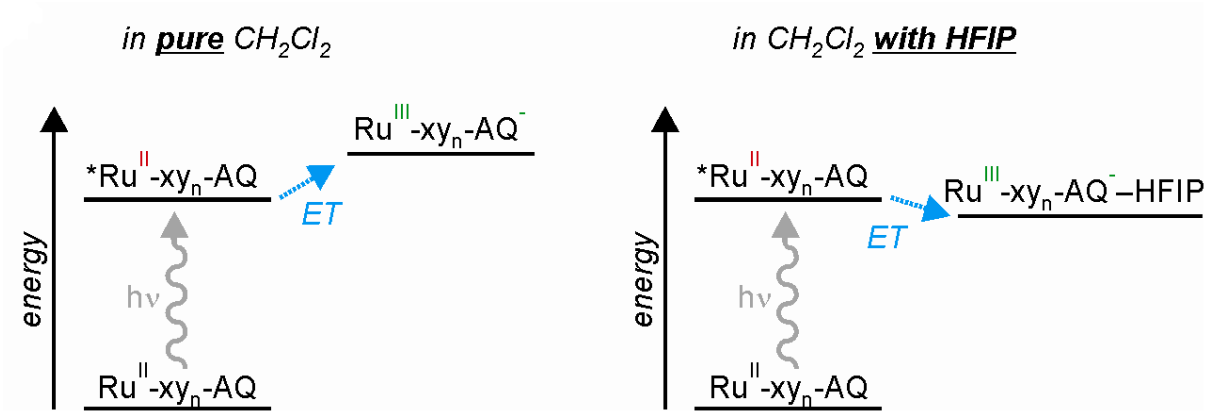

Scheme 1.12: Energetics for photoinduced Ru to AQ electron transfer in pure CH_2Cl_2 (left) and in CH_2Cl_2 with HFIP (right).

Hence, it can be expected that the ^{3}MLCT excited state of the Ru-xy_1-AQ dyad will undergo an intramolecular electron transfer from Ru to AQ when HFIP is added to the CH_2Cl_2 solution.

In fact, the quenching in the luminescence lifetimes supports our expectation. Figure 1.18 (left panel) shows the ^{3}MLCT luminescence decays of the Ru-xy_1-AQ dyad in presence of increasing concentration of HFIP. The lifetime varies from 929 ns in the case of 0.0 M of HFIP to 249 ns upon addition of 1.0 M of HFIP.

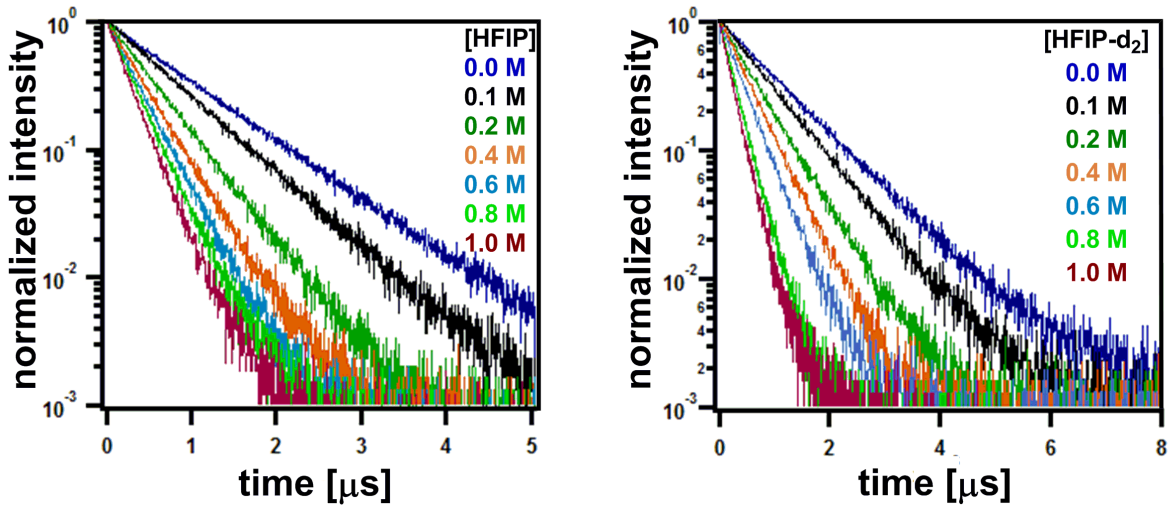

Figure 1.18: ^{3}MLCT luminescence decay of Ru-xy$_1$-AQ in dichloromethane solution in presence of increasing concentrations of HFIP (left) and HFIP-d_2 (right). Excitation was at 450 nm and detection at 610 nm.

When HFIP was added to a deoxygenated dichloromethane solution of $Ru(bpy)_3^{2+}$, one observes a shortening of the lifetime: In deoxygenated pure CH_2Cl_2 the lifetime is 659 ns while in presence of 1.0 M of HFIP the lifetime decreases by a factor of 1.4 (τ = 455 ns) (Figure 1.19).

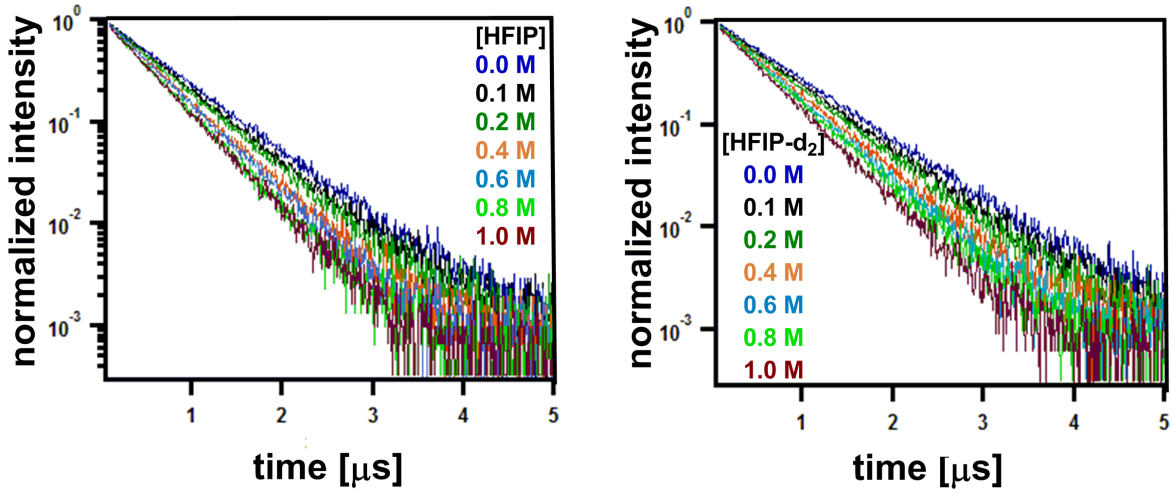

Figure 1.19: ^{3}MLCT luminescence decay of $Ru(bpy)_3^{2+}$ in dichloromethane solution in presence of increasing concentrations of HFIP (left) and HFIP-d_2 (right). Excitation was at 450 nm and detection at 610 nm.

This shortening in the lifetime in presence of HFIP is caused by a nonradiative relaxation likely due to the high-frequency vibrations of the O-H stretch in HFIP which are known to be efficient luminescence killers [35].

When compared to the Ru-xy_1-AQ dyad, the lifetime quenching in $Ru(bpy)_3^{2+}$ is significantly less pronounced. Thus, one may conclude that the lifetime shortening in Ru-xy_1-AQ is indeed caused by hydrogen-bonding from HFIP to AQ.

References

[1] Balzani, V., *Electron transfer in chemistry*. VCH Wiley: Weinheim, 2001; Vol. 3.

[2] Wenger, O. S., *Coord. Chem. Rev.* **2009,** *253*, 1439.

[3] Opperman, K. A., Mecklenburg, S. L., Meyer, T. J., *Inorg. Chem.* **1994**, *33*, 5295.

[4] Hanss, D.; Wenger, O. S., *Inorg. Chem.* **2008,** *47*, 9081.

[5] Hanss, D.; Walther, M. E.; Wenger, O. S., *Coord. Chem. Rev.* **2010,** *254*, 2584.

[6] Wenger, O. S., *Chem. Soc. Rev.* **2011,** *40*, 3538.

[7] Goldsmith, R. H.; Sinks, L. E.; Kelley, R. F.; Betzen, L. J.; Liu, W. H.; Weiss, E. A.; Ratner, M. A.; Wasielewski, M. R., *Proc. Natl. Acad. Sci. U. S. A.* **2005,** *102*, 3540.

[8] Weiss, E. A.; Ahrens, M. J.; Sinks, L. E.; Gusev, A. V.; Ratner, M. A.; Wasielewski, M. R., *J. Am. Chem. Soc.* **2004,** *126*, 5577.

[9] Sjödin, M.; Styring, S.; Åkermark, B.; Sun, L. C.; Hammarström, L., *J. Am. Chem. Soc.* **2000,** *122*, 3932.

[10] Walther, M. E.; Wenger, O. S., *Inorg. Chem.* **2011,** *50*, 10901.

[11] Mecklenburg, S. L.; McCafferty, D. G.; Schoonover, J. R.; Peek, B. M.; Erickson, B. W.; Meyer, T. J., *Inorg. Chem.* **1994,** *33*, 2974.

[12] Lopéz, R.; Leiva, A. M.; Zuloaga, F.; Loeb, B.; Norambuena, E.; Omberg, K. M.; Schoonover, J. R.; Striplin, D.; Devenney, M.; Meyer, T. J., *Inorg. Chem.* **1999,** *38*, 2924.

[13] Lewis, F. D.; Thazhathveetil, A. K.; Zeidan, T. A.; Vura-Weis, J.; Wasielewski, M. R., *J. Am. Chem. Soc.* **2010,** *132*, 444.

[14] Weller, A., *Z. Phys. Chem.* **1982,** *133*, 93.

[15] Kilså, K.; Kajanus, J.; Macpherson, A. N.; Mårtensson, J.; Albinsson, B., *J. Am. Chem. Soc.* **2001,** *123*, 3069.

[16] Gurzadyan, G. G.; Steenken, S., *Chem. Eur. J.* **2001,** *7*, 1808.

[17] Turro, N. J., *Molecular Photochemistry*. New York, Amsterdam, 1967.

[18] Hanss, D.; Walther, M. E.; Wenger, O. S., *Chem Commun.,* **2010,** *46*, 7034.

[19] Walther, M. E.; Wenger, O. S., *ChemPhysChem,* **2009,** *10*, 1203.

[20] Gagliardi, L. G.; Castells, C. B.; Rafols, C.; Roses, M.; Bosch, E., *J. Chem. Eng. Data* **2007,** *52*, 1103.

[21] Yamada, Y. United States Patent Application: Anti-Allergen Agent. 2010.

[22] Babaei, A.; Connor, P. A.; McQuillan, A. J.; Umapathy, S., *J. Chem. Ed.* **1997,** *74*, 1200.

[23] Huynh, M. H. V.; Meyer, T. J., *Chem. Rev.* **2007,** *107*, 5004.

[24] Mayer, J. M., *Annu. Rev. Phys. Chem.* **2004,** *55*, 363.

[25] Hammarström, L.; Styring, S., *Energy Environ. Sci.* **2011,** *4*, 2379.

[26] Costentin, C.; Robert, M.; Savéant, J.-M., *Acc. Chem. Res.* **2010,** *43*, 1019.

[27] Mataga, N.; Tsuno, S., *Bull. Chem. Soc. Jpn.* **1957,** *30*, 368.

[28] Mataga, N.; Tsuno, S., *Bull. Chem. Soc. Jpn.* **1957,** *30*, 711.

[29] Biczok, L.; Gupta, N.; Linschitz, H., *J. Am. Chem. Soc.* **1997,** *119*, 12601.

[30] Steed, J. W.; Atwood, J. L., *Supramolecular chemistry*. John Wiley&Sons., Ltd.: 2009.

[31] Pecile, C.; Lunelli, B., *J. Chem. Phys.* **1967,** *46*, 2109.

[32] Büschel, M.; Stadler, C.; Lambert, C.; Beck, M.; Daub, J., *J. Electroanal. Chem.* **2000,** *484*, 24.

[33] Gupta, N.; Linschitz, H., *J. Am. Chem. Soc.* **1997,** *119*, 6384.

[34] Ahmed, S.; Khan, A. Y.; Qureshi, R.; Subhani, M. S., *Russ. J. Electrochem.* **2007,** *43*, 811.

[35] Brunold, T. C.; Güdel, H. U., *Inorganic Electronic Structure and Spectroscopy*. Wiley: New York, 1999; Vol. 1, p 259.

Chapter II
Photoinduced Electron Transfer in Linear Triarylamine-Photosensitizer-Anthraquinone Triads

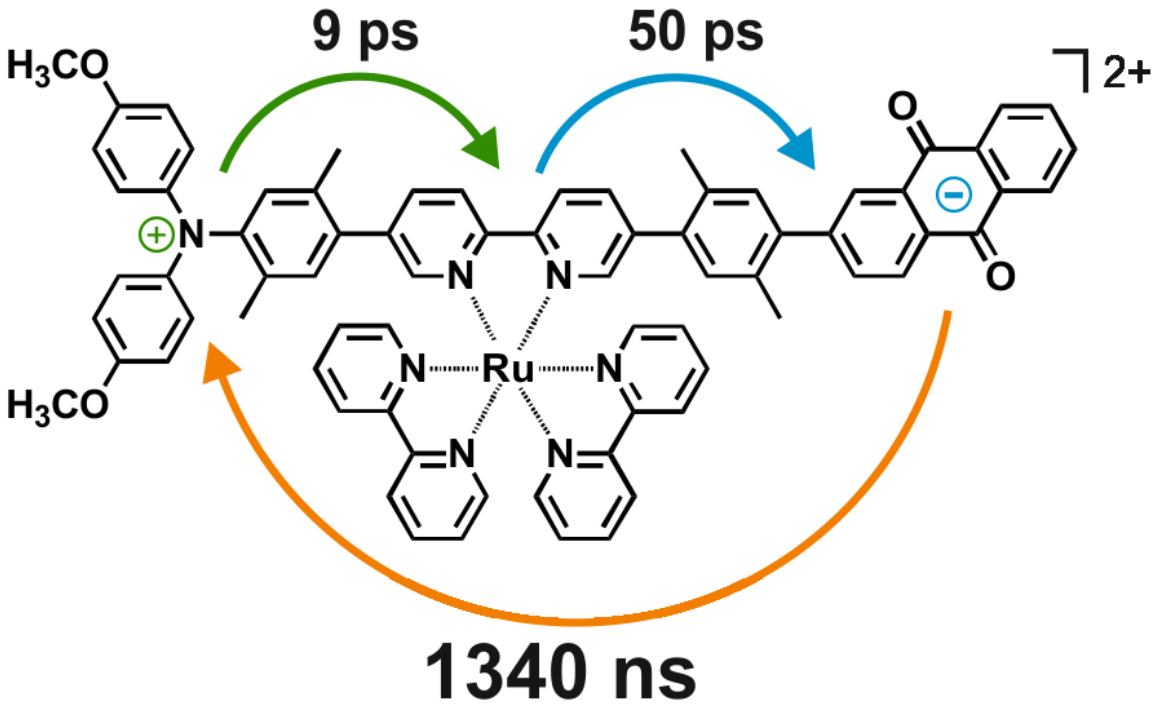

Introduction

Photoinduced electron transfer in triad systems based on ruthenium as a photosensitizer has been investigated by several research groups [1]. But none, to the best of my knowledge, has reported the synthesis of linear triads using $Ru(bpy)_3^{2+}$ wherein the electron donor and acceptor are attached to the same 2,2'-bipyridine ligand (Scheme 2.1a). Such molecules enable vectorial photoinduced electron transfer and have numerous advantages: (i) This design avoids the formation of isomers which occurs when having the donor and the acceptor linked to different bipyridine ligands [2-7] (Scheme 2.1b), (ii) it is not necessary to use 2,2';6',2''-terpyridine (tpy) as a ligand connected to the ruthenium [8-14] (Scheme 2.1c) for obtaining linear triads. This is important because $Ru(tpy)_2^{2+}$ has a short excited state lifetime compared to $Ru(bpy)_3^{2+}$, and this is detrimental for photoinduced electron transfer[15]. (iii) Furthermore, it will not be necessary to involve a ligand such as bis(diquinolinyl)pyridine [16-19] (Scheme 2.1d) which is difficult to synthesize.

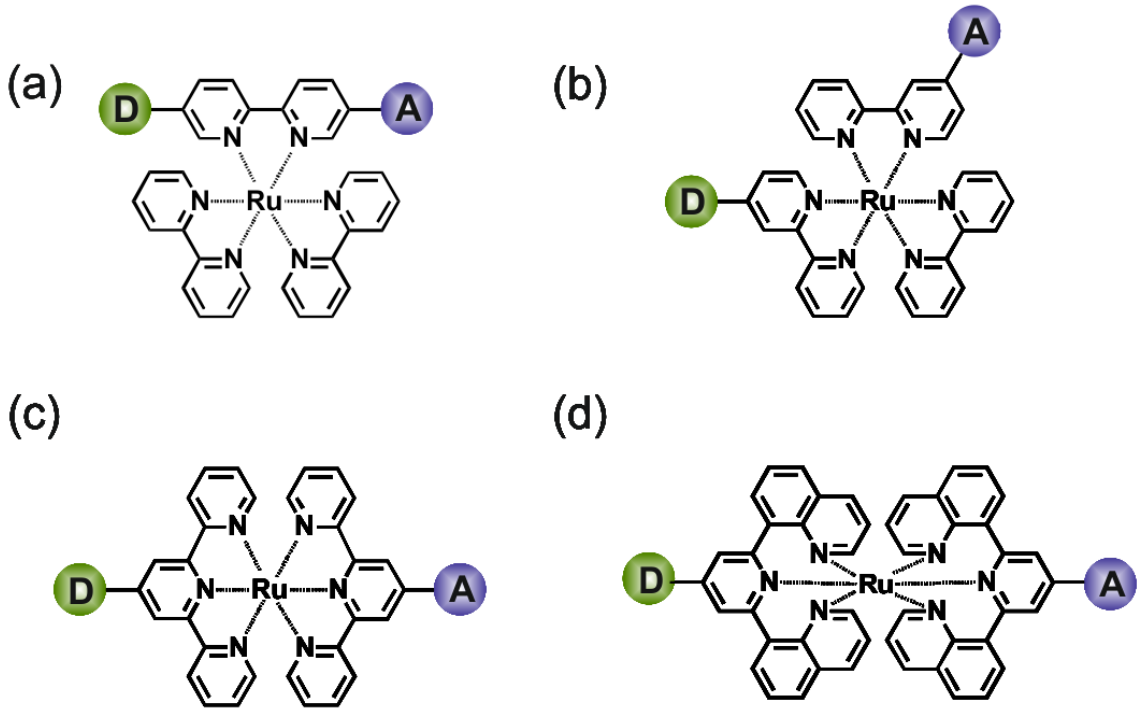

Scheme 2.1: Chemical structures of ruthenium triads with different ligands and substitution positions for the electron donor (D) and the electron acceptor (A).

II-1. Triads and dyads that incorporate $Ru(bpy)_3^{2+}$ as photosensitizer

A molecular triad designated as **TAA-Ru^{2+}-AQ** based on $Ru(bpy)_3^{2+}$ as a photosensitizer has been synthesized and thoroughly studied (Scheme 2.2) as part of this thesis. In addition, corresponding dyads in which ruthenium is connected either with the electron donor alone (**TAA-Ru**) or solely with the electron acceptor (**Ru-AQ**) have been synthesized and investigated as well.

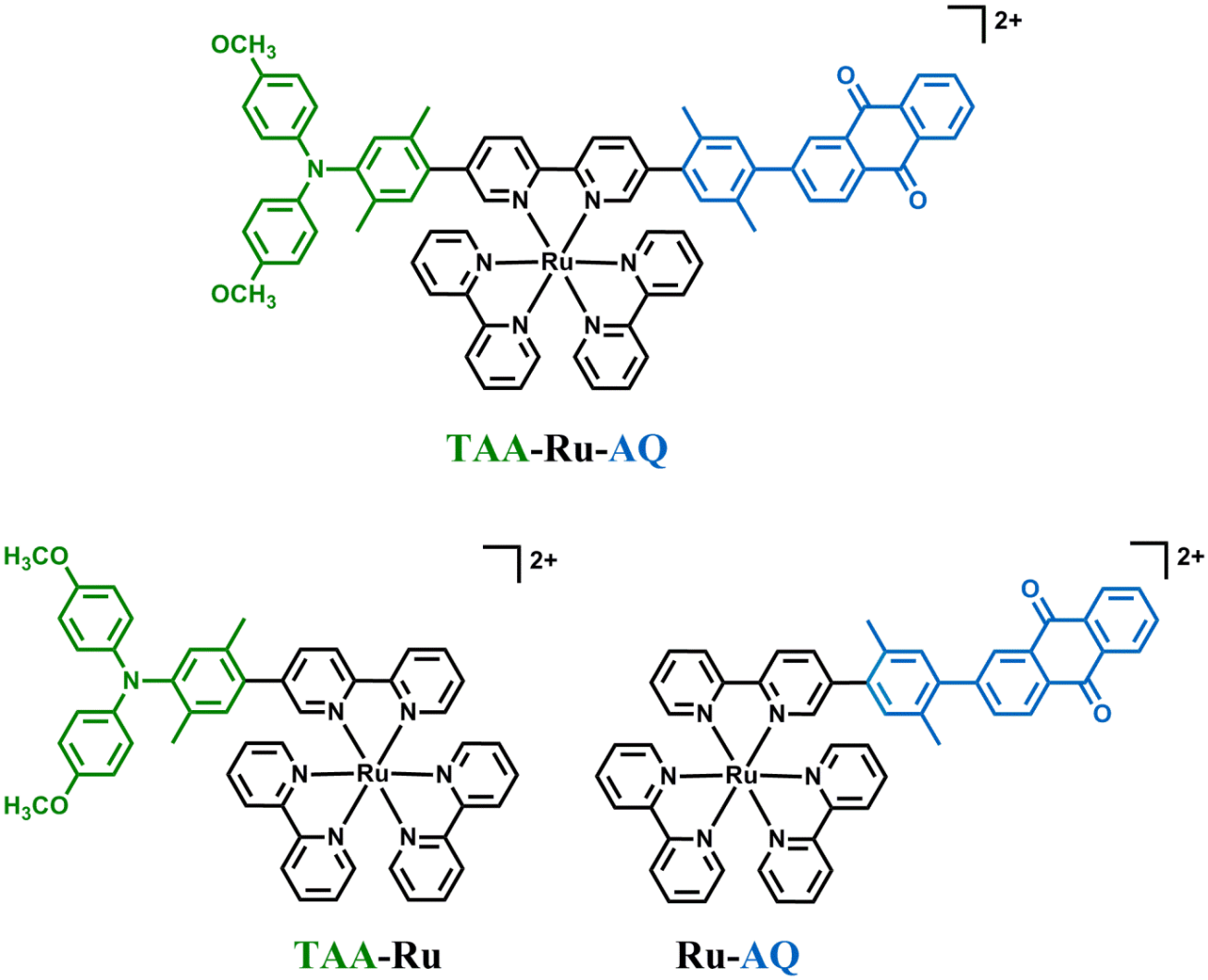

Scheme 2.2: Molecular structures of the investigated ruthenium triad with two relevant dyads.

Upon photoexcitation of the triad molecule shown in Scheme 2.2, an electron transfer is expected to occur first from the triarylamine (**TAA**) electron donor to $Ru(bpy)_3^{2+}$ (**Ru**) leading to the formation of the trianisylamine radical cation (TAA^+). Then, the electron

should be transferred from **Ru** to the 9,10-anthraquinone (**AQ**) electron acceptor allowing the formation of the radical anion (AQ^-). Therefore, a TAA^+-Ru^{2+}-AQ^- state will be obtained. This state is a so-called fully charge-separated state containing two radical species: the oxidized amine (TAA^+) and the quinone monoanion (AQ^-).

An important target of this work is to determine the lifetime of the fully charge-separated state of the photogenerated radical species (TAA^+-Ru^{2+}-AQ^-) after excitation of the ruthenium. In addition, the quantum yield for the formation of this state will be as well determined.

Due to the chemical versatility of the overall ligand backbone, triads with $Os(bpy)_3^{2+}$ and $[Ir(2\text{-}(p\text{-tolyl})pyridine)_2(bpy)]^+$as photosensitizers have been also involved in this study (Scheme 2.3) which, despite their chemical similarity to the ruthenium triad, present different photophysical and photochemical properties.

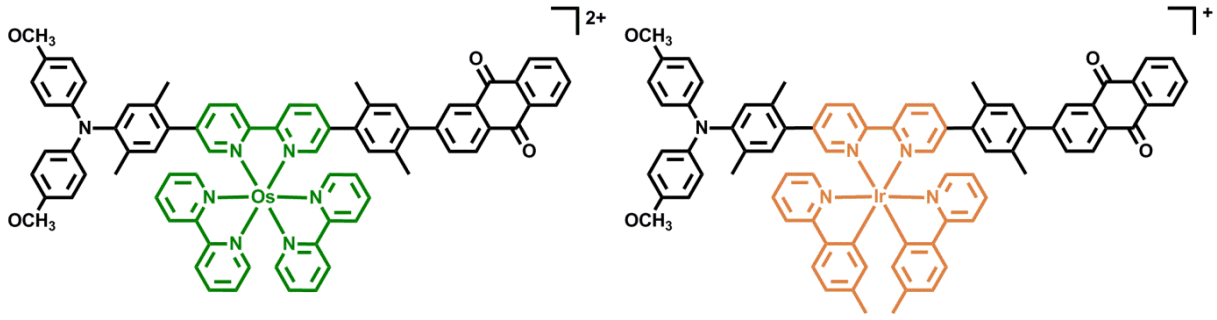

TAA-Os-AQ **TAA-Ir-AQ**

Scheme 2.3: Triad molecules based on osmium and iridium complexes as photosensitizers.

The experimental techniques used for the investigation of all these triads and their relevant dyads are: Electrochemistry, spectroelectrochemistry, optical absorption spectroscopy, steady-state luminescence spectroscopy, nanosecond transient absorption spectroscopy and femtosecond transient absorption spectroscopy. The latter technique was performed in collaboration with a research group in Finland.

II-1.1 Synthesis of TAA-Ru^{2+}-AQ molecule

Several synthetic steps are needed in order to obtain the ruthenium triad. These steps are illustrated below in Scheme 2.4.

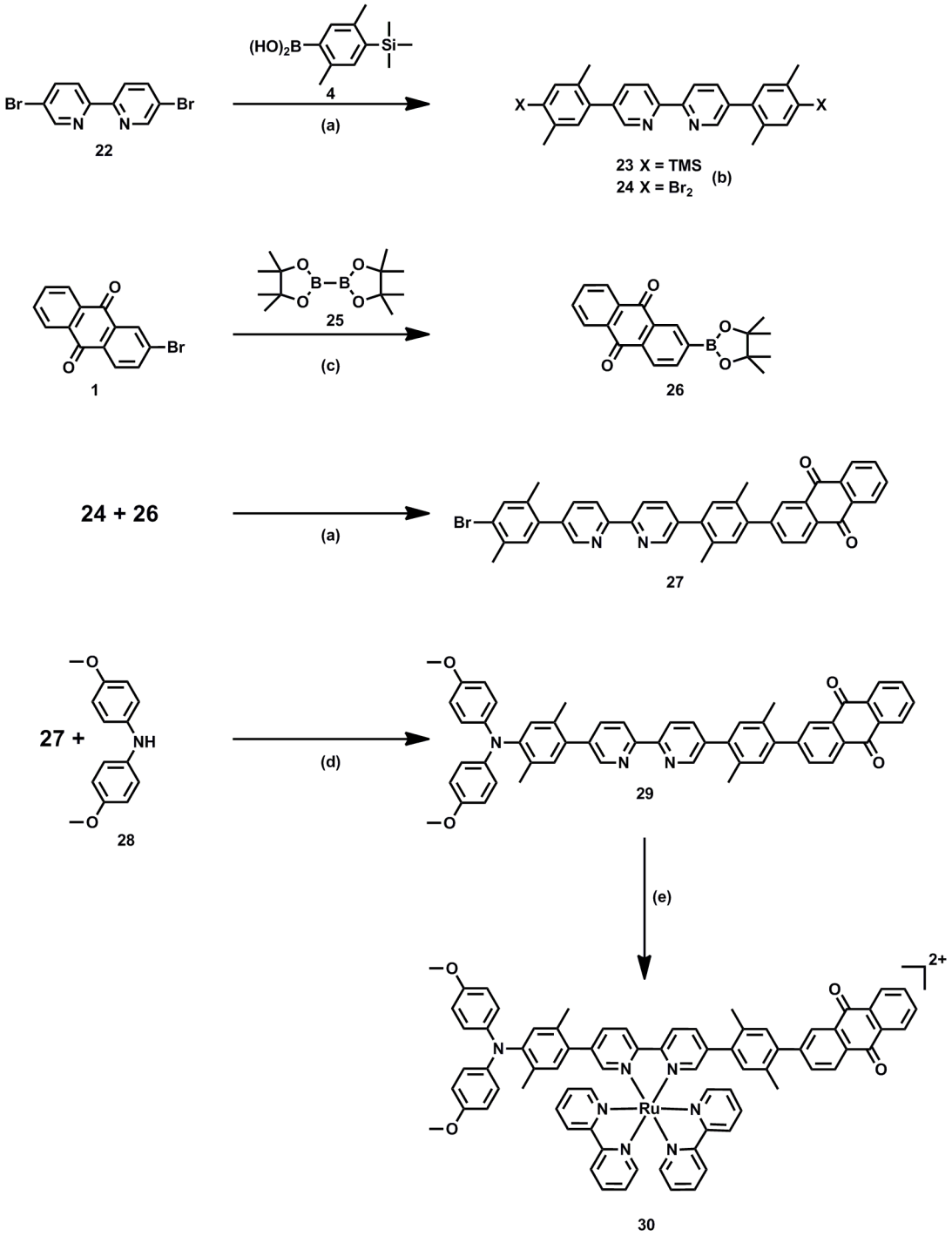

(a) $Pd(PPh_3)_4$, Na_2CO_3, THF/water 1:1(reflux), (b) Br_2, NaOAc, THF, 0°C, (c) $PdCl_2(dppf).CH_2Cl_2$, KOAc, DMSO, 80°C, (d) ^{t}BuOK, Pd(dba), $P(tbu)_3$, toluene, 60°C, (e) $Ru(bpy)_2Cl_2$, ethanol/chloroform 10:3 (reflux).

Scheme 2.4: Synthetic strategy leading to the ruthenium triad.

To summarize Scheme 2.4, 5,5'-dibromo-2,2'-bipyridine (**22**) is coupled to 2,5-dimethoxy-4-trimethylsilylphenylboronic acid (**4**) using an efficient $Pd(PPh_3)_4$ catalyst. The resulting TMS product (**23**) is deprotected through reaction with bromine (Br_2) in order to give product **24**. To synthesize molecule **26**, two commercial compounds namely 2-bromoanthraquinone (**1**) and bis(pinacolato)diboron (**25**) are coupled together using $PdCl_2(dppf)\cdot CH_2Cl_2$ as a catalyst for this reaction.

Consecutively, to build the first part of the ligand (**27**) which contains the electron acceptor (AQ), a Suzuki-coupling reaction has been performed between **24** and **26**. The next step was effected by adding the electron donor (**28**) to molecule **27** in order to get the final ligand **29**. Toward this end, an N-C coupling reaction between **27** and the commercial electron donor molecule 4,4'-dimethoxydiphenylamine (**28**) has been carried out. The final ligand (**29**) containing both AQ and TAA is then reacted with $Ru(bpy)_2Cl_2$ yielding to TAA-Ru^{2+}-AQ (**30**) in 75 % yield. The resulting complex is now ready for the spectroscopic measurements.

The overall yield starting from molecule **22** to reach the final ligand (**29**) is about 33%.

II-1.2 Optical absorption spectroscopy

Figure 2.1 shows the optical absorption spectra of the ruthenium triad (**TAA-Ru^{2+}-AQ**) and the corresponding two dyads. In fact, in the **Ru-TAA** dyad the electron is transferred only from TAA to Ru, whereas in **Ru-AQ** dyad the electron is transferred from Ru to AQ. These two dyads are necessary in order to understand the electron transfer in the triad molecule which contain both ways of electron transfer: first from TAA to Ru and then from Ru to AQ. $Ru(bpy)_3^{2+}$, abbreviated as **Ru** is used as a reference complex.

In all four absorption spectra, the ^{1}MLCT band is located at 450 nm. Another prominent band with high extinction coefficient is at 290 nm which is attributed to a bpy-localized π-π* transition. An absorption band due to the anthraquinone units seems to be between 310 nm and 380 nm, and it is observed in Ru-triad and Ru-AQ. The TAA unit absorbs at wavelengths below 300 nm.

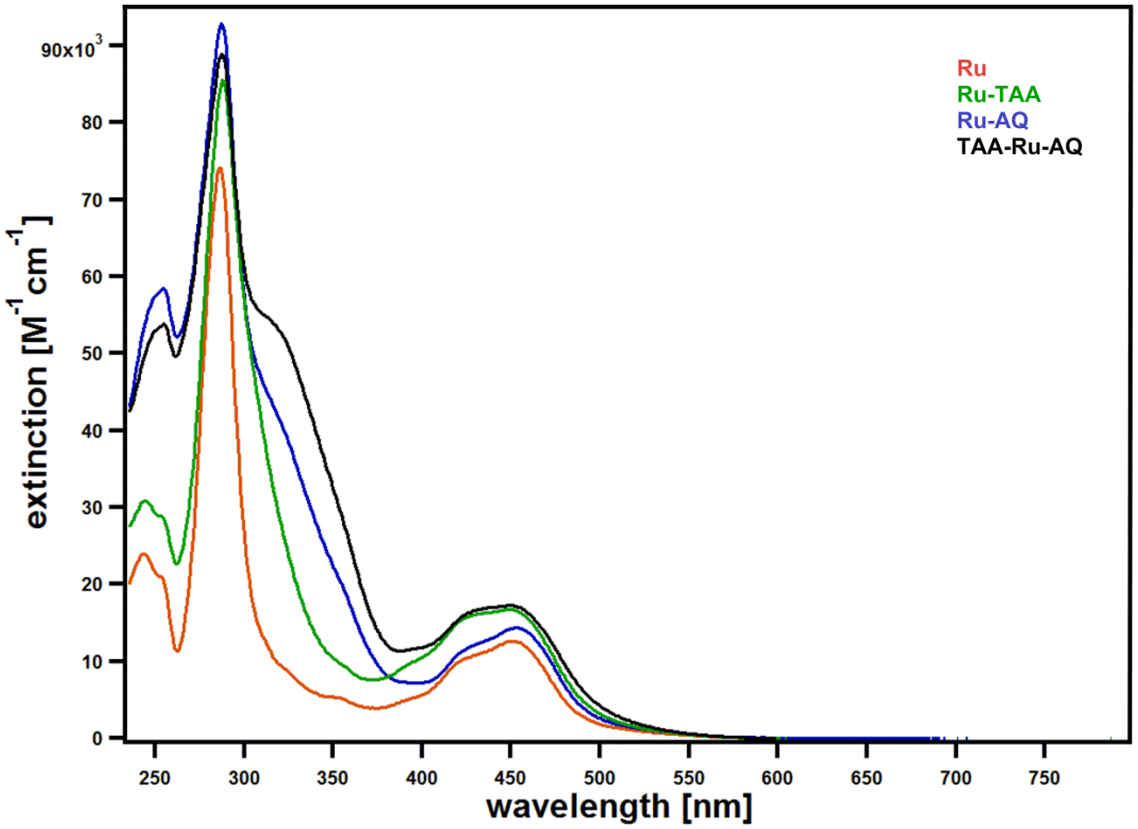

Figure 2.1: UV-Vis absorption spectra in acetonitrile solution of the investigated ruthenium triad and dyads with $Ru(bpy)_3^{2+}$ as molecular reference.

II-1.3 Steady-state luminescence spectroscopy

The ^{3}MLCT emission bands of the triad, the two dyads and that of the ruthenium reference complex are represented in Figure 2.2. Excitation of these complexes occurred at 450 nm and the detection was taking place between 470 and 780 nm. The maximum of the four bands is at 610 nm. The emission intensity in Ru-AQ is similar to that of the reference indicating that the luminescence is not affected in presence of the AQ unit, whereas significant luminescence quenching is detected in the case of TAA-Ru^{2+}-AQ and Ru-TAA. This quenching indicates that the excited state is deactivated either by a photoinduced electron transfer mechanism or by a triplet-triplet energy transfer process. The latter process is thermodynamically unlikely since the triplet excited states of AQ (~2.7 eV) and TAA (~3.2 eV) are energetically higher than the triplet excited state of Ru (2.12 eV).

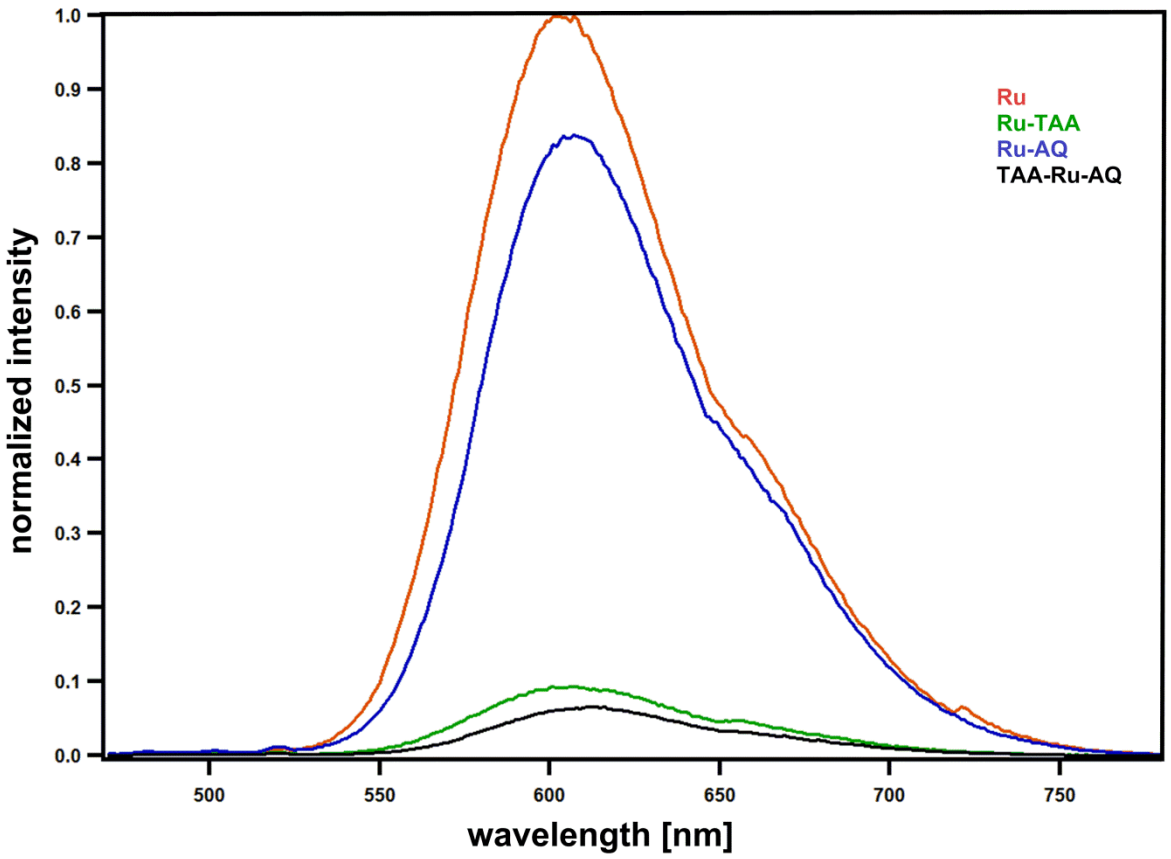

Figure 2.2: Luminescence spectra of the four complexes measured in aerated acetonitrile solution. Excitation occurred at 450 nm.

II-1.4 Electrochemistry experiments and establishing of the energy level diagram for the TAA-Ru^{2+}-AQ triad

The cyclic voltammograms of the four compounds shown in Figure 2.3 were measured in deoxygenated acetonitrile solution using a platinum disk as the working electrode. All redox waves are calibrated with respect to the oxidation wave of ferrocene at 0.0 V which was added to the solution in relatively small amounts. Tetrabutlyammonium hexafluorophosphate ($TBAPF_6$) was used as supporting electrolyte.

The four complexes present a common wave around 0.9 V which is assigned to the oxidation of $Ru^{2+}$to Ru^{3+}. Three well-defined waves between -1.7 and -2.1 correspond to the reduction of the three bpy ligands. These waves are present in all compounds considered here. In order to simplify, the first reduction bpy wave is designated as the reduction wave of the entire ruthenium complex (Ru^{2+}/Ru^{+}). In Ru-TAA and TAA-Ru^{2+}-AQ, a wave at 0.3 V is attributed

to the oxidation of TAA (TAA^{+}). The anthraquinone reduction wave is at -1.28 V and it appears in TAA-Ru^{2+}-AQ and Ru-AQ. All these potential values are summarized in Table 2.1 The similarity in the redox potentials of the individual Ru, TAA and AQ components in the triad and dyad systems with those of their isolated species [20-26] lead to the conclusion that these components are electronically weakly coupled to each other in these particular systems.

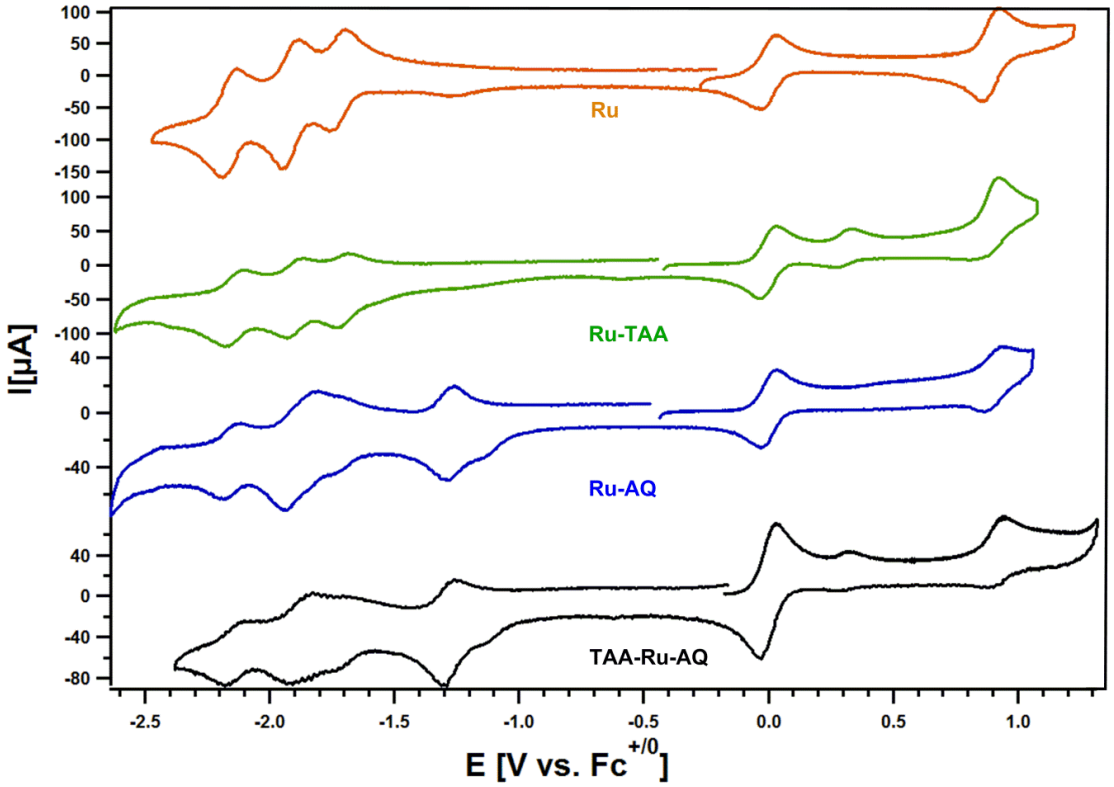

Figure 2.3: Cyclic voltammograms of the four relevant complexes measured in acetonitrile solution in presence of 0.1 M of $TBAPF_6$. The scan rate was 100 mV/s.

	Ru	Ru-TAA	Ru-AQ	TAA-Ru-AQ
Ru^{3+}/Ru^{2+}	0.89	0.89	0.90	0.92
$TAA^{+/0}$		0.30		0.30
$AQ^{0/-}$			-1.28	-1.27
$bpy^{0/-}$	-1.72	-1.70	-1.72	-1.73
$bpy^{0/-}$	-1.91	-1.90	-1.90	-1.86
$bpy^{0/-}$	-2.15	-2.13	-2.14	-2.13

Table 2.1: Redox potential values in Volts vs. Fc^{+}/Fc extracted from the data from Figure 2.3.

Once the redox potentials of the triad and dyads systems are known, the energy levels of the different states that could be obtained while exciting the triad molecule can be established. In order to calculate these relevant levels, equation 1.1 from chapter 1 and the potentials from the Table 2.1 have been used for this purpose. The energy level diagram in Scheme 2.5 was obtained. The ^{3}MLCT excited state of the ruthenium triad is designated as TAA-*Ru^{2+}-AQ (2.12 eV above the ground state). From this excited state, the system may undergo either an oxidative quenching leading to the formation of the TAA-Ru^{3+}-AQ^{-} state at 2.19 eV or a reductive quenching to produce the TAA^{+}-Ru^{+}-AQ state at 2.03 eV.

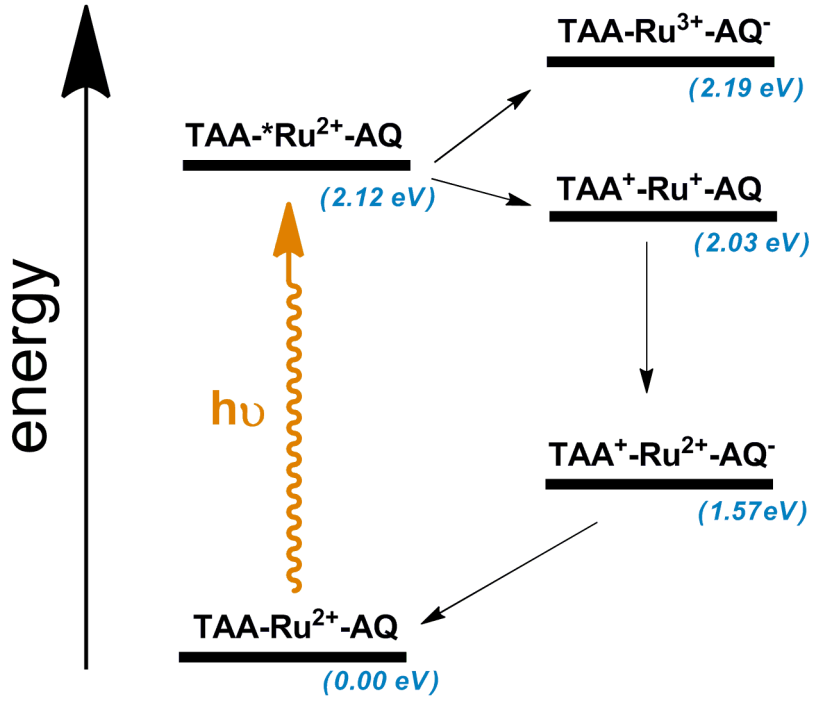

Scheme 2.5: Energy level diagram for the TAA-Ru^{2+}-AQ triad.

II-1.5 Transient absorption spectroscopy and spectroelectrochemistry experiments

In the above diagram (Scheme 2.5), one may notice that the initial electron transfer step from *Ru^{2+} to AQ is endergonic by 0.07 eV in acetonitrile solution. By contrast, the driving force for electron transfer from TAA to *Ru^{2+} seems to be exergonic by 0.09 eV. Hence, we may predict that upon photoexcitation of Ru, the electron is probably transferred first from TAA to Ru and then from Ru to AQ rather than the opposite sequence (Ru to AQ and then TAA to Ru). The formation of the radical cation (TAA^{+}) first and the radical anion (AQ^{-}) second leads

to the charge-separated state at 1.57 V. The overall process from the initial ^{3}MLCT excited state is highly exergonic (ΔG_{ET} = 0.55 eV) (Scheme 2.5).

In order to detect the formation of the relevant radicals, nanosecond transient absorption spectroscopy has been used. The results obtained are corroborated by spectroelectrochemistry data discussed below.

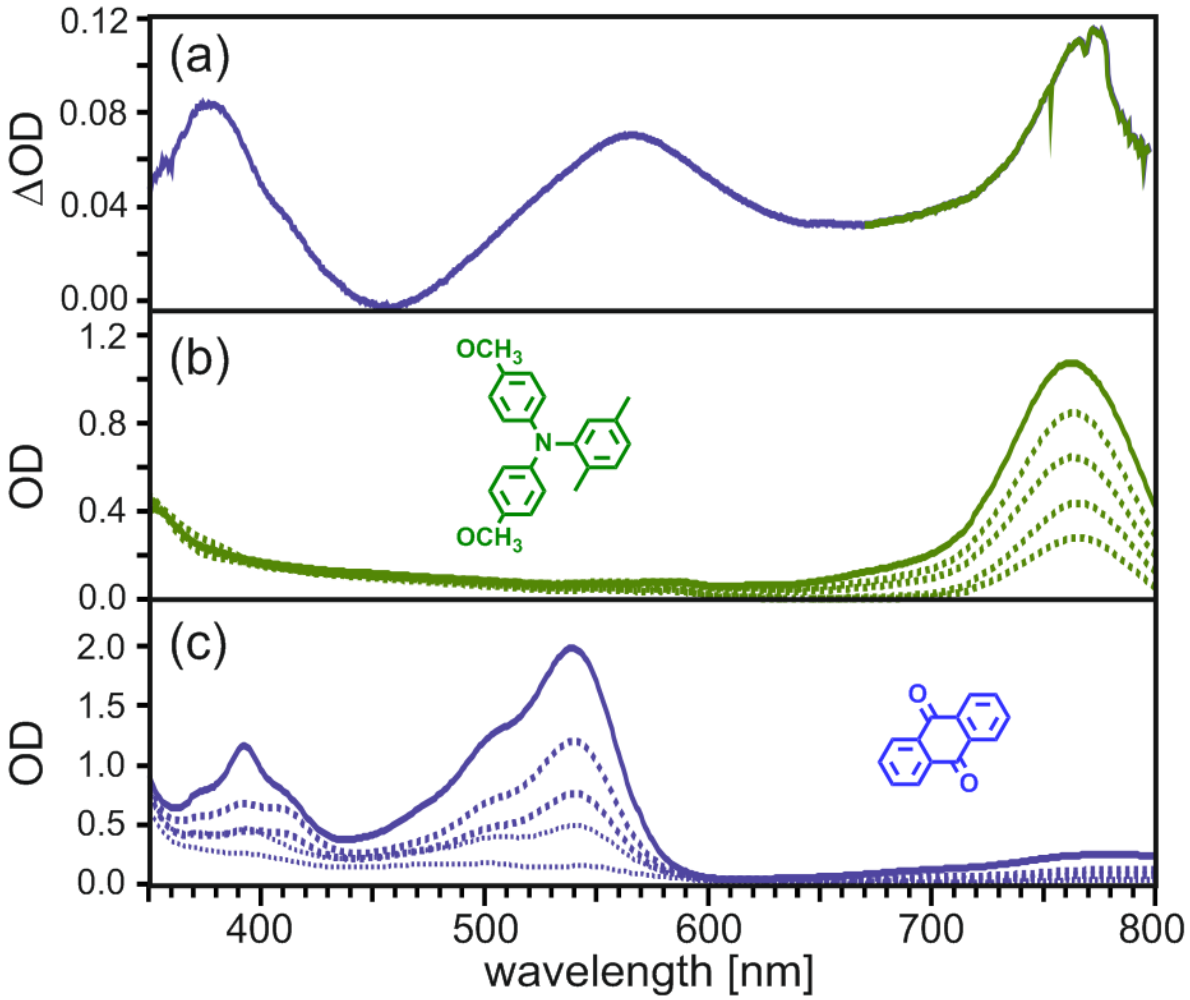

Figure 2.4: (a) Transient absorption spectrum of TAA-Ru^{2+}-AQ in deoxygenated acetonitrile solution; (b) aborption band detected during the oxidation of a TAA reference (inset) in acetonitrile solution; (c) absorption band detected during the reduction of AQ compound (inset) in dichloromethane solution.

Figure 2.4a shows the transient absorption spectrum of the TAA-Ru^{2+}-AQ triad. This spectrum is measured in deoxygenated acetonitrile solution. Excitation occurred at 450 nm with 8 ns laser pulses. The signal was detected in a 200 ns time window immediately after the

pulse. Three bands with maxima at 770, 570 and 380 nm are observed and are clearly related to the formation of the radical species.

Although we have a preliminary idea about which bands belong to TAA^+ and which to the monoanion radical AQ^- [22,23,26-30], spectroelectrochemistry measurements were necessary in order to clarify this point. Figure 2.4b shows the absorption bands of a TAA reference molecule during its electrochemical oxidation at a potential of 0.5 V vs. Fc^+/Fc. An absorption maximum appears at 770 nm. Figure 2.4c presents the absorption spectrum of AQ monoanion detected at 540 nm and 392 nm. These bands were obtained upon electrochemical reduction of AQ at a potential more negative than -1.2 V vs. Fc^+/Fc in CH_2Cl_2. Therefore, we may now be sure that the band at 770 nm is indeed belonging to the radical cation (TAA^+), whereas the two absorption bands at 570 nm and 380 nm are due to the radical monoanion (AQ^-).

After providing direct experimental evidence for the formation of the fully charge-separated state TAA^+-Ru^{2+}-AQ^-, we may expect that these two radicals should decay simultaneously back to the ground state (Scheme 2.5).

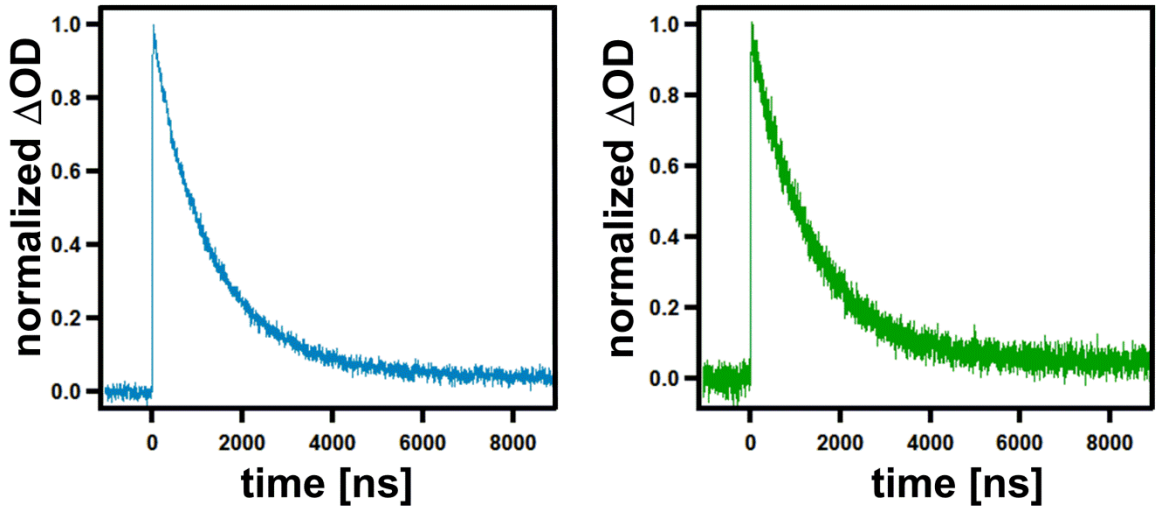

Figure 2.5: Decay kinetics at 570 nm (left) and 770 nm (right) of the ruthenium triad in acetonitrile.

Figure 2.5 shows the decays of the transient absorption spectra from Figure 2.4a at 570 nm and 770 nm in deoxygenated acetonitrile solution. Single exponential fits yield a decay time of 1300 ns at 570 nm and 1342 at 770 nm. These two decays are identical within experimental

accuracy. This result is in agreement with our expectation since TAA^+ and AQ^- disappear together in a thermal charge-recombination event (Scheme 2.5).

II-1.6 Determination of the quantum yield for formation of charge-separated states

In order to estimate the quantum yield for formation of the fully charge-separated state TAA^+-Ru^{2+}-AQ^-, the rate constants for the formation of each state from Scheme 2.5 are still missing. After calculating the relevant rate constants (details presented in the next paragraph), Scheme 2.6 has been established.

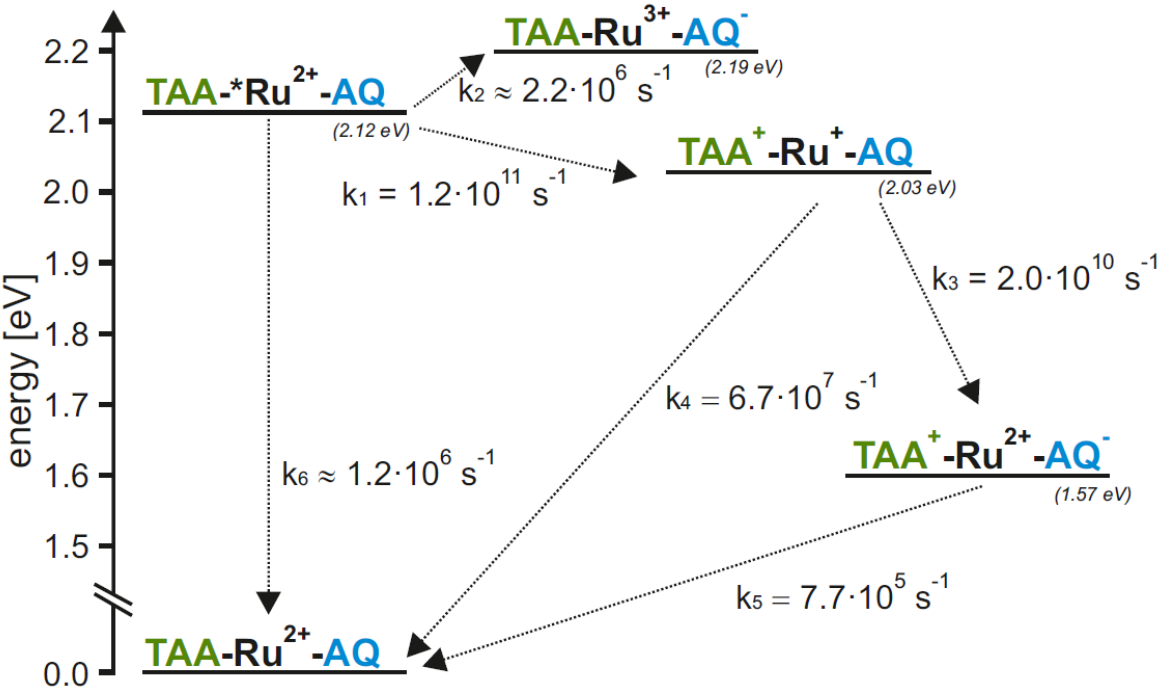

Scheme 2.6: Energy level scheme of the different excited states of the TAA-Ru^{2+}-AQ triad.

The rise times of the radical species (TAA^+ and AQ^-) were measured using a femtosecond transient absorption instrument which is available in the group of Prof. Lemmetyinen at Tampere University of Technology in Finland. Figure 2.6 shows rises of the transient absorption signal of AQ^- at 570 nm (a) and TAA^+ at 770 nm (b). These two radicals are formed in 9 ps and 50 ps, respectively.

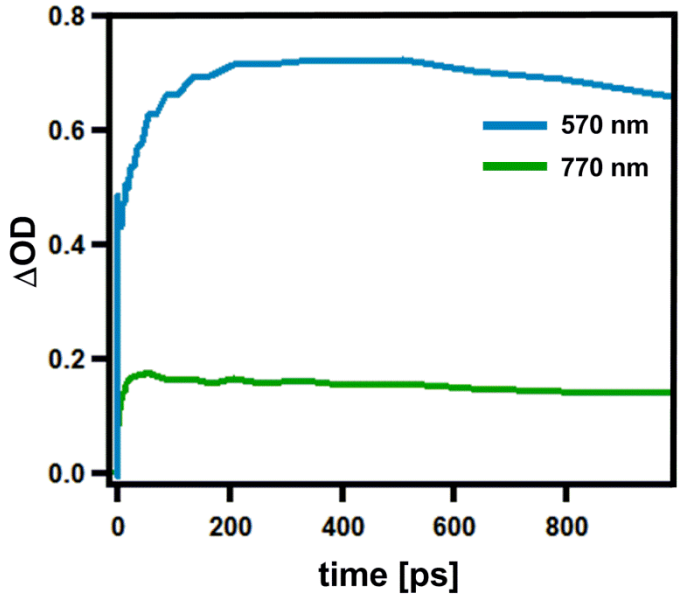

Figure 2.6: Rise of the transient absorption signals at 570 nm (blue trace) and at 770 nm (green trace) after excitation of a deoxygenated acetonitrile solution of TAA-Ru^{2+}-AQ at 450 nm with femtosecond laser pulses.

In other words, the forward electron transfer happens from TAA to Ru^{2+} with a time constant of $k_1 = 1.2 \cdot 10^{11}$ s^{-1} leading to the TAA^{+}-Ru^{+}-AQ state at 2.03 eV. Then the electron is transferred from Ru^{+}-to-AQ with a time constant of $k_3 = 2.0 \cdot 10^{10}$ s^{-1} while maintaining the hole at the TAA^{+}. Therefore, the fully charge-separated state (TAA^{+}-Ru^{2+}-AQ^{-}) is built within 100 ps. It then exhibits lifetime of 1340 ns corresponding to a rate constant of $k_5 = 7.7 \cdot 10^{5}$ s^{-1} (Scheme 2.6).

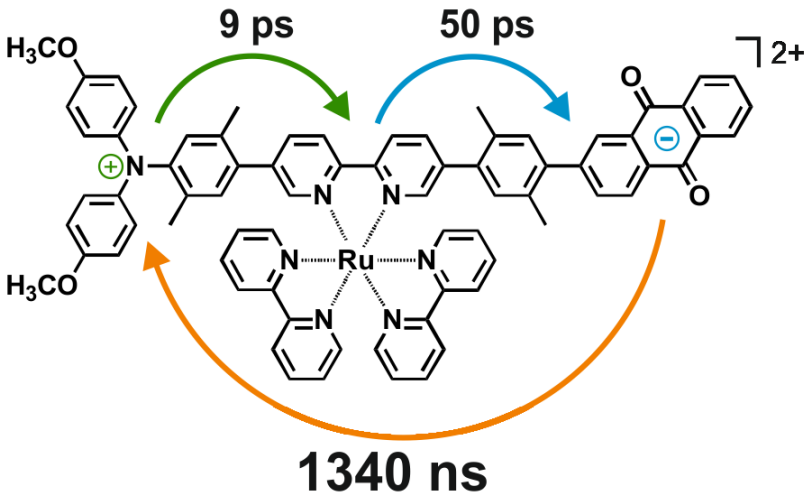

Scheme 2.7: Formation and disappearance of the fully charge-separated state in TAA-Ru^{2+}-AQ.

The rate constant $k_2 = 2.2 \cdot 10^6\ s^{-1}$ for Ru^{2+} to AQ electron transfer has been reported already in chapter 1. It was obtained from time-resolved luminescence data of the Ru^{2+}-AQ dyad in deoxygenated acetonitrile solution. The TAA^+-Ru^+-AQ state at 2.03 eV may undergo Ru^+ to TAA^+ back electron transfer with a time constant of $k_4 = 6.7 \cdot 10^7\ s^{-1}$ (Scheme 2.6). This rate constant was estimated from the decay time (15 ns) of the TAA-Ru^{2+} dyad at 770 nm (Figure 2.7). From this value, one may conclude that once the TAA^+-Ru^+-AQ state at 2.03 eV is formed, the system is much more likely to undergo Ru^+ to AQ electron transfer ($k_1 = 1.2 \cdot 10^{11}\ s^{-1}$) rather than Ru^+ to TAA^+ back electron transfer ($k_4 = 6.7 \cdot 10^7\ s^{-1}$) (Scheme 2.6).

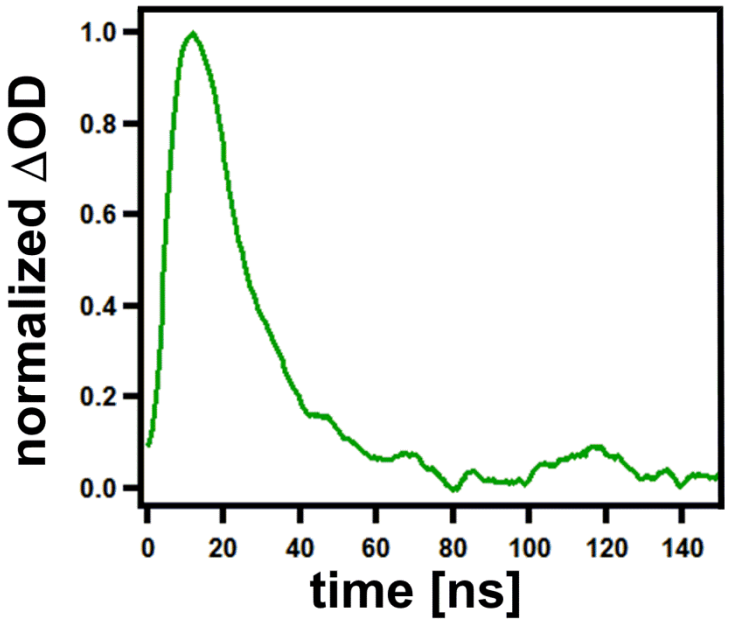

Figure 2.7: Decay of the transient absorption signal at 770 nm in the TAA-Ru^{2+} dyad in deoxygenated acetonitrile solution.

In order to estimate the quantum yield for formation of TAA^+-Ru^{2+}-AQ^- state, knowledge of the ^{3}MLCT lifetime of the reference complex $Ru(bpy)_3^{2+}$ is further necessary. It has been measured previously (chapter 1) and it was about 866 ns in deoxygenated acetonitrile solution. This lifetime corresponds to a rate constant of $k_6 = 1.2 \cdot 10^6\ s^{-1}$.

Based on the kinetic data from Scheme 2.6, the quantum yield Φ for the formation of the fully charge-separated state TAA^+-Ru^{2+}-AQ^- is estimated to be 99.7%. It means that almost every photon put into the $Ru(bpy)_3^{2+}$ ^{3}MLCT state at 2.12 eV leads to the formation of a molecule in the TAA^+-Ru^{2+}-AQ^- state at 1.57 eV.

In the following sections, analogous series of osmium and iridium triads and dyads have been investigated. In the ruthenium triad the charge-separated state was obtained via electron transfer from TAA to Ru and then from Ru to AQ. In the osmium triad, the opposite sequence is expected to take place. In other words, we are expecting an electron transfer from AQ to Os first and then from the reduced Os to TAA. In the analogous iridium triad both ways are thermodynamically possible and therefore kinetically competitive. In spite of three different sequences, the energy of the fully charge separated states is expected to be independent of the metal. Therefore an identical decay around 1.3 μs is expected in all three cases. All these informations will be detailed subsequently.

Our main interest behind the synthesis of osmium and iridium complexes is to study the rates and quantum yields for formation of the fully charge-separated states in these two series compared to that of ruthenium and to explore whether they will be affected by the fact that this state is formed via different reaction pathways.

II-2.Triads and dyads that incorporate $Os(bpy)_3^{2+}$ as a photosensitizer

Scheme 2.8 represents the molecular structure of the osmium triad (TAA-Os^{2+}-AQ) containing both TAA electron donor and AQ electron acceptor, while the osmium dyads contain either the electron donor (TAA-Os) or the electron acceptor (Os-AQ). $Os(bpy)_3^{2+}$ (Os) is used as a reference molecule.

In order to synthesize the TAA-Os^{2+}-AQ molecule, the same strategy as for TAA-Ru^{2+}-AQ was followed. The only difference is in the final step for which $Ru(bpy)_2Cl_2$ was replaced by $Os(bpy)_2Cl_2$.

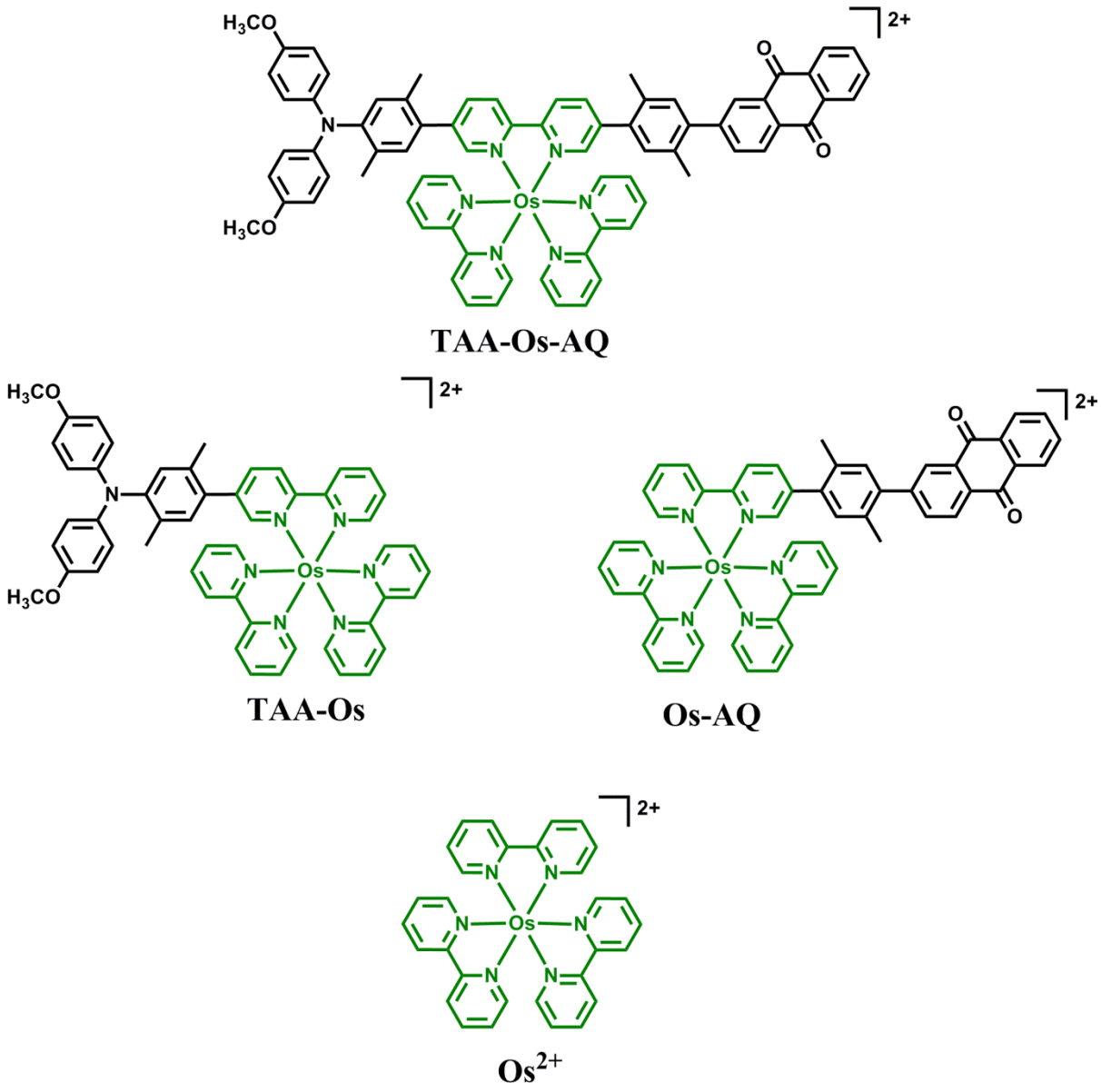

Scheme 2.8: Molecular structures of osmium triad, dyads, and reference complex.

II-2.1 Optical absorption and steady-state luminescence spectroscopy

Figure 2.8 shows the absorption spectra of the osmium series of complexes in acetonitrile solution. The ^{1}MLCT state band caused by the transition from a d-metal orbital to a ligand-based orbital (π^*) is located in the range of 400-520 nm. An additional band was detected between 520 and 700 nm, and this is most likely due to a ^{3}MLCT absorption which becomes detectable because of the relaxation of spin selection rule in the 5d-metal. Another characteristic band is a bpy-localized π-π^* absorption located at 290 nm. For the absorption of

the anthraquinone moiety bands between 310 and 380 nm were detected, and they are observable in TAA-Os^{2+}-AQ and Os-AQ.

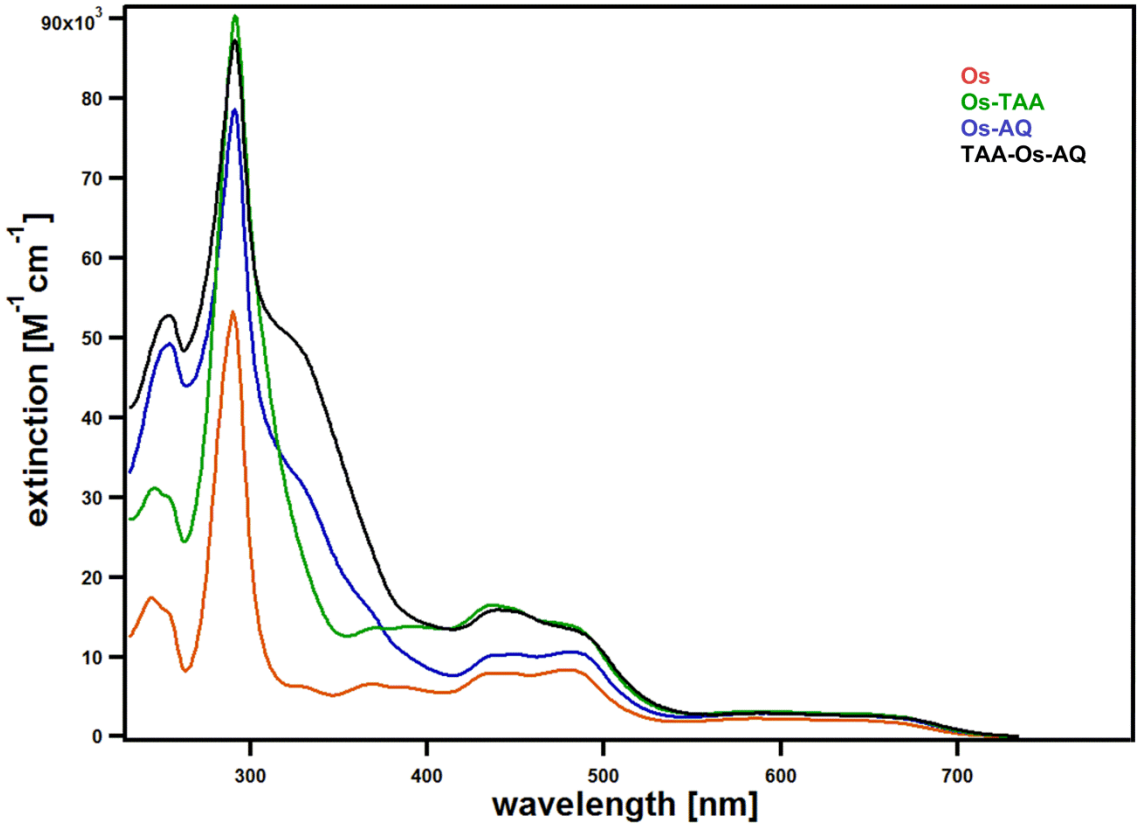

Figure 2.8: Absorption spectra of the four osmium complexes in acetonitrile solution.

The absorption spectrum of the osmium dyads and triad correspond more or less to the sum of the absorption spectra of the individual molecular components. This finding indicates that in the triad and dyads systems the different components are electronically weakly coupled, as noted already for the ruthenium systems.

II-2.2 Steady-state luminescence spectroscopy

The steady-state luminescence spectra in acetonitrile solution are represented in Figure 2.9. They were obtained after excitation of the osmium complexes at 600 nm. The luminescence seems to be susceptible to the presence of AQ which causes more quenching in Os-AQ and TAA-Os^{2+}-AQ compared to Os-TAA. This luminescence quenching is due to a photoinduced electron transfer which dominates over the triplet-triplet energy transfer since the triplet

excited-state of Os (1.79 eV) is lower than the triplet energy states of AQ (2.69 eV) and TAA (3.2 eV).

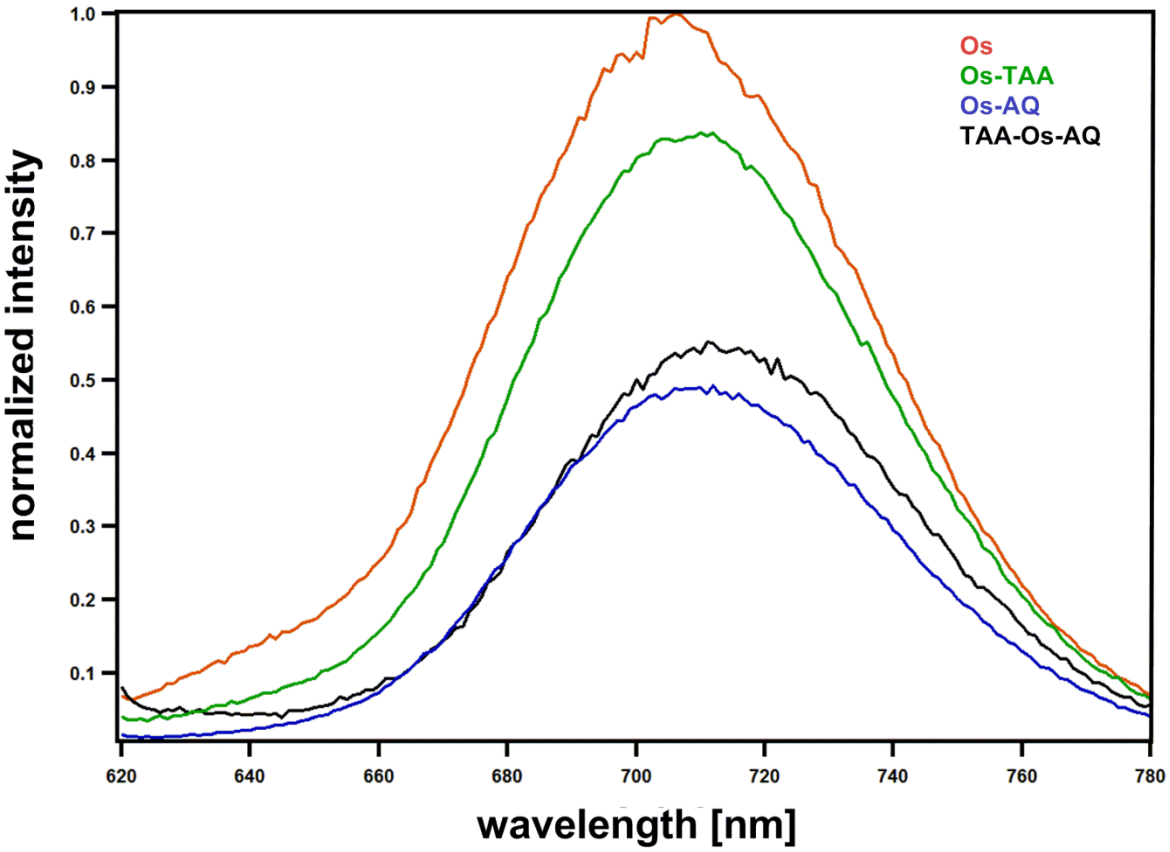

Figure 2.9: Luminescence spectra for osmium compounds in acetonitrile solution. Excitation occurred at 600 nm.

II-2.3 Electrochemistry

Figure 2.10 shows the cyclic voltammograms of the osmium complexes in deoxygenated acetonitrile solution at room temperature, in presence of ferrocene (Fc) used as an internal reference. The half-wave redox potentials extracted from these voltammograms are reported in Table 2.2.

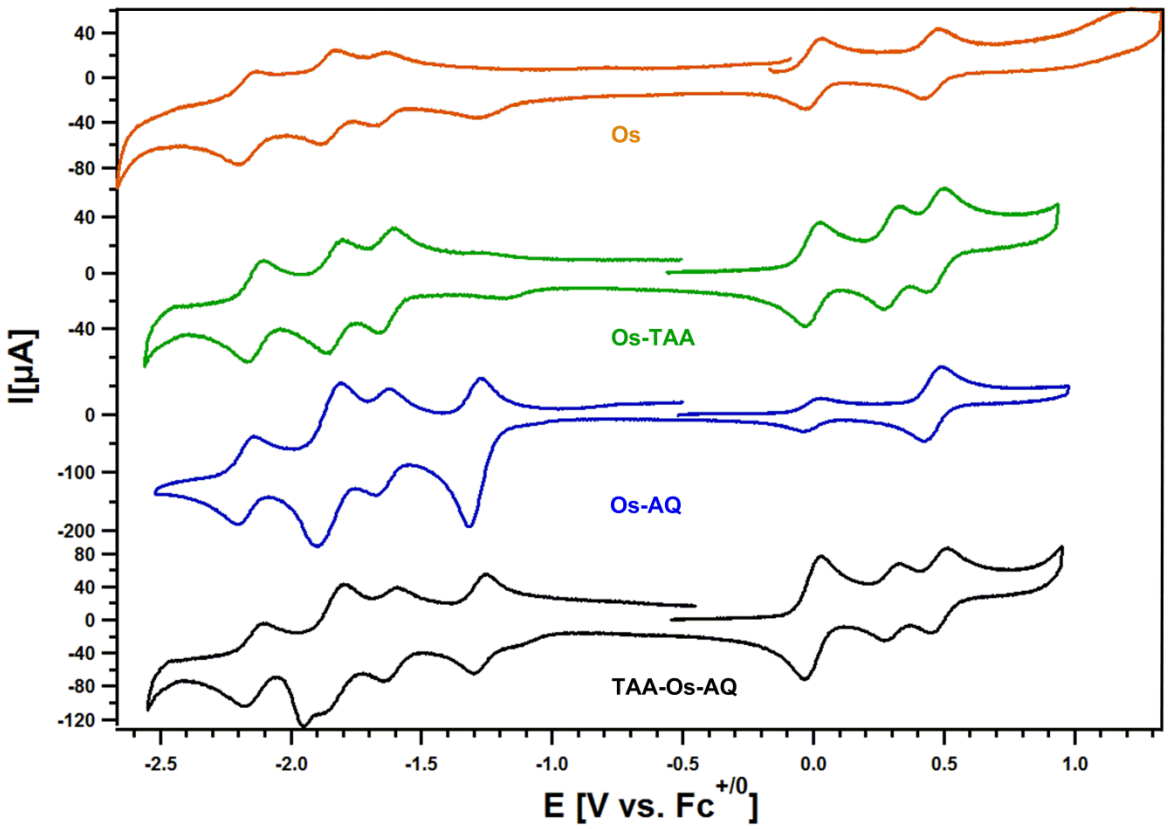

Figure 2.10: Voltammograms of TAA-Os^{2+}-AQ complex with the corresponding two dyads and the reference complex measured in deoxygenated acetonitrile solution. $TBAPF_6$ is used as electrolyte.

	Os	Os-TAA	Os-AQ	TAA-Os-AQ
Os^{3+}/Os^{2+}	0.45	0.47	0.46	0.48
$TAA^{+/0}$		0.30		0.30
$AQ^{0/-}$			-1.29	-1.28
$bpy^{0/-}$	-1.67	-1.63	-1.65	-1.62
$bpy^{0/-}$	-1.86	-1.84	-1.85	-1.83
$bpy^{0/-}$	-2.16	-2.13	-2.17	-2.14

Table 2.2: Redox potentials extracted from Figure 2.10. These values are reported versus the oxidation wave of ferrocene at 0.0 V

When comparing the redox potentials of the osmium complexes (Table 2.2) with those of ruthenium complexes (Table 2.1), TAA, AQ, and bpy redox potentials seem to be unaffected

by the change in metal. Only the metal oxidation wave (Os^{3+}/Os^{2+}) changes and it occurs at ~ 0.46 V in line with previous investigations [31]. As for ruthenium, the first reduction wave of the bpy ligand is considered as the reduction of the entire $Os(bpy)_3^{2+}$ complex to $Os(bpy)_3^{+}$. This process occurs at ~ -1.65 V (Table 2.2).

II-2.4 Energy level diagram

Based on the electrochemical potentials shown in Table 2.2, an energy level diagram can be established (Scheme 2.9) in analogous manner as described in chapter 1.

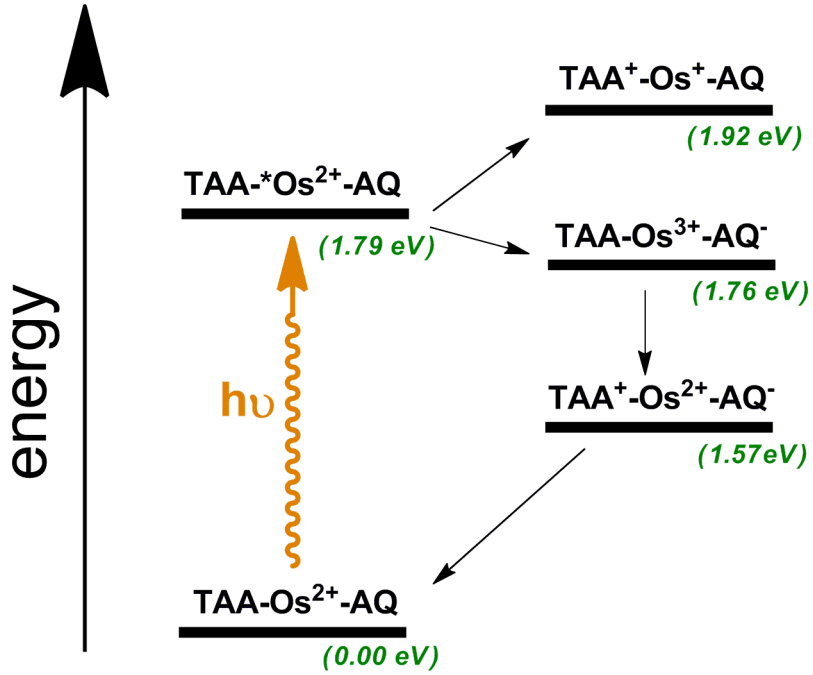

Scheme 2.9: Energy level scheme showing the different states that are accessible after photoexcitation of the osmium triad.

This energy level shows that the reductive quenching (electron transfer from TAA to $*Os^{2+}$) is an endergonic process, whereas the oxidative quenching (electron transfer from $*Os^{2+}$ to AQ) is exergonic by 0.03 eV. In fact, this result is in line with the steady-state luminescence spectra (Figure 2.9) and may explain the reason for the luminescence quenching in the complexes in presence of AQ and not in presence of TAA. The fully charge-separate state TAA^{+}-Os^{2+}-AQ^{-} lies at an energy of 1.57 eV which is the same as for TAA^{+}-Ru^{2+}-AQ^{-} (Scheme 2.5).

II-2.5 Transient absorption spectroscopy

The transient absorption spectrum of the osmium triad shown in Figure 2.11 exhibits identical absorption bands as in the case of ruthenium triad (Figure 2.4a). This spectrum is measured in deoxygenated acetonitrile solution. Excitation occurred at 532 nm with 8 ns laser pulses. The signal was detected in a 200 ns time window immediately after the pulse.

Not surprisingly, the fully charge-separated state at 1.57 eV is formed which is manifested by the formation of the relevant radical signals. The TAA^+ radical absorbs at 770 nm, while the AQ^- radical absorbs at 565 and 380 nm.

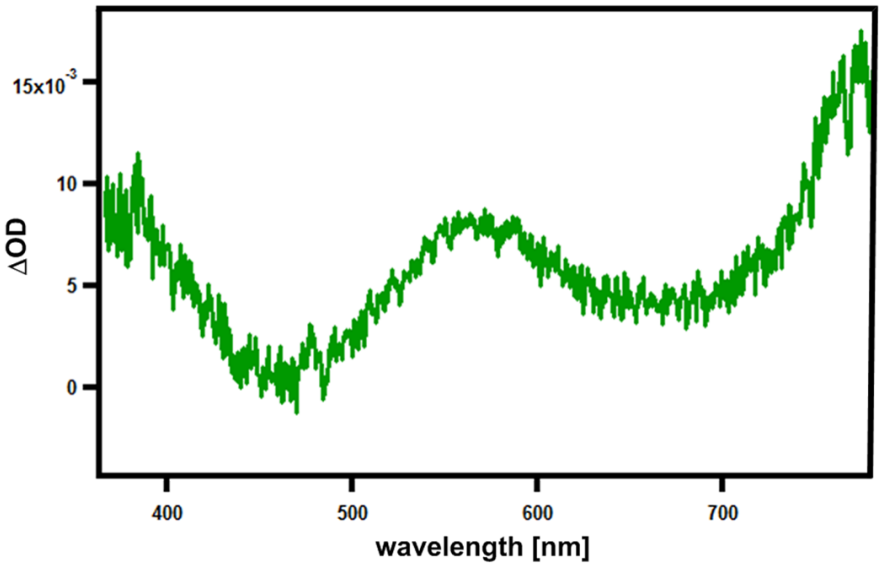

Figure 2.11: Transient absorption spectrum of the osmium triad measured in deoxygenated acetonitrile solution.

Moreover, we would expect a similar decay as in TAA^+-Ru^{2+}-AQ^- because the fully charge separated state is independent of the metal (Scheme 2.5 and 2.9). Therefore, a decay time around 1.3 µs should be detected. Our expectation was not fulfilled in TAA^+-Os^{2+}-AQ^-. A peculiar observation was made in this case: The recombination of the two relevant radicals occurs within 80 ns (Figure 2.12). This unexpected observation will be discussed in a subsequent paragraph.

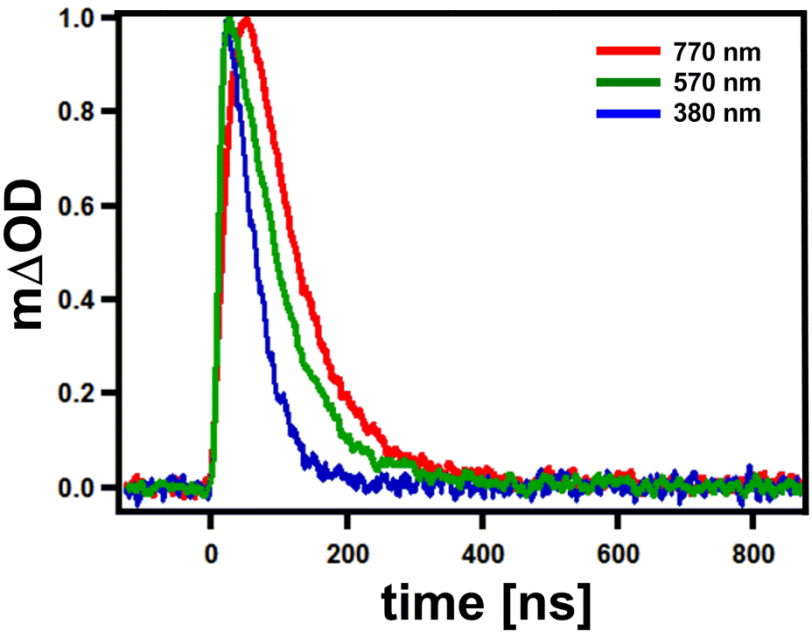

Figure 2.12: Decay kinetics at 770 nm (red trace), 570 nm (green trace) and 380 nm (blue trace) of the TAA-Os^{2+}-AQ molecule.

II-2.6 Kinetics and quantum yields for formation of charge-separated states in the osmium complexes.

For the determination of the quantum yield for the formation of the fully charge-separated state TAA^{+}-Os^{2+}-AQ^{-}, the rate constants of the levels presented in Scheme 2.9 must be calculated. Scheme 2.10 contains all the information that we need.

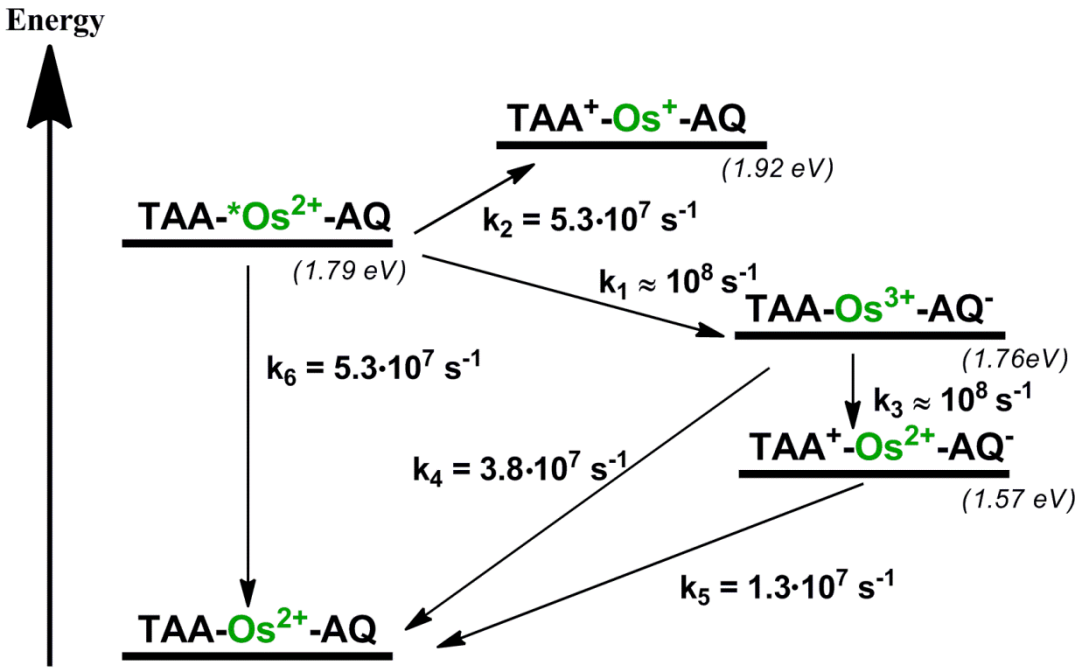

Scheme 2.10: Energy level scheme after excitation of TAA^{+}-Os^{2+}-AQ^{-} showing the rate constants of the different states.

Upon photoexcitation of TAA-Os^{2+}-AQ at 532 nm, oxidative quenching of the excited-state by AQ is thermodynamically likely since the electron transfer from Os to AQ is slightly exergonic (ΔG_{ET} = - 0.03 eV, Scheme 2.10). The TAA-Os^{3+}-AQ^{-} state is formed at 1.76 eV with a rise time of 10 ns ($k_1 \approx 10^8$ s^{-1}) as extracted from the rise of the transient absorption signal at 550 nm (Figure 2.13a, blue trace). The value of 10 ns is not accurate due to instrument limitation.

From the TAA-Os^{3+}-AQ^{-} state, there are two possibilities: (i) The electron is transferred from TAA to Os^{3+} giving the fully charge separated-state (TAA^{+}-Os^{2+}-AQ^{-}) at 1.57 eV (Scheme 2.10), and the radical cation (TAA^{+}) detected at 770 nm is formed in approximately 20 ns ($k_2 \approx 10^8$ s^{-1}) (Figure 2.13a, green trace). (ii) Thermal charge recombination between Os^{3+} and AQ^{-} leading back to the ground state TAA-Os^{2+}-AQ. In order to study the second possibility, transient absorption experiment was carried out on the Os-AQ dyad, where the AQ^{-} signal at 570 nm decays with a time constant of 26 ns (Figure 2.13b), corresponding to a rate constant of $k_4 = 3.8.10^7$ s^{-1}.

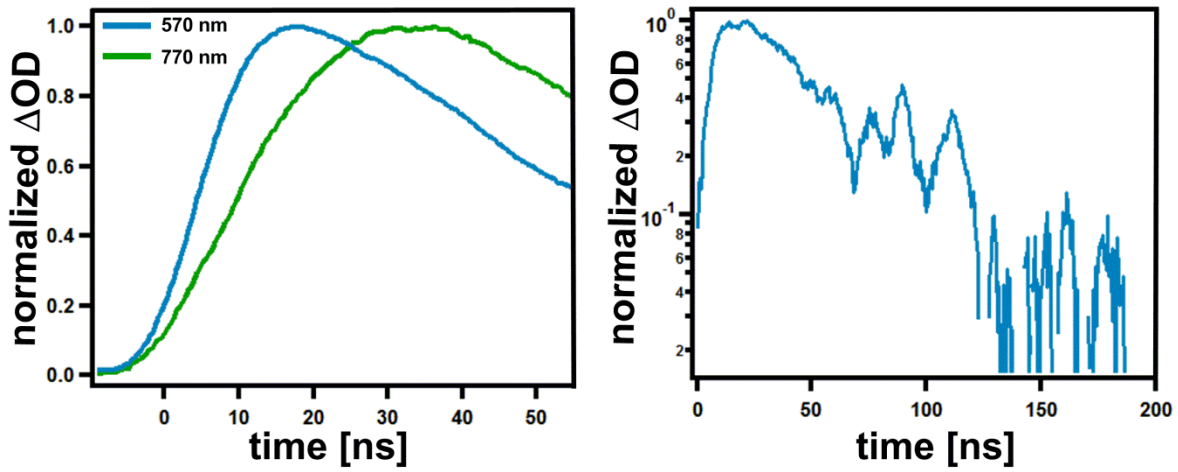

Figure 2.13: Left panel: Rise of the transient absorption signals at 570 nm (blue trace) and 770 nm (green trace) after excitation of the TAA-Os^{2+}-AQ triad at 450 nm with laser pulses of ~10 ns width (CH_3CN solution). Right panel: Decay of the transient absorption signal of the Os^{2+}-AQ dyad at 570 nm (AQ^- disappearance) after excitation at 450 nm with laser pulses of ~10 ns width (CH_3CN solution).

One piece of information is still missing in order to estimate the quantum yield for formation of the fully charge separated-state: the lifetime of the ^{3}MLCT excited-state of Os. For this purpose, a time-resolved luminescence spectroscopy experiment was performed with the $Os(bpy)_3^{2+}$ reference complex. It was found that the ^{3}MLCT decay rate constant of $Os(bpy)_3^{2+}$ is $k_6 = 5.3.10^7\ s^{-1}$ in deoxygenated acetonitrile solution.

From the rate constants in Scheme 2.10, one may conclude that the fully charge-separated state is formed with a quantum yield of ~ 46% out of the initially excited $Os(bpy)_3^{2+}$ ^{3}MLCT state.

To understand why the fully charge-separated state (TAA^+-Os^{2+}-AQ^-) decays within 80 ns instead of ~ 1.3 µs as for the TAA^+-Ru^{2+}-AQ^- state, one possible explanation could be as follows: Given the fact that the TAA-Os^{3+}-AQ^- at 1.76 eV is energetically only 0.18 eV above the fully charge separated state at 1.58 eV (Scheme 2.10), a thermal one-back-electron transfer from AQ^- to Os^{2+} might be possible in this case. In other words, both states (TAA-Os^{3+}-AQ^- and TAA^+-Os^{2+}-AQ^-) will be populated due to the rather small energy gap between them. Hence, the thermal population of the state TAA-Os^{3+}-AQ^- at 1.76 eV and rapid charge

recombination from this state ($k_4 = 3.8.10^7\ s^{-1}$) might be responsible for the comparatively fast depopulation (80 ns) of the TAA^+-Os^{2+}-AQ^- state at 1.58 eV.

Another possible explanation is that once the TAA^+-Os^{2+}-AQ^- state at 1.57 eV is formed, charge recombination of TAA^+ and AQ^- radicals could lead back to the ^{3}MLCT excited state at 1.79 eV which is only 0.21 eV above the fully charge-separated state.

II-3. Triads and dyads that incorporate $[Ir(2\text{-}(p\text{tolyl})pyridine)_2(bpy)]^+$ as a photosensitizer

In the previous sections, we thoroughly studied two systems based on ruthenium and osmium as photosensitizers. We have found that after photoexcitation of the metal, the initial electron transfer is not the same. In the ruthenium system reductive quenching dominates, whereas in the osmium system oxidative quenching occurs first. Therefore, it was obvious to enlarge our investigations into a system where both oxidative and reductive quenching are thermodynamically possible and therefore kinetically competitive.

For this purpose, the TAA-Ir^{3+}-AQ triad and its corresponding dyads (TAA-Ir and Ir-AQ) containing cyclometalated iridium as a photosensitizer have been synthesized (Scheme 2.11). $[Ir(2\text{-}(p\text{-tolyl})pyridine)_2(bpy)]^+$ was used as a reference complex and it was designated as Ir.

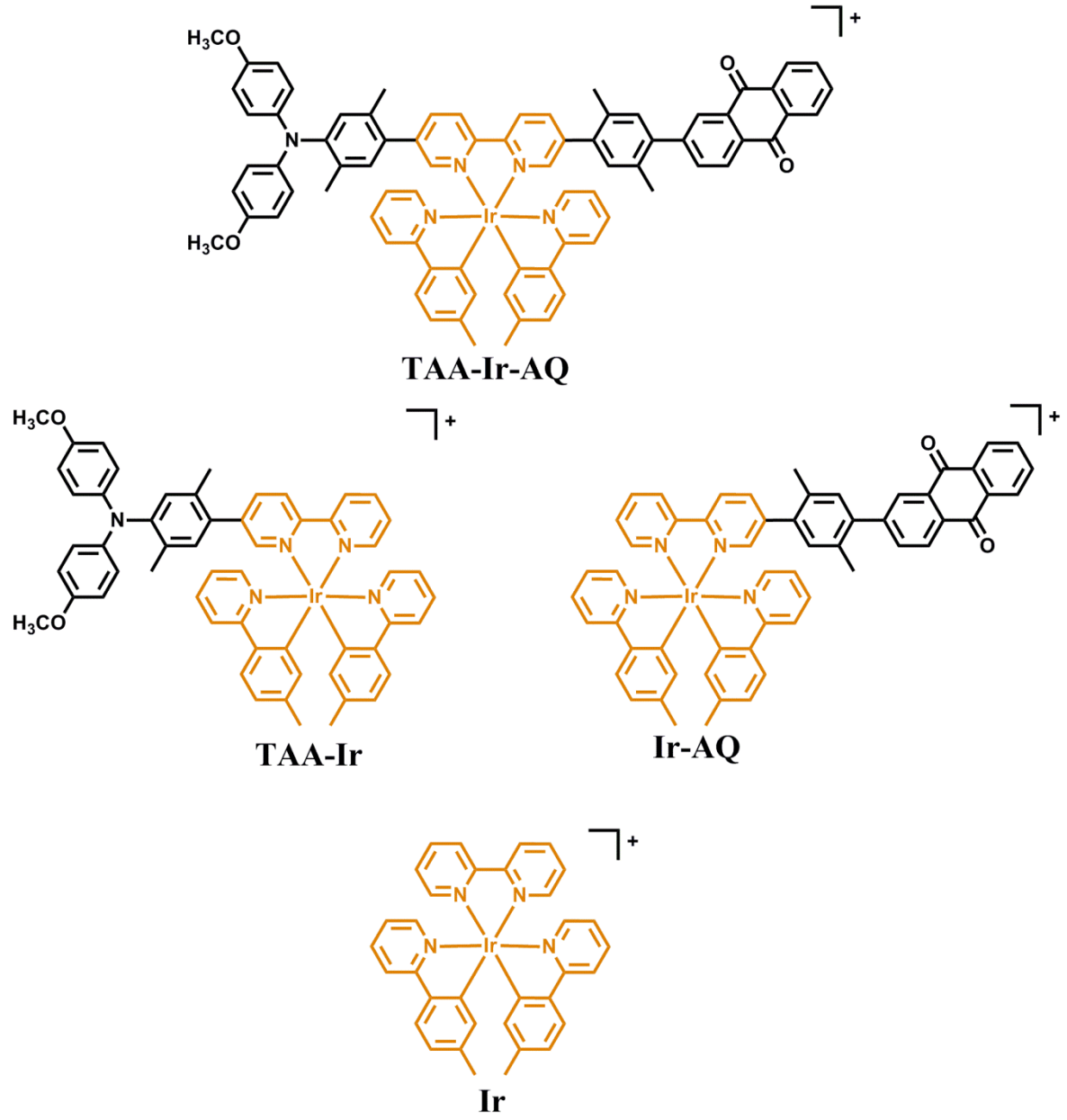

Scheme 2.11: Iridium triad with the relevant two dyads and the reference complex.

The synthesis of the ligand for the triad complex was reported previously in this chapter (ligand 29, Scheme 2.4). Thus, in order to get the final triad complex, the [Ir(2-(*p*-tolyl)pyridine)$_2$(Cl)]$_2$ precursor complex was used and was reacted with ligand **29** in 87 % yield.

II-3.1 Optical absorption and luminescence spectroscopy

Figure 2.14 (left) shows the optical absorption spectra of the complexes shown in Scheme 2.11. In Addition to bpy-localized absorptions in the range of 255-275 nm, the iridium

complexes exhibit ^{1}MLCT and ^{3}MLCT absorption bands around 400 nm. For Ir-TAA and TAA-Ir^{3+}-AQ, a broad absorption band at 450 nm was observed. This band is likely due to an electronic interaction between the individual molecular moieties. This observation was previously made in other iridium systems [32].

Figure 2.14 (right) illustrates the steady-state luminescence spectra measured in acetonitrile solution after excitation at 400 nm. The fact that the triad and the dyads exhibit a quasi-total luminescence quenching with respect to the reference complex confirms our expectation that in these iridium systems both oxidative and reductive excited-state quenching pathways are thermodynamically allowed. Triplet-triplet energy transfer is ruled out in this case since iridium has its emissive excited state at 2.37 eV. An electrochemistry experiment was carried out in order to establish the energy level diagram for the iridium triad.

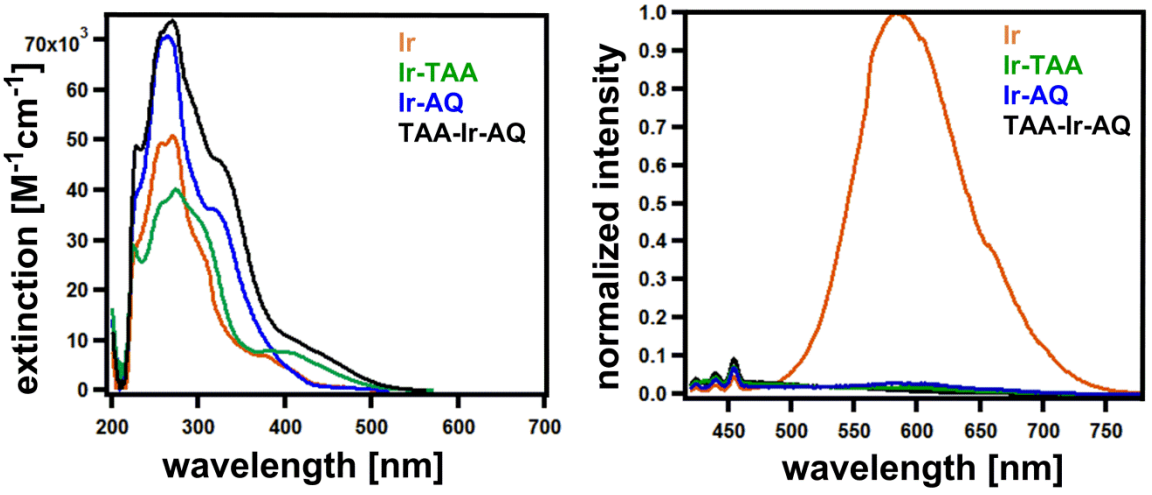

Figure 2.14: UV-vis (left) of the iridium complexes; Steady-state luminescence spectra after excitation of these systems at 400 nm. Detection occurred between 420 nm and 780 nm. In both experiments, deoxygenated acetonitrile solution was used.

II-3.2 Cyclic voltammetry experiment and establishement of the energy level diagram

The cyclic voltammograms for the iridium complexes in Figure 2.15 are less rich on the reductive side than the ruthenium and osmium data, and the bpy reduction wave at ~ -1.75 V is considered as the reduction of the entire iridium complex (Ir^{3+}/Ir^{2+}). Metal oxidation

(Ir^{4+}/Ir^{3+}) takes place at 0.92 V in the reference complex (Ir), while in the triad and dyads it occurs at less positive potentials (0.84 V). One may conclude that in these systems the iridium sensitizer has a significant interaction with TAA and AQ moieties, which is not the case in ruthenium and osmium systems (Tables 2.1 and 2.2). On the other hand, oxidation of the triarylamine (TAA) and the reduction of anthraquinone (AQ) are the same in the triad and the dyads and occur at 0.30 V and ~ -1.27 V respectively (Table 2.3).

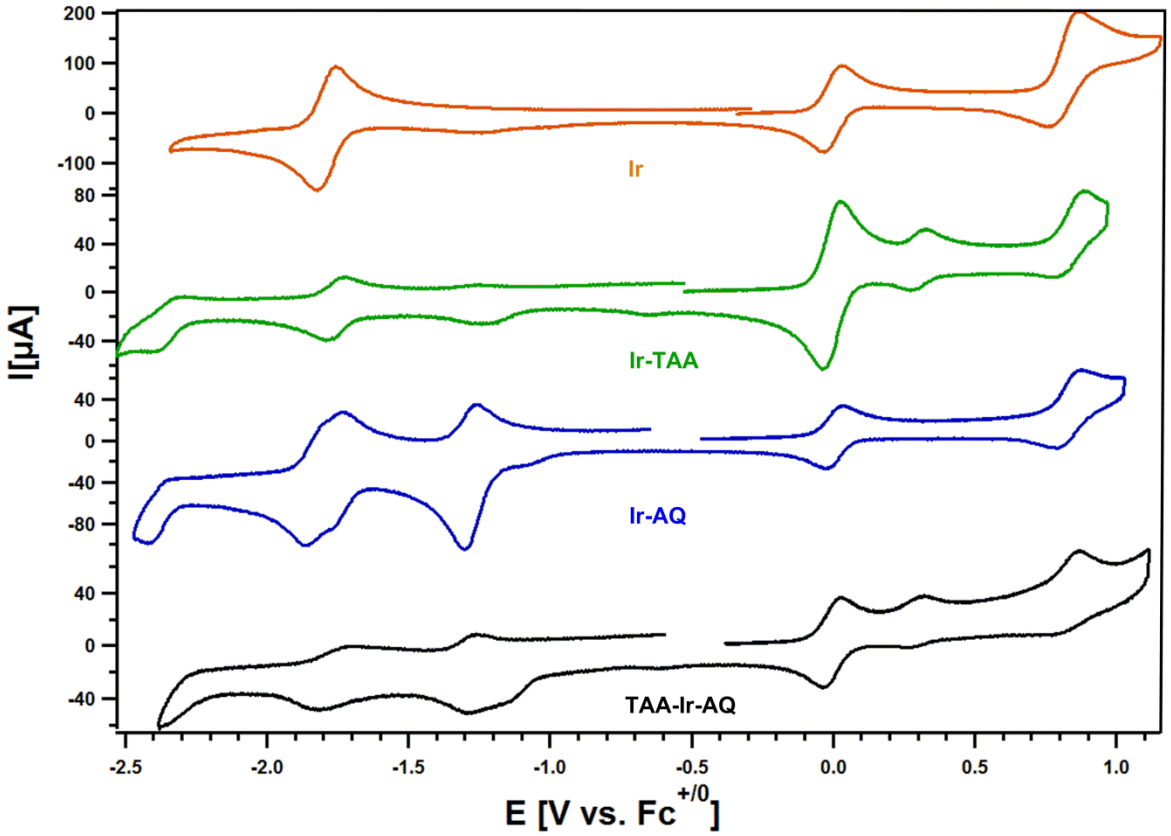

Figure 2.15: Cyclic voltammograms of the four iridium complexes measured in deoxygenated acetonitrile solution in presence of 0.1 M of $TBAPF_6$.

	Ir^{3+}	TAA-Ir	Ir-AQ	TAA-Ir-AQ
Ir^{4+}/Ir^{3+}	0.92	0.84	0.84	0.84
$TAA^{+/0}$		0.30		0.30
$AQ^{0/-}$			-1.28	-1.26
$bpy^{0/-}$	-1.79	-1.76	-1.80	-1.75

Table 2.3: Elechtrochemical potentials extracted from Figure 2.15 and are reported in Volts versus ferrocene (Fc^+/Fc).

Based on the redox potential data in Table 2.3, the energy level diagram for TAA-Ir^{3+}-AQ (Scheme 2.12) could be established.

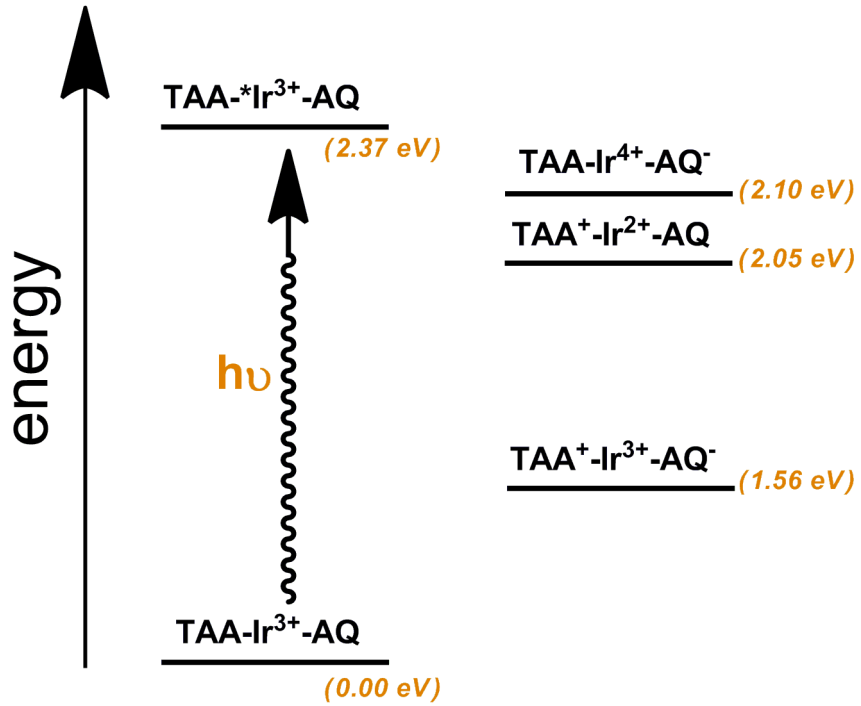

Scheme 2.12: Energy level scheme illustrating the possible states which can be populated after photoexciting the TAA-Ir^{3+}-AQ molecule.

As it appears from Scheme 2.12, there are two possibilities leading to the fully charge-sepatated state TAA^{+}-Ir^{3+}-AQ^{-} (i) either oxidative quenching by electron transfer from $*Ir^{3+}$ to AQ (exergonic by 0.27 eV), (ii) or reductive quenching by electron transfer from TAA to $*Ir^{3+}$ (exergonic by 0.32 eV). Therefore, the strong quenching observed in the luminescence spectra in Figure 2.14 (right) of the triad and the dyads with respect to the reference complex must be due to the fact that the oxidative and reductive quenching are thermodynamically downhill from the initial TAA-$*Ir^{3+}$-AQ state at 2.37 eV. Furthermore, once again the fully charge-separated state is independent of the metal, and it has an energy of 1.56 eV. Therefore, here too, we expect a similar decay of the two radical species (Scheme 2.12) as in the ruthenium system where TAA^{+} and AQ^{-} disappear simultaneously within 1340 ns, unless several factors may play a role in order to prevent this from happening as in the case of the osmium triad where both radicals decay within 80 ns instead of 1340 ns.

II-3.3 Nanosencond transient absorption spectroscopy

After exciting a deoxygenated acetonitrile solution of the iridium triad at 355 nm, a transient absorption spectrum was obtained (Figure 2.16, left panel). Three signals have been detected with maxima at 770, 570, and 380 nm. As discussed previously, these signals are attributed to the oxidized amine (TAA^+) at 770 nm and the reduced anthraquinone (AQ^-) at 570 and 380 nm.

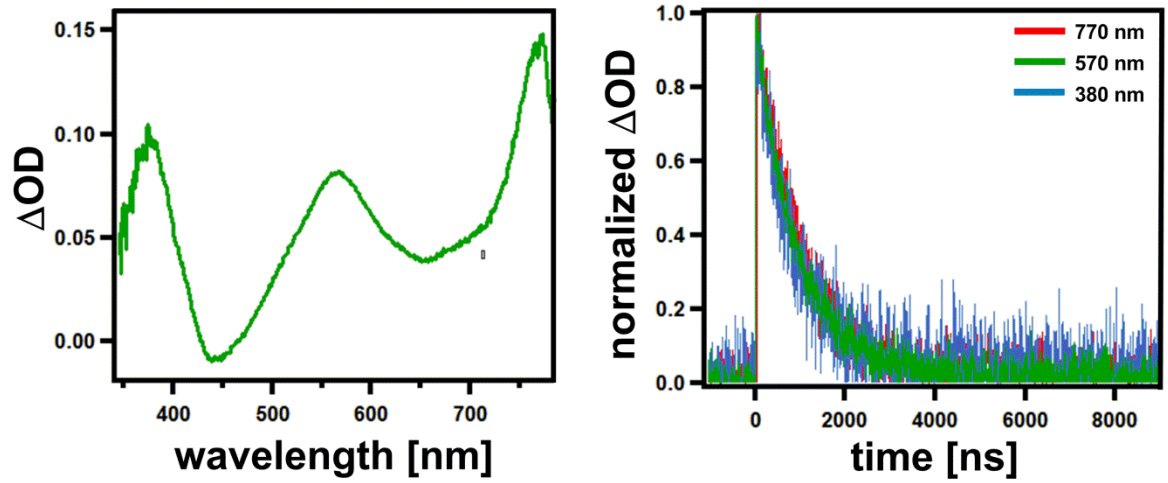

Figure 2.16: Left panel: Transient absorption spectrum obtained after excitation of a deoxygenated acetonitrile solution of the TAA-Ir^{3+}-AQ triad. Excitation occurred at 355 with 8 ns laser pulses. The signals were detected in a 200 ns time window immediately after the pulse. Right panel: The corresponding decays at three wavelengths.

As mentioned above, a decay of the two radical species (TAA^+ and AQ^-) in the range of 1.3 µs is expected. Figure 2.16 (right panel) shows the decays of the transient absorption intensities at 380 nm (blue trace), 570 nm (green trace), and 770 nm (red trace). Exponential fits yield a decay time of 890 ns at the three wavelengths within experimental accuracy. This result is in line with our expectation by taking into account instrumental error.

II-3.4 Kinetics and quantum yields for formation of charge-separated states in the iridium systems

The case of the TAA-Ir^{3+}-AQ triad is somewhat more complicated than for ruthenium and osmium. While photoexciting the triad, we have realized that we were unable to excite solely the iridium, but we were exciting both the iridium metal and the TAA moiety. In other words, in the iridium system, we have two excited-states prior to electron transfer: the TAA-*Ir^{3+}-AQ state and the newly introduced state named *(TAA-Ir^{3+})-AQ. Hence, Scheme 2.12 is no longer fully appropriate for this situation, and therefore Scheme 2.13 has been established.

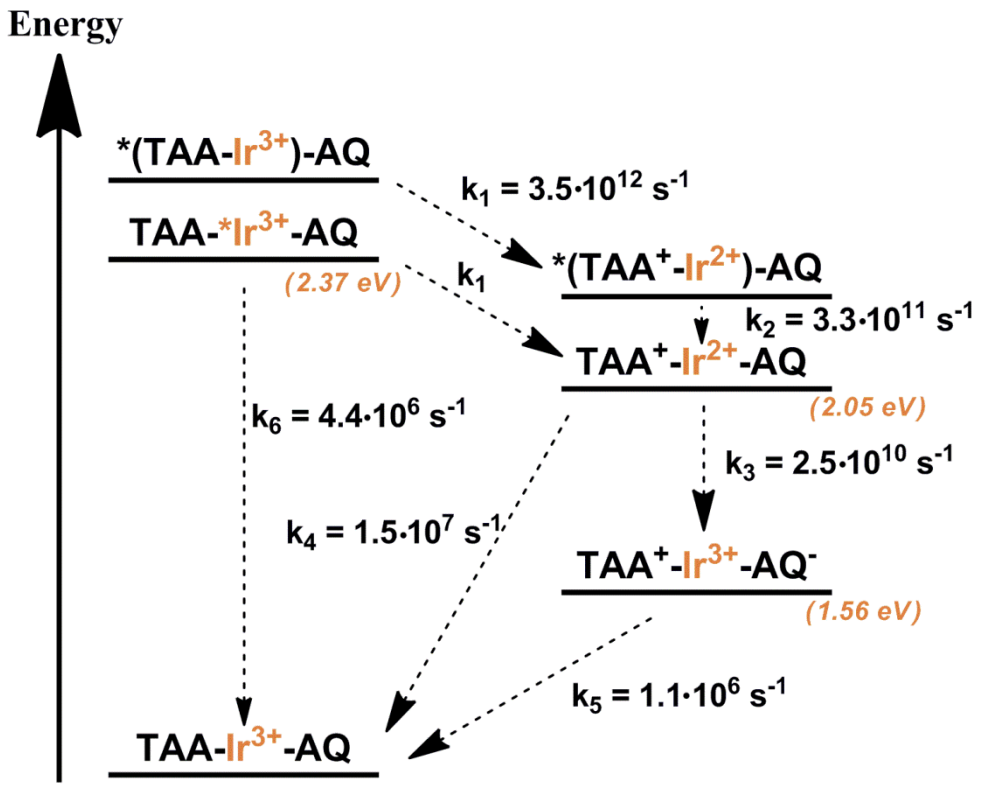

Scheme 2.13: Energy scheme with the different states obtained after excitation of the iridium triad

In Scheme 2.13, the TAA-Ir^{4+}-AQ^{-} state at 2.10 eV from the prior energy level scheme (Scheme 2.12) has been removed since there is no experimental evidence for its formation in the triad. For that reason, the new diagram (Scheme 2.13) reflects better the situation in iridium triad.

Upon photoexcitation of a deoxygenated acetonitrile solution of the iridium triad at 420 nm with 1 ps delay after the excitation, a signal appears at 770 nm which has been previously assigned to the formation of TAA^+ (Figure 2.17, red trace). In addition, there is an absorption band observed between 500 nm and 650 nm which is probably due to a reduced iridium species (Ir^{2+}). We note that same observation was made while exciting the TAA-Ir dyad with 10 ns laser pulses. From Figure 2.18, one may extract the risetime for the formation of the TAA^+ radical at 770 nm. It appears to be 0.4 ps, and this corresponds to a rate constant of $k_1 = 3.5 \cdot 10^{12}\ s^{-1}$.

The black trace in Figure 2.17 was measured from the same sample but this time detected with a delay of 3 ps. In other words, once the *(TAA^+-Ir^{2+})-AQ state has been formed in 0.4 ps, it undergoes an electronic relaxation to form the TAA^+-Ir^{2+}-AQ state at 2.05 V (Scheme 2.13) with a time constant of 3 ps ($k_2 = 3.3 \cdot 10^{11}\ s^{-1}$).

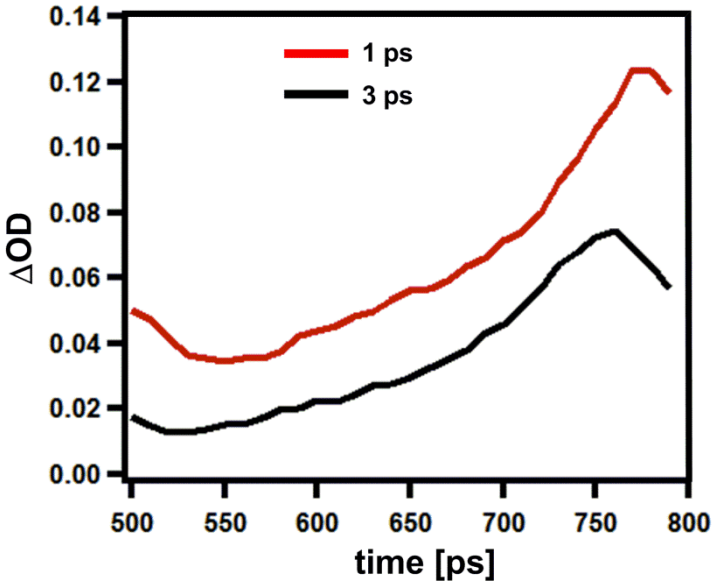

Figure 2.17: Red trace: Transient absorption spectrum detected with a delay of 1 ps after excitation of an acetonitrile solution of TAA-Ir^{3+}-AQ at 420 nm; black trace: transient absorption spectrum from the same sample detected with a delay of 3 ps.

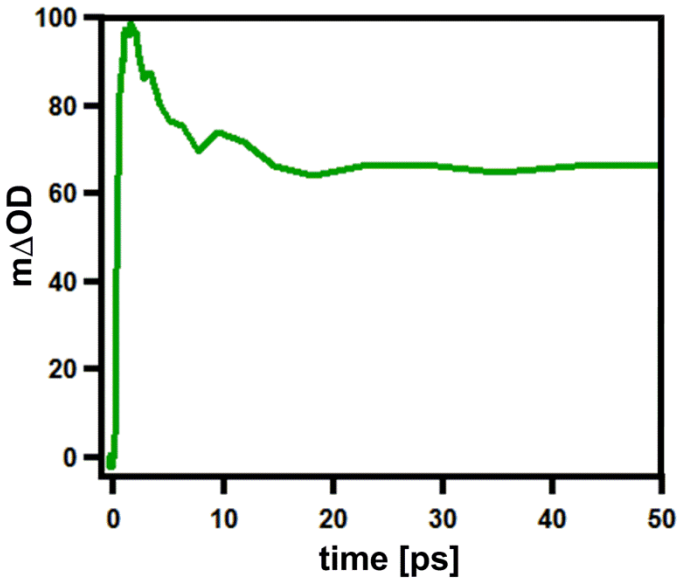

Figure 2.18: Time profile of the transient absorption at 770 nm after excitation at 420 nm with laser pulses of 150 fs width.

Once TAA^{+}-Ir^{2+}-AQ state has been reached at 2.05 eV, two processes can occur. The first process is a charge recombination between TAA^{+} and Ir^{2+} and leads back to the ground state. To study this possibility, experiments were performed with the TAA-Ir dyad. Figure 2.19 shows the transient absorption decay of the TAA-Ir dyad in which TAA^{+} and Ir^{2+} decay with a time constant of 67 ns ($k_4 = 1.5 \cdot 10^7\ s^{-1}$).

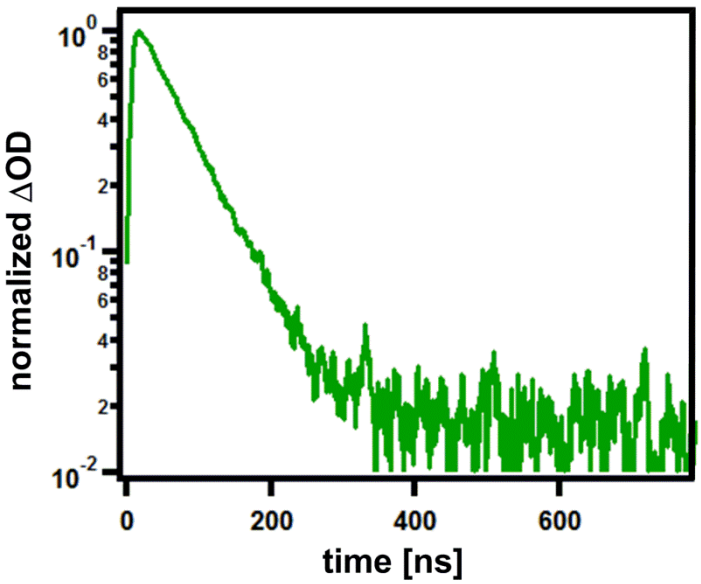

Figure 2.19: Decay of the transient absorption at 770 nm after excitation of the TAA-Ir^{3+} dyad (in deoxygenated CH_3CN) at 355 nm with ~10-ns laser pulses.

The second process will allow the formation of the fully charge-separated state TAA^{+}-Ir^{3+}-AQ^{-} at 1.56 eV due to electron transfer from Ir^{2+} to AQ (Scheme 2.13). The radical monoanion (AQ^{-}) seems to be formed with a time constant of 40 ps ($k_4 = 2.5 \cdot 10^{10}$ s^{-1}), and it was detected at 570 nm (Figure 2.20, blue trace). At the same time, a signal at 770 nm was also detected (Figure 2.20, green trace) due to TAA^{+} radical.

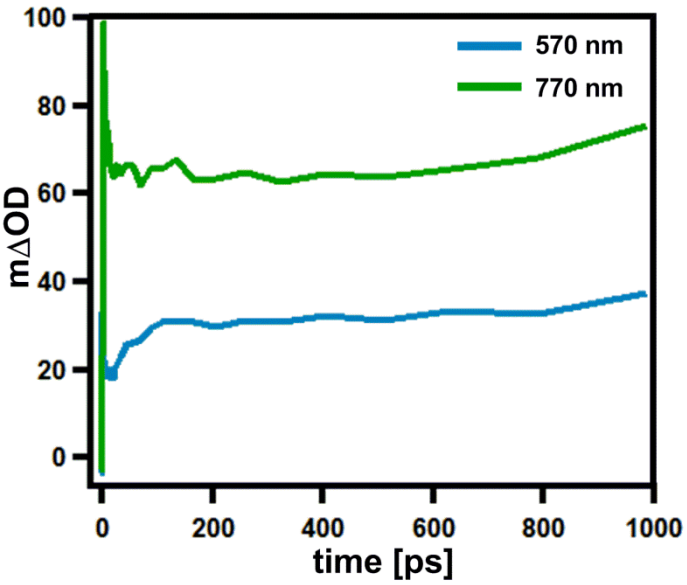

Figure 2.20: Time profiles of the transient absorption at 550 nm (purple trace) and 770 nm (blue trace) after 420-nm excitation of the TAA-Ir^{3+}-AQ triad in CH_3CN (laser pulse width: 150 fs).

Thermal charge recombination occurs between TAA^{+} and AQ^{-} at 1.56 eV with a time constant of 890 ns and a rate constant of $k_5 = 1.1 \cdot 10^{6}$ s^{-1}.

The lifetime of the ^{3}MLCT excited state was measured in the reference iridium complex. It appears that ^{3}MLCT state is deactivated within 230 ns ($k_6 = 4.4 \cdot 10^{6}$ s^{-1}) (Scheme 2.13).

Based on the rate constants shown in Scheme 2.13, the quantum yield for the formation of the fully charge-separated state TAA^{+}-Ir^{3+}-AQ^{-} from the initial ground state TAA-Ir^{3+}-AQ is approximately 100 %.

References

[1] Balzani, V., *Electron transfer in chemistry*. VCH Wiley: Weinheim, 2001; Vol. 3.

[2] Opperman, K. A.; Mecklenburg, S. L.; Meyer, T. J., *Inorg. Chem.* **1994,** *33*, 5295-5301.

[3] Treadway, J. A.; Chen, P. Y.; Rutherford, T. J.; Keene, F. R.; Meyer, T. J., *J. Phys. Chem. A* **1997,** *101*, 6824-6826.

[4] Borgström, M.; Johansson, O.; Lomoth, R.; Baudin, H. B.; Wallin, S.; Sun, L. C.; Åkermark, B.; Hammarström, L., *Inorg. Chem.* **2003,** *42*, 5173-5184.

[5] Falkenström, M.; Johansson, O.; Hammarström, L., *Inorg. Chim. Acta* **2007,** *360*, 741-750.

[6] Wenger, O. S., *Coord. Chem. Rev.* **2009,** *253*, 1439-1457.

[7] Dupont, N.; Ran, Y. F.; Jia, H. P.; Grilj, J.; Ding, J.; Liu, S. X.; Decurtins, S.; Hauser, A., *Inorg. Chem.* **2011,** *50*, 3295-3303.

[8] Collin, J.-P.; Guillerez, S.; Sauvage, J.-P.; Barigelletti, F.; De Cola, L.; Flamigni, L.; Balzani, V., *Inorg. Chem.* **1991,** *30*, 4230-4238.

[9] Collin, J.-P.; Guillerez, S.; Sauvage, J.-P.; Barigelletti, F.; Flamigni, L.; De Cola, L.; Balzani, V., *Coord. Chem. Rev.* **1991,** *111*, 291-296.

[10] Collin, J.-P.; Guillerez, S.; Sauvage, J.-P.; Barigelletti, F.; De Cola, L.; Flamigni, L.; Balzani, V., *Inorg. Chem.* **1992,** *31*, 4112-4117.

[11] Sauvage, J.-P.; Collin, J.-P.; Chambron, J.-C.; Guillerez, S.; Coudret, C.; Balzani, V.; Barigelletti, F.; De Cola, L.; Flamigni, L., *Chem. Rev.* **1994,** *94*, 993-1019.

[12] Collin, J.-P.; Dixon, I. M.; Sauvage, J.-P.; Williams, J. A. G.; Barigelletti, F.; Flamigni, L., *J. Am. Chem. Soc.* **1999,** *121*, 5009-5016.

[13] Dixon, I. M.; Collin, J.-P.; Sauvage, J.-P.; Barigelletti, F.; Flamigni, L., *Angew. Chem. Int. Ed.* **2000,** *39*, 1292-1295.

[14] Dixon, I. M.; Collin, J.-P.; Sauvage, J.-P.; Flamigni, L.; Encinas, S.; Barigelletti, F., *Chem. Soc. Rev.* **2000,** *29*, 385-391.

[15] Roundhill, D. M., *Photochemistry and Photophysics of Metal Complexes*. Plenum Press: NewYork, 1994.

[16] Abrahamsson, M.; Jager, M.; Osterman, T.; Eriksson, L.; Persson, P.; Becker, H. C.; Johansson, O.; Hammarström, L., *J. Am. Chem. Soc.* **2006,** *128*, 12616-12617.

[17] Abrahamsson, M.; Jager, M.; Kumar, R. J.; Osterman, T.; Persson, P.; Becker, H. C.; Johansson, O.; Hammarström, L., *J. Am. Chem. Soc.* **2008,** *130*, 15533-15542.

[18] Hammarström, L.; Johansson, O., *Coord. Chem. Rev.* **2010,** *254*, 2546-2559.

[19] Kumar, R. J.; Karlsson, S.; Streich, D.; Jensen, A. R.; Jager, M.; Becker, H. C.; Bergquist, J.; Johansson, O.; Hammarström, L., *Chem.-Eur. J.* **2010,** *16*, 2830-2842.

[20] Balzani, V.; Juris, A.; Venturi, M.; Campagna, S.; Serroni, S., *Chem. Rev.* **1996,** *96*, 759-833.

[21] Juris, A.; Balzani, V.; Barigelletti, F.; Campagna, S.; Belser, P.; Von Zelewsky, A., *Coord. Chem. Rev.* **1988,** *84*, 85-277.

[22] Geiss, B.; Lambert, C., *Chem. Commun.* **2009**, 1670-1672.

[23] Sreenath, K.; Suneesh, C. V.; Gopidas, K. R.; Flowers, R. A., *J. Phys. Chem. A* **2009,** *113*, 6477-6483.

[24] Furue, M.; Maruyama, K.; Oguni, T.; Naiki, M.; Kamachi, M., *Inorg. Chem.* **1992,** *31*, 3792-3795.

[25] Anderson, P. A.; Keene, F. R.; Meyer, T. J.; Moss, J. A.; Strouse, G. F.; Treadway, J. A., *J. Chem. Soc., Dalton Trans.* **2002**, 3820-3831.

[26] Sreenath, K.; Thomas, T. G.; Gopidas, K. R., *Org. Lett.* **2011,** *13*, 1134-1137.

[27] Mecklenburg, S. L.; McCafferty, D. G.; Schoonover, J. R.; Peek, B. M.; Erickson, B. W.; Meyer, T. J., *Inorg. Chem.* **1994,** *33*, 2974.

[28] Lopéz, R.; Leiva, A. M.; Zuloaga, F.; Loeb, B.; Norambuena, E.; Omberg, K. M.; Schoonover, J. R.; Striplin, D.; Devenney, M.; Meyer, T. J., *Inorg. Chem.* **1999,** *38*, 2924.

[29] Lewis, F. D.; Thazhathveetil, A. K.; Zeidan, T. A.; Vura-Weis, J.; Wasielewski, M. R., *J. Am. Chem. Soc.* **2010,** *132*, 444.

[30] Lambert, C.; Nöll, G., *J. Am. Chem. Soc.* **1999,** *121*, 8434-8442.

[31] Creutz, C.; Chou, M.; Netzel, T. L.; Okumura, M.; Sutin, N., *J. Am. Chem. Soc.* **1980,** *102*, 1309-1319.

[32] Baranoff, E.; Dixon, I. M.; Collin, J.-P.; Sauvage, J.-P.; Ventura, B.; Flamigni, L., *Inorg. Chem.* **2004,** *43*, 3057-3066.

Chapter III
Increasing the Lifetime of a Charge-Separated State in Molecular Triads by Hydrogen-Bonding Solvents

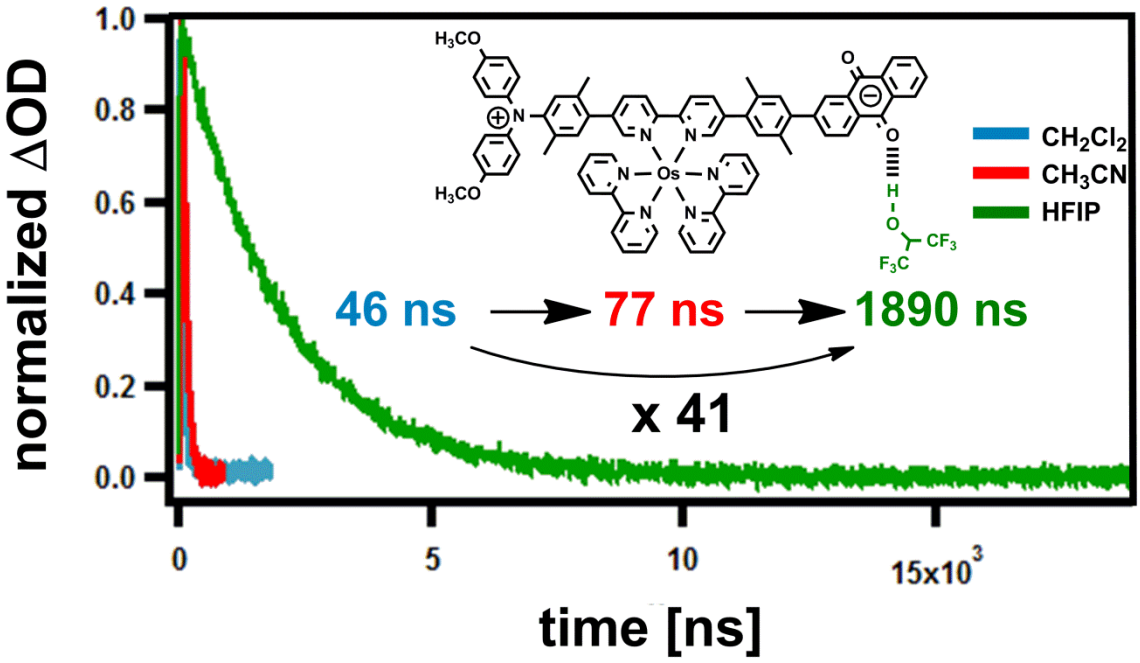

Introduction

Despite numerous studies exploring the role of hydrogen-bonding in proton coupled electron transfer mechanism (PCET) [1-8], only few shed light on how hydrogen-bonding could affect the thermodynamics and kinetics of a photoinduced electron transfer reaction [9-14]. Moreover, increasing the lifetime of charge-separated states (τ_{CR}) via hydrogen-bonding has received limited attention [10].

My main focus in this chapter is to highlight the change in the lifetimes of the charge-separated states of TAA^{+}-Ru^{2+}-AQ^{-} and TAA^{+}-Os^{2+}-AQ systems (triads from chapter 2) while going from aprotic solvent (CH_2Cl_2) to one of the strongest hydrogen-bond donors (hexafluoroisopropanol). It will be demonstrated that the hydrogen-bond donor ability of the solvent is responsible for the increase of τ_{CR} in the molecular triads and not its dielectric constant.

III-1. Electrochemistry in CH_2Cl_2 solvent

The cyclic voltammograms shown in Figure 3.1 have been measured in dichloromethane solution at room temperature in presence of ferrocene and 0.1 M $TBAPF_6$. The orange trace corresponds to the molecular triad TAA-Ru^{2+}-AQ, while the green trace is obtained from the TAA-Os^{2+}-AQ molecule.

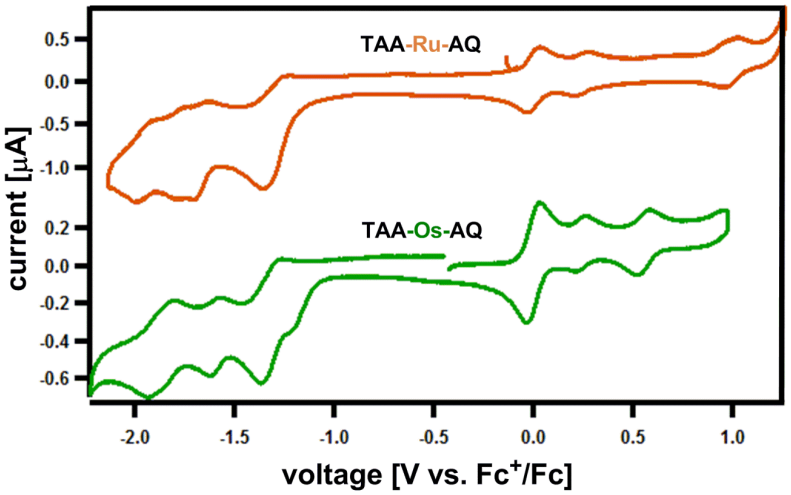

Figure 3.1: Cyclic voltammograms of TAA-Ru^{2+}-AQ (orange trace) and TAA-Os^{2+}-AQ (green trace) triads measured in dichloromethane solution in presence of 0.1 M of $TBAPF_6$.

The redox potentials extracted from Figure 3.1 are as follows and are reported in Volts versus the Fc^+/Fc couple (0.0 V): Metal oxidation occurs at 0.95 V for Ru^{3+}/Ru^{2+}, while the osmium(II) is oxidized at less positive potentials (0.56 V). On the reduction side, the ruthenium complex is reduced at -1.71 V (Ru^{2+}/Ru^+), and the osmium complex at -1.59 V (Os^{2+}/Os^+). Triarylamine oxidation (TAA^+/TAA) takes place at 0.2 V for TAA-Ru^{2+}-AQ and at 0.24 V for TAA-Os^{2+}-AQ. Anthraquinone is reduced at -1.39 V in the ruthenium triad and at less negative potentials (-1.3 V) in the case of the osmium triad.

III-2. Electrochemistry in CH_2Cl_2 with increasing amounts of HFIP

Following the addition of HFIP to a solution of TAA-Ru^{2+}-AQ (left panel of Figure 3.2) and TAA-Os^{2+}-AQ (right panel) in dichloromethane only the wave around -1.3 V which corresponds to the reduction of anthraquinone is affected and shifts to less negative potentials (Figure 3.2, dashed vertical line). At [HFIP] = 4 mM, the AQ/AQ^- wave has shifted positively by 150 mV in both triads. Redox waves around 0.3 V (TAA^+/TAA), 0.9 V (Ru^{3+}/Ru^{2+}), 0.6 V (Os^{3+}/Os^{2+}), and the first bpy localized reduction near -1.7 V remain unchanged upon adding HFIP (Figure 3.2).

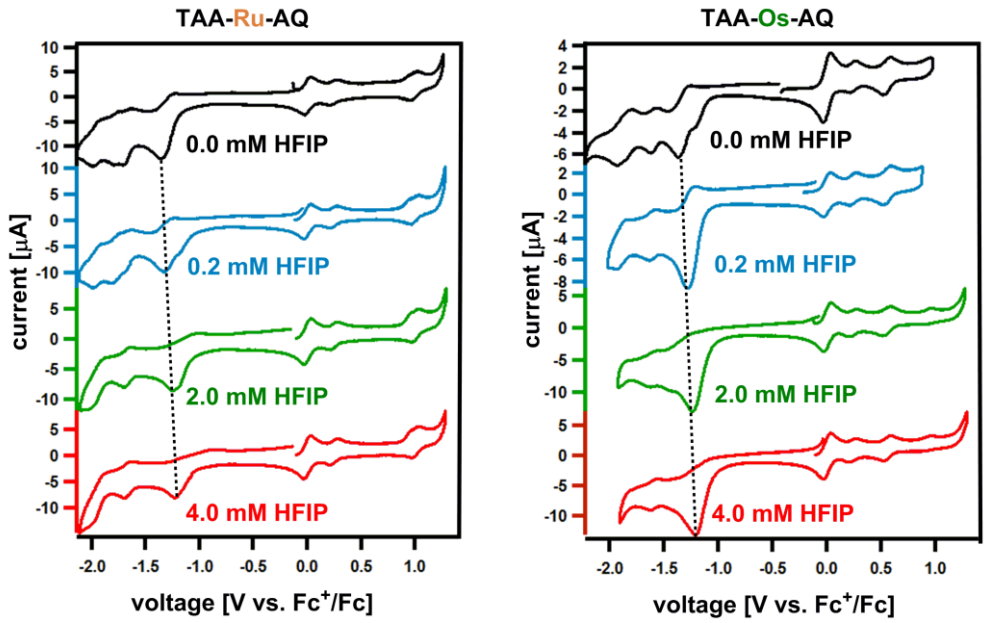

Figure 3.2: Cyclic voltammograms of TAA-Ru^{2+}-AQ (left panel) and TAA-Os^{2+}-AQ (right panel) measured in deoxygenated dichloromethane solution. Increasing concentrations of HFIP were added in presence of $TBAPF_6$. Small amounts of ferrocene were used for internal voltage calibration.

The shift of the reduction wave of AQ to less negative values while adding HFIP (Figure 3.2) suggests that hydrogen-bonding between the carbonyl group of AQ and the hydroxyl group of HFIP (Figure 3.3) might be present.

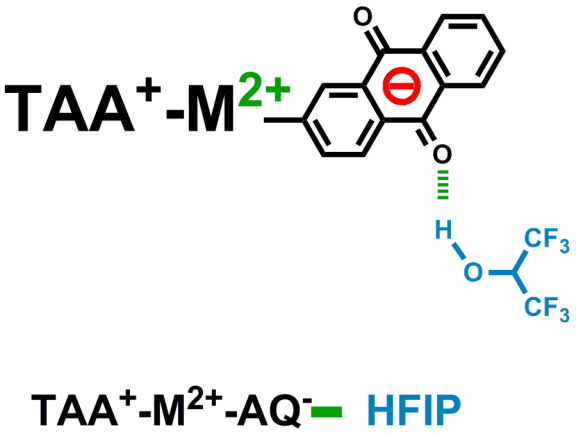

Figure 3.3: Illustration of the hydrogen-bonding between photoreduced AQ and HFIP in the triads. '**M**' corresponds to the metal (either Ru or Os).

Based on what was discussed in chapter 1, it seems reasonable to assume that a chemical equilibrium is obtained between free TAA^{+}-M^{2+}-AQ^{-} and TAA^{+}-M^{2+}-AQ^{-} hydrogen-bonded to *n* molecules of HFIP (eq. 3.1).

$$TAA^{+}\text{-}M^{2+}\text{-}AQ^{-} + n\ HFIP \leftrightarrow TAA^{+}\text{-}M^{2+}\text{-}AQ^{-} \text{—} HFIP_n \qquad \text{(eq. 3.1)}$$

In order to determine the equilibrium constant (K_{eq}) of the above reaction, equation 3.2 [15,16] was used:

$$\Delta E_{red} = n \cdot 2.3 \cdot (R \cdot T/F) \cdot \log([HFIP]) + (R \cdot T/F) \cdot \ln(K_{eq}) \qquad \text{(eq. 3.2)}$$

In equation 3.2, ΔE_{red} is the difference between the electrochemical reduction at a given HFIP concentration and the respective potential in pure CH_2Cl_2, R is the gas constant, T is the temperature, and F is the Faraday constant.

Straight lines are obtained by plotting ΔE_{red} versus log([HFIP]) for TAA-Ru^{2+}-AQ (circles) and TAA-Os^{2+}-AQ (squares) (Figure 3.4). Linear regression fits give a slope of 0.061 V for

the ruthenium triad and 0.045 V for the osmium triad. Therefore, n = 1.0 is obtained for TAA-Ru^{2+}-AQ and n = 0.8 for TAA-Os^{2+}-AQ, implying that one molecule of HFIP is bound to AQ^- in the triads under these conditions.

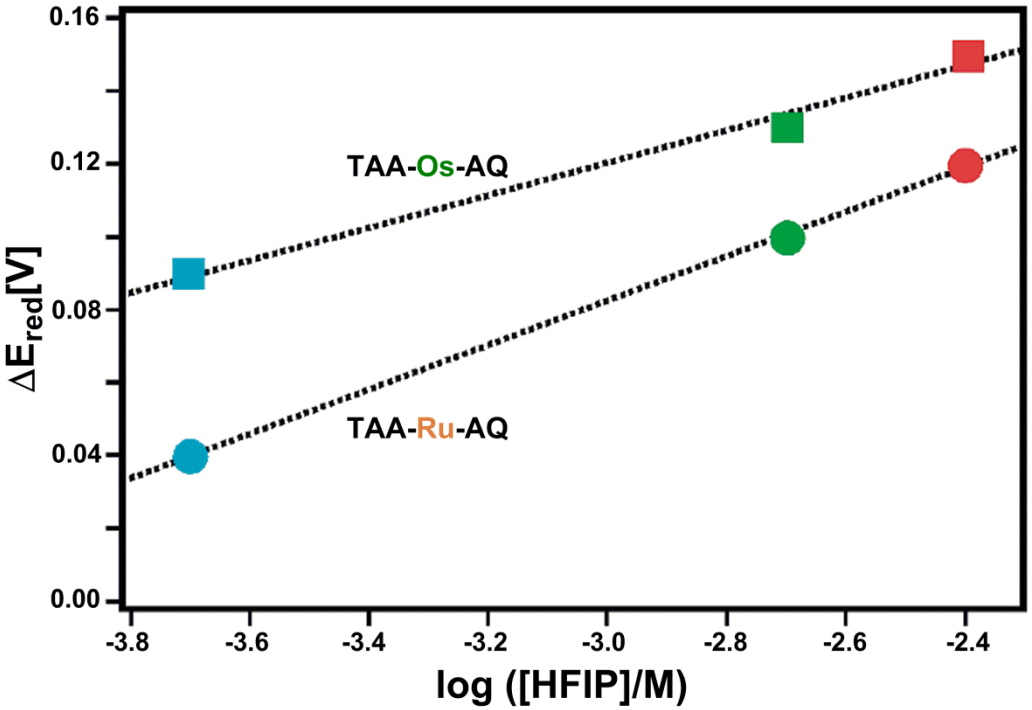

Figure 3.4: Shifts of the anthraquinone reduction potentials between CH_2Cl_2 and HFIP (ΔE_{red}) plotted versus log([HFIP]) in TAA-Ru^{2+}-AQ (circles) and TAA-Os^{2+}-AQ (squares).

From the intercepts (0.266 V for ruthenium and 0.254 V for osmium triad), the equilibrium constant from equation 3.1 can be determined. One obtains $K_{eq} = 3.2 \cdot 10^4$ M^{-1} for TAA-Ru^{2+}-AQ and $K_{eq} = 2.0 \cdot 10^4$ M^{-1} for TAA-Os^{2+}-AQ. In fact, these values of K_{eq} are relatively large, but their magnitude can potentially be explained by the fact that one is adding a very strong hydrogen-bond donor (HFIP) to an aprotic solution (CH_2Cl_2) of a good hydrogen-bond acceptor (AQ^-).

The reduction potential of AQ cannot be measured directly in pure HFIP. Consequently, in order to have a rough idea about the shift of the AQ reduction wave when going from pure CH_2Cl_2 to pure HFIP, equation 3.2 was applied. In fact, based on the data (slope and intercept) extracted from the corresponding linear regression fits (dotted lines in Figure 3.4),

and by taking [HFIP] = 9.5 M (log[HFIP] = 1), one may extrapolate $\Delta E_{red} \approx 0.30$ V for the ruthenium and osmium triads.

The redox potentials of the ruthenium and osmium triads in different solvents are summarized in Table 3.1. The data obtained in CH_3CN are already discussed in chapter 2. The potentials in CH_2Cl_2 are extracted from Figure 3.1. As mentioned above, in HFIP the redox potentials of the individual components in the triads complexes remain the same as in CH_2Cl_2 except for the reduction of anthraquinone which shifts positively by ~ 0.3 V. Hence, one may conclude that in HFIP all states containing AQ^- are shifted by 0.3 eV with respect to the states in CH_2Cl_2.

Redox couple	TAA-Ru-AQ CH_3CN	TAA-Ru-AQ CH_2Cl_2	TAA-Ru-AQ HFIP	TAA-Os-AQ CH_3CN	TAA-Os-AQ CH_2Cl_2	TAA-Os-AQ HFIP
$M^{3+/2+}$	0.92	0.95	0.95	0.48	0.56	0.56
$TAA^{+/0}$	0.30	0.20	0.20	0.30	0.24	0.24
$AQ^{0/-}$	-1.27	-1.39	-1.09	-1.27	-1.30	-1.00
$M^{2+/+}$	-1.73	-1.71	-1.71	-1.62	-1.59	-1.59

Table 3.1: Electrochemical potentials (in Volts vs. Fc^+/Fc) of the individual components in the ruthenium and osmium triads obtained in CH_3CN, CH_2Cl_2 and HFIP. 'M' corresponds to the metal (Ru or Os).

III-3. Energy level diagram in CH_3CN, CH_2Cl_2 and HFIP

Based on the electrochemical potentials reported in Table 3.1, it is possible to establish energy level schemes (Scheme 3.1). As seen above, in HFIP the TAA^+-Ru^{2+}-AQ^- and TAA^+-Os^{2+}-AQ^- charge-separated states are energetically lowered by 0.3 eV compared to those in CH_2Cl_2.

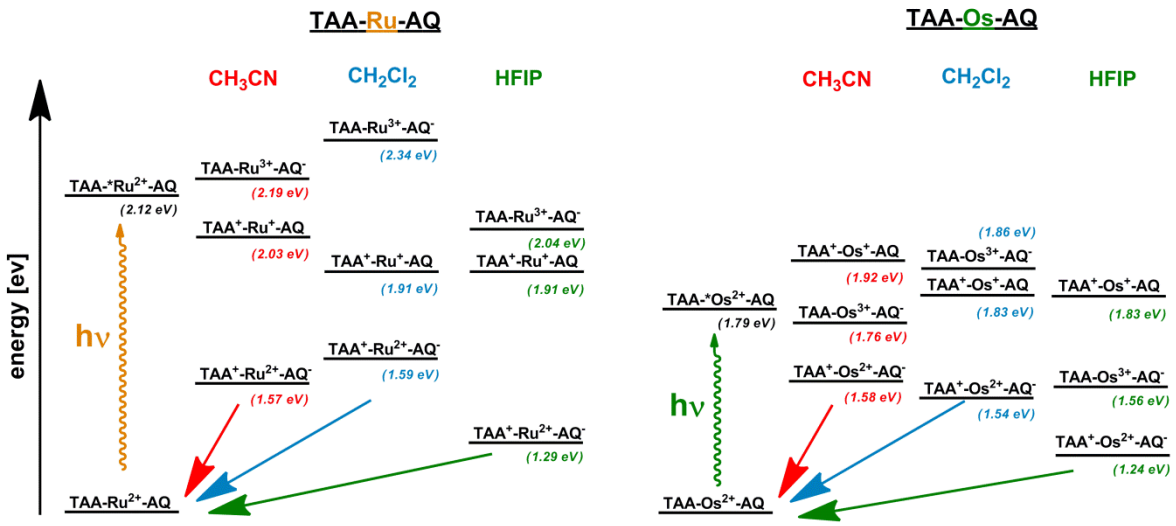

Scheme 3.1: Energy level scheme of all the relevant states obtained after excitation of the TAA-Ru^{2+}-AQ (left) and TAA-Os^{2+}-AQ (right) molecules in CH_3CN, CH_2Cl_2, and HFIP.

III-4. Transient absorption spectroscopy

Transient absorption spectra of the TAA-Ru^{2+}-AQ and TAA-Os^{2+}-AQ triads are presented in Figure 3.5. These spectra are measured in three different solvents (CH_2Cl_2, CH_3CN, and HFIP). Similar spectra are obtained for the ruthenium and osmium triads in dichloromethane and acetonitrile solutions. In both solvents, three bands with maxima at 380 nm, 570 nm, and 770 nm were detected. According to what has been previously reported (chapter 2), the band at 770 nm is assigned to the oxidized amine (TAA^+), while the bands at 380 nm and 570 nm are attributed to the reduced anthraquinone (AQ^-).

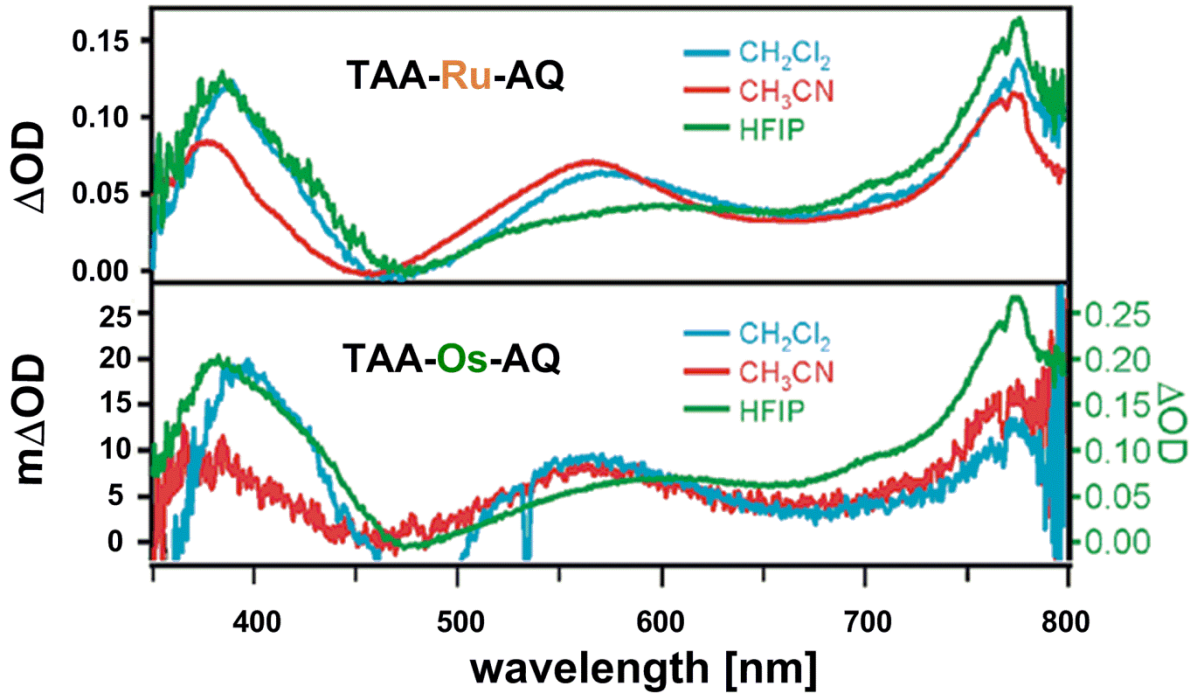

Figure 3.5: Transient absorption spectra of TAA-Ru^{2+}-AQ (upper panel) and TAA-Os^{2+}-AQ (lower panel) triads measured in three solvents. Excitation occurred at 532 nm in both triads with 10 ns laser pulses. Detection was in a 200 ns window starting immediately after the pulse.

In HFIP solution the situation differs. The maximum of the band related to AQ^- is shifted from 570 nm to 600 nm in both triads (green trace in Figure 3.5), while the TAA^+ signal keeps the same position at 770 nm as in the case of CH_2Cl_2 and CH_3CN solvents. This result suggests that there are interactions between AQ^- and HFIP. These interactions, as mentioned above, are presumably hydrogen bonds between the two species.

It should be kept in mind that in our case we have excluded the possibility of protonation of AQ^- by HFIP (this was discussed thoroughly in chapter 1). It is much more plausible to have formation of hydrogen bonds after excitation of the triads in HFIP solution. To further confirm our interpretation, we performed spectroelectrochemistry experiments in dichloromethane solution of free AQ molecule (Figure 3.6, blue trace), and of AQ in presence of 3 mM of HFIP (Figure 3.6, green trace).

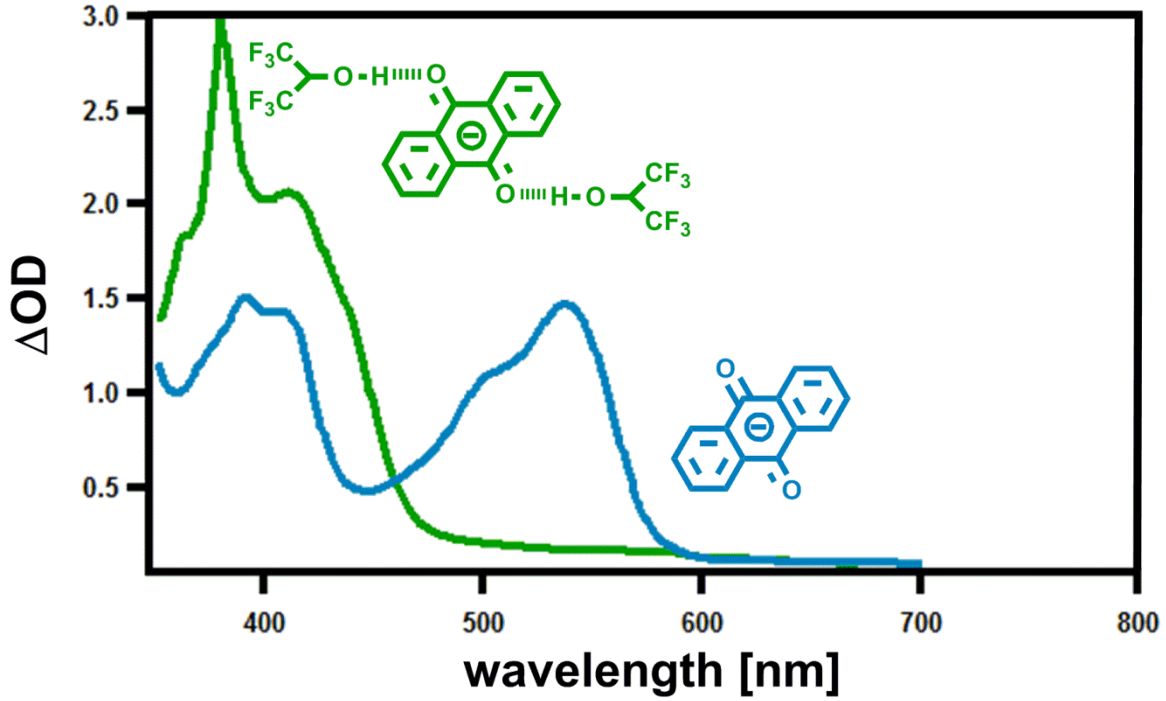

Figure 3.6: Spectroelectrochemical data obtained while applying negative potentials of -1.5 V to a CH_2Cl_2 solution of 9,10-anthraquinone (blue trace), and of 9,10-anthraquinone in presence of hexafluoroisopropanol (green trace).

The green spectrum from Figure 3.6 shows that instead of the two bands at 380 nm and 570 nm observed in pure CH_2Cl_2 solution of AQ without HFIP (blue trace), one detects a sharp peak at 375 nm and a broad band at 410 nm in solution of AQ with HFIP. Prior investigations [17] attributed these two bands to the formation of the AQH_2 species (twofold reduced and twofold protonated AQ).

However, the bands of AQH_2 observed in Figure 3.6 (green trace) are absent in the transient absorption spectra from Figure 3.5 (green traces). This result excludes the possibility of having AQ^- protonated by HFIP at least as far as twofold reduction and twofold protonation is concerned. Instead, a new species is formed which is most likely AQ^-─HFIP. This species contributes to the shift of the band at 570 nm to longer wavelengths (Figure 3.5, green traces).

III-5. Transient absorption decays in CH_2Cl_2, CH_3CN, and HFIP

Figure 3.7 shows the decays of the transient absorption signals from Figure 3.5 detected at 770 nm after photoexcitation of TAA-Ru^{2+}-AQ in three different solvents. The lifetimes of the TAA^+-Ru^{2+}-AQ^- charge separated state extracted from the decays are: τ_{CR} = 747 ns in CH_2Cl_2 (blue color), 1381 ns in CH_3CN (red color), and 3019 ns in HFIP (green color). (I should note that τ_{CR} obtained at 380 and 570 nm is similar to τ_{CR} at 770 nm).

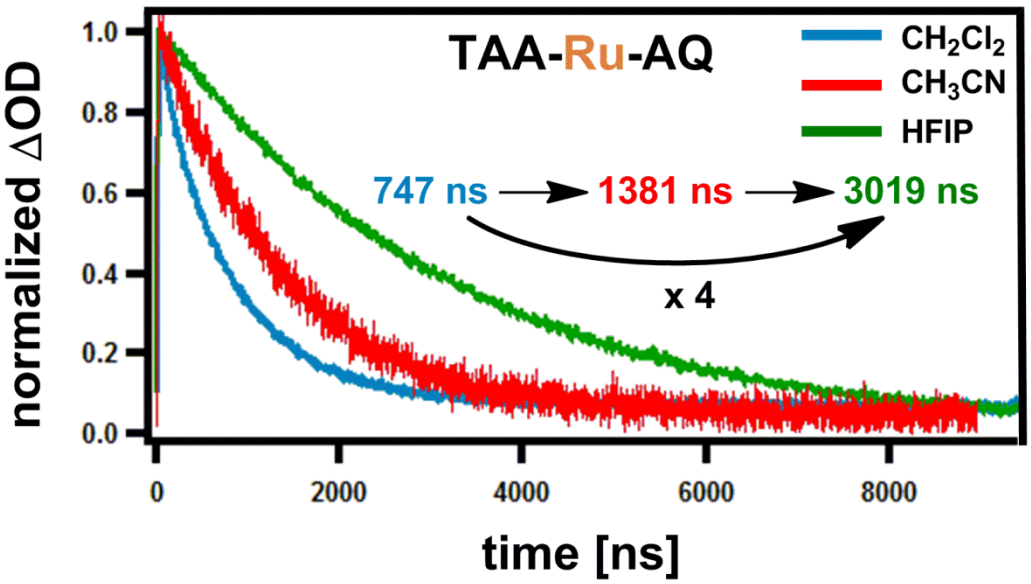

Figure 3.7: Decays of the radical species detected at 770 nm after photoexcitation of solutions of TAA-Ru^{2+}-AQ in deoxygenated CH_2Cl_2, CH_3CN, and HFIP.

In acetonitrile τ_{CR} is a factor of 1.8 longer than in dichloromethane, while τ_{CR} increases by a factor of 4 when going from CH_2Cl_2 to HFIP. This increase is most likely due to hydrogen-bonding between HFIP and the anthraquinone monoanion (Figure 3.3). In fact, hydrogen-bonding contributes to the thermodynamic and kinetic stabilization of the photoproduced charge separated state, as discussed below.

Thermodynamic stabilization could be explained based on the electrochemical investigations in section III-2, where the TAA^+-Ru^{2+}-AQ^- state is thermodynamically stabilized by ~ 0.3 eV. Therefore the time constant for the charge recombination (k_{CR}) between TAA^+ and (AQ^-—HFIP) will be longer than between TAA^+ and AQ^-.

Kinetic stabilization results in by less driving-force for charge recombination: ΔG_{CR} = ~1.6 eV in CH_2Cl_2 versus ΔG_{CR} = ~1.3 eV in HFIP (Scheme 3.1). In addition, hydrogen-bonding could possibly lead to a change in the reorganization energy (λ) accompanying charge-recombination. According to Marcus theory, an increase in λ can be accompanied by a decrease in k_{CR}. Figure 3.8 shows how a decrease in $-\Delta G_{CR}$ may lead to a decrease in k_{CR} in the Marcus normal regime. In other words, τ_{CR} will be longer.

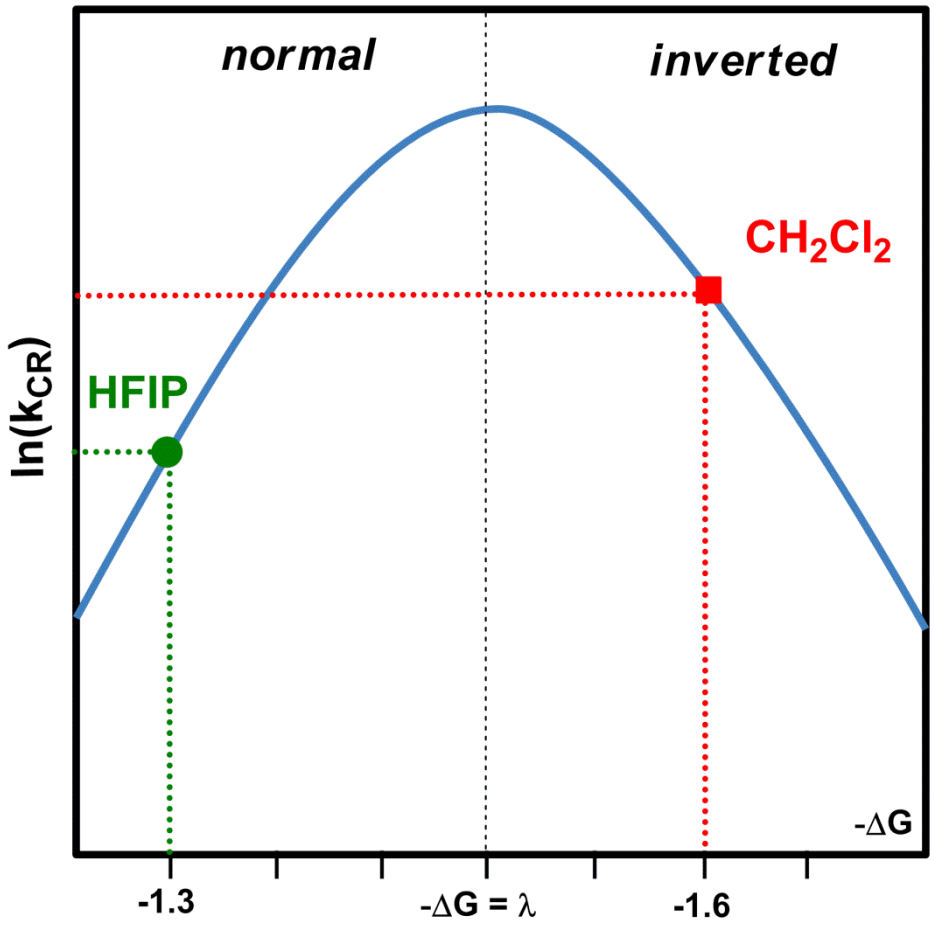

Figure 3.8: Plot $\ln(k_{CR})$ versus $-\Delta G$ in order to illustrate the decrease in k_{CR} between CH_2Cl_2 and HFIP.

The most spectacular result upon solvent variation was found in the case of TAA-Os^{2+}-AQ. Figure 3.9 shows the decays of the transient absorption signals (Figure 3.5) detected at 770 nm after photoexcitation of TAA-Os-AQ in CH_2Cl_2, CH_3CN, and HFIP. The lifetimes of the TAA^+-Os^{2+}-AQ^- charge-separated state are τ_{CR} = 46 ns in CH_2Cl_2 (blue color), 77 ns in CH_3CN (red color), and 1890 ns in HFIP (green color). In other words, we observed lengthening of τ_{CR} by a factor of 41 when going from CH_2Cl_2 to HFIP (Figure 3.9).

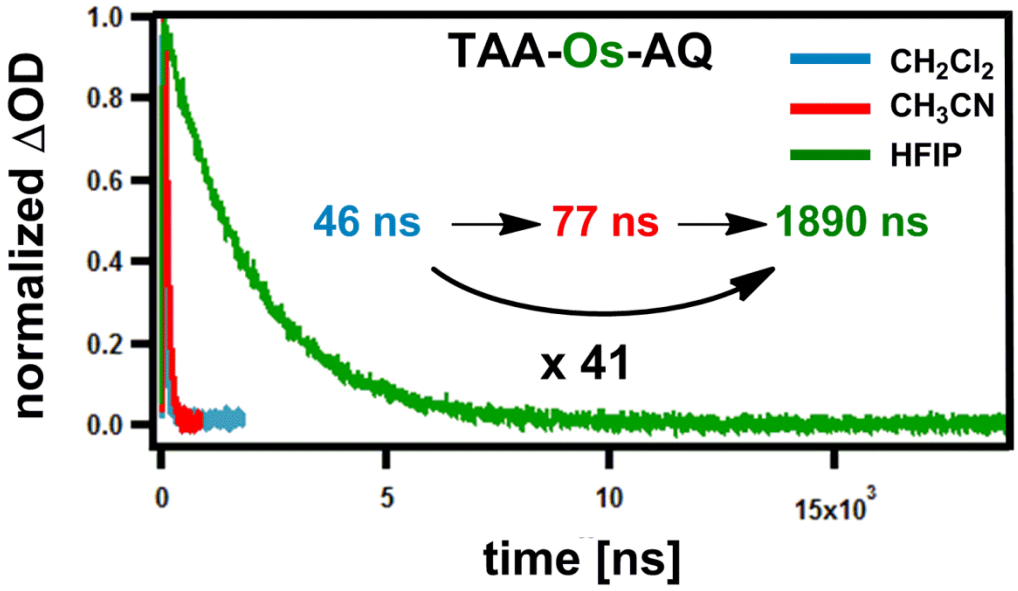

Figure 3.9: Decays of the radical species detected at 770 nm after photoexcitation of three solutions of TAA-Os^{2+}-AQ in CH_2Cl_2, CH_3CN, and HFIP.

III-6. Influence of solvent hydrogen-bond donor strength on τ_{CR}

As discussed above, the idea behind this study was to provide evidence that the large increase in the lifetimes of the charge-separated states correlates with the hydrogen-bond donor strength of the solvent but not with the solvent dielectric constant (ε_s). Therefore, 6 solvents have been compared together based on their Gutmann acceptor numbers (AN), their Reichardt parameter (E_T^N), and their dielectric constant (ε_r) (Table 3.2).

Solvent	AN	E_T^N	ε_r	τ_{CR} [ns] TAA-Ru-AQ	τ_{CR} [ns] TAA-Os-AQ
Hexafluoroisopropanol	66.3	1.068	16.6	3019	1890
Trifluoroethanol	53.3	0.898	26.7	2870	692
Methanol	41.3	0.762	32.66	2359	218
n-Propanol	33.5	0.617	20.45	1856	209
Acetonitrile	18.9	0.460	35.94	1381	77
Dichloromethane	20.4	0.309	8.93	747	46

Table 3.2: Gutmann acceptor numbers (AN), Reichardt parameter (E_T^N), and dielectric constant of the solvents (ε_r). Lifetimes of TAA^+-Ru^{2+}-AQ^- and TAA^+-Os^{2+}-AQ^- measured in 6 different solvents under deoxygenated conditions.

AN is a measure for the Lewis acidity of a solvent [18]. In the present case the Lewis acidity may be interpreted as a measure of hydrogen-bond donor strength when the reduced AQ moiety in TAA^+-Ru^{2+}-AQ^- and TAA^+-Os^{2+}-AQ^- is present. E_T^N represents an alternative measure of the Lewis acidity of a solvent [19-20]. The lifetimes of the charge-separated states of the triads in 6 solvents are reported in the fifth and sixth column in Table 3.2. Transient absorption decays measured in different solvents at 570 nm and 770 nm are shown in Figure 3.10.

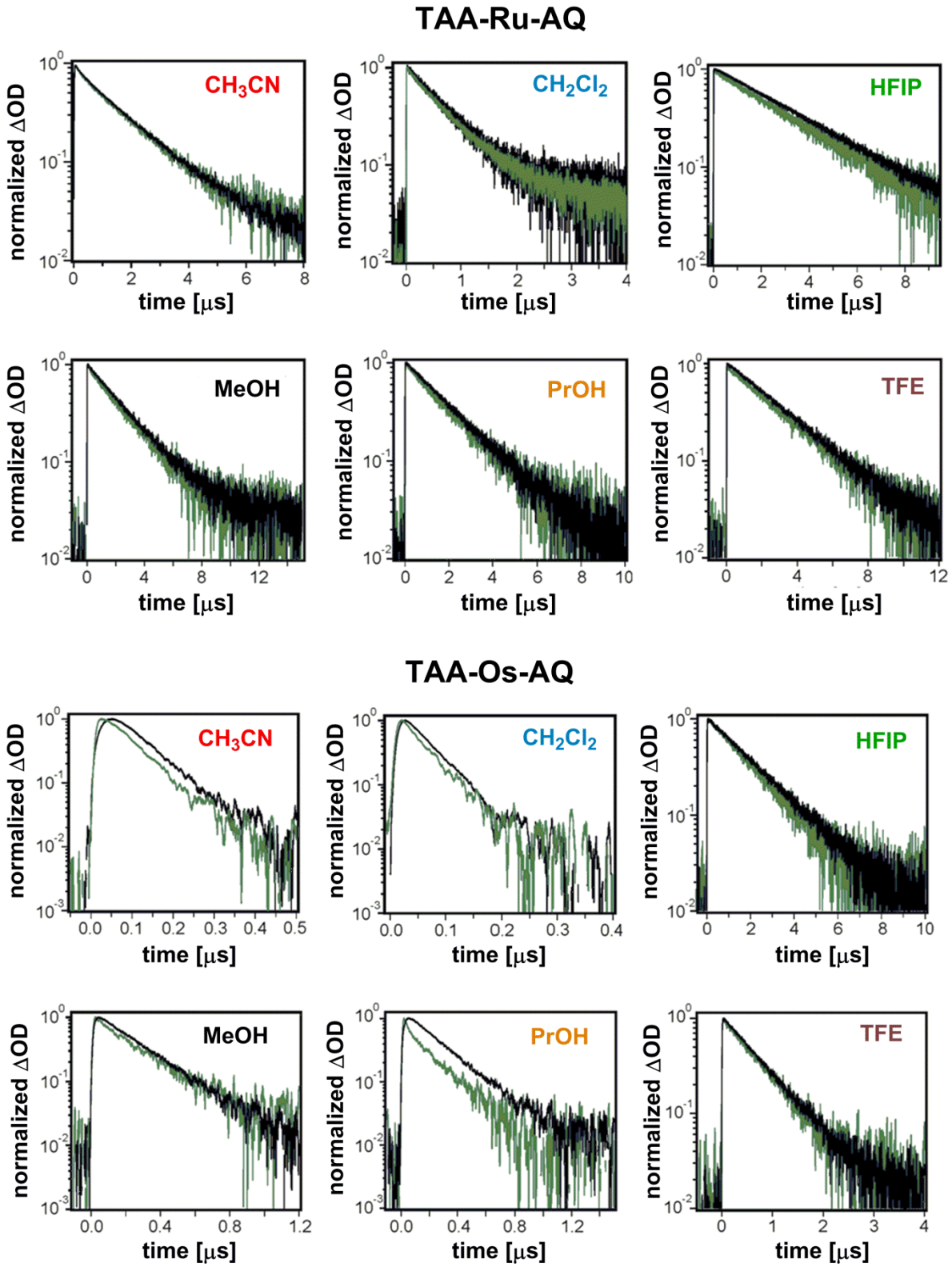

Figure 3.10: Transient absorption decays at 570 nm (green traces) and 770 nm (black traces) of TAA-Ru^{2+}-AQ and TAA-Os^{2+}-AQ in CH_3CN, CH_2Cl_2, HFIP, *n*-propanol (PrOH), methanol (MeOH), and trifluoroethanol (TFE).

From Table 3.2 we see that τ_{CR} increases with the increase of AN number and E_T^N parameter (Figure 3.11a). For instance when going from CH_2Cl_2 (E_T^N = 0.309) to HFIP (E_T^N = 1.068), τ_{CR} increases from 747 ns to 3019 ns in the ruthenium triad and from 46 ns to 1890 ns in the osmium triad, respectively. By contrast, it is obvious that ε_r does not correlate at all with τ_{CR} (Figure 3.11b). In fact, if the lengthening in τ_{CR} were due to the increase of the dielectric constant ε_r, acetonitrile with ε_r = 35.94 should have the longest lifetimes, which is not the case.

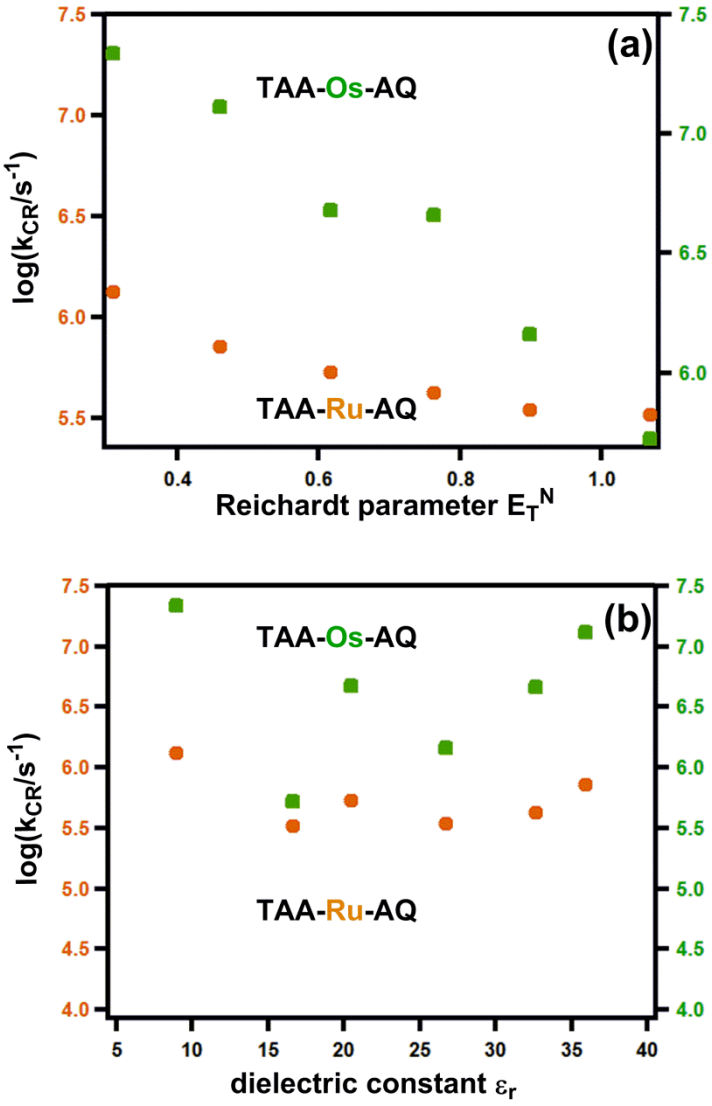

Figure 3.11 (a) Plot of log(k_{CR}) versus Reichardt parameter in TAA-Ru-AQ (orange circles), and TAA-Os-AQ (green squares), (b) Plot of log(k_{CR}) versus dielectric constant of the solvent in TAA-Ru-AQ (orange circles), and TAA-Os-AQ (green squares).

References

[1] Mayer, J. M., *Annu. Rev. Phys. Chem.* **2004,** *55*, 363.

[2] Reece, S. Y.; Nocera, D. G., *Annu. Rev. Biochem.* **2009,** *78*, 673.

[3] Hammes-Schiffer, S., *Acc. Chem. Res.* **2009,** *42*, 1881.

[4] Dempsey, J. L.; Winkler, J. R.; Gray, H. B., *Chem. Rev.* **2010,** *110*, 7024.

[5] Wenger, O. S., *Chem.-Eur. J.* **2011,** *17*, 11692.

[6] Hammarström, L.; Styring, S., *Energy Environ. Sci.* **2011,** *4*, 2379.

[7] Hammes-Schiffer, S.; Stuchebrukhov, A. A., *Chem. Rev.* **2010,** *110*, 6939.

[8] Warren, J. J.; Tronic, T. A.; Mayer, J. M., *Chem. Rev.* **2010,** *110*, 6961.

[9] Hung, S. C.; Macpherson, A. N.; Lin, S.; Liddell, P. A.; Seely, G. R.; Moore, A. L.; Moore, T. A.; Gust, D., *J. Am. Chem. Soc.* **1995,** *117*, 1657.

[10] Kawai, K.; Osakada, Y.; Takada, T.; Fujitsuka, M.; Majima, T., *J. Am. Chem. Soc.* **2004,** *126*, 12843.

[11] Okamoto, K.; Fukuzumi, S., *J. Phys. Chem. B* **2005,** *109*, 7713.

[12] Fukuzumi, S.; Okamoto, K.; Yoshida, Y.; Imahori, H.; Araki, Y.; Ito, O., *J. Am. Chem. Soc*. **2003,** *125*, 1007.

[13] Fukuzumi, S.; Yoshida, Y.; Okamoto, K.; Imahori, H.; Araki, Y.; Ito, O., *J. Am. Chem. Soc*. **2002,** *124*, 6794.

[14] Malferrari, M.; Francia, F.; Venturoli, G., *J. Phys. Chem. B* **2011,** *115*, 14732.

[15] Gupta, N.; Linschitz, H., *J. Am. Chem. Soc.* **1997,** *119*, 6384.

[16] Ahmed, S.; Khan, A. Y.; Qureshi, R.; Subhani, M. S., *Russ. J. Electrochem.* **2007,** *43*, 811.

[17] Babaei, A.; Connor, P. A.; McQuillan, A. J.; Umapathy, S., *J. Chem. Ed.* **1997,** *74*, 1200.

[18] Gutmann, V., *Coord. Chem. Rev.* **1976,** *18*, 225.

[19] Reichardt, C., *Angew. Chem. Int. Ed.* **1965,** *4*, 29-40.

[20] Reichardt, C., *Chem. Rev.* **1994,** *94*, 2319-2358.

Summary and Conclusions

The aim of this thesis was to study photoinduced electron transfer in dyad and triad systems. Although this topic was and still is explored by many research groups, I am positive that I brought new insights that are useful to many scientists in this field. As can be seen on several occasions in this thesis, large numbers of experiments have been carefully performed, and the results are discussed thoroughly and accurately.

In the first part of chapter **1**, I have demonstrated that despite a low driving force for electron transfer in a ruthenium-anthraquinone dyad in CH_2Cl_2, changing different parameters can have a strong impact on the photoinduced electron transfer:

- Upon increasing the dielectric constant of the solvent (ε_r) when going from CH_2Cl_2 (ε_r = 8.93) to CH_3CN (ε_r = 35.94), intramolecular photoinduced electron transfer in molecular ruthenium-anthraquinone dyads is accelerated and becomes competitive with other excited-state deactivation processes inherent to the $Ru(bpy)_3^{2+}$ photosensitizer. A change from pure acetonitrile to a 1:1 CH_3CN/H_2O solvent mixture (ε_r = 55.7) reveals a more important increase of electron transfer rates. I initially searched for PCET in CH_3CN/H_2O mixtures with these anthraquinone systems but so far was not successful in this respect.

- Introducing *tert*-butyl substituents in the bpy ancillary ligands leads to an increase in the driving force which was manifested by an acceleration of the rate constant (k_{ET}) by an order of magnitude.

- Replacement of the *p*-xylene spacer by a *p*-dimethoxybenzene units leads to a decrease in the donor-acceptor energy gap and causes an increase in electron transfer rate by a factor of 3.5.

This part of my thesis was published in the RSC journal *Physical Chemistry Chemical Physics.* [1]

In the second part of chapter **1**, my investigations have been mainly focused on the influence of hydrogen-bonding solvent on photoinduced intramolecular electron transfer. Prior to electron transfer in the dyad systems, one molecule of HFIP is weakly bound to the charge-neutral AQ in dichloromethane solution. The hydrogen-bonding association constant (K_{eq}) is on the order of 1 M^{-1}. Upon photoexcitation of the dyads, an anthraquinone radical anion is

formed (AQ^-) which is considered as a good hydrogen-bond acceptor. I found that on average 2.5 of HFIP molecules are tightly hydrogen-bonded to the anthraquinone monoanion with a relatively large association constant per individual HFIP molecule ($K_{eq} = 1.6 \times 10^4 M^{-1}$).

I have also demonstrated in this second part that based on the pK_a values HFIP cannot protonate neither the charge-neutral AQ nor the reduced AQ (AQ^-). I arrived at the conclusion that instead of having full proton transfer as in the case of proton-coupled electron transfer (PCET), the photoinduced process in my dyad may be regarded as partial transfer of proton density from the hydrogen-bond donor towards the hydrogen-bond acceptor. In other words, hydrogen bonds are strengthened.

This part of my thesis was published in the *Journal of Physical Chemistry A*. [2]

In chapter **2**, I have demonstrated vectorial electron transfer in three linear triads incorporating $Ru(bpy)_3^{2+}$, $Os(bpy)_3^{2+}$, and $[Ir(2\text{-}(p\text{-tolyl})pyridine)_2(bpy)]^+$ complexes as photosenitizers. Photoexcitation of these triads leads to fully charge-separated states containing an oxidized triarylamine (TAA^+) which absorbs at 770 nm and a reduced anthraquinone (AQ^-) manifested by two absorption bands at 380 nm and 570 nm in transient absorption spectroscopy.

The formation of the radical species in the fully charge-separated states occurred in two steps with lifetimes in the picosecond regime. These states are formed through different kinetic pathways: In the ruthenium triad reductive quenching of the initially excited state is kinetically favored, while in the osmium triad oxidative quenching is most likely predominant. In the iridium triad, both pathways are kinetically competitive, but reductive quenching dominates.

By contrast, thermal charge-recombination between TAA^+ and AQ^- back to the ground state occurs in one step with lifetimes on the order of microseconds in the ruthenium and the iridium triads. These long-lived charge-separated states are kinetically stabilized by three factors: (i) inverted driving-force effect, (ii) spin selection rule, (iii) long electron-hole separation distance (~ 22 Å).

Surprisingly, τ_{CR} in the osmium triad is approximately an order of magnitude shorter than in the ruthenium and iridium triads. This has been explained by the thermal population of the

energetically close-by TAA-Os^{3+}-AQ^- and the TAA^+-Os^{2+}-AQ^- states which probably quench the fully charge-separated state.

The quantum yield for the formation of the charge-separated states is almost 100 % for the ruthenium and iridium triads and about 46 % for the osmium triad.

Extracts of this part of my thesis were published in *Chemical Communications*.[3] A full paper has been submitted recently.

In chapter **3**, I have demonstrated that the lifetime of the charge-separated state (τ_{CR}) in the TAA-Ru-AQ triad increases by a factor of 4 when changing the solvent from CH_2Cl_2 to HFIP, while in the TAA-Os-AQ triad τ_{CR} increases by a factor of 41. This significant increase in τ_{CR} is presumably due to hydrogen-bonding between the anthraquinone radical anion (AQ^-) and HFIP (considered as strong hydrogen-bond donor). Moreover, based on my investigations in different solvents, it was found that τ_{CR} correlates with the hydrogen-bond strength of the solvent, while there is absence of any correlation with the dielectric constant of the solvent. Hydrogen-bonding contributes to both thermodynamic and kinetic stabilization of the fully charge-separated states. Thermodynamically, the TAA^+-M^{2+}-AQ^- state is stabilized by roughly 0.3 eV when going from CH_2Cl_2 to HFIP. Hydrogen-bonding may also lead to an increase of the reorganization energy.

Extracts of this of my thesis were communicated in *Chemistry - A European Journal*.[4] A full paper has been submitted recently.

References

[1] Hankache, J.; Wenger, O. S., *Phys. Chem. Chem. Phys.* **2012,** *14*, 2685.

[2] Hankache, J.; Hanss, D.; Wenger, O. S., *J. Phys. Chem. A* **2012**, *13*, 3347.

[3] Hankache, J.; Wenger, O. S., *Chem. Commun.* **2011,** *47*, 10145.

[4] Hankache, J.; Wenger, O. S., *Chem.-Eur. J.* **2012**, *18*, 6443.

Experimental Section




1. Scientific instrumentation used for experimental investigations

Commercially available chemicals were used as received without further purification. For thin-layer chromatography, Polygram SIL G/UV254 plates from Machery-Nagel were used. Silica Gel 60 from Macherey-Nagel was used for preparative column chromatography.

^{1}H NMR spectra have been recorded on a Bruker Avance 300 MHz or 400 MHz spectrometer. All chemical shifts are reported relative to the tetramethylsilane signal.

Electron ionization mass spectrometry (ESI-MS) was performed using a FTCIR-MS APEX IV (Bruker) instrument and elemental analysis was performed on a Vario EL III CHNS analyzer from Elementar.

Cyclic voltammograms were obtained using a Versastat3-200 potentiostat from Princeton Applied Research. A platinum disk was used as a working electrode. A platinum wire served as a quasi-reference electrode and a silver wire was used as a counter electrode. Voltage sweeps occurred at rates of 100 mV/s, solutions were deoxygenated by bubbling N_2 gas prior to measurements.

Optical absorption spectra were recorded on a Cary 300 spectrometer from Varian.

Spectro-electrochemical experiments were performed using the Cary 300 spectrometer, the potentiostat mentioned above, and an optically transparent thin-layer (OTTLE) cell from Specac.

Steady-state luminescence spectra were measured on a Fluorolog-3 instrument (FL322) from Horiba Jobin-Yvon, equipped with a TBC-07C detector from Hamamatsu.

Transient absorption and time-resolved luminescence in the nanosecond time domain was measured using an LP920-KS instrument from Edinburgh Instruments. The detection system of the LP920-KS spectrometer consisted of an R928 photomultiplier and an iCCCD camera from Andor. The excitation source was a Quantel Brilliant b laser (frequency-doubled or -tripled).

2. Synthetic protocols and product characterization data

TMS-xy-Br

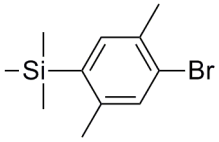

1,4-dibromo-*p*-xylene (10.00 g, 38 mmol) was dissolved in dry THF (70 ml) under inert atmosphere. 28.4 ml of *n*-BuLi (1.6 M in hexane) was added dropwise at -78°C. This temperature was maintained for 1 hour, and trimethylsilyl chloride (5.74 ml) was added slowly. After stirring overnight at room temperature, the product was extracted with CH_2Cl_2 and dried over $MgSO_4$. The combined organic solvents were removed to afford the desired compound as a colorless oil (9.78 g, 100 %).

^{1}H NMR: (400 MHz, $CDCl_3$, 25°C): δ [ppm] = 0.31 (s, 9 H, TMS), 2.36 (s, 3 H, CH_3), 2.39 (s, 3 H, CH_3), 7.27 (s, 1 H, xy), 7.34 (s, 1 H, xy).

TMS-xy-B(OH)$_2$

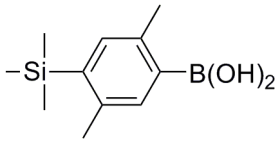

Grains of magnesium (1.017 g, 42 mmol) were suspended in dry THF (10 ml). A solution of TMS-xy-Br (9.78 g, 38 mmol) in the same solvent (40 ml) was added very slowly to the suspension of magnesium under inert atmosphere at 60°C. The mixture was heated to reflux for 1 hour, then cooled to room temperature and finally to -78°C. Then $B(OCH_3)_3$ (4.34 g, 42 mmol) was added, and the reaction mixture was stirred at room temperature overnight. Aqueous HCl solution (2 M, 50 ml) was added slowly with stirring for 10 minutes. The product was extracted with CH_2Cl_2, and the solvents were removed under vacuum. This gave the product as a white solid (7.5 g, 89 %).

^{1}H NMR: (400 MHz, acetone-d_6/D_2O (3/1), 25°C): δ [ppm] = 0.16 (s, 9 H, TMS), 2.36 (s, 3 H, CH_3), 2.39 (s, 3 H, CH_3), 7.06 (s, 1 H, xy), 7.23 (s, 1 H, xy).

bpy-xy$_0$-AQ

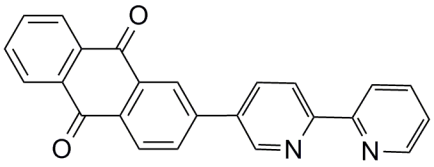

5-(tri-*n*-butylstannyl)-2,2'-bipyridine [1] (0.20 g, 0.45 mmol) was added to a solution of 2-bromoanthraquinone (0.10 g, 0.34 mmol) in 30 ml of *m*-xylene. Once the solution was deoxygenated by bubbling with nitrogen gas, $Pd(PPh_3)_4$ catalyst (0.06 g, 0.05 mmol) was added, and the solution was refluxed for two days. The solvent was removed by rotary evaporation. The crude product was purified by flash column chromatography over silica gel using a mixture of CH_2Cl_2/CH_3OH (9/1). The bpy-xy$_0$-AQ product was obtained as a yellow solid (0.035 g, 30% yield).

^{1}H NMR (300 MHz, $CDCl_3$, 25°C): δ [ppm] = 7.36 (m, 1 H, xy), 7.84 (m, 3 H, AQ), 8.14 (dd, *J* = 8.0 Hz, 2.0 Hz, 2 H, bpy), 8.55 (m, 6 H), 8.73 (d, *J* = 4.0 Hz, 1 H, bpy), 9.06 (m, 1 H, bpy).

TMS-xy-AQ

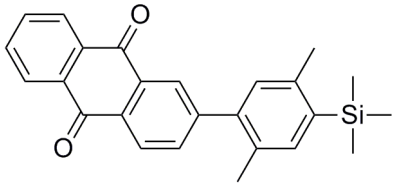

2-bromoanthraquinone (5.00 g, 17.4 mmol), 4-trimethylsilyl-2,5-dimethylphenylboronic acid (TMS-xy-B(OH)$_2$) (4.64 g, 0.02 mol) and a solution of Na_2CO_3 (5.53 g, 52.2 mmol) in de-ionized water were dissolved in a solvent mixture comprised of 30 ml toluene and 5 ml ethanol. The solution was deoxygenated for 30 minutes before adding the $Pd(PPh_3)_4$ catalyst and heating to reflux overnight. The product was extracted with CH_2Cl_2 and purified by silica gel column chromatography. The eluent was a 1:1 pentane/dichloromethane mixture. A yellow solid was obtained (6.45 g, 96% yield).

^{1}H NMR: (400 MHz, $CDCl_3$, 25°C): δ [ppm] = 0.38 (s, 9 H, TMS), 2.30 (s, 3 H, CH_3), 2.49 (s, 3 H, CH_3), 7.11 (s, 1 H, xy), 7.4 (s, 1 H, xy), 7.82 (m, 3 H, AQ), 8.35 (m, 4 H, AQ).

I-xy-AQ

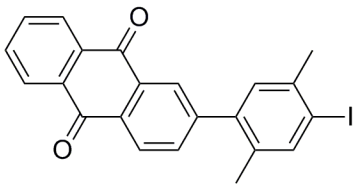

TMS-xy-AQ (4.47 g, 0.011 mol) was dissolved in dichloromethane (20 ml). ICl (3.78 g, 0.023 mol) in an acetonitrile solution (80 ml) was added dropwise under nitrogen at 0°C to the dichloromethane solution. After stirring at room temperature overnight, the mixture was washed with an aqueous solution of $Na_2S_2O_3$ (5% in water, 250 ml). The two resulting phases were separated. Afterwards, the yellow organic phase was dried over $MgSO_4$ and filtered. The solvent was evaporated, and the desired product was obtained as a yellow powder in essentially quantitative yield.

^{1}H NMR: (400 MHz, $CDCl_3$, 25°C): δ [ppm] = 2.23 (s, 3 H, CH_3), 2.45 (s, 3 H, CH_3), 7.14 (s, 1 H, xy), 7.73 (dd, *J* = 8.0 Hz, 2.0 Hz, 1 H, AQ), 7.79 (s, 1 H, AQ), 7,83 (m, 2 H, AQ), 8.25 (d, *J* = 1.6 Hz, 1 H, xy), 8.35 (m, 3 H, AQ).

bpy-xy-AQ

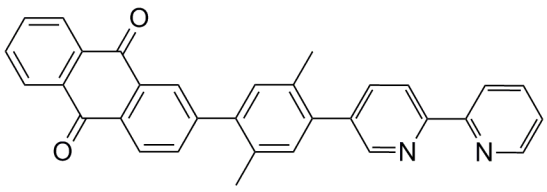

$Pd(PPh_3)_4$ (0.04 g, 0.03 mmol) was added under inert atmosphere to a stirred and deoxygenated suspension of I-xy-AQ (0.30 g, 0.68 mmol) and 5-(tri-*n*-butylstannyl)-2,2'-bipyridine (0.40 g, 0.90 mmol) in *m*-xylene (30 ml). The yellow suspension was deoxygenated for an additional 10 minutes, and then the reaction was carried out at reflux during 48 hours. After cooling to room temperature, the solvent was removed under reduced pressure. The dark brown remaining solid was purified by three consecutive silica gel column chromatographies, using a mixture of CH_2Cl_2/CH_3OH (9/1) to give the product as a yellow solid (0.12 g, 38% yield).

^{1}H NMR (400 MHz, $CDCl_3$, 25°C): δ [ppm] = 2.35 (m, 6 H, *J* = 3.2 Hz, CH_3), 7.27 (s, 1 H, xy), 7.34 (ddd, *J* = 4.8 Hz, 1.2 Hz, 0.8 Hz, 1 H, xy), 7.85 (m, 5 H, AQ), 8.35 (m, 3 H), 8.40

(d, *J* = 8.0 Hz, 1 H, bpy), 8.46 (td, *J* = 8.0 Hz, 0.8 Hz, 1 H, bpy), 8.5 (dd, *J* = 8.0 Hz, 0.8 Hz, 1 H, AQ), 8.72 (m, 2 H, bpy).

TMS-xy$_2$-AQ

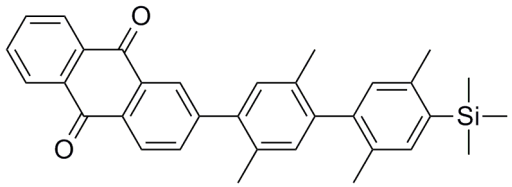

I-xy-AQ (3.00 g, 6.84 mmol) and TMS-xy-B(OH)$_2$ (1.67 g, 7.55 mmol) were dissolved together in toluene (100 ml). Then, a solution of Na_2CO_3 (2.18 g, 0.02 mol) in de-ionized water (20 ml) was added. The yellow mixture was deoxygenated by bubbling nitrogen gas during 30 minutes. After addition of the $Pd(PPh_3)_4$ catalyst (0.395 g, 0.14 mmol), the reaction mixture was heated to 90°C overnight under nitrogen atmosphere. After cooling to room temperature, the organic layer was extracted with CH_2Cl_2, dried over $MgSO_4$, and filtered. The solvent was removed under reduced pressure. A yellow solid was obtained, and the raw product was purified by silica gel column chromatography using an 80% pentane / 20% dichloromethane eluent mixture (3.18 g, 95% yield).

^{1}H NMR (400 MHz, $CDCl_3$, 25°C): δ [ppm] = 0.37 (s, 9 H, TMS), 2.11 (s, 6 H, CH_3), 2.30 (s, 3 H, CH_3), 2.45 (s, 3 H, CH_3), 6.96 (s, 1 H, xy), 7.07 (s, 1 H, xy), 7.55 (s, 1 H, xy), 7.35 (s, 1 H, xy), 7.82 (m, 3 H, AQ), 8.35 (m, 4 H, AQ).

I-xy$_2$-AQ

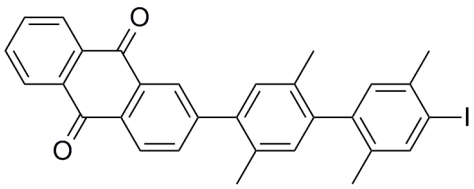

TMS-xy$_2$-AQ (3.18 g, 6.51 mmol) was dissolved in dichloromethane (80 ml). ICl (2.11 g, 0.013 mol) in an acetonitrile solution (60 ml) was added dropwise under inert atmosphere at 0°C. After stirring for one night at room temperature, excess iodine monochloride was destroyed by adding an aqueous saturated solution of $Na_2S_2O_3$. The organic phase was extracted with CH_2Cl_2, dried over $MgSO_4$, and filtered. The solvent was removed under reduced pressure to give a yellow powder (3.1 g, 88% yield).

^{1}H NMR (400 MHz, $CDCl_3$, 25°C): δ [ppm] = 2.05 (s, 3 H, CH_3), 2.07 (s, 3 H, CH_3), 2.30 (s, 3 H, CH_3), 2.43 (s, 3 H, CH_3), 7.02 (s, 2 H, xy), 7.19 (s, 1 H, xy), 7.75 (s, 1 H, xy), 7.83 (m, 3 H, AQ), 8.36 (m, 4 H, AQ).

bpy-xy$_2$-AQ

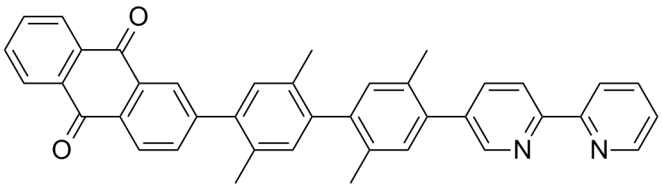

For the Stille coupling reaction, I-xy$_2$-AQ (0.31 g, 0.57 mmol) was dissolved in *m*-xylene (30 ml) with 5-(tri-*n*-butylstannyl)-2,2'-bipyridine [1] (0.33 g, 0.74 mmol). The $Pd(PPh_3)_4$ catalyst (0.066 g, 0.057 mmol) was added once the mixture was deoxygenated by bubbling nitrogen gas for 15 minutes. Afterwards, an additional deoxgenation was carried out, and the solution was heated to reflux under nitrogen during 2 days. The solvent was evaporated, and the resulting black solid was chromatographed on silica gel using a 99:1 dichloromethane/methanol eluent mixture affording a light yellow solid (0.11 g, 35% yield).

^{1}H NMR (300 MHz, $CDCl_3$, 25°C): δ [ppm] = 2.16 (s, 6 H, CH_3), 2.33 (d, *J* = 3 Hz, 6 H, CH_3), 7.12 (s, 2 H, CH_3, xy), 7.22 (d, *J* = 3 Hz, 2 H, xy), 7.33 (ddd, *J* = 3 Hz, 6 Hz, 9 Hz, 1 H, bpy), 7.85 (m, 5 H), 8.36 (m, 4 H), 8.47 (m, 2 H, bpy), 8.72 (ddd, *J* = 0.87 Hz, 1.7 Hz, 4.8 Hz, 1 H, bpy), 8.75 (dd, *J* = 0.72 Hz, 2.2 Hz, 1 H, bpy).

TMS-xy$_3$-AQ

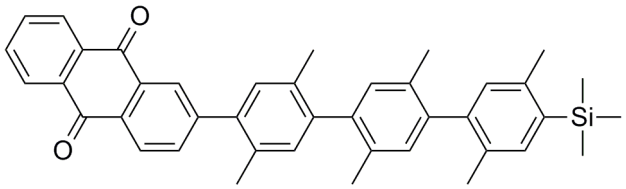

I-xy$_2$-AQ (2.80 g, 5.16 mmol) and TMS-xy-B(OH)$_2$ (1.26 g, 5.68 mmol) were dissolved in toluene (100 ml) and ethanol (20 ml). A solution of Na_2CO_3 (1.64 g, 0.015 mol) in de-ionized water (20 ml) was added, and the yellow solution was deoxygenated by bubbling nitrogen gas during 30 minutes. $Pd(PPh_3)_4$ catalyst (0.30 g, 0.26 mmol) was added, followed by heating the mixture to 90°C overnight. After cooling to room temperature, the organic layer was extracted with CH_2Cl_2, dried over $MgSO_4$, and filtered. The solvent was removed under reduced pressure. A yellow solid was obtained. This raw product was purified by silica gel column chromatography using a mixture of pentane/dichloromethane (first 8:2 and then 1:1) to give the pure product (2.40 g, 78% yield).

1H NMR (400 MHz, $CDCl_3$, 25°C): δ [ppm] = 0.37 (s, 9 H, TMS), 2.08 (s, 3 H, CH_3), 2.11 (m, 6 H, CH_3), 2.15 (d, *J* = 5.2 Hz, 3 H, CH_3), 2.33 (s, 3 H, CH_3), 2.46 (s, 3 H, CH_3), 6.99 (s, 1 H, xy), 7.03 (t, *J* = 5.2 Hz, 2 H, xy), 7.15 (s, 1 H, xy), 7.22 (s, 1 H, xy), 7.35 (s, 1 H, xy), 7.84 (m, 3 H, AQ), 8.37 (m, 4 H, AQ).

I-xy$_3$-AQ

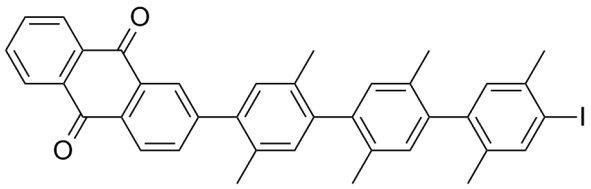

To a solution of TMS-xy$_3$-AQ (1.25 g, 2.10 mmol) in dichloromethane (80 ml), ICl (0.69 g, 4.21 mmol) dissolved in acetonitrile (60 ml) was added dropwise under inert atmosphere at 0°C. After stirring at room temperature overnight, an aqueous saturated solution of $Na_2S_2O_3$ was added. The organic layer was extracted with CH_2Cl_2, dried over $MgSO_4$ and filtered. The solvent was removed under reduced pressure. This yielded a yellow powder (1.18 g, 87% yield).

^{1}H NMR (400 MHz, $CDCl_3$, 25°C): δ [ppm] = 0.37 (s, 9 H, TMS), 2.11 (s, 6 H, CH_3), 2.30 (s, 3 H, CH_3), 2.45 (s, 3 H, CH_3), 6.96 (s, 1 H, xy), 7.07 (s, 1 H, xy), 7.55 (s, 1 H, xy), 7.35 (s, 1 H, xy), 7.82 (m, 3 H, AQ), 8.35 (m, 4 H, AQ).

bpy-xy$_3$-AQ

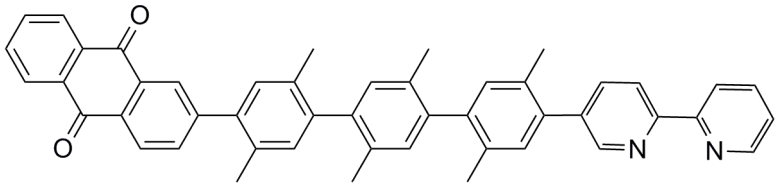

Pd(PPh$_3$)$_4$ catalyst (0.053 g, 0.04 mmol) was added to a deoxygenated solution of I-xy$_3$-AQ (0.30 g, 0.46 mmol) and 5-(tri-*n*-butylstannyl)-2,2'-bipyridine [1] (0.27 g, 0.60 mmol) in 30 ml of *m*-xylene. The reaction mixture was heated to reflux for 48 hours. The desired yellow compound was obtained after evaporation of the solvent and subsequent purification with silica gel column chromatography using pure dichloromethane as the eluent (0.08 g, 26% yield).

^{1}H NMR (300 MHz, $CDCl_3$, 25°C): δ [ppm] = 2.13 (s, 6 H, CH_3), 2.16 (m, 6 H, CH_3), 2.34 (s, 6 H, CH_3), 7.07 (m, 2 H, xy), 7.16 (s, 2 H, xy), 7.21 (s, 1 H, xy), 7.23 (s, 1 H, xy), 7.35 (m, 1

H, bpy), 7.85 (m, 5 H), 8.41 (m, 4 H, AQ), 8.47 (m, 2 H, bpy), 8.72 (m, 1 H, bpy), 8.76 (m, 1H, bpy).

TMS-xy$_4$-AQ

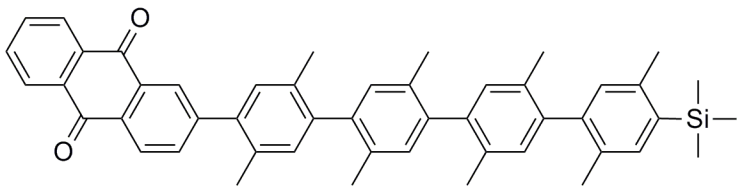

TMS-xy$_4$-AQ was obtained by cross-coupling of I-xy$_3$-AQ (0.87 g, 1.34 mmol) to TMS-xy-B(OH)$_2$ (0.33 g, 1.48 mmol) in toluene/ethanol (80/20 ml). A solution of Na_2CO_3 (0.043 g, 4 mmol) in de-ionized water was added. After deoxygenating the mixture by bubbling nitrogen gas, Pd(PPh$_3$)$_4$ (0.08 g, 0.07 mmol) was added, and the solution was heated to 90° C during 2 days. After cooling to room temperature, the organic layer was extracted with CH_2Cl_2. Solvent removal under reduced pressure afforded a yellow solid which was purified by column chromatography on silica gel using a 1:1 pentane/dichloromethane eluent mixture (0.89 g, 76% yield).

^{1}H NMR (400 MHz, $CDCl_3$, 25°C): δ [ppm] = 0.37 (s, 9 H, TMS), 2.10 (m, 15 H, CH_3), 2.17 (d, *J* = 4.8 Hz, 3 H, CH_3), 2.34 (s, 3 H, CH_3), 2.46 (s, 3 H, CH_3), 7.00 (m, 2 H, xy), 7.06 (m, 3 H, xy), 7.17 (s, 1 H, xy), 7.23 (s, 1 H, xy), 7.34 (s, 1 H, xy), 7.83 (m, 3 H, AQ), 8.38 (m, 4 H, AQ).

I-xy$_4$-AQ

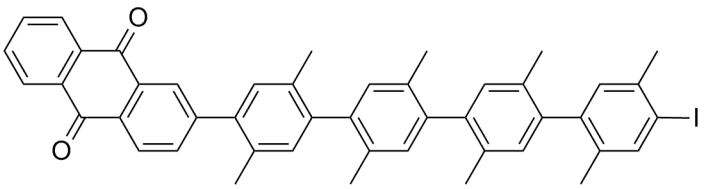

0.89 g of TMS-xy$_4$-AQ (0.12 mmol) was suspended in a mixture of 20 ml dichloromethane and 40 ml acetonitrile in the dark at 0^{o}C. A solution of ICl (0.42 g, 0.25 mmol) in acetonitrile was added slowly to the cooled mixture under inert atmosphere. After stirring at room temperature overnight, 50 ml of an aqueous solution of $Na_2S_2O_3$ was added, and the organic layer was extracted with CH_2Cl_2. Evaporation of the solvent afforded the desired product as a yellow solid in essentially quantitative yield.

bpy-xy$_4$-AQ

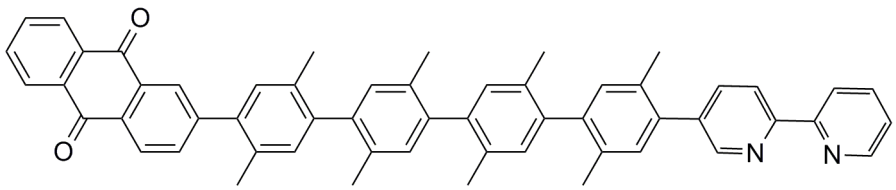

I-xy$_4$-AQ (0.17 g, 0.22 mmol) was dissolved in 30 ml of *m*-xylene. 5-(tri-*n*-butylstannyl)-2,2'-bipyridine [1] (0.13 g, 0.29 mmol) was added, and the solution was deoxygenated for 15 min by bubbling nitrogen gas before and after adding the Pd(PPh$_3$)$_4$ catalyst (0.046 g, 0.039 mmol). The reaction mixture was heated to reflux for 2 days. The solvent was evaporated, and the crude product was purified by silica gel chromatography using a mixture of 99:1 dichloromethane/methanol. A yellow solid was obtained (50 mg, 30% yield).

^{1}H NMR: (300 MHz, $CDCl_3$, 25°C): δ [ppm] = 2.14 (s, 12 H, CH_3), 2.17 (m, 6 H, CH_3), 2.35 (s, 6 H, CH_3), 7.09 (m, 4 H, xy), 7.17 (s, 2 H, xy), 7.22 (m, 2 H, xy), 7.34 (m, 1 H, bpy), 7.85 (m, 5 H), 8.37 (m, 4 H), 8.47 (m, 2 H, bpy), 8.74 (m, 2 H, bpy).

Ru-xy$_0$-AQ

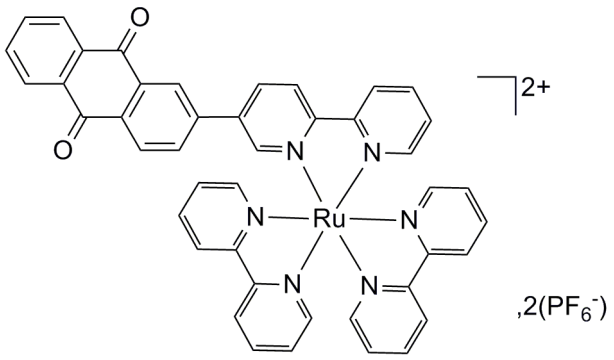

A solution of bpy-xy$_0$-AQ (0.035 g, 0.09 mmol) in 3 ml of chloroform and a solution of Ru(bpy)$_2$Cl$_2$ (0.046 g, 0.09 mmol) in 10 ml of ethanol were mixed together and heated to reflux overnight. Then, the solvents were evaporated, and the product was chromatographed on silica gel using a mixture of acetone/water/aqueous saturated solution of KNO_3 (80/19/1). Subsequently, the acetone was removed on a rotary evaporator. Upon addition of an aqueous saturated solution of KPF_6, an orange precipitate was obtained. This orange solid was filtrated, washed with water and diethyl ether, and finally dried under vaccum (0.071 g, 70% yield).

^{1}H NMR (300 MHz, $CDCl_3$, 25°C): δ [ppm] = 7.43 (m, 5 H), 7.77 (m, 4 H), 7.90 (m, 5 H), 8.08 (m, 5 H), 8.28 (m, 4 H), 8.44 (m, 1 H), 8.53 (m, 4 H), 8.62 (m, 2 H).

ES-MS m/z = 388.073 (calculated 388.075 for $C_{44}H_{30}N_6O_2Ru^{2+}$).

Anal. Calcd. for $C_{44}H_{30}N_6O_2RuP_2F_{12}$: C 49.59, H 2.84, N 7.89. Found: C 49.26, H 2.95, N 8.49.

Ru-xy$_1$-AQ

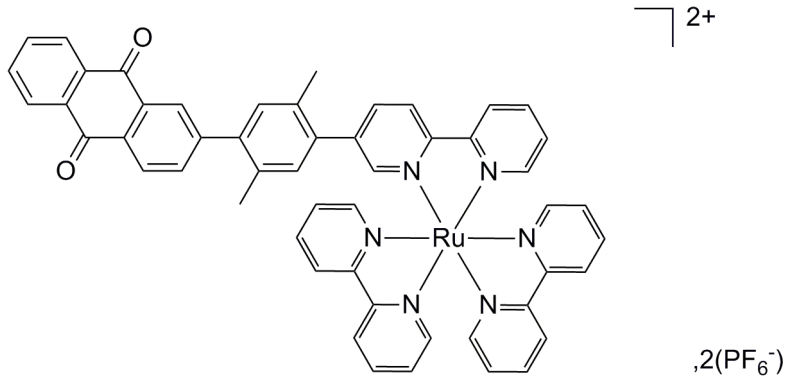

A suspension of bpy-xy-AQ (0.05 g, 0.1mmol) and $Ru(bpy)_2Cl_2$ (0.058 g, 0.1 mmol) in a mixture of $CHCl_3$/EtOH (3/10) was heated to reflux overnight under nitrogen atmosphere. The resulting red-orange solution was evaporated under reduced pressure. The remaining dark solid was purified by column chromatography on silica gel, using first pure acetone, then a mixture of acetone/H_2O/aqueous saturated KNO_3 (90/10/1) as the eluent. The resulting product was dissolved in minimum of acetone, and a saturated solution of KPF_6 in water was added. The orange precipitate was filtered, washed with water and diethyl ether, and finally dried under vacuum. The yield was 78%.

^{1}H NMR: (400 MHz, CD_3CN, 25°C): δ [ppm] = 2.02 (s, 3 H, CH_3), 2.25 (s, 3 H, CH_3), 7.13 (s, 1 H, xy), 7.22 (s, 1 H, xy), 7.44 (m, 5 H), 7.65 (d, *J* = 5.6 Hz, 1 H), 7.76 (d, *J* = 5.6 Hz, 3 H), 7.80 (d, *J* = 5.6 Hz, 1 H), 7.82 (d, *J* = 1.6 Hz, 8 Hz, 1 H), 7.90 (m, 3 H), 8.08 (m, 7 H), 8.19 (d, *J* = 1.6 Hz, 1 H), 8.30 (m, 3 H), 8.56 (m, 8 H).

ES-MS m/z = 440.1056 (calculated 440.1044 for $C_{52}H_{38}N_6O_2Ru^{2+}$).

Anal. Calcd. for $C_{52}H_{38}N_6O_2RuP_2F_{12}$ · H_2O · CH_3COCH_3: C 53.02, H 3.72, N 6.74. Found C 53.03, H 3.59, N 6.66.

Ru-xy_2-AQ

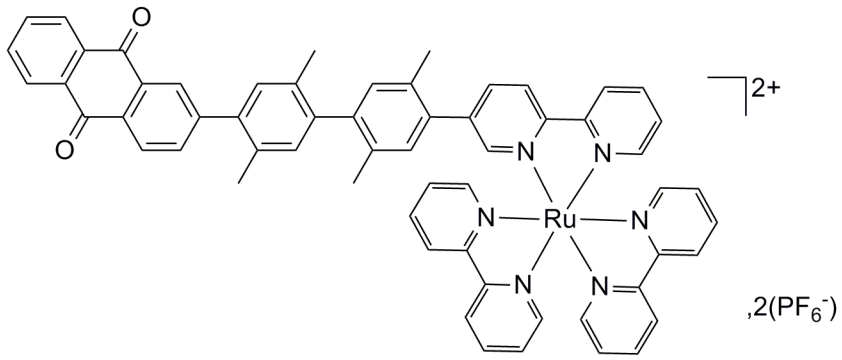

Ru-xy_2-AQ was obtained by refluxing bpy-xy_2-AQ (0.05 g, 0.087 mmol) and $Ru(bpy)_2Cl_2$ (0.04 g, 0.087 mmol) in a chloroform / ethanol mixture (3 ml / 10 ml) overnight. After removal of the solvent, the solid was chromatographed on silica gel using an eluent mixture comprised of 90% acetone, 9% water and 1% saturated aqueous solution of KNO_3. The acetone was evaporated, and the desired complex was precipitated by adding a saturated aqueous KPF_6 solution. The resulting red orange solid was isolated by filtration, washed with water and diethyl ether, and dried under vacuum (0.08 g, 72% yield).

^{1}H NMR (300 MHz, CD3CN, 25°C): δ [ppm] = 1.96 (m, 3 H, CH_3), 2.04 (m, 6 H, CH_3), 2.28 (s, 3 H, CH_3), 7.01 (s, 2 H, xy), 7.09 (d, *J* = 3.5 Hz, 1 H, xy), 7.27 (s, 1 H, xy), 7.44 (m, 5 H), 7.68 (m, 1 H), 7.76 (m, 4 H), 7.89 (m, 4 H), 8.07 (m, 6 H), 8.29 (m, 4 H), 8.52 (m, 5 H), 8.58 (m, 1 H).

ES-MS: m/z = 492.1363 (calculated 492.1363 for $C_{60}H_{46}N_6O_2Ru^{2+}$).

Anal. Calcd. for $C_{60}H_{46}N_6O_2RuP_2F_{12}$ · xylene: C 59.17, H 4.09, N 6.09. Found: C 58.96, H 4.06, N 6.34.

Ru-xy$_3$-AQ

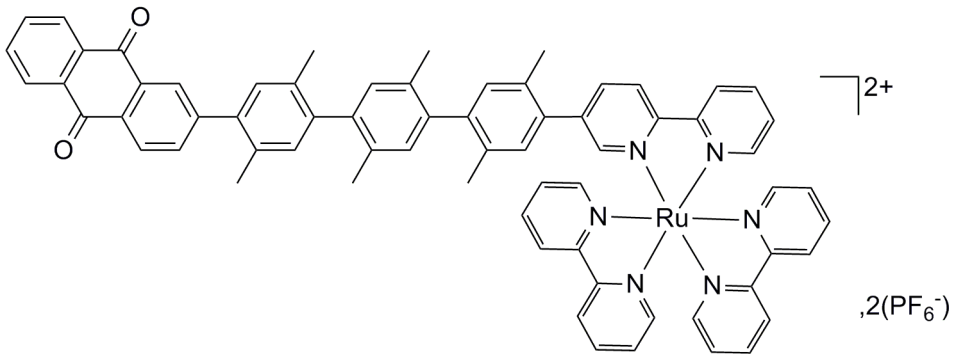

To a solution of bpy-xy$_3$-AQ (0.04 g, 0.06 mmol) in 3 ml of $CHCl_3$ was added a solution of Ru(bpy)Cl_2 (0.029 g, 0.06 mmol) in ethanol. The mixture was deoxygenated by bubbling nitrogen for 15 minutes, and then it was put to reflux overnight. The next day, the solvents were evaporated and the product was chromatographed on silica gel using a mixture of acetone/water/aqueous saturated solution of KNO_3 (80/19/1). After removing acetone, an aqueous saturated solution of KPF_6 was added, leading to an orange precipitate. The latter was filtrated, washed with water and diethyl ether, and dried under vaccum (0.07 g, 85% yield).

^{1}H NMR (400 MHz, $CDCl_3$, 25°C): δ [ppm] = 1.99 (m, 6 H, CH_3), 2.07 (m, 12 H, CH_3), 2.29 (s, 3 H, CH_3), 6.96 (s, 1 H, xy), 7.01 (s, 1 H, xy), 7.07 (m, 2 H, xy), 7.26 (s, 1 H, xy), 7.21 (s, 1 H, xy), 7.45 (m, 5 H), 7.82 (m, 5 H), 7.88 (m, 4 H), 8.08 (m, 6 H), 8.26 (m, 4 H), 8.56 (m, 6 H).

ES-MS: m/z = 544.1682 (calculated 544.1676 for $C_{68}H_{54}N_6O_2Ru^{2+}$).

Anal. Calcd. for $C_{68}H_{54}N_6O_2RuP_2F_{12}\cdot 1.5H_2O$: C 58.12, H 4.09, N 5.98. Found: C 58.06, H 4.09, N 5.82.

Ru-xy$_4$-AQ

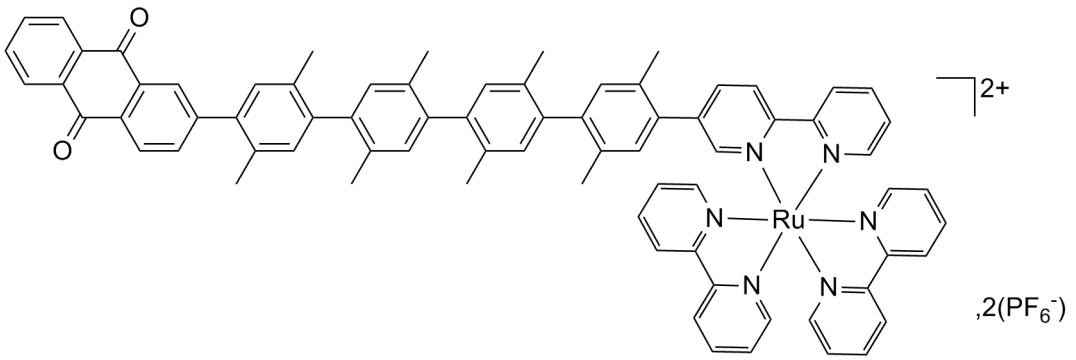

A solution of bpy-xy$_4$-AQ (0.04 g, 0.051 mmol) and Ru(bpy)$_2$Cl$_2$ (0.025 g, 0.051 mmol) in ethanol/chloroform (10/3) was heated to reflux for 48 hours. The solvents were evaporated under reduced pressure. The obtained solid was purified by silica gel column chromatography using a mixture of acetone/water/aqueous saturated solution of KNO_3 (80/19/1). Acetone was evaporated, and an aqueous saturated KPF_6 solution was added. An orange solid was precipitated, filtered, washed with water and diethyl ether, and dried over vacuum (0.026 g, 35% yield).

^{1}H NMR: (300 MHz, $CDCl_3$, 25°C): δ [ppm] = 1.99 (m, 3 H, CH_3), 2.03 (s, 3 H, CH_3), 2.09 (m, 12 H, CH_3), 2.14 (m, 6 H, CH_3), 6.97 (s, 1 H), 7.09 (m, 6 H), 7.31 (s, 1 H), 7.42 (m, 5 H), 7.70 (s, 1 H), 7.77 (m, 4 H), 7.90 (m, 4 H), 8.11 (m, 6 H), 8.31 (m, 4 H), 8.52 (m, 4 H), 8.59 (m, 2 H).

ES-MS: m/z = 596.2001 (calculated 596.1989 for $C_{76}H_{62}N_6O_2Ru^{2+}$)$^{\cdot}$.

Anal. Calcd. for $C_{76}H_{62}N_6O_2RuP_2F_{12}$: C 61.58, H 4.22, N 5.67. Found: C 61.27, H 4.45, N 5.59.

Ru(*t*Bu)-xy-AQ

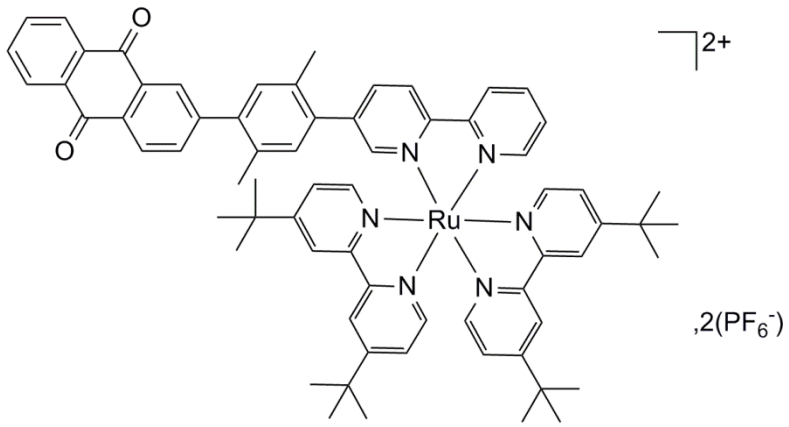

The same synthetic procedure as described for the Ru-xy-AQ was used. Ru(*t*Bu)-xy-AQ was obtained in 72% yield, by using ($Ru(^tBu\text{-}bpy)_2Cl_2$) [*t*Bu-bpy = 4,4'-di(*t*-butyl)-2,2'-bipyridine] instead of $Ru(bpy)_2Cl_2$.

^1H NMR: (400 MHz, $CDCl_3$, 25°C): δ [ppm] = 1.40 (m, 36 H, CH_3), 1.99 (s, 3 H, CH_3), 2.26 (s, 3 H, CH_3), 7.10 (s, 1 H, xy), 7.22 (s, 1 H, xy), 7.46 (m, 1 H), 7.50 (m, 1 H), 7.54 (m, 2 H), 7.63 (m, 2 H), 7.72 (m, 5 H), 7.82 (m, 2 H), 7.96 (td, *J* = 8.0 Hz, 1.3 Hz, 1 H), 8.07 (dd, *J* = 8.0 Hz, 2.0 Hz, 1 H), 8.19 (m, 4 H), 8.24 (m, 2 H), 8.32 (m, 3 H), 8.46 (m, 1 H), 8.55 (m, 1 H).

ES-MS m/z = 552.229 (calculated 552.229 for $C_{68}H_{70}O_2N_6Ru^{2+}$).

Anal. Calcd. for $C_{68}H_{70}N_6O_4RuP_2F_{12} \cdot 2H_2O$: C 57.10, H 5.21, N 5.88. Found C 57.02, H 5.24, N 5.65.

Br-dmb-TMS

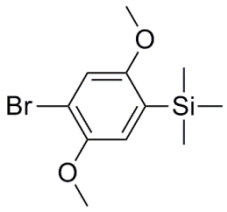

In a double-neck flask, 23.2 ml of *n*-BuLi (1.6 M in hexane) was added dropwise at -78°C to a solution of 1,4-dibromo-2,5-dimethoxybenzene (10.0 g, 0.033 mol) in dry THF (80 ml) under nitrogen at -78°C. After stirring for 1 hour at -78°C, 4.27 ml of trimethylsilyl chloride was added dropwise, and then the reaction was stirred overnight at room temperature. The organic layer was extracted with CH_2Cl_2 and evaporated to dryness. The crude product was purified by silica gel column chromatography using pentane as the eluent. The product (3.8 g, 39% yield) was obtained as a colorless oil which crystallized upon standing.

^{1}H NMR: (400 MHz, $CDCl_3$, 25°C): δ [ppm] = 0.26 (s, 9 H, TMS), 3.76 (s, 3 H, OCH_3), 3.86 (s, 3 H, OCH_3), 6.92 (s, 1 H, dmb), 7.01 (s, 1 H, dmb).

$B(OH)_2$-dmb-TMS

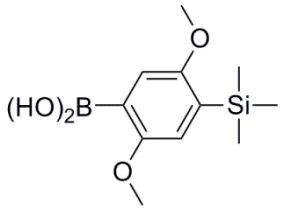

Br-dmb-TMS (3.8 g, 13 mmol) was dissolved in dry THF (50 ml) under inert atmosphere. 9.85 ml of *n*-BuLi (1.6 M in hexane) was added dropwise at -78°C. After 1 hour, triisopropylborate (4.55 ml, 20.0 mmol) was added at -78°C and the reaction was stirred overnight at room temperature. An aqueous solution of HCl (2 M, 50 ml) was added slowly, and the product was extracted by CH_2Cl_2. After evaporation of the solvent, the brown oil was purified by silica gel column chromatography using a mixture of pentane-dichloromethane (1:1) to afford the product as a pale brown solid (1.98 g, 60% yield).

^{1}H NMR: (400 MHz, Acetone-d_6/D_2O (3/1), 25°C): δ [ppm] = 0.28 (s, 9 H, TMS), 3.80 (s, 3 H, CH_3), 3.90 (s, 3 H, CH_3), 6.94 (s, 1 H, dmb), 7.27 (s, 1 H, dmb).

TMS-dmb-AQ

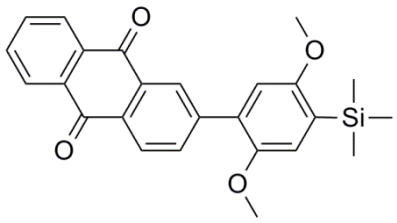

2-Bromoanthraquinone (5.00 g, 0.017 mol), 4-trimethylsilyl-2,5-dimethoxyphenylboronic acid ($B(OH)_2$-dmb-Br) (5.31 g, 0.02 mol) were dissolved in 120 ml toluene and 20 ml ethanol. A saturated solution of Na_2CO_3 (5.53 g, 0.05 mol) in de-ionized water was added. The mixture was deoxygenated by bubbling nitrogen gas during 30 minutes, then, $Pd(PPh_3)_4$ (1.00 g, 0.8 mmol) was added, and the reaction was carried out at 90°C overnight. The product was extracted with CH_2Cl_2 and purified by silica gel column chromatography using eluent mixture of 1:1 pentane/dichoromethane to obtain an orange solid (6.7 g, 92% yield).

^{1}H NMR: (400 MHz, $CDCl_3$, 25°C): δ [ppm] = 0.33 (s, 9 H, TMS), 3.81 (s, 3 H, OCH_3), 3.85 (s, 3 H, OCH_3), 6.90 (s, 1 H, dmb), 7.06 (s, 1 H, dmb), 7.80 (m, 2 H, AQ), 8.01 (dd, *J* = 8.0 Hz, 1.2 Hz, 1 H, AQ), 8.32 (m, 3 H, AQ), 8.48 (d, *J* = 1.6 Hz, 1 H, AQ).

I-dmb-AQ

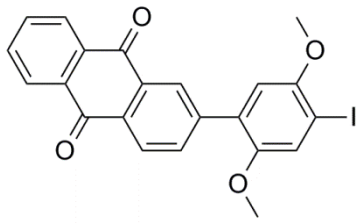

TMS-dmb-AQ (3.05 g, 7.3 mmol) was dissolved in CH_2Cl_2 (20 ml). Under nitrogen atmosphere, a solution of ICl (2.38 g, 14.6 mmol) in acetonitrile (70 ml) was added dropwise at 0°C. After stirring for 2 days at room temperature, the mixture was washed with an aqueous solution of meta-bisulfite (5% in water, 20 ml). The organic phase was extracted with CH_2Cl_2, dried over $MgSO_4$, filtered and evaporated under reduced pressure. A yellow powder was obtained (3.44 g, 82% yield).

^{1}H NMR: (400 MHz, $CDCl_3$, 25°C): δ [ppm] = 3.80 (s, 3 H, OCH_3), 3.90 (s, 3 H, OCH_3), 6.87 (s, 1 H, dmb), 7.43 (s, 1 H, dmb), 7.82 (m, 2 H, AQ), 7.97 (dd, *J* = 8.0 Hz, 2.0 Hz, 1 H, AQ), 8.34 (m, 3 H, AQ), 8.43 (d, *J* = 1.6 Hz, 1 H, AQ).

bpy-dmb-AQ

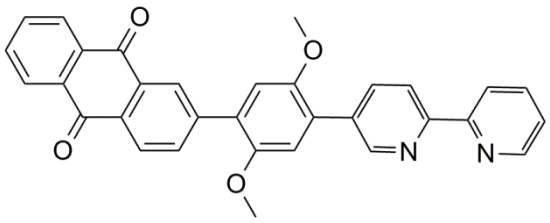

In a double-neck flask, I-dmb-AQ (0.25 g, 0.53 mmol) and 5-(tri-*n*-butylstannyl)-2,2'-bipyridine [1] (0.30 g, 0.69 mmol) were dissolved in *m*-xylene (30 ml). The mixture was deoxygenated for 30 minutes by bubbling nitrogen gas, and then the $Pd(PPh_3)_4$ catalyst (0.06 g, 0.053 mmol) was added. The reaction mixture was heated to reflux for 48 hours. After cooling to room temperature, the solvent was evaporated, a red-orange solid was obtained, and this solid was purified by silica gel column chromatography using a CH_2Cl_2/CH_3OH/triethylamine (99:1:1) eluent mixture (0.18 g, 69% yield).

^{1}H NMR: (400 MHz, $CDCl_3$, 25°C): δ ppm = 3.87 (d, *J* = 1.6 Hz, 6 H, OCH_3), 7.08 (s, 1H, dmb), 7.09 (s, 1 H, dmb), 7.34 (ddd, *J* = 8.0 Hz, 4.8 Hz, 1.2 Hz, 1 H, AQ), 7.83 (m, 3 H, AQ), 8.07 (m, 2 H, AQ), 8.35 (m, 3 H, AQ/bpy), 8.48 (m, 2 H, bpy), 8.53 (d, *J* = 1.6 Hz, 1 H, bpy), 8.71 (m, 1 H, bpy), 8.93 (d, *J* = 1.6 Hz, 1 H, bpy).

Ru-dmb-AQ

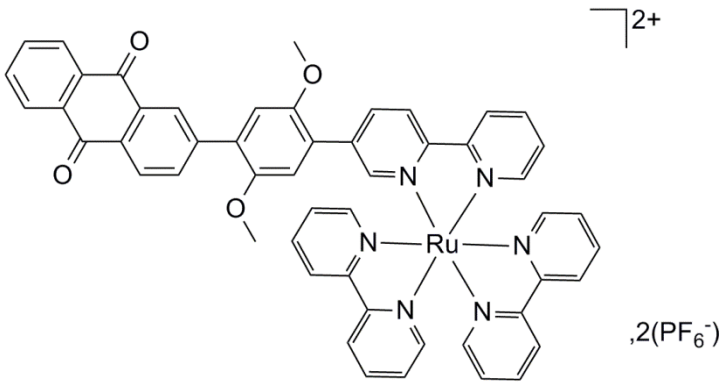

bpy-dmb-AQ (0.05 g, 0.1 mmol) and $Ru(bpy)_2Cl_2$ (0.048 g, 0.1 mmol) were dissolved in a mixture of ethanol and chloroform (10:3). The solution was deoxygenated and heated at reflux for 1 night. The solvent was evaporated, and the purple solid was purified by silica gel column chromatography using first acetone as the eluent and then a mixture of acetone/H_2O/KNO_3 saturated solution in water (9:1:1). The resulting product was dissolved in minimum of acetone, and a saturated solution of KPF_6 in water was added. The resulting precipitate was filtered and washed with water, then with diethyl ether, and dried under vacuum to give an orange solid (70 mg, 62% yield).

^{1}H NMR: (400 MHz, $CDCl_3$, 25°C): δ [ppm] = 3.60 (s, 3 H, OCH_3), 3.77 (s, 3 H, OCH_3), 7.02 (s, 1 H, dmb), 7.05 (s, 1 H, dmb), 7.44 (m, 5 H), 7.83 (m, 7 H), 8.06 (m, 7 H), 8.26 (m, 3 H), 8.30 (dd, *J* = 8.8 Hz, 2.0 Hz, 1 H), 8.39 (d, *J* = 2.0 Hz, 1 H), 8.58 (m, 6 H).

ES-MS m/z = 456.1 (calculated 456.1 for $C_{52}H_{38}N_6O_4Ru^{2+}$).

Anal. Calcd. for $C_{52}H_{38}N_6O_4RuP_2F_{12}$ · $3H_2O$: C 49.73, H 3.53, N 6.69. Found C 49.60, H 3.46, N 6.47.

Ru(^{t}Bu)-dmb-AQ

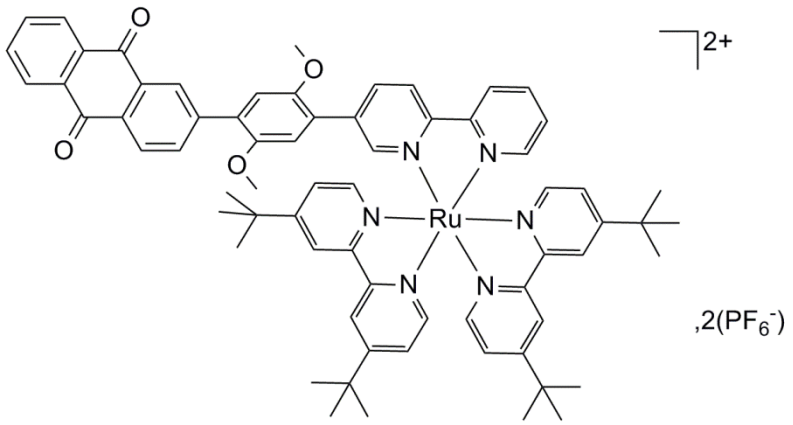

Ru(^{t}Bu)-dmb-AQ was prepared following the same protocol as described above, and by replacing $Ru(bpy)_2Cl_2$ with $Ru(^tBu\text{-}bpy)_2Cl_2$ (79% yield).

^{1}H NMR: (400 MHz, Acetone-d_6, 25°C): δ [ppm] = 1.35 (m, 36 H, CH_3), 3.65 (s, 3 H, OCH_3), 3.80 (s, 3 H, OCH_3), 7.05 (s, 1 H, dmb), 7.20 (s, 1 H, dmb), 7.52 (m, 2 H), 7.58 (dd, *J* = 6.0 Hz, 2.0 Hz, 2 H), 7.61 (dd, *J* = 6.0 Hz, 2.0 Hz, 1 H), 7.78 (m, 1 H), 7.86 (m, 3 H), 7.92 (m, 2 H), 7.98 (m, 2 H), 8.05 (dd, *J* = 7.0 Hz, 1.0 Hz, 1 H), 8.16 (m, 4 H), 8.29 (d, *J* = 1.7 Hz, 1 H), 8.36 (dd, *J* = 8.5 Hz, 1.8 Hz, 1 H), 8.87 (m, 6 H).

ES-MS m/z = 568.223 (calculated for 568.224 $C_{52}H_{38}N_6O_4Ru^{2+}$).

Anal. Calcd. for $C_{68}H_{70}N_6O_4RuP_2F_{12} \cdot 0.6CHCl_3$: C 55.00, H 4.75, N 5.61. Found C 55.23, H 4.87, N 5.10.

Br-bpy-Br

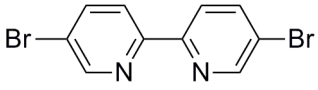

A solution of hexabutylditin (17.22 g, 29 mmol), 5-bromo-2-iodopyridine (16.85 g, 59 mmol), and 80 ml of dry *m*-xylene was well deoxygenated by bubbling nitrogen gas. $Pd(PPh_3)_4$ (0.68

g, 0.59 mmol) was added, and the mixture was allowed to reflux for 3 days until all the starting materials were consumed. The black solid was filtered, and then the filtrate was evaporated. Recrystalization of the crude product from chloroform leads to an off-white solid. The latter was filtered, washed with pentane and dried under vacuum (8.1 g, 89% yield).

^{1}H NMR (300 MHz, $CDCl_3$, 25°C): δ [ppm] = 7.93 (dd, *J* = 8.5 Hz, 2.3 Hz, 2 H), 8.28 (dd, *J* = 8.5 Hz, 0.6 Hz, 2 H), 8.70 (dd, *J* = 2.3 Hz, 0.6 Hz, 2 H).

TMS-xy-bpy-xy-TMS

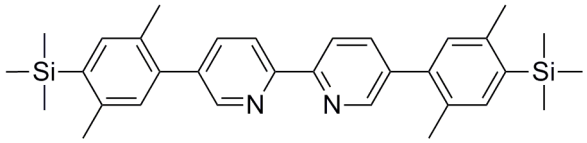

In a 250 ml double neck flask, 5,5'-Dibromo-2,2'-bipyridine (3.10 g, 9.87 mmol) was coupled to TMS-xy-$B(OH)_2$ (4.82 g, 21.7 mmol) in presence of 15.00 g Na_2CO_3 in 80 ml THF and 60 ml de-ionized water. The biphasic solution was deoxygenated by bubbling nitrogen gas for 30 minutes, and the $Pd(PPh_3)_4$ (0.57 g, 0.49 mmol) was added, and the solution was deoxygenated for another 15 minutes. The reaction mixture was refluxed overnight, and the workup was done by extracting the organic phase with CH_2Cl_2, drying with anhydrous $MgSO_4$, and evaporation of the solvents. The resulting solid was recrystallized from pentane to yield 78% of white product.

^{1}H NMR (300 MHz, $CDCl_3$, 25°C): δ [ppm] = 0.40 (s, 18 H, TMS), 2.32 (s, 6 H, CH_3), 2.49 (s, 6 H, CH_3), 7.11 (s, 2 H, xy), 7.40 (s, 2 H, xy), 7.82 (dd, *J* = 8.1 Hz, 2.2 Hz, 2 H, bpy), 8.48 (dd, *J* = 8.1 Hz, 0.7 Hz, 2 H, bpy), 8.70 (dd, *J* = 2.1 Hz, 1.4 Hz, 2 H, bpy).

Br-xy-bpy-xy-Br

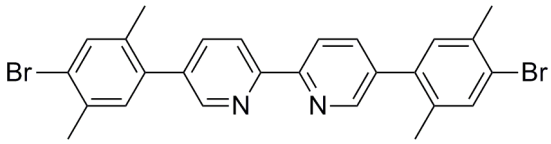

Bromine (0.88 ml, 17.13 mmol) was added dropwise to a stirred and ice-cooled suspension of TMS-xy-bpy-xy-TMS (2.18 g, 4.28 mmol) and NaOAc (0.70 g, 8.56 mmol) in THF (40 ml) in the dark. After 5 minutes, the ice bath was removed and the reaction mixture was stirred for 2 hours at room temperature. Et_3N (4.77 ml, 34.27 mmol) was added and the excess of bromine was destroyed by addition of a saturated aqueous $Na_2S_2O_3$ solution. The two resulting phases were separated, and the organic phase was dried over $MgSO_4$ and filtered. The solvent was evaporated and the residue purified by chromatography on silica gel, using a mixture of pentane/diethylether (1:1) as the eluent, to give a pure white solid (1.76 g, 79%).

^{1}H NMR (300 MHz, $CDCl_3$, 25°C): δ [ppm] = 2.27 (s, 6 H, CH_3), 2.42 (s, 6 H, CH_3), 7.15 (s, 2 H, xy), 7.50 (s, 2 H, xy), 7.77 (dd, *J* = 8.1 Hz, 2.2 Hz, 2 H, bpy), 8.48 (dd, *J* = 8.1 Hz, 0.7 Hz, 2 H, bpy), 8.64 (dd, *J* = 2.2 Hz, 0.7 Hz, 2 H, bpy).

AQ-boronic ester

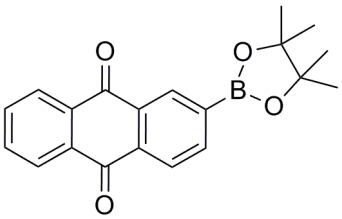

2-bromoanthraquinone (1.00 g, 3.48 mmol), bis(pinacolate)diboron (1.06 g, 4.17 mmol), $PdCl_2$(dppf)·CH_2Cl_2 (dppf = 1,1′-Bis(diphenylphosphino)ferrocene) (0.14 g, 0.17 mmol), KOAc (1.02 g, 10.00 mmol), and 30 ml of anhydrous DMSO were added to a dried 100 ml double neck flask. The reaction mixture was stirred at 80°C for 2 days; afterwards a saturated aqueous NH_4Cl solution was added. The organic phase was extracted with EtOAc, dried over

$MgSO_4$, and evaporated under reduced pressure. Recrystallization of the crude product from pentane leads to a yellow solid (0.56 g, 48%).

^{1}H NMR (300 MHz, $CDCl_3$, 25°C): δ [ppm] = 1.38 (s, 12 H, CH_3), 7.80 (m, 2 H, AQ), 8.20 (dd, *J* = 7.5 Hz, 1.1 Hz, 1 H, AQ), 8.31 (m, 3 H, AQ), 8.75 (d, *J* = 0.5 Hz, 1 H, AQ).

Br-xy-bpy-xy-AQ

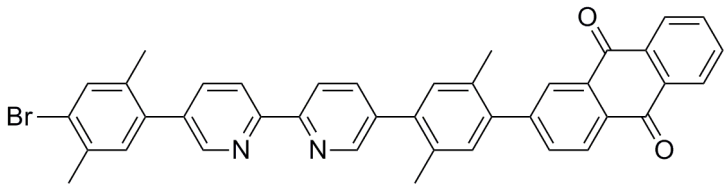

$Pd(PPh_3)_4$ (0.13 g, 0.19 mmol) was added under inert atmosphere to a stirred and deoxygenated suspension of AQ-boronic ester (0.40 g, 1.19 mmol), Br-xy-bpy-xy-Br (1.56 g, 2.99 mmol), and 5 g of Na_2CO_3 in a 1:1 mixture of THF and de-ionized water (20 ml:20 ml). After refluxing overnight, the product was extracted with CH_2Cl_2, dried over $MgSO_4$, filtered and the solvents were removed under reduced pressure. A yellow solid (0.56 g, 72%) was obtained by recrystallization from pentane.

^{1}H NMR (300 MHz, $CDCl_3$, 25°C): δ [ppm] = 2.28 (s, 3 H, CH_3), 2.36 (s, 3 H, CH_3), 2.37 (s, 3 H, CH_3), 2.43 (s, 3 H, CH_3), 7.16 (s, 1 H, xy), 7.27 (s, 2 H, xy), 7.51 (s, 1 H, xy), 7.81 (m, 4 H, AQ), 7.88 (dd, *J* = 8.1 Hz, 2.2 Hz, 1 H, bpy), 8.35 (m, 3 H, AQ), 8.40 (d, *J* = 8.0 Hz,1 H, bpy), 8.51 (dd, *J* = 8.1 Hz, 4 Hz, 2 H, bpy), 8.66 (dd, *J* = 2.1 Hz, 0.5 Hz, 1 H, bpy), 8.75 (dd, *J* = 2.1 Hz, 0.5 Hz, 1 H, bpy).

TAA-xy-bpy-xy-AQ

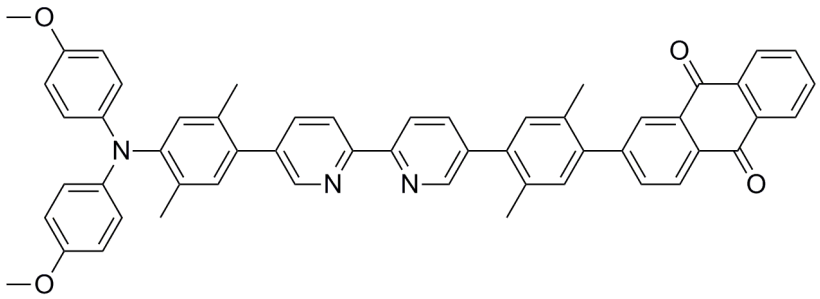

To a dried two-neck flask charged with 4,4'-dimethoxydiphenylamine (0.19 g, 0.86 mmol), AQ-xy-bpy-xy-Br (0.56 g, 0.86 mmol), potassium *tert*-butoxide (0.14 g, 1.29 mmol), and Pd(dibenzylidene-acetone)$_2$ (0.02 g, 0.03 mmol), were added freshly distilled toluene (30 ml) and a 1 M solution of tri-*tert*-butylphosphine (0.03 ml, 0.03 mmol) under nitrogen atmosphere. The yellow suspension was heated to 60°C overnight, until all starting material was consumed. The solvent was evaporated and the resulting brown product was purified by column chromatography on a silica gel, using dichloromethane/acetone (9:1) as eluent mixture. This gave a pure solid (0.51 g, 75%).

^{1}H NMR (300 MHz, $CDCl_3$, 25°C): δ [ppm] = 2.03 (s, 3 H, CH_3), 2.23 (s, 3 H, CH_3), 2.36 (d, *J* = 3.6 Hz, 6 H, CH_3), 3.79 (s, 6 H, OCH_3), 6.80 (m, 4 H, C_6H_4), 6.93 (m, 4 H, C_6H_4), 6.99 (s, 1 H, xy), 7.13 (s, 1 H, xy), 7.27 (s, 2 H, xy), 7.85 (m, 5 H, AQ/bpy), 8.35 (m, 3 H, AQ), 8.41 (d, *J* = 8.0 Hz, 1 H, bpy), 8.51 (t, *J* = 8.0 Hz, 2 H, bpy), 8.68 (dd, *J* = 2.2 Hz, 0.6 Hz, 1 H, bpy), 8.77 (dd, *J* = 2.2 Hz, 0.6 Hz, 1 H, bpy).

Anal. Calcd. for $C_{54}H_{43}N_3O_4$: C 81.28, H 5.43, N 5.27. Found: C 81.03, H 5.42, N 4.90.

TAA-Ru^{2+}-AQ

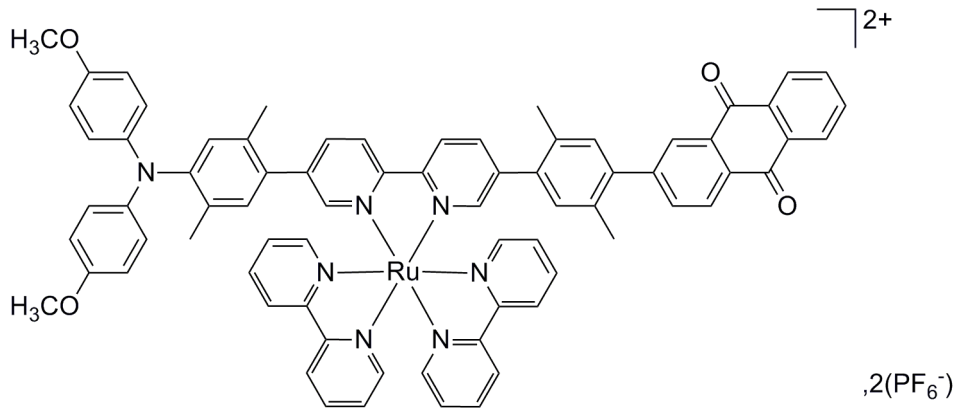

Metal complexation occurred by refluxing TAA-xy-bpy-xy-AQ (0.15 g, 0.18 mmol) and $Ru(bpy)_2Cl_2$ (0.09 g, 0.18 mmol) in a chloroform/ethanol mixture (6 ml/20 ml) overnight. After removing the solvent, the solid was chromatographed on silica gel using an eluent mixture comprised of 90% acetone, 9% water and 1% aqueous saturated KNO_3 solution. Acetone was evaporated, and the desired complex was precipitated from the remaining aqueous phase by adding an aqueous saturated potassium hexafluorophosphate solution. The orange solid was separated by filtration, and then washed with de-ionized water and diethylether. Finally, it was dried under vacuum (0.21 g, 75%).

^{1}H NMR (300 MHz, CD_2Cl_2, 25°C): δ [ppm] = 1.77 (s, 3 H, CH_3), 1.87 (s, 3 H, CH_3), 1.93 (s, 3 H, CH_3), 2.21 (s, 3 H, CH_3), 3.69 (s, 6 H, OCH_3), 6.73 (m, 8 H, C_6H_4), 6.95 (s, 1 H, xy), 7.09 (s, 1 H, xy), 7.12 (s, 1 H, xy), 7.49 (m, 2 H, bpy), 7.51 (m, 2 H, bpy), 7.63 (dd, *J* = 6.6 Hz, 1.7 Hz, 2 H, bpy), 7.69 (m, 3 H, bpy), 7.78 (m, 2 H, AQ), 7.84 (m, 2 H, bpy), 8.01 (m, 7 H, AQ/bpy), 8.16 (d, *J* = 1.6 Hz, 1 H, bpy), 8.25 (m, 3 H, AQ/bpy), 8.40 (m, 4 H, bpy), 8.53 (dd, *J* = 8.4 Hz, 4.4 Hz, 2 H, bpy).

ES-MS: m/z = 605.684 (calculated 605.685 for $C_{74}H_{59}N_7O_4Ru^{2+}$).

Anal. Calcd. for $C_{74}H_{59}N_7O_4RuP_2F_{12}$ · 4 H_2O: C 56.41, H 4.29, N 6.23. Found: C 56.48, H 4.17; N 6.16.

bpy-xy-TMS

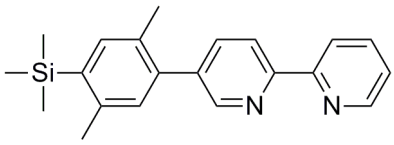

Br-bpy (4.44 g, 18.8 mmol)[1], TMS-xy-$B(OH)_2$ (4.61 g, 20.0 mmol) and Na_2CO_3 (6.01 g, 56.0 mmol) were dissolved in a mixture of toluene (150 ml), water (50 ml) and ethanol (50 ml). The solution was deoxygenated by three subsequent nitrogen/vacuum cycles, then $Pd(PPh_3)_3$ (0.43 g, 0.30 mmol) was added under nitrogen atmosphere. After heating the solution to reflux overnight, the solvents were evaporated and a yellow oil was obtained. The latter was purified by flash chromatography using a mixture of pentane/diethylether (1:1) as the eluent. A colorless oil, which was crystallized upon prolonged standing, was obtained (4.82 g, 76%).

^{1}H NMR (300 MHz, CD_2Cl_2, 25°C): δ [ppm] = 0.37 (s, 9 H, TMS), 2.30 (s, 3 H, CH_3), 2.48 (s, 3 H, CH_3), 7.09 (s, 1 H, xy), 7.32 (m, 1 H, bpy), 7.39 (s, 1 H, xy), 7.83 (m, 2 H, bpy), 8.44 (m, 2 H, bpy), 8.70 (m, 2 H, bpy).

bpy-xy-Br

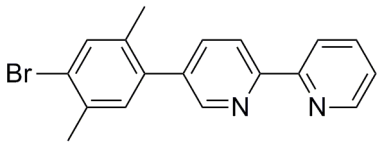

To an ice-cooled suspension of bpy-xy-TMS (4.81 g, 14.0 mmol) and NaOAc (3.55 g, 43.0 mmol) in 50 ml of THF placed in the dark, bromine (1.49 ml, 29.0 mmol) was added. After stirring for 2 hours at room temperature, Et_3N (16.12 ml, 11.5 mmol) was added, followed by addition of a saturated aqueous $Na_2S_2O_3$ solution (50 ml). The organic phase was extracted with CH_2Cl_2 and the solvents were removed under vacuum. Silica gel column chromatography was necessary to purify the crude product, using a mixture of pentane/diethylether (1:1) as the eluent. A yellow oil was obtained (3.98 g, 84%).

^{1}H NMR (300 MHz, CD_2Cl_2, 25°C): δ [ppm] = 2.25 (s, 3 H, CH_3), 2.41 (s, 3 H, CH_3), 7.13 (s, 1 H, xy), 7.32 (m, 1 H, bpy), 7.49 (s, 1 H, xy), 7.80 (m, 2 H, bpy), 8.44 (m, 2 H, bpy), 8.70 (m, 2 H, bpy).

TAA-xy-bpy

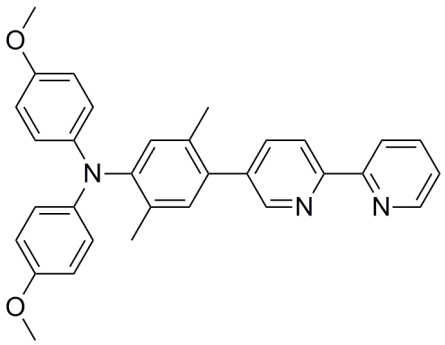

N-C coupling between bpy-xy-Br (0.28 g, 0.82 mmol) and 4,4-dimethoxydiphenylamine (0.19 g, 0.82 mmol) was performed as follows: To the flask containing the two coupling partners, potassium *tert*-butoxide (0.13 g, 1.23 mmol), Pd(dibenzylidene-acetone)$_2$ (0.02 g, 0.03 mmol) and 30 ml of dry toluene was added. After 20 minutes of bubbling nitrogen, tri-*tert*-butylphosphine was added, and the reaction mixture was heated to 80°C for 2 days. Once the reaction was stopped, the solvent was removed under reduced pressure, and the resulting oil was chromatographed on silica gel, using an eluent mixture of pentane/ethylacetate (9:1). A purple solid was obtained (64.0 mg, 15 %).

^{1}H NMR (300 MHz, $CDCl_3$, 25°C): δ [ppm] = 2.01 (s, 3 H, CH_3), 2.21 (s, 3 H, CH_3), 3.78 (s, 6 H, OCH_3), 6.80 (m, 4 H, C_6H_4), 6.91 (m, 4 H, C_6H_4), 6.98 (s, 1 H, xy), 7.10 (s, 1 H, xy), 7.31 (m, 1 H, bpy), 7.83 (m, 2 H, bpy), 8.44 (m, 2 H, bpy), 8.70 (m, 2 H, bpy).

TAA-Ru^{2+}

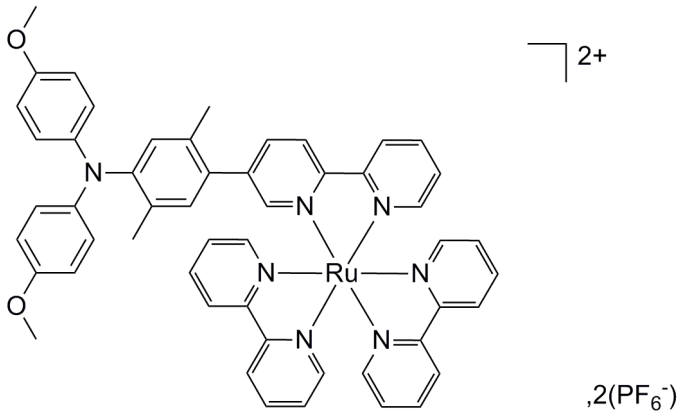

TAA-xy-bpy (64.0 mg, 0.13 mmol) in 3 ml of $CHCl_3$ was added to a suspension of $Ru(bpy)_2Cl_2$ (69.9 mg, 0.13 mmol) in 10 ml of EtOH. The reaction mixture was refluxed under nitrogen atmosphere overnight. Then, the solvents were removed under reduced pressure, and the crude product was purified by column chromatography on silica gel. The eluent was a mixture of acetone/water/aqueous saturated KNO_3 solution (90/9/1). After acetone removal under reduced pressure, addition of a saturated aqueous solution of potassium hexafluorophosphate induced precipitation of the desired product. The orange solid was filtered, washed with water and diethylether, and dried under vaccum.

^{1}H NMR (300 MHz, CD_2Cl_2, 25°C): δ [ppm] = 1.80 (s, 3 H, xy), 1.90 (s, 3 H, xy), 3.73 (s, 6 H, OCH_3), 6.76 (m, 8 H, C_6H_4), 6.95 (s, 1 H), 7.46 (m, 5 H), 7.70 (m, 6 H), 8.05 (m, 7 H), 8.44 (m, 6H).

ES-MS: m/z = 450.634 (calculated 450.635 for $C_{52}H_{47}N_7O_2Ru^{2+}$).

Anal. Calcd. for $C_{52}H_{45}N_7O_2RuP_2F_{12} \cdot 0.5H_2O$: C 52.05, H 3.86, N 8.17. Found: C 52.36, H 4.12; N 7.89

For all the osmium complexes, same synthetic procedure has been followed:

A mixture of starting materials in ethylene glycol was refluxed overnight under nitrogen atmosphere. After cooling to room temperature water was added, and the aqueous phase was extracted with CH_2Cl_2. The organic phase was dried over $MgSO_4$, and the solvent was removed under reduced pressure. Product purification occurred by column chromatography on silica gel using a mixture comprised of acetone/water/aqueous saturated KNO_3 solution (90/9/1) as the eluent. The desired product was precipitated from the aqueous solution (after acetone removal) by addition of saturated aqueous KPF_6 solution.

TAA-Os^{2+}

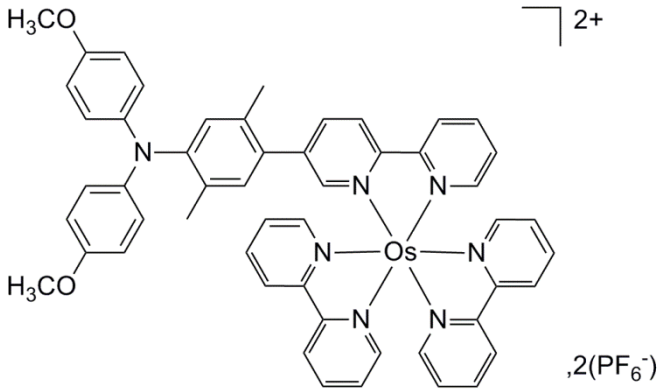

Starting materials: TAA-xy-bpy (30.0 mg, 0.061 mmol) and $Os(bpy)_2Cl_2$ (35.0 mg, 0.061 mmol). Green solid was obtained (53 mg, 68 % yield).

^{1}H NMR (300 MHz, CD_2Cl_2, 25°C): δ [ppm] = 1.79 (s, 3 H, xy), 1.90 (s, 3 H, xy), 3.73 (s, 6 H, OCH_3), 6.76 (m, 9 H, C_6H_4/xy), 6.95 (s, 1 H, xy), 7.36 (m, 5 H), 7.61 (m, 6 H), 7.86 (m, 6 H), 8.41 (m, 6 H).

ES-MS: m/z = 495.66 (calculated 495.66 for $C_{52}H_{45}N_7O_2Os^{2+}$).

Anal. Calcd. for $C_{52}H_{45}N_7O_2OsP_2F_{12}$: C 48.79, H 3.54, N 7.66. Found: C 48.44, H 3.47, N 7.50.

AQ-Os^{2+}

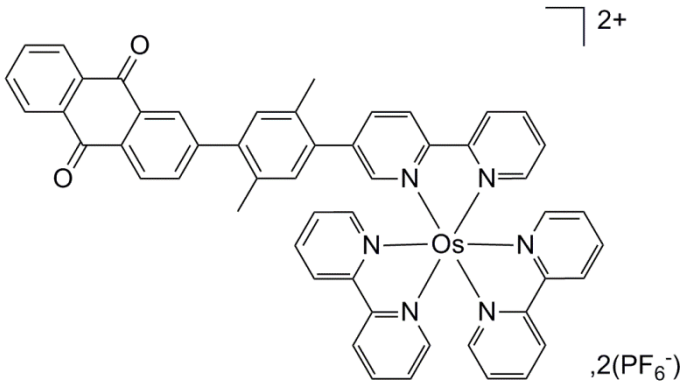

Starting materials: AQ-xy-bpy (0.05 g, 0.1mmol) and $Os(bpy)_2Cl_2$ (61.0 mg, 0.1 mmol). Green solid was obtained (64 mg, 49 % yield).

^{1}H NMR: (300 MHz, CD_3CN, 25°C): δ [ppm] = 2.02 (s, 3 H, CH_3), 2.25 (s, 3 H, CH_3), 7.12 (s, 1 H, xy), 7.22 (s, 1 H, xy), 7.32 (m, 5 H), 7.56 (d, *J* = 1.5 Hz, 1 H), 7.67 (m, 4 H), 7.83 (m, 4 H), 7.90 (m, 6 H), 8.12 (d, *J* = 1.6 Hz, 1 H), 8.29 (m, 3 H), 8.50 (m, 6 H).

ES-MS m/z = 485.133 (calculated 485.135 for $C_{52}H_{38}N_6O_2Os^{2+}$).

Anal. Calcd. for $C_{52}H_{38}N_6O_2OsP_2F_{12}$ ·1.5 H_2O: C 48.56, H 3.21, N 6.53. Found C 48.66, H 3.13, N 6.49

TAA-Os^{2+}-AQ

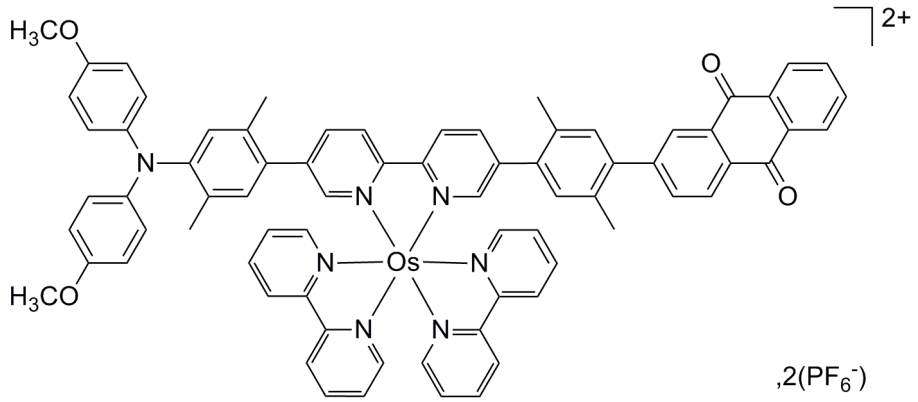

Starting materials: TAA-xy-bpy-xy-AQ (30.0 mg, 0.037 mmol) and $Os(bpy)_2Cl_2$ (21.0 mg, 0.037 mmol). Green solid was obtained (42 mg, 72% yield).

^{1}H NMR (300 MHz, CD_2Cl_2, 25°C): δ [ppm] = 1.81 (s, 3 H, CH_3), 1.91 (s, 3 H, CH_3), 1.97 (s, 3 H, CH_3), 2.34 (s, 3 H, CH_3), 3.74 (s, 6 H, OCH_3), 6.77 (m, 8 H, amine), 6.99 (s, 1 H), 7.14 (s, 1 H), 7.16 (s, 1 H), 7.35 (m, 2 H), 7.46 (m, 3 H), 7.57 (m, 2 H), 7.67 (m, 2 H), 7.73 (m, 1 H), 7.82 (m, 6 H), 7.92 (m, 4H), 8.20 (m, 1 H), 8.30 (m, 3 H), 8.45 (m, 4 H), 8.59 (m, 2 H).

ES-MS: m/z = 650.71 (calculated 650.71 for $C_{74}H_{59}N_7O_4Os^{2+}$).

Anal. Calcd. for $C_{74}H_{59}N_7O_4OsP_2F_{12}$ · 2 H_2O: C 54.64, H 3.90, N 6.03. Found: C 54.41, H 3.79, N 6.04

In order to synthesize the irdium complexes, the sarting materials was refluxed overnight in a mixture comprised of 10 ml of ethanol and 3 ml of chloroform. After cooling down to room temperature, a yellow-orange solid was obtained upon addition of an aqueous saturated solution of KPF_6. The solid was filtered, washed with water and diethylether, and dried under vaccum.

TAA-Ir$^+$

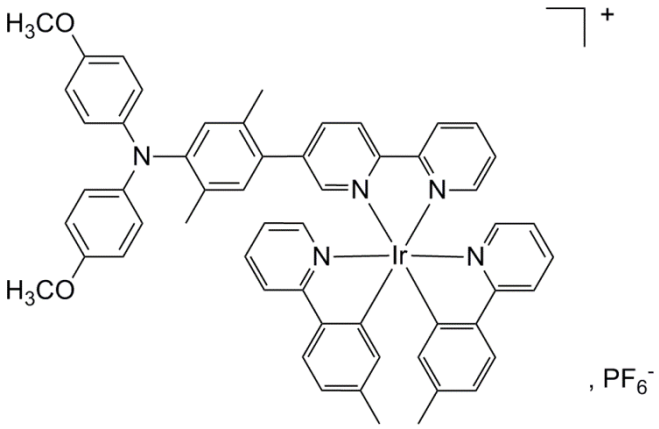

Starting materials: TAA-xy-bpy (28.0 mg, 0.058 mmol), Ir(tolyl-py)$_2$Cl$_2$ (30.0 mg, 0.026 mmol). Orange solid was obtained (22 mg, 73%).

^{1}H NMR (300 MHz, CD_2Cl_2, 25°C): δ [ppm] = 1.80 (s, 3 H, CH_3), 1.92 (s, 3 H, CH_3), 2.10 (m, 6 H, CH_3), 3.73 (s, 6 H, OCH_3), 6.08 (s, 1 H), 6.15 (s, 1 H), 6.78 (m, 9 H), 6.93 (m, 5 H), 7.43 (m, 1 H), 7.56 (m, 4 H), 7.74 (m, 2 H), 7.88 (m, 2 H), 8.05 (m, 4 H), 8.51 (m, 2 H).

ES-MS: m/z = 1016.35 (calculated 1016.35 for $C_{56}H_{49}N_5O_2Ir^+$).

Anal. Calcd. for $C_{56}H_{49}N_5O_2IrPF_6 \cdot H_2O$: C 57.04, H 4.36, N 5.94. Found: C 57.10, H 4.22, N 5.87.

AQ-Ir$^+$

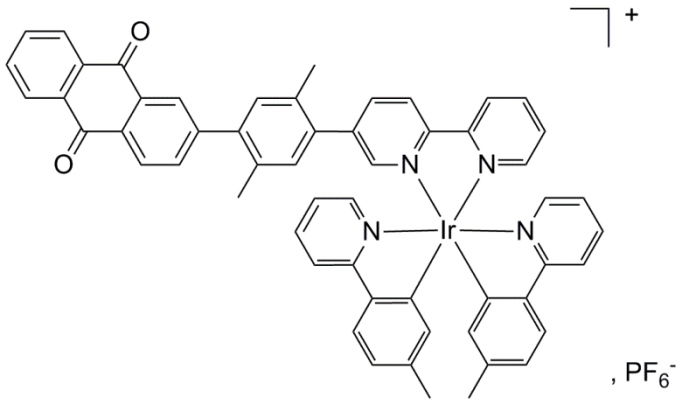

Starting materials: AQ-xy-bpy (27.0 mg, 0.058 mmol), Ir(tolyl-py)$_2$Cl$_2$ (30.0 mg, 0.026 mmol). Yellow solid was obtained (24 mg, 80%).

^{1}H NMR: (300 MHz, CD_3CN, 25°C): δ [ppm] = 1.99 (s, 3 H, CH_3), 2.07 (s, 3 H, CH_3), 2.11 (s, 3 H, CH_3), 2.27 (s, 3 H, CH_3), 6.12 (s, 1 H), 6.17 (s, 1 H), 6.88 (m, 2 H), 7.01 (m, 2 H), 7.16 (s, 1 H), 7.23 (s, 1 H), 7.52 (m, 1 H), 7.63 (m, 1 H), 7.69 (m, 3 H), 7.83 (m, 3 H),7.90 (m, 2 H), 8.00 (m, 4 H), 8.17 (m, 3 H), 8.29 (m, 3 H), 8.57 (m, 2 H).

ES-MS m/z = 995.29 (calculated 995.29 for $C_{56}H_{42}N_4O_2Ir^+$).

Anal. Calcd. for $C_{56}H_{42}N_4O_2IrPF_6$ ·0.3 $CHCl_3$: C 57.50, H 3.63, N 4.76. Found C 57.74, H 3.41, N 4.73.

TAA-Ir^{+}-AQ

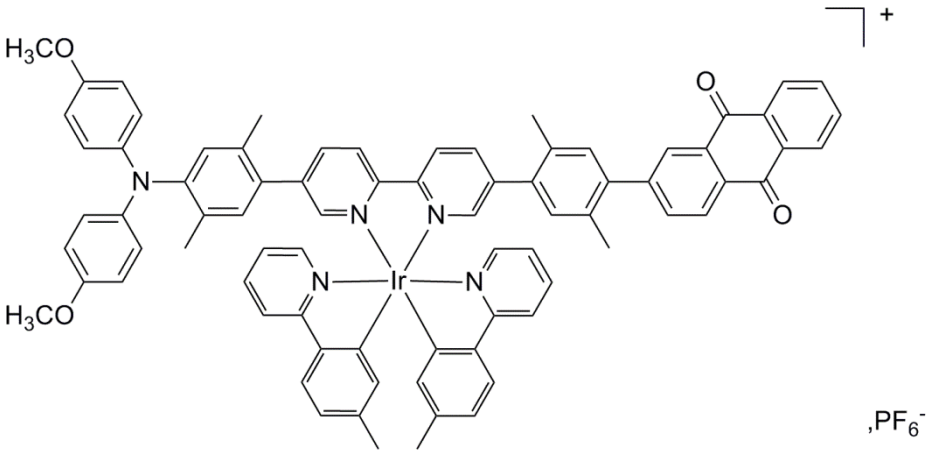

Starting materials: TAA-xy-bpy-xy-AQ (46.0 mg, 0.026 mmol), Ir(tolyl-py)$_2$Cl$_2$ (30.0 mg, 0.058 mmol). Orange solid was obtained (34 mg, 87 % yield).

^{1}H NMR (300 MHz, CD_2Cl_2, 25°C): δ [ppm] = 1.81 (s, 3 H, CH_3), 1.93 (s, 3 H, CH_3), 1.97 (s, 3 H, CH_3), 2.10 (m, 6 H, xy), 2.28 (s, 3 H, xy), 3.75 (s, 6 H, OCH_3), 6.15 (m, 2 H), 6.78 (m, 8 H, C_6H_4), 6.88 (m, 2 H), 6.99 (m, 3 H), 7.17 (m, 2 H), 7.62 (m, 4 H), 7.77 (m, 3 H), 7.83 (m, 2 H), 7.89 (m, 2 H), 8.10 (m, 2 H), 8.16 (m, 2 H), 8.30 (m, 5 H), 8.58 (m, 2 H).

ES-MS m/z = 1326.45 (calculated 1326.45 for $C_{78}H_{63}N_5O_4Ir^+$).

Anal. Calcd. for $C_{78}H_{63}N_5O_4IrPF_6$: C 63.66, H 4.32, N 4.76. Found C 64.00, H 4.45, N 4.78

Reference

[1] Hanss, D.; Wenger, O. S., *Inorg. Chem.* **2009**, *48*, 671-680.

List of Publications

a) Publications resulting from my Ph.D. work

Photoinduced electron transfer in linear triarylamine-photosensitizer-anthraquinone triads with ruthenium(II), osmium(II), and iridium(III)
Hankache, J.; Marja, N.; Lemmetyinen, H.; Wenger, O. S., *Inorg. Chem.* **2012**, *51*, 6333-6344.

Increasing the lifetime of a charge-separated state in a molecular triad by hydrogen-bonding solvent
Hankache, J.; Wenger, O. S., *Chem.-Eur. J.* **2012**, *18*, 6443-6447.

Hydrogen-bond strengthening upon photoinduced electron transfer in ruthenium–anthraquinone dyads interacting with hexafluoroisopropanol or water
Hankache, J.; Hanss, D.; Wenger, O. S., *J. Phys. Chem. A* **2012**, *13*, 3347-3358.

Photoinduced electron transfer in covalent ruthenium-anthraquinone dyads: Relative importance of driving-force, solvent polarity, and donor-bridge energy gap
Hankache, J.; Wenger, O. S., *Phys. Chem. Chem. Phys.* **2012,** *14*, 2685-2692.

Microsecond charge recombination in a linear triarylamine-$[Ru(bpy)_3]^{2+}$-anthraquinone triad
Hankache, J.; Wenger, O. S., *Chem. Commun.* **2011,** *47*, 10145-10147.

Organic Mixed Valence
Hankache, J.; Wenger, O. S., *Chem. Rev.* **2011**, *111*, 5138-5178.

b) Publications resulting from prior work as a Master student

Influence of experimental parameters on the synthesis of gold nanoparticles by electroless deposition
Bechelany, M.; Elias, J.; Hankache, J.; Brodard, P.; Philippe, L. ; Michler, J., *Advanced Materials Research* **2011**, *324*, 125-128.

Synthesis Mechanisms of Organized Gold Nanoparticles: Influence of Annealing Temperature and Atmosphere
Bechelany, M.; Maeder, X.; Riesterer, J.; Hankache, J.; Lerose, D.; Christiansen, S.; Michler, J.; Philippe, L., *Cryst. Growth Des.* **2010**, *10*, 587-596.

Acknowledgements

Making Ph.D. is a long and hard path. I couldn't be able to finish without the help and the assistance of many people, in particular my supervisor.

The passion, the guidance and support from my supervisor Prof. Dr. Oliver Wenger are something that I will remember for a long time. His attitude is beyond limit and expectations. Finishing my Ph.D. today is because of his great help. Without a single doubt, being part of his group was my best choice ever. To say the word 'thanks' is not enough.
But, he was not an angel all the time. Behind his kindness, he is a very tough boss, a very precise supervisor, and very demanding person. He made me crazy and angry several times. I will always remember his expressions: be precise, do not be lazy, be serious, help the reader….

I would like to express my sincere gratitude to Prof. Dr Franc Meyer for accepting to be my co-supervisor, while he has a lot of students and too much work.

I address my gratefulness to Prof. Dr. Dietmar Stalke, to Jun-Prof. Dr. Guido Clever, to Prof. Dr. Joerg Schroeder, and to Prof. Dr. Philipp Vana for their kind and prompt response regarding the acceptance to take part in my dissertation committee.

I had the privilege to start my Ph.D. in Geneva and finish what I started in Goettingen. I had the opportunity to meet and work with friendly colleagues in both sides. In Geneva, I was lucky to meet DaDa (Le Méchant) and MatMat (Mon Ami) who helped me a lot and taught me how to work in lab. JoJo (Beau Gosse) and WiWi (Zombie Guy) thanks for making my life like hell. I will miss the days while working together. Hard to leave these guys but too hard to stay with them. Believe me.

Here in Gottingen, we were a team from different continents, different culture, and different thinking. We worked together in a friendly environment. I was very happy to work with every single person in the group. Mr. He my labmate: I think you suffered a lot from my complaining. Catherine: Thanks for everything. Martin: Mein Freund. Luisa and Annabell: I will miss the 'German Rules'.

Finally, I would like to thank my parents. In the beginning they opposed my idea of doing a Ph.D., but I learned something in my life: Sometimes if we want to aim high, we need to fight hard and work hard to reach it. I would like to tell them now that I have overcome all the obstacles, and finally I did it.